Bucket foundations under lateral cyclic loading

Submitted for the degree of doctor of philosophy

Foglia, Aligi

Publication date:
2015

Document Version
Publisher's PDF, also known as Version of record

Bucket foundations under lateral cyclic loading

Submitted for the degree of doctor of philosophy

Aligi Foglia

DEPARTMENT OF CIVIL ENGINEERING
AALBORG UNIVERSITY

ISSN 1901-7294
DCE Thesis No. 68

Aalborg University
Department of Civil Engineering

DCE Thesis No. 68

Bucket foundations under lateral cyclic loading

Submitted for the degree of doctor of philosophy

by

Aligi Foglia

September 2014

Scientific Publications at the Department of Civil Engineering

Technical Reports are published for timely dissemination of research results and scientific work carried out at the Department of Civil Engineering (DCE) at Aalborg University. This medium allows publication of more detailed explanations and results than typically allowed in scientific journals.

Technical Memoranda are produced to enable the preliminary dissemination of scientific work by the personnel of the DCE where such release is deemed to be appropriate. Documents of this kind may be incomplete or temporary versions of papers—or part of continuing work. This should be kept in mind when references are given to publications of this kind.

Contract Reports are produced to report scientific work carried out under contract. Publications of this kind contain confidential matter and are reserved for the sponsors and the DCE. Therefore, Contract Reports are generally not available for public circulation.

Lecture Notes contain material produced by the lecturers at the DCE for educational purposes. This may be scientific notes, lecture books, example problems or manuals for laboratory work, or computer programs developed at the DCE.

Theses are monograms or collections of papers published to report the scientific work carried out at the DCE to obtain a degree as either PhD or Doctor of Technology. The thesis is publicly available after the defence of the degree.

Latest News is published to enable rapid communication of information about scientific work carried out at the DCE. This includes the status of research projects, developments in the laboratories, information about collaborative work and recent research results.

Published 2014 by
Aalborg University
Department of Civil Engineering
Sofiendalsvej 9-11,
DK-9200 Aalborg SV, Denmark

Printed in Aalborg at Aalborg University

ISSN 1901-7294
DCE Thesis No. 68

Preface

This doctoral thesis addresses problems regarding the behaviour of monopod bucket foundations under cyclic loading. The monopod bucket foundation is a sub-structure concept for offshore wind turbines which has been developed in Denmark by the company Universal Foundation A/S in collaboration with Aalborg University. The supervisor and coordinator of my Ph.D. project, Lars Bo Ibsen, is one of the main developers of the monopod bucket foundation concept. The present volume includes five introductory chapters and five scientific papers. The introductory chapters outline the premises, the aims and the conclusions of the scientific work. The five papers form the scientific content of the Ph.D. thesis.

I have been employed at Aalborg University from August 2011 to September 2014. The Ph.D. project was financially supported by "The Danish National Advanced Technology Foundation"through the platform "Cost-effective deep water foundations for large offshore wind turbines". The financial support is greatly acknowledged. During the period spent at Aalborg University, I have been involved in the following activities: conducting experiments on bucket foundations, post-processing and analysis of experimental data collected in the laboratory, giving lectures of soil mechanics and supervising master students.

The first six months of my Ph.D. studies were spent on designing and setting up a laboratory rig and on gaining insight into the behaviour of bucket foundations. The following two years were spent on carrying out an experimental campaign and on post-processing the experimental data. Within these two years, I worked for four months with the geotechnical research group of the University of Bologna. The researchers of the University of Bologna have extended knowledge on the behavioural patterns of shallow foundations on sand and, together with them, I was able to analyse thoroughly the experimental data and develop a new interpretation model. The last eight months of my experience were dedicated to writing scientific papers based on the main outcome of the Ph.D. project.

Aalborg, September 2014

Aligi Foglia

Acknowledgements

The doctorate of philosophy is a solitary experience. However, personal and professional connections are essential to it.

I need first of all to thank Lea for being so inspiring and so indispensable.

In the first months of my experience I had the chance to work together with Søren Peder Hyldal Sørensen. I wish to thank him for wisely taming some of my naive ideas driven by inexperience.

The period spent at Bologna University was fruitful beyond expectations and I wish to thank the geotechnical engineering research group for that. In particular, I want to express my gratitude to Guido Gottardi and Laura Govoni with whom I could have crucial discussions which shaped not only this thesis but also my ethic and my professional personality.

In the course of my doctorate I had the privilege to have brief but illuminating discussions with David Muir Wood, Marc Randolph and Roy Butterfield. I wish to thank them for the encouragement and for the outstanding contributions they gave to the geotechnical engineering discipline.

During my doctorate I had the pleasure to supervise Matthias Mücke, Giulio Nicolai and Benedetto Laerte Aiello. I wish to thank them for helping in the laboratory and for bringing new and fresh ideas to the research.

I finally wish to express my gratitude to my inexhaustible supervisor, who gave me the opportunity to grow surrounded by great Danish values.

Summary in English

To enable a prosperous development of offshore wind energy, economically feasible technologies must be developed. The monopod bucket foundation is likely to become a cost-effective sub-structure for offshore wind turbines and has the potential to make offshore wind more cost-competitive in the energy market. This thesis addresses issues concerning monopod bucket foundations in the hope of providing tools and ideas that could be used to optimize the design of this sub-structure.

The work is focussed on the behaviour of bucket foundations under lateral cyclic loading. Other related and propaedeutic topics, such as bucket foundations under transient lateral loading and under monotonic lateral loading, are also investigated. All the scientific work is fundamentally based on small-scale experimental tests of bucket foundations in dense water-saturated sand.

The most important scientific documents on bearing capacity and installation of bucket foundations are reviewed and the results from the models found in literature are compared to the experimental results obtained in the current study. Monotonic tests of bucket foundations under lateral loading until failure are compared with existing failure envelopes. A jacked installation test is successfully compared with existing models.

Tests of bucket foundations under lateral loading applied at different loading rates are analysed. As expected, the bearing capacity of bucket foundations under transient lateral loading increases dramatically with the loading rate. Though, there is no difference in the initial stiffness. Pore pressure transducers inside and around the foundations recorded the distribution of the pore water pressure during loading. Horizontal and rotational displacements are not found to be influenced by the loading rate.

A comprehensive experimental campaign of bucket foundations under lateral cyclic loading is interpreted with an existing empirical model that calculates the long-term rotation. The model is calibrated for dense sand. The model calibration reveals that the parameters are significantly dependent on the relative density but not on the embedment ratio. The ultimate capacity of bucket foundations pre-subjected

to cyclic loading is found to be larger than the monotonic capacity recorded with standard quasi-static tests.

A macro-element model for bucket foundations supporting offshore wind turbines is developed on the base of monotonic tests. To simulate the cyclic loading response, a boundary surface model is integrated into the macro-model. The model is able to reproduce the monotonic and cyclic experimental results quite well. Nevertheless, a proper strategy on how to evaluate the parameters of the boundary surface model is yet to be established.

Resumé (Summary in Danish)

For at sikre en positiv udvikling af offshore-vindenergi må økonomisk rentable teknologier udvikles. Bøttefundamentet bliver sandsynligvis en omkostningseffektiv substruktur for havvindmøller og har potentialet til at gøre offshore-vind mere prismæssigt konkurrencedygtigt. Denne afhandling omhandler problemstillinger i forbindelse med bøttefundamenter i håb om at frembringe redskaber og ideer, der kan bruges til at optimere udformningen af denne sub-struktur.

Arbejdet er fokuseret på bøttefundamentets opførsel under cyklisk belastning. Andre relaterede emner, såsom bøttefundamenter udsat for tværlast med forskellige hastigheder, bliver også undersøgt. Alle videnskabelige arbejder er grundlæggende baseret på småskala-forsøg med bøttefundamenter installeret i vandmættet, fastlejret sand.

De vigtigste videnskabelige dokumenter omhandlende bæreevne og installation af bøttefundamenter gennemgås, og resultaterne fra litteraturen holdes op imod resultater opnået i dette studie. Forsøg med bøttefundamenter under sideværts ensidig belastning sammenlignes med eksisterende brudflader. Forskellige brudflader sammenlignes, og der vises god indbyrdes overensstemmelse. Den målte modstand for et forsøg med nedpresset installation stemmer godt overens med eksisterende modeller.

Otte forsøg med tværbelastede bøttefundamenter ved fire forskellige belastningshastigheder analyseres. Som forventet stiger bæreevnen drastisk med belastningshastigheden dette på trods af, at der ingen forskel er i den oprindelige stivhed. Poretryksmålere i og omkring fundamenterne registrerer fordelingen af poretryk under belastning. Horisontale flytninger og rotationer er ikke påvirket af belastningshastigheden.

Et omfattende forsøgsprogram af cyklisk tværbelastede bøttefundamenter fortolkes i forhold til en eksisterende model, der beregner den permanente rotation. Modellen er kalibreret til fast sand. Kalibrering af modellen viser, at parametrene er væsentligt afhængige af den relative lejringstæthed, men ikke af penetrationsforholdet. Den ultimative kapacitet af et bøttefundament, som indledningsvis har været udsat for cyklisk last, påvises at være større end kapaciteten ved en ensidig påvirkning.

En makroelementmodel er udviklet på basis af monotone og cykliske forsøg. Modellen er i stand til at gengive både monotone og cykliske forsøgsresultater ganske godt. Ikke desto mindre er en ordentlig strategi for, hvordan man vurderer de cykliske parametre, endnu ikke udviklet.

Contents

CHAPTER 1

Renewable Energy in Europe

Nowadays society is facing a great challenge: getting off fossil fuels. This must be done for at least two reasons. First; more than 100 years of fossil resources usage has most likely led to significant global warming and climate change. Second; fossil fuel is so limited that humanity can no longer rely on that only. Coping with these challenges requires a multi-directional plan that includes all the different aspects of the issue (MacKay, 2009). For a carbon-free revolution to happen, society should start living more sustainably by adjusting its lifestyle, by adopting smart energy devices and by replacing fossil-fuel-based power plants with renewable energy power plants.

During the last two decades, renewable energies have emerged in the global energy market. The statistics given in the following refer to the year 2013 and are taken from two reports of the European Wind Energy Association (EWEA, 2013; EWEA, 2014). Figure 1 illustrates that at the end of 2013, the share of renewable energies in Europe was around 38% of the total installed capacity. Of the total renewable energy installed, 34% was wind energy. Figure 2 shows the breakdown of new capacity installed in 2013 in Europe. Renewable energies seem to have the prominent majority and wind energy has the largest percentage of new installed capacity. In Figures 1 and 2, PV stands for photovoltaic systems.

Among the renewable energies, offshore wind is going to be a key technology especially in those European countries characterised by long cost lines and noticeably windy seas. At the end of 2013, around 5.6% of the total wind power capacity (6526 MW) was installed offshore. In the decades to come, its development rate is likely to increase significantly. Only for offshore wind, the forecast of the European Wind Energy Association for the coming years is: 40 GW by 2020, 150 GW by 2030 and 460 GW by 2050 (EWEA, 2013).

Wind turbine performance is enhanced on sea water, where wind is faster and steadier than on land. Moreover, offshore wind seems to be more generally accepted by civil society avoiding the so-called "not in my back yard"issue. The advantages of open sea sites are however outweighed by the large initial investment required for offshore wind energy converters. Indeed, this technology is relatively young and still a high risk is associated to that. This makes potential investors often sceptical and reluctant to overtake such projects. A major part of the costs involves the sub-structures of offshore wind turbines (OWTs). To discern the real cost of sub-structures construction and installation from the total investment cost is not an easy task. According to the specifics of each project, the costs of construction, installation and maintenance of sub-structures fluctuate from 20% to 30% of the total investment.

Another raising cost factor related to sub-structures for OWTs is the large area involved in offshore wind projects. Traditional offshore structures, such as oil and gas platforms, require only very limited seabed area to be investigated and the cost of the sub-structure might be small in comparison to the total investment. On the contrary, offshore wind farms need an extensive area to be investigated and a universal foundation concept capable to provide a firm support on different stratigraphies. Pursuing research on cost-competitive offshore wind sub-structures is one way by which the cost of offshore wind energy can be reduced significantly.

In the next chapter, foundations and sub-structures for OWTs are presented. Particular attention is given to the most commonly used technologies and to the innovative concepts that might save initial investment costs and eventually reduce the cost of energy.

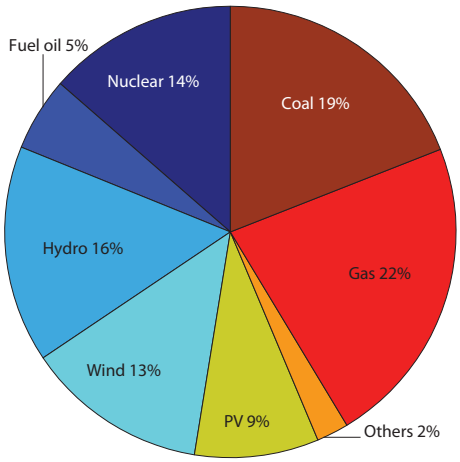

Figure 1: Breakdown of power mix in 2013 in Europe (EWEA, 2014)

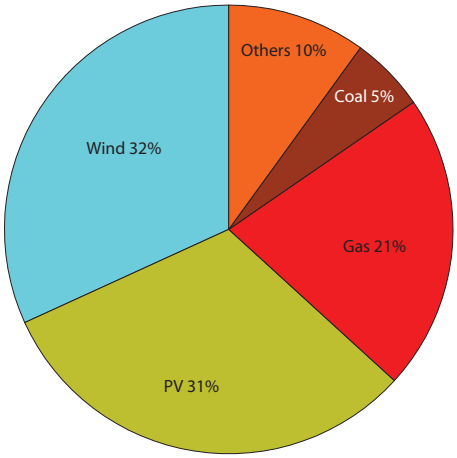

Figure 2: Breakdown of new power installations in 2013 in Europe (EWEA, 2014)

CHAPTER 2

Foundations and sub-structures

Strictly speaking, sub-structures and foundations are not the same thing. Although the two terminologies are sometimes interchangeably used, here a clear definition is given as follows. Support structures include all the structural elements below an offshore wind turbine, *cf.* Figure 3a. Two main components are included in the support structure, the tower and the sub-structure. The part of the sub-structure that is interfaced with the soil is the foundation.

Before presenting the general characteristics of foundations for offshore structures and sub-structures for offshore wind, it is fundamental to underline the unique loading condition of OWTs. In general, sub-structures for offshore wind converters have to withstand a very large overturning moment together with a relatively large horizontal load and a small vertical load. In Figures 3b and 3c, the loading configurations applied to sub-structures (dashed line) and foundations (solid bold line) are shown. If the sub-structure has multiple foundations (sub-structure with multipod foundation), Figure 3c, the overturning moment is transferred to the soil by means of axial loading in tension and compression distributed over the foundations. If, on the contrary, the sub-structure has one foundation only (sub-structure with monopod foundation), Figure 3b, the foundation has to withstand the overturning moment directly.

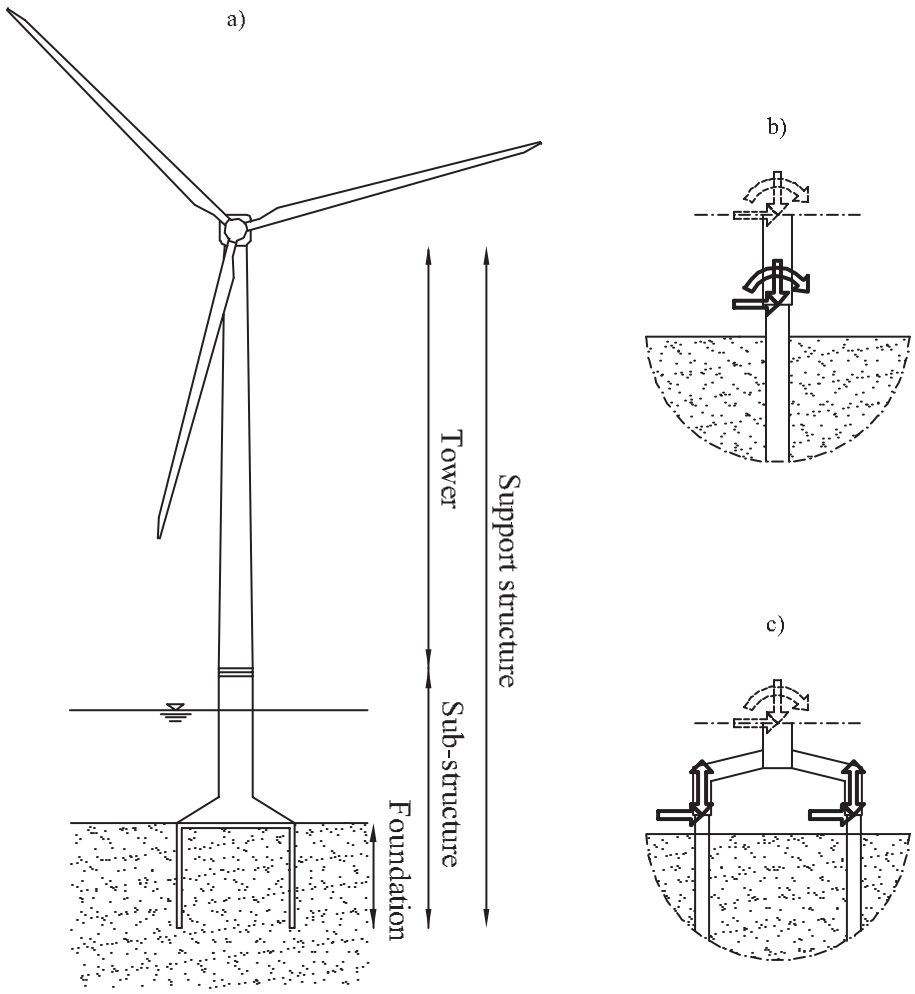

Figure 3: a) components of an offshore wind turbine system; b) load configuration of a sub-structure with monopod foundation; c) load configuration of a sub-structure with multipod foundation

In the oil and gas industry, foundations are mostly used to support jacket structures and to hold floating facilities (anchoring systems). Conversely, OWTs have been by far bottom-fixed sub-structures with monopod foundations. The overturning moment has therefore much more importance in the design compared with foundations for oil and gas facilities. This aspect becomes even more relevant since OWTs are relatively lighter than oil and gas platforms and thus more susceptible to overturning moment. The dimensionless group $V/(\gamma' D^3)$, where V is the vertical load, γ' the effective unit weight of the soil and D the foundation diameter, is larger than 3 for jackets for oil and gas platforms (Randolph and Gourvenec, 2011) while it ranges between 0.1 and 1 for OWTs. As it will be explained in greater details in the articles attached to this thesis, this feature influences the behaviour of the foundations. Before applying design criteria conceived for oil and gas platforms to offshore wind

turbines, clear proves of applicability should be given.

Throughout this doctoral thesis only planar loading (*i.e.* vertical load, horizontal load and overturning moment acting in the same plane) is considered. The reader should bear in mind that this is a simplification; real offshore loading conditions act in multiple directions in the three-dimensional space. However, this simplified approach does not prevent behavioural patterns of offshore foundations from being investigated.

In the following, the main features of each foundation and sub-structure concept are briefly described. Most of the general information given is taken from two main sources: Randolph and Gourvenec (2011) and Lesny (2011).

2.1 Offshore Foundations

The foundations are the parts of the support structure that interact with the seabed. Depending on the sub-structure, one or more foundations distribute the loads coming from the superstructures to the soil strata. The most common non-temporary foundations present in the offshore environment include: deep (or piled) foundations, shallow foundations and anchoring systems. Anchoring systems are widely used in the offshore environment but are not included here as they have not been extensively used for offshore wind turbines. Anchoring systems will perhaps be adopted more in the future when floating sub-structures will be optimised for commercial use.

2.1.1 Deep foundations

Piled foundations can be subdivided into large diameter piles (between 4 and 8 m in diameter), for sub-structures with monopod foundations, and small diameter piles (from 2 to 4 m in diameter), for sub-structures with multipod foundations. Piled foundations are the best option for offshore structures when the shallow soil encountered is soft or when there is the likelihood of foundation slide problems due to large horizontal loads. Most piles are driven into the soil with hydraulic hammers. In the presence of soil strata such as calcareous sediments or rock, also drilled and grouted piles can be adopted. Piles supporting jackets are driven into the seabed through the sleeves integrated at the jacket base (post-piling) or through mobile piling templates transported by the jackup vessels (pre-piling). Large diameter piles are hammered down through a frame leaning out from the installation vessel. A crucial aspect when assessing the capacity of a piled foundation is the evaluation of the post-installation soil conditions. To model the load transferred to the soil, the soil-pile interaction is schematised with non-linear springs (*cf.* Figure 4). t-z curves describe the relationship between mobilised shear stress and vertical displacement of axially loaded piles. p-y curves describe the relationship between soil resistance

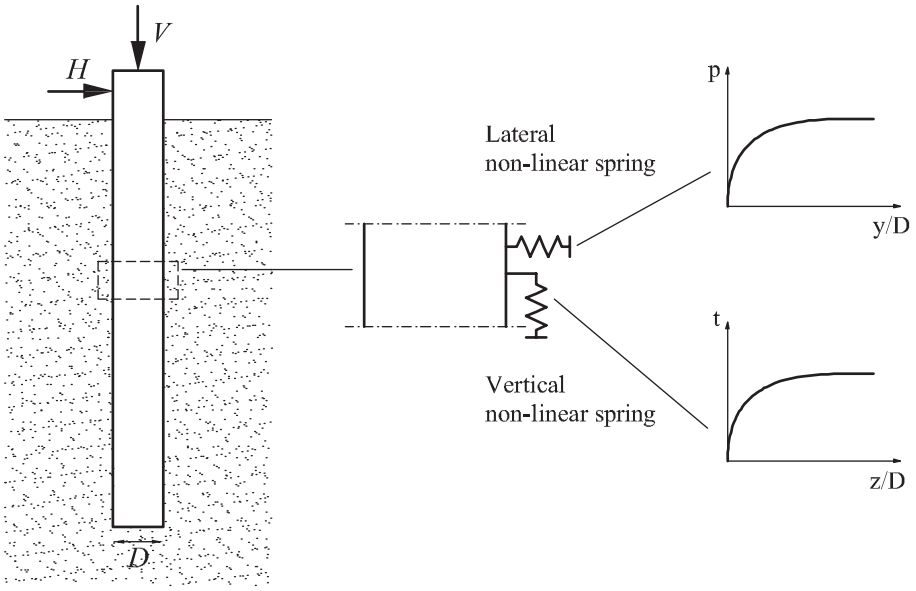

Figure 4: Simplified scheme of soil-structure interaction for axially loaded piles and horizontally loaded piles. After Randolph and Gourvenec (2011)

and lateral displacement of laterally loaded piles. Piles supporting jacket structures (small diameter piles) are mainly subjected to vertical loading. The axial capacity of a piled foundation has two contributions: the base resistance and the shaft resistance. In sandy soils the shaft resistance is assessed based on the cone resistance whereas in clayey soils it is quantified as a function of the undrained shear strength. The ultimate base resistance is defined with an allowable vertical displacement criterion and is calculated by summing the two contributions of pile wall and soil plug. The response of axially loaded piles is influenced by cyclic loading. The main effect of cyclic loading is the shaft resistance degradation. This is caused by pore pressure development in cohesive soils and by soil densification in sandy soils. To take cyclic degradation into account some rules for updating the spring stiffness of each cycle can be implemented in numerical models. Jardine et al. (2012) review the methods to estimate the cyclic loading effects of piles.

Large diameter piles have to bear large lateral loads in terms of combined moment and horizontal load. The current design base for laterally loaded piles is the well-known p-y curves approach. This method was developed some decades ago for slender piles. Whether this design method is appropriate for large diameter (and thus stiffer) piles or not is a controversial and ongoing topic of discussion among researchers (LeBlanc et al., 2010; Haigh, 2014). Furthermore, the standard p-y method considers simplistically the cyclic loading response. Some of the cyclic loading effects such as gapping, change in stiffness and ultimate post-cyclic resistance are nowadays widely investigated (Achmus et al., 2009; Kirkwood and High, 2014; Klinkvort and Hededal, 2014).

2.1.2 Shallow foundations

Shallow foundations are the obvious alternative to pile foundations when bedrock or very stiff soils are present. These foundations transfer the loads to the superficial layers of soil. In case of weak superficial soil strata, shallow foundations are provided with a skirt that transfers the loads to deeper and stronger soil. In Figure 5, flat and skirted foundations are depicted together with the possible loading configurations. Shallow flat foundations are normally subjected to combined loading. The bearing capacity of flat footings under combined loading relies on the compressive behaviour of the most superficial soil strata. Shallow flat foundations do not have any resistance against tension, except for their own weight. The prominent moment loading featured by OWTs might cause the foundation to be only partly in compression. If the foundation is required to be only in compression, significant ballast should be provided or the diameter should be enlarged.

Commonly, skirted foundations have embedment length to diameter ratio smaller than one. In addition to the increase in bearing capacity, the skirt allows pure tensile loads to be sustained as a result of suction generated within the foundation. This characteristic makes this foundation ideal for sub-structures with multiple foundations. Skirted foundations react to combined loading with both base resistance and skin friction. According to geometry and loading condition, skirted foundations can also be named as: suction caissons, suction bucket, bucket foundations or suction anchors. As suggested by Clukey et al. (1995), "suction"is a suitable term that identifies two distinct characteristics of the foundation. First, the foundation is installed by pump-induced under pressure. Second, when a certain loading rate is exceeded, suction passively develops underneath the foundation under tensile or general loading. Shallow foundations are preliminary designed with the classic baring capacity method. More accurate estimation of their response can be obtained with interaction diagrams, macro-models and numerical models. The effect of short-term cyclic loading can be evaluated with the well-known method proposed by Andersen (2009) and based on cyclic model tests.

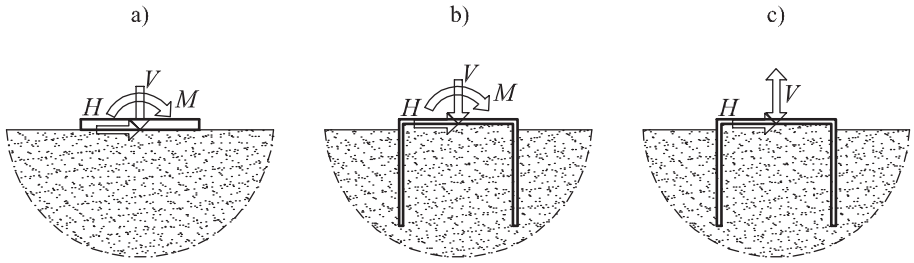

Figure 5: a) flat foundation for sub-structures with monopod foundation; b) skirted foundation for sub-structure with monopod foundation; c) skirted foundation for sub-structure with multipod foundation

2.2 Sub-structures for OWTs

Sub-structures are made of concrete or steel and connect the turbine tower to the seabed. Sub-structures can have three general configurations: sub-structures with monopod foundation (gravity based foundation, monopile, monopod bucket foundation), sub-structures with multipod foundation (jackets, tripods, tripiles) and floating sub-structures (Hywind, Windfloat, Blue H, etc.). As mentioned earlier, sub-structures govern the way in which the loads from the superstructure are transferred to the foundations.

2.2.1 Sub-structures with monopod foundation

Monopod structures are connected to the ground by means of one foundation only. The load transferred to the foundation consists of predominant overturning moment, considerable horizontal load and relatively small vertical load.

Gravity based foundations Gravity based foundations (GBFs) are made of reinforced concrete or steel and withstand the environmental forces by means of a prominent vertical load due to self-weight and ballast. GBFs are normally built on dry docks and transported offshore on vessels. Some types of GBFs reach the installation site by floating, towed by barges. The ballast material used to sink the structure and ensure its stability can be concrete, water, sand or gravel. Frequently, before laying the structure, the seabed must be adjusted in order to obtain a horizontal profile. GBFs have been favoured over other sub-structures in the early stage of the offshore wind development. This was certainly due to their technical simplicity in very shallow water depths. However, the large amount of material used to ensure a sufficient stabilising vertical load and the soil preparation procedure increase the cost of these sub-structures. Even though GBFs are generally considered uneconomical, they are currently being considered as possible options for some consented wind parks in the North Sea (4C Offshore, 2014).

Monopiles Monopiles have been used as the predominant type of sub-structure for offshore wind turbines in the last two decades. This structure is composed by a pile foundation supporting a transition piece which is the interface between the foundation and the turbine tower. Few years ago there was scepticism in using monopiles in water depth exceeding 20-25 m. Nowadays 6 MW wind turbines can be mounted on monopiles in water depths up to 30 m. Furthermore, new projects are being developed for the installation of monopiles in water depths exceeding 35 m (Seidel, 2014). As pointed out by Seidel (2014) with monopiles being installed in deeper water, not only the magnitude of loads increase but also the type of loading is prone to change in favour of a more significant action of the waves. The

wall thickness of a standard monopile goes from 40 to 70 mm. In the last years, a lot of research effort has been put into optimizing the design of these structures. Currently, important research projects on monopiles are undertaken by the PISA project. So far, monopiles have been driven into the seabed by ramming with hydraulic hammers. Limiting values for the noise emission during pile driving were introduced by the German authorities (BSH, 2013). To cope with these stringent regulations, new installation methods such as drilled monopiles (Hautmann, 2013) and vibro-piles (LeBlanc et al., 2013) are being investigated. Beside these two new technologies, also noise mitigation techniques for the installation of monopiles are being tested (Reimann et al., 2013).

Monopod bucket foundations Monopod bucket foundations are made of steel and consist of three main components: a flange on which the turbine tower is mounted, a skirted foundation, and a lid that interfaces flange and foundation. A picture of a monopod bucket structure with diameter 15 m and embedment length 7.5 m is shown in Figure 6. All the steel elements are welded to one another onshore and the entire structure is then transported offshore with a jackup vessel.

Figure 6: Real-scale monopod bucket foundation on the deck of a jackup vessel

Figure 7: Real-scale installation of a monopod bucket foundation in Frederikshavn, Denmark

Once the structure has reached the designated location, the foundation is installed by means of suction applied within the bucket. In 2002 a monopod bucket was installed a few meters off the shore of Frederikshavn to support a 3.0 MW wind turbine (Ibsen, 2008). A picture of the monopod bucket foundation installed in Frederikshavn in 2002 is illustrated in Figure 7. In 2009 a monopod bucket foundation for a met mast was towed from the port of Frederikshavn to the wind park Horns Rev 2 and installed by suction (LeBlanc, 2009). In September 2013 a monopod bucket foundation supporting a met mast was installed at Dogger Bank, in the British sector of the North Sea.

2.2.2 Sub-structures with multipod foundation

Sub-structures with multipod foundation are connected to the ground by means of three or four foundations. The large overturning moment from the superstructures is transferred to the foundations through vertical load in compression and in tension. Sub-structures with multiple foundations are conceived to support wind turbines with nominal power output larger than 5 MW in water depths exceeding 35 m.

Jackets Jackets are three or four legged steel frames founded on shallow foundations or piles. These systems were already fully developed for offshore oil and gas platforms. For this reason, jackets are generally considered very reliable and have been the most common sub-structures with multipod foundation so far adopted. The majority of the jackets for OWTs have four legs and are founded on piles. The construction of the steel frame is completed onshore. The sub-structure is then transported offshore and lifted with a crane of adequate capacity. Once the structure has reached a stable position on the seafloor, piles are driven into the soil through guiding sleeves at the four corners of the jacket. Pre-piling installation technologies, where the foundations are installed before laying the jacket, can also be adopted.

As demonstrated by oil and gas platform projects such as Draupner E and Sleipner SLT (Bye et al., 1995), jackets can be founded also on skirted foundations. Dong Energy is currently working on a three legged jacket structure founded on bucket foundations.

Tripods and Tripiles Tripods and tripiles are steel structures which consist of three legs founded on three piles. For tripods, the three legs are connected below the water level. For tripiles, the connecting node is situated above the water level. Tripods and tripiles were installed in the German sector of the North Sea to support 5 MW wind turbines in around 40 m water depth. While tripiles were only used in the wind park Bard 1, tripods have been used more often (Alpha Ventus, Borkum Phase 1 and Global Tech 1) and could be competitors of jacket structures in future projects.

2.3 Floating sub-structures

As reported in EWEA (2013), a significant European offshore wind potential is situated at water depths grater than 60 m, where conventional bottom-fixed sub-structures would not be feasible. For example, water depths between 50 m and 220 m cover the 66% of the North Sea. Besides, the Atlantic Ocean and the Mediterranean Sea present even deeper water. In light of these observations, floating sub-structures for OWTs could play a relevant role in the future. Floating sub-structures are anchored to the ground by means of tethers or mooring lines. Tethers transfer the environmental forces to the foundations through tensile load whereas mooring lines through horizontal load. Floating sub-structure technologies are still in their infancy and will need at least another five years to enter competitively the offshore wind market (EWEA, 2013). Two well-known examples of floating sub-structures are Hywind and Windfloat. A prototype of Hywind supporting a 2.3 MW wind turbine was installed in 2009 off the west coast of Norway. In 2011 a prototype of Windfloat was deployed off the coast of Portugal. Most of the projects are still on pilot or prototype stage. Some of these technologies will perhaps be mature enough to be commercially deployed by 2017.

CHAPTER 3

Aims and objectives

3.1 Overall aim

As emphasised in Chapter 1, offshore wind energy is necessary to enable the transition to renewable energy in Europe. In light of this, it is of fundamental importance to pursue research on offshore wind energy aiming at reducing its cost.

The cost of construction and installation of sub-structures can represent 30% of the total investment of a wind farm. Monopod bucket foundations are the object of this thesis as they could be a convenient sub-structure in various design situations.

The monopod bucket foundation could be ideal for the following reasons:

- no transition piece is needed. This would reduce the wind turbine installation time and avoid the problems related to the grouted connections of the transition piece
- the installation process, being very silent, is not dangerous for sea mammals. This might be a key feature, especially in the German sea sectors
- as opposite to monopiles, the installation process is theoretically fully reversible, meaning that the whole structure could be potentially recovered at the end of its life-time

The research presented in this thesis is dedicated to the development of tools and ideas that aim at optimizing the design of monopod bucket foundations. More specifically, geotechnical aspects regarding the skirted foundation response under environmental loading are investigated.

3.2 Brief literature review and specific objectives

The literature review extensively presented in the first paper attached to this thesis reveals that bucket foundations for oil and gas platforms have been widely investigated. In fact, the vast majority of the studies on bucket foundations addresses issues concerning the installation process and the response of the foundation under predominant axial loading.

Monotonic response of monopod bucket foundations under general loading has recently received attention in works such as Villalobos et al. (2009), Achmus et al. (2013a) and Ibsen et al. (2014). Villalobos et al. (2009) experimentally derive a yield surface for skirted foundations with embedment ratios equal to 0.5 and 1. Achmus et al. (2013a) run numerical simulations in order to extrapolate a normalised failure surface for the preliminary design of monopod bucket foundations. Ibsen et al. (2014) also derive a failure surface on the base of small-scale expeimental tests. Relatively few studies on bucket foundations cover the response of the structure under short-term cyclic combined loading. The well-established approach of Andersen (2009) estimates the settlements of shallow foundations subjected to different packages of load cycles in drained and undrained conditions. Byrne and Houlsby (2004) and Nguyen-Sy (2006) adopt the framework of hyperplasticity to model the response of bucket foundation under short-term cyclic general loading.

Offshore wind turbines supported by monopod bucket foundations have to withstands millions of load cycles during their lifetime. The estimation of the cyclic loading-induced irreversible displacements accumulated during the normal operational time of the turbine is a key element for serviceability and fatigue limit state design (DNV, 2014). The behaviour of monopod bucket foundations under lateral cyclic loading is thus of vital importance but yet not fully explored. Zhu et al. (2013) carried out a comprehensive experimental programme regarding cyclic lateral loading of a bucket foundation with embedment ratio equal to 0.5. Based on the experimental results, Zhu et al. (2013) calibrates the empirical framework proposed by LeBlanc et al. (2010) and define also how stiffness and displacement components change with the number of cycles. By means of the stiffness degradation method (Achmus et al., 2009), Achmus et al. (2013b) analyse the cyclic response of bucket foundations. The numerical simulations indicate an influence of the skirt length on the cyclic response and also an effect of the load magnitude on the rate of accumulation.

This doctoral project deals primarily with investigations on the long-term response of skirted foundations for monopod sub-structures under cyclic loading. Preparatory topics such as bucket foundations subjected to monotonic loading and transient loading, are also explored. According to the bibliographic research, the effect of embedment ratio on the cyclic lateral response has not been explored with a physical model. Besides, an all-embracing macro-model capable of describing monotonic and

long-term cyclic response of bucket foundations for offshore wind turbines has not been developed. On the basis of these observations, the specific objectives of this thesis are:

- to create a comprehensive database of small-scale cyclic loading tests of bucket foundations with different embedment ratios under monotonic and cyclic lateral loading
- to give an empirical interpretation of the experimental data aiming at extending the empirical model proposed by Zhu et al. (2013) to buckets with different embedment ratios in dense sand
- to refine the data interpretation by developing a more sophisticated analytical model. In particular, it is attempted to integrate the cyclic loading behaviour within the framework of macro-element models based on the theory of elasto-plasticity

CHAPTER 4

Description of the research project

The research content of this thesis is included in five scientific papers. The five papers have basically two common topics: geotechnical physical modelling and behaviour of bucket foundations. This chapter outlines the content of the scientific documents describing premises, objectives and methodologies adopted. Besides, the connections between the five contributions are highlighted.

4.1 Paper I - Bucket foundations: a literature review

Skirted foundations have been used for oil and gas platforms since the early eighties (Hogervost, 1980). A great deal of studies on installation and bearing capacity of these structures is available in literature. The first enclosed paper is an internal report dealing with the state of the art of bearing capacity and installation of bucket foundations. In addition to a review on previous studies, the paper contains a number of comparisons between models found in literature and novel experimental data collected during the doctoral project. The objectives of this paper are:

- to have a background knowledge on shallow foundations and to identify the research area that still needs to be explored
- to check the quality of some experimental results by comparing the test data with models existing in literature
- to provide an up-to-date list of essential scientific documents on shallow foundations and bucket foundations

The report starts with the analysis of shallow footings and shows a comparison between the best-known methods to evaluate the bearing capacity. The analysis is then extended to skirted foundations and the result of two physical experiments is interpreted with three different models. A section of the report is entirely dedicated to a close examination of the interaction diagrams of flat footings and skirted foundations. A number of experimental points are plotted together with the relevant interaction diagrams present in literature. The pushing penetration mechanism of bucket foundations is analysed and three analytical models are used to interpret the experimental results. Two sections of Paper I gather a list of recommended readings concerning bucket foundations for offshore wind turbines and oil and gas platforms.

4.2 Paper II - A preliminary study on bucket foundations under transient lateral loading

The second scientific document is a corrected version of the conference article Foglia et al. (2013). In the course of the doctoral project, a mistake regarding the interpretation of the pore pressure distribution was found in Foglia et al. (2013). In the revised version of the article enclosed here, the pore pressure interpretation is corrected and the part of the conclusions related to that is changed accordingly.

One of the design drivers of monopod bucket foundations for offshore wind turbines is the drained response of the foundation. However, when the structure is hit by extreme or rare events such as freak waves or emergency stop of the rotor, the suction caused by the high loading rate of these actions induces an enhancement in bearing capacity. This aspect is not taken into account by the current standards. Paper II deals with the physical modelling of bucket foundations under transient loading. A short experimental campaign including eight tests on two different buckets is presented with the following objectives:

- to understand which loading rate causes transient loading on small-scale bucket foundations
- to obtain information on the pore pressure distribution under and around a bucket foundation subjected to transient loading
- to gain insight into bearing capacity and displacement patterns of bucket foundations in partially drained conditions

The physical model is described and the experimental programme is presented. A preliminary interpretation of the results in terms of load-displacement curves, displacement trajectories and pore pressure distribution is attempted. The information regarding the loading rate effects were taken into consideration when designing the experimental campaign presented in the third paper.

It should be mentioned that the author did not perform the experimental tests. The contribution of the author to this paper is to be found in the physical model design and in the presentation and interpretation of the experimental observations.

4.3 Paper III - Monopod bucket foundations under cyclic lateral loading

Understanding the response of offshore foundations under long-term lateral cyclic loading is necessary to ensure that serviceability and fatigue limit states are not breached during the lifetime of the structure. The dangerous effects that must be prevented are drastic changes in the natural frequency of the system and the accumulation of significant irreversible displacements. A practical empirical model to estimate the long-term plastic rotation of monopiles was proposed by LeBlanc et al. (2010). The model was then calibrated for bucket foundations in loose sand by Zhu et al. (2013).

In the third paper attached to this thesis, the issue of bucket foundations under lateral cyclic loading is dealt with. The document includes the bulk of the experimental campaign conducted during the doctoral project. The experimental programme presented comprises 7 tests series, for a total number of 33 tests of bucket foundations under monotonic and cyclic loading. The experimental data is interpreted with the following aims:

- to calibrate the empirical model of LeBlanc et al. (2010) for bucket foundations in dense saturated sand
- to understand how the long-term displacement accumulation is affected by embedment ratio, relative density and loading frequency
- to investigate the post-cyclic monotonic response of bucket foundations

After presenting the problem and the attempted solutions, the attention is focussed on the physical model design. In the latter section the theoretical design of the modelling is thoroughly described and details on the experimental programme and on the test setup are given. The calibration of the empirical model for bucket foundations with three different embedment ratios in very dense silica sand is then accomplished on the base of the experimental post-processed data. The last section of the paper describes a real design situation in which the empirical model is used together with a finite element simulation to preliminary estimate the long-term accumulated rotation.

4.4 Paper IV - Investigations on macro-element modelling of bucket foundations for offshore wind turbines

The interpretation of the experimental data proposed in Paper III is merely empirical and may not be sufficient to model complex soil-foundation-superstructure interaction problems. The fourth paper covers a more sophisticated interpretation of the experimental results based on the macro-element approach. As elucidated in Wood (2012), macro-element models can reveal behavioural patterns of non-linear geotechnical problems. Well-established macro-elements for shallow and embedded footings for oil and gas facilities exist in literature and are used by industry practice (Zhang et al., 2014; Houlsby and Cassidy, 2002). Much more limited are the studies on cyclic behaviour of shallow foundations for offshore wind turbines (Nguyen-Sy, 2006). The main objective of this work is to create a macro-element model capable to reproduce the experimental monotonic and cyclic behavioural patterns of bucket foundations for offshore wind turbines.

The first chapter includes a literature review of macro-models for shallow foundations. In the following chapter the physical experiments used to calibrate and validate the model are reported. Then, all the components of the macro-model are presented and their validity discussed. The macro-model is finally implemented in a Matlab script and comparisons between experimental data and analytical model are shown.

4.5 Paper V - Laboratory experiments of bucket foundations under cyclic loading

Long-term cyclic loading experimental tests of monopod bucket foundations are very rare in the literature (Zhu et al., 2013). Paper V is an internal report which describes in detail all the procedures that have been necessary to carry through the experimental program. The entire experimental programme is listed with the main features of each test. The most important plots are shown and information on how to handle the raw data is given. The objectives of this document are:

- to give practical and detailed information on the physical model used in order to enable future researchers to perform analogous experiments
- to establish a database of experiments of bucket foundations for offshore wind turbines against which various models could be calibrated and validated

CHAPTER 5

Conclusions

To optimise the design of monopod bucket foundations, issues concerning their response under cyclic loading must be addressed. In the five scientific papers included in this thesis, the behaviour of bucket foundations under lateral cyclic loading and other related topics, are explored. This chapter contains the conclusions of each paper and some recommendations for future research. No conclusion is drawn about the fifth paper since it is merely illustrative and descriptive.

5.1 Paper I - Bucket foundations: a literature review

The bibliographic research reveals that bucket foundations have been studied for over fifty years as optimum solutions for offshore structures. The installation procedure seems to be by now well-established and its reliability has been proven in many real-scale projects and in various soils. However, an interesting remark is that large-scale tests and real-scale monitoring of the bucket bearing capacity were mostly performed on suction anchors and on multiple bucket foundations.

Using the standard DNV (2014) to estimate the bearing capacity of flat footings under pure vertical loading could be very conservative. Perhaps, the ultimate bearing capacity of flat footings should be estimated with more innovative methods such as the method of characteristics (Martin, 2003).

Considering now the bearing capacity of skirted foundations under combined loading, it seems that the failure envelopes of standard methods and those of more innovative methods (experimentally derived interaction diagrams) give the same capacity in the region of the load space relevant for offshore wind turbines. Interaction diagrams

though, should not be underestimated since they can better model the soil-structure non-linearity.

An experimentally derived interaction diagram evaluated with a reasonable value of the friction angle appears to be in agreement with the preliminary design tool developed by Achmus et al. (2013a).

A reassuring finding is that the novel experimental tests of installation and bearing capacity of bucket foundations, are successfully compared with the methods suggested in literature.

5.2 Paper II - A preliminary study on bucket foundations under transient lateral loading

The foundations tested were instrumented with multiple pore pressure transducers around and inside the bucket. The physical model results may be valuable to calibrate numerical simulations of the pore pressure distribution of bucket foundations subjected to rapid lateral loading. In addition, the information on the development of the pore pressure was necessary to design the experimental campaign on cyclic loading presented in Papers III and V.

The analysis of the displacement trajectory demonstrates that the vertical displacement is greatly influenced by the loading rate whereas the horizontal and the rotational displacements are not.

As expected, a high loading rate leads to an increased bearing capacity and consequent reduction of the vertical displacement. However, the data indicates that the effect becomes significant only when a very large displacement (exceeding the serviceability limit state) is mobilised. Indeed, the initial stiffness and the initial vertical displacement trajectory are not affected by the loading rate. This discovery, which was already pointed out by various authors, corroborates the idea that the undrained capacity can be considered only when designing the foundation with respect to rare and extreme events.

The measurements performed with the laboratory rig can be considered entirely reliable. However, the actuator showed limited capacity when dealing with high loads to be exerted in a very short time. This finding led to substantial modifications and improvements of the experimental rig.

5.3 Paper III - Monopod bucket foundations under cyclic lateral loading

Three monotonic lateral loading tests of bucket foundations with embedment ratios 1, 0.75 and 0.5, show different failure mechanisms. Even though the soil samples were very dense, only the bucket with embedment ratio equal to 1 shows a pronounced softening branch after the loading peak. This kind of behaviour could be seen in analogy with the findings of Vesić (1973) for shallow foundations under pure vertical loading.

One of the test series was designed to investigate the rate of rotation accumulation as a function of increasing load magnitude. From these tests it can be observed that plastic adaptation (*i.e.* accumulation rate of the rotational displacement tending to 0) occurred within the first 300-400 cycles, even for high load magnitudes.

The examination of the post-cyclic monotonic tests disclosed an interesting trend. The ultimate capacity becomes greater than that of a standard monotonic test, as though the failure surface would expand during the cyclic loading phase. This effect is attributed to the soil densification occurring during the cyclic loading phase. Perhaps more trivially, the initial stiffness of the post-cyclic tests was also found greater than the monotonic one. One test series deals with tests having the same loading configuration but different loading frequency (within 0.025 and 0.1 Hz). Since the sand sample was water saturated a marked difference in displacement patter among the tests was expected to be observed. Nonetheless, the experiments do not show any marked and consistent difference.

All the tests under a certain value of load magnitude are found to be in substantially drained conditions. These tests are employed to calibrate the empirical framework of LeBlanc et al. (2010) for bucket foundations in dense saturated sand. As already pointed out by previous authors, the relative density of the material affects the model parameters. More importantly, the calibration of the empirical method revealed that the three foundations tested respond equally to cyclic loading. The method though remains small-scale based, and thus applicable to real cases only with strict engineering judgement.

5.4 Paper IV - Investigations on macro-element modelling of bucket foundations for offshore wind turbines

A macro-element model capable to represent the experimental results of a bucket foundation under monotonic and cyclic lateral loading is derived.

A yield surface, originally thought for shallow footings (Nova and Montrasio, 1991), is modified to account for the presence of the skirt. For loading paths relevant to offshore wind turbines, the surface shows to be in good agreement with another yield surface derived for bucket foundations. The yield surface at failure (failure surface) is calibrated against eight monotonic tests with five different eccentricity over diameter ratios. Two (out of four) parameters of the hardening rule are extrapolated from a pure vertical load test until failure. One (out of two) parameter of the plastic potential and another parameter of the hardening law are obtained by using the displacement trajectory of a monotonic test with negligible horizontal load. The remaining two parameters are estimated by trial and error against the experimental results. Load-displacement curves and displacement trajectories of experimental tests and analytical simulations are compared. The comparison is fairly successful except for the horizontal displacement of two tests which is underestimated by the model by a factor 2.

To incorporate the modelling of the cyclic loading response, the boundary surface model of di Prisco et al. (2003) is simplified and integrated in the flow rule of the monotonic macro-model. The additional parameters required are calibrated by trial and error against four cyclic loading tests. The cyclic macro-element model shows a good prediction ability with respect to the long-term normalised accumulated rotation of the foundation. The results shown in the paper enhance confidence in using macro-element models for monopod bucket foundations supporting offshore wind turbines.

5.5 Future work

The experimental observations and the tools presented in this thesis are meant to be a step forward in the understanding and modelling of skirted foundations under long-term cyclic lateral loading. Some future research directions are suggested below.

The analysis of the long-term behaviour of bucket foundations concerned only accumulated displacement and post-cyclic response. Dynamic properties such as stiffness and hysteresis loops should also be investigated on the base of the experimental results.

The experimental tests were proven to be in substantially drained conditions. However, it is of interest to explore other drainage conditions by using a less permeable material or by increasing the loading frequency. It is then suggested that future long-term analysis should be carried out with different materials and with an instrumentation capable of trustfully measuring the pore pressure development during cyclic loading.

As already mentioned, all the loading conditions considered in this thesis are planar

(moment, horizontal load and vertical load acting in the same plane). More realistic response could be obtained by increasing the degrees of freedom of the system. Besides, more sophisticated investigations should include multidirectional and multi-magnitudes packages of loading.

Small-scale experiments in single gravity can give broad indications on general pattern of response of geotechnical structures. The direct implications of $1g$ tests to real-scale foundations are indeed very limited. To gain more insight into geotechnical problems, the findings of small-scale experiments should be corroborated with centrifuge tests, with numerical simulations and ultimately with large-scale tests.

The results achieved with the macro-model presented are promising. Nevertheless, seven new parameters are necessary for the boundary surface model definition. To understand the real meaning of each parameter a sensitivity analysis of the cyclic parameters should be performed. Furthermore, this would help to deepen the knowledge of the model and perhaps to elaborate a systematic strategy with which the cyclic parameters could be calibrated over a reasonable number of tests.

Bibliography

4C Offshore (2014). Global Offshore Wind Farms Database. Retrieved from the website *www.4coffshore.com*

Achmus, M., Kuo, Y.-S. and Abdel-Rahman, K. (2009). Behavior of monopile foundations under cyclic lateral load. *Computer and Geotechnics* 36, No. 5, 725-735

Achmus, M., Akdag, C. T. and Thieken, K. (2013a). Load-bearing behavior of suction bucket foundations in sand. *Applied Ocean Research* 43, 157-165

Achmus, M., Thieken, K., Akdag, C. T., Schröder, C. and Spohn, C. (2013b). Load bearing capacity of bucket foundations in sand. In *Proceeding of the 3rd International Symposium on Computational Geomechanics (ComGeoIII), Krakov*, 586-597

Andersen, K. H. (2009). Bearing capacity under cyclic loading - offshore, along the coast, and on land. The 21st Bjerrum Lecture presented in Oslo, 23 November 2007. *Canadian Geotechnical Journal* 46, No. 5, 513-535

BSH (2013).*Offshore Wind Farms Measuring Specification for the Quantitative - Determination of the Effectiveness of Noise Control Systems*. Bundesamt für Seeschifffahrt und Hydrographie

Bye, A., Erbrich, C., Rognlien, B. and Tjelta, T. I. (1995). Geotechnical design of bucket foundations. *Proc. of Offshore Technology Conference (OTC), Houston*, paper 7793

Byrne, B. W. and Houlsby, G. T. (2004). Experimental investigations of the response of suction caissons to transient combined loading. *Journal of Geotechnical and Geoenvironmental Engineering* 130, No. 3, 240-253

Clukey, E. C., Morrison, M. J., Garnier, J. and Corté, J. F. (1995). The response of suction caissons in normally consolidated clays to cyclic TLP loading conditions. *Offshore Technology Conference (OTC), Houston*, paper 7796

di Prisco, C., Nova, R. and Sibilia, A. (2003). Shallow footings under cyclic loading: experimental behaviour and constitutive modeling. In *Geotechnical analysis of seismic vulnerability of historical monuments*, Maugeri M. and Nova R. (Eds). Patron, Bologna

DNV (2014). *Design of Offshore Wind Turbine Structures*. Det Norske Veritas, offshore standard DNV-OS-J101

EWEA (2013). *Deep water - The next step for offshore wind energy*. The European Wind Energy Association

EWEA (2014). *Wind in power - 2013 European statistics*. The European Wind Energy Association

Foglia, A., Ibsen, L.B., Nielsen, S.K. and Mikalauskas, L. (2013). A Preliminary Study on Bucket Foundations under Transient Lateral Loading. In *Proceeding of the Twenty-third International Offshore and Polar Engineering (ISOPE), Anchorage*

Haigh, S. K. (2014). Foundations for offshore wind turbines. In *Proceedings of the 8th International Conference of Physical Modelling in Geotechnics (ISFOG), Perth*, Gaudin C. and White D. J. (Eds). CRC Press

Hautmann, D. (2013). Profound progress. *New Energy* 3, May 2013

Hogervost, J. R. (1980). Field trials with large diameter suction piles. *Offshore Technology Conference (OTC), Houston*, paper 3817

Houlsby, G. T. and Cassidy, M. J. (2002). A plasticity model for the behaviour of footings on sand under combined loading. *Géotechnique* 52, No. 2, 117-129

Ibsen, L. B. (2008). Implementation of a new foundations concept for offshore wind farms. Keynote of the *Nordic Geotechnical Meeting (NGM), Copenaghen*

Kirkwood, P. B. and Haigh, S. K. (2014). Centrifuge testing of monopiles subject to cyclic lateral loading. In *Proceedings of the 8th International Conference of Physical Modelling in Geotechnics (ISFOG), Perth*, Gaudin C. and White D. J. (Eds). CRC Press

Klinkvort, R. T. and Hededal, O. (2013). Lateral response of monopile supporting an offshore wind turbine. *Geotechnical Engineering* 166, No. 2, 147-158

Jardine, R., Puech, A. and Andersen, K. H. (2012). Cyclic loading of offshore piles: potential effects and practical design. In *Proceedings of the 7th International Conference of Offshore Site Investigation and Geotechnics (OSIG): Integrated Geotechnologies, London*

LeBlanc, C. (2009). *Design of Offshore Wind Turbine Support Structures*. Ph.D. thesis, Aalborg University

LeBlanc, C., Byrne, B. W. and Houlsby, G. T. (2010). Response of stiff piles in sand to long-term cyclic lateral loading. *Géotechnique* 60, No. 2, 79-90

LeBlanc, C., Lingaard, M. A., Shajarati, A., Kallehave, D. and Gretlund, J. S. (2013). Vibro-driving of monopiles - experience from Anholt Offshore Wind Farm. Presentation at *Offshore EWEA 2013, Amsterdam*

Lesny, K. (2011). *Foundations for Offshore Wind Turbines - Tools for Planning and Design*. VGE Verlag GmbH

Ibsen, L. B., Larsen, K. A. and Barari, A. (2014). Calibration of Failure Criteria for Bucket Foundations on Drained Sand under General Loading. *Journal of Geotechnical and Geoenvironmental Engineering* 140, No. 7

MacKay, D. J. C. (2009). *Sustainable energy - without the hot air*. UIT Cambridge Ltd

Martin, C. M. (2003). *User guide for ABC - Analysis of Bearing Capacity*. Report No. OUEL 2261/03, Department of Engineering Science, Oxford University

Nguyen-Sy, L. (2006). *The theoretical modelling of circular shallow foundations for offshore wind turbines*. Ph.D. thesis, Oxford University

Nova, R. and Montrasio, L. (1991). Settlements of shallow foundations on sand. *Géotechnique* 41, No. 2, 243-256

Randolph, M. F. and Gourvenec, S. (2011). *Offshore geotechnical engineering*. Spon press

Reimann, K., Schwarz, M. and Grabe, J. (2013). Acoustic emisssions due to offshore piling - field measurements at an offshore wind energy construction site. *In Proceedings of the 23rd International Ocean and Polar Engineering Conference (ISOPE), Anchorage*

Seidel, M. (2014). Substructures for offshore wind turbines - Current trends and developments. In *Festschrift Peter Schaumann, Hannover*

Vesić, A. S. (1973). *Analysis of Ultimate Loads of Shallow Foundations. JSMFD*, ASCE 99, 45-73

Villalobos, F. A., Byrne, B. W. and Houlsby, G. T. (2009). An experimental study of the drained capacity of suction caisson foundations under monotonic loading for offshore applications. *Soils and Foundations* 49, No. 3, 477-488

Wood, D. M. (2012). Macroelement Modelling. In *Mechanical Behaviour of Soils under Environmentally Induced Cyclic Loads*, di Prisco C. and Wood D. M. (Eds), CISM, Udine

Zhang, Y., Cassidy, M. J., Bienen, B (2014). A plasticity model for spudcan foundations in soft clay. *Canadian Geotechnical Journal* 51, 629-646

Zhu, B., Byrne, B. W. and Houlsby, G. T. (2013). Long-term lateral cyclic response of suction caisson foundations in sand. *Journal of Geotechnical and Geoenvironmental Engineering* 139, No. 1, 73-83

Enclosed scientific papers

Paper I

Foglia, A. and Ibsen, L. B. (2014). *Bucket foundations: a literature review.* DCE Technical Report No. 176, Department of Civil Engineering, Aalborg University

Paper II

Foglia, A., Ibsen, L. B., Nielsen, S. K. and Mikalauskas, L. (2013). *A preliminary study on bucket foundations under transient lateral loading.* In *Proceedings of the International Ocean and Polar Engineering Conference (ISOPE), Anchorage.* (corrected version)

Paper III

Foglia, A. and Ibsen, L. B. (2014). *Monopod bucket foundations under cyclic lateral loading.* DCE Technical Memorandum No. 49, Department of Civil Engineering, Aalborg University. (submitted for publication to the International Journal of Physical Modelling in Geotechnics)

Paper IV

Foglia, A., Govoni, L., Gottardi, G. and Ibsen, L. B. (2014). *Investigations on macro-element modelling of bucket foundations for offshore wind turbines.* DCE Technical Memorandum No. 48, Department of Civil Engineering, Aalborg University. (submitted for publication to Applied Ocean Research)

Paper V

Foglia, A. and Ibsen, L. B. (2014). *Laboratory experiments of bucket foundations under cyclic loading.* DCE Technical Report No. 177, Department of Civil Engineering, Aalborg University

Paper I

Title:

Bucket foundations: a literature review

Authors:

Foglia, A. and Ibsen, L. B.

Year of publication:

2014

Published in:

DCE Technical Report No. 176, Department of Civil Engineering, Aalborg University

Number of pages:

37

Bucket foundations: a literature review

Aligi Foglia and Lars Bo Ibsen

Department of Civil Engineering, Aalborg University

In this report, bearing behaviour and installation of bucket foundations are reviewed. Different methods and standards are compared with the experimental data presented in Foglia and Ibsen (2014a). The most important studies on these topics are suggested. The review is focussed on the response of monopod bucket foundations supporting offshore wind turbines.

1 Introduction

Settlements and bearing capacity of shallow foundations have been studied for over one century and yet many issues are still to be addressed and resolved. This technical report covers some of the fundamental topics that were experimentally and/or theoretically explored throughout the experimental campaign conducted by Foglia and Ibsen (2014a). This literature review compares different approaches and, when relevant, the comparison is integrated with the experimental results collected in Foglia and Ibsen (2014a).

The bearing capacity of rigid flat footings is the necessary starting point to understand the response of bucket foundations under general loading. The focus is then shifted towards the bearing capacity of bucket foundations, as these are the main object of the experimental work (Foglia and Ibsen, 2014a). Two methods are used to predict the bearing capacity of the experi-

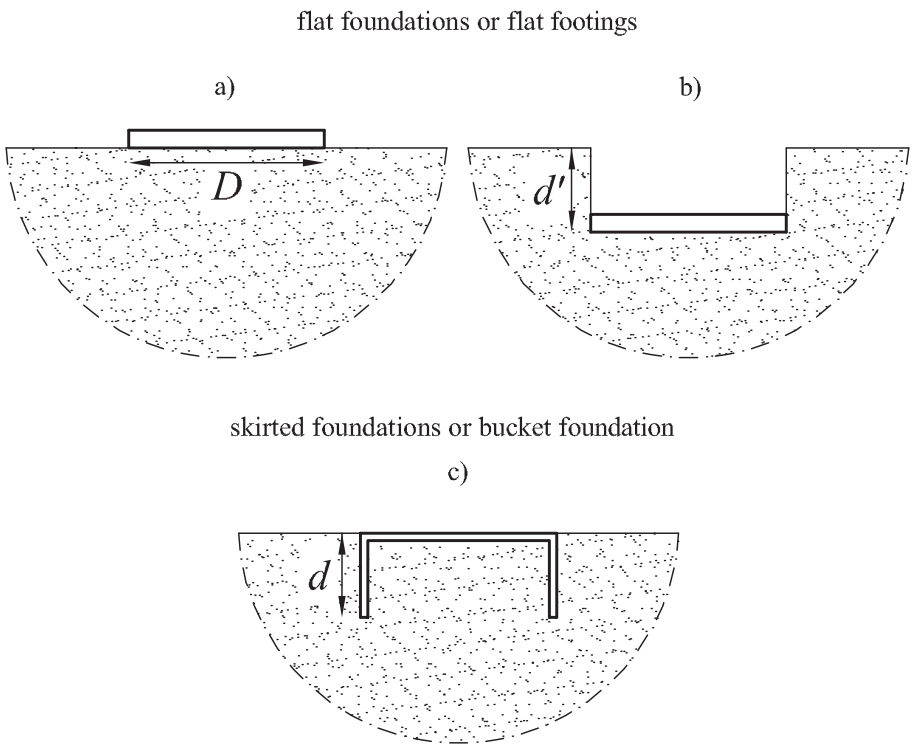

Figure 1: a) standard flat footing; b) buried or embedded footing; c) skirted foundation or bucket foundation

mental tests. Innovative and more traditional methods to evaluate the bearing capacity of bucket foundations under general loading are discussed. The installation process is described and three methods are used to interpret the jacked installation of a small-scale foundation.

Figure 1 illustrates the types of shallow foundations examined in this study. Throughout the report, the terms bucket foundation and skirted foundation are used interchangeably.

2 Bearing capacity under vertical loading

2.1 Flat footings

Shallow foundations under pure vertical loading are traditionally designed on the base of the classic bearing capacity theory proposed by Terzaghi (1943). For a flat embedded footing with

width, D, and area, $A = DL$, the bearing capacity can be expressed as:

$$q_u = \frac{V_\mathrm{u}}{A} = cN_c s_c + qN_q + 0.5\gamma' D N_\gamma s_\gamma \tag{1}$$

where N_c, N_q and N_γ are the bearing capacity factors, c is the cohesion of the material, q is the surcharge ($q = \sigma'_\mathrm{v}(d') = \gamma' d'$; where d' is the depth of excavation), γ' is the effective unit weight of the soil and s_c and s_γ are the shape factors that account for rectangular and circular shapes of the foundation. For most of the authors, the shape factors are functions of D, L, and, for some calculation methods (Brinch Hansen, 1970; Vesić, 1973), also of the friction angle, ϕ'. Circular and square footings have $D = L$ and thus their shape is considered to affect the bearing capacity in the same manner (CEN, 2004; Fang, 1991).

By multiplying q_u by the area of the foundation, the ultimate vertical load of the footing, V_u, can be obtained. In practice, equation 1, uncouples and superimposes the three terms influencing the bearing capacity. The solution proposed by Terzaghi (1943) is based on the work conducted by Prandtl (1920) who adopted the theory of plasticity to analytically solve the problem of a rigid body penetrating into a granular material. The bearing capacity factors are by definition functions of the friction angle and, after Terzaghi (1943), many authors have proposed new formulations for their estimation (Meyerhof, 1963; Brinch Hansen, 1970; Vesić, 1973). Among the authors there is general agreement about the value of the factors N_c and N_q. On the contrary, N_γ can vary significantly, especially for friction angles larger than 40° (Bowles, 1996). Meyerhof (1963) Brinch Hansen (1970) and Vesić (1973) propose also that the depth factors, d_c, d_q and d_γ, and one further shape factor, s_q, are to be included in equation 1. Though, the depth factors are not included in current standards (CEN, 2004; DNV, 2014).

More recently, Bolton and Lau (1993) and Martin (2005) have used the method of characteristics to obtain the exact value of the bearing capacity factors for strip and circular footings with rough and smooth interface. In Bolton and Lau (1993) and Martin (2005) the depth and shape factors

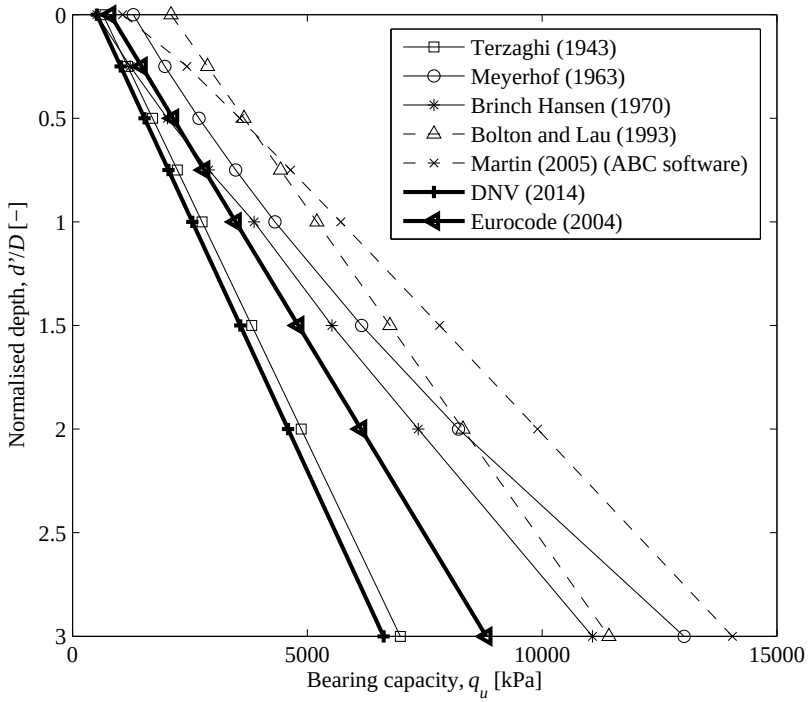

Figure 2: Estimation of the bearing capacity of a flat circular footing with seven different methods

are not evaluated since the bearing capacity factors obtained with the method of characteristics already embrace the effects of shape and depth. Exact values of the vertical bearing capacity of shallow foundations can be obtained with the software ABC developed by Martin (2003) and based on the method of characteristics. Houlsby and Martin (2003) used the same method to estimate the bearing capacity factors of spudcan foundations on clays considering the effects of embedment, roughness, strength heterogeneity and cone angle.

In Figure 2 the evaluation of the bearing capacity of a circular foundation ($D = 5$ m) on sand ($\phi' = 35°$) with seven different methods is illustrated. A rough soil-footing interface is chosen for the estimation. In Figure 2 it can be observed that the bearing capacity equation given by DNV (2014) seems to be the most conservative. Furthermore, depending on the normalised

depth, the approaches of Martin (2005) and Bolton and Lau (1993) give the largest value of q_u.

2.2 Skirted foundations

As mentioned by Villalobos (2006), when the ultimate vertical load of a bucket foundation, V_{s}, is being investigated, multiple issues emerge. For example, the soil plug inside the foundation can be assumed to be rigid or flexible. If the soil plug is assumed to act as a rigid block, the bearing capacity is calculated at the level of embedment ($d = d'$; where d is the length of the skirt):

$$\frac{V_{\mathrm{s}}}{A} = qN_q d_q s_q + 0.5\gamma' D N_\gamma d_\gamma s_\gamma \tag{2}$$

Equation 2 is written for a skirted foundation in non-cohesive soil.

Clearly, assuming rigid skirt and flexible soil plug would be more realistic. In case of pure vertical loading though, the result would not change dramatically. Conversely, in case of combined loading, Bransby and Yun (2009) showed that due to a failure mechanism inside the skirt, the capacity of skirted foundations with flexible soil plug could be significantly lower than that of solid embedded foundations. For this reason, as recommended in Randolph and Gourvenec (2011), internal skirts should be included in the bucket foundation design to ensure a non-flexible soil plug.

Another issue is related to the effect of installation on the volume of material surrounding the foundations. This aspect is discussed in Chapter 4.

The contribution of the friction on the outer surface of the skirt should also be taken into account. A straightforward estimation of the skin friction resistance, V_{f}, can be obtained by integrating a constant shear stress, τ_{o}, over the skirt length d:

$$V_{\mathrm{f}} = 2\pi R \int_0^d \tau_{\mathrm{o}} dz = \pi R \gamma' K tan(\delta) d^2 \tag{3}$$

where τ_{o} is the shear stress on the outer surface of the skirt, R is the outer radius of the bucket, K is the lateral earth pressure coefficient and δ is the interface friction angle.

In an attempt to estimate the vertical bearing capacity of bucket foundations, small-scale vertical loading tests until failure were carried out at different scales and on different sands by Villalobos (2006) and Larsen (2008). Villalobos (2006) run displacement controlled vertical loading tests of buckets with D = 50.9 mm and with seven different embedment ratios (d/D from 0 to 2), on loose and dense sand samples. As expected, he found punching shear mechanism for the loose samples and general shear mechanism for the dense samples. He interpreted his results with the bearing capacity equation:

$$V_{\mathrm{s}} = D\pi \int_0^d \tau_{\mathrm{o}} dz + A\left(qN_q + 0.5\gamma' D N_\gamma\right) \tag{4}$$

where it was assumed K = 2 and δ= 16°. N_q and N_γ were calculated for smooth interface according to Bolton and Lau (1993) and to Martin (2005), respectively. He found that by using the peak friction angle, the estimation of V_{s} overestimates the experimental results for both loose and dense sample.

Larsen (2008) carried out several vertical loading tests of buckets with diameter varying between 50 and 200 mm and four different embedment ratios (d/D from 0 to 1). Larsen (2008) calculated V_{s} as a linear function of d/D and V_{u}:

$$\frac{V_{\mathrm{s}}}{V_{\mathrm{u}}} = 1 + c\left(\frac{d}{D}\right) \tag{5}$$

Larsen (2008) estimated the parameter c as 2.9 while the bearing capacity factors for V_{u} were deducted according to Martin (2005). Equation 5 was first put forward by Byrne and Houlsby (1999) who estimated c as 0.89.

In Foglia and Ibsen (2014a) the results of two vertical loading tests until failure performed with a novel experimental rig, are presented. A detailed description of the test setup is given in Vaitkunaite et al. (2014). Two buckets with D = 300 mm were tested. One foundation had d/D = 1 (test S64) and the other had d/D = 0.75 (test S63). It is worth to emphasise that, given the dimension of the foundations tested, laboratory tests of such a kind are rare. The

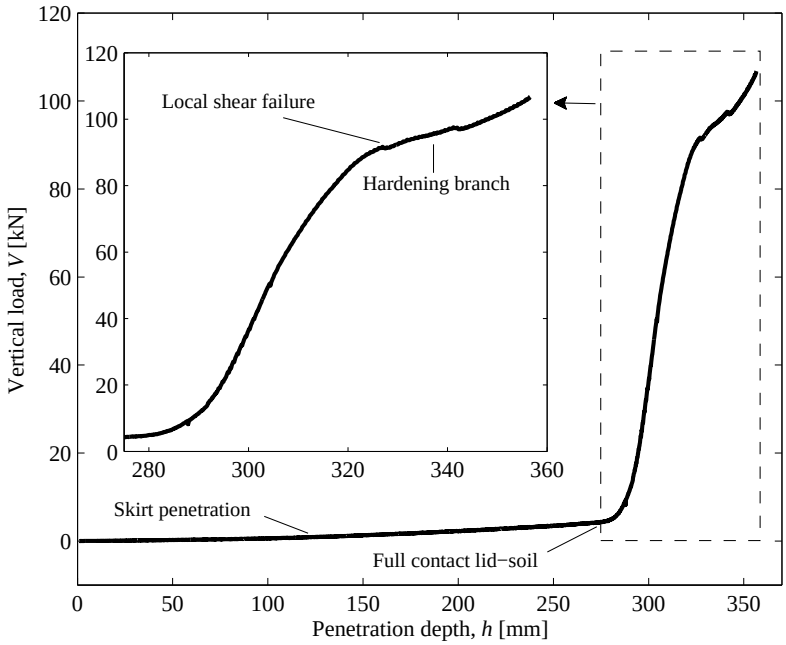

Figure 3: Installation and bearing capacity test until failure, test S64

relative density, D_r, of the sand sample was estimated with a small-scale cone penetration test as 77%. The $V - h$ curve of test S63 is shown in Figure 3, where h is the penetration depth of the foundation. In the figure, the part of the curve after the full contact lid-soil (full skirt penetration) is shown in a magnified inner plot. The entire curve can be divided in two different parts. In the first part the increase in V is due only to the skirt resistance. This part of the curve is, in reality, the jacked installation phase, which is analysed in section 4.2. Once full contact lid-soil (full skirt penetration) is established, the penetration curve has a sudden stiffness increase caused by the lid which becomes the predominant bearer. According to Vesić (1973), the soil supporting a footing under vertical load can fail following three mechanisms: general shear, local shear and punching shear. Figure 3 clearly shows that no general shear failure of the soil occurred. During the test, soil bulging was observed meaning that the soil around the foundation (unloaded soil) was visibly involved in the failure mechanism. According to this observation

a local shear failure of the soil appears to have occurred (Vesić, 1973). As already mentioned, general failure was reported by Villalobos (2006) in all the tests on dense sand ($D_r = 88\%$ and $D_r = 83\%$). This difference in failure mechanism can be attributed to the different scale of the physical models or to the discrepancy in relative density.

The ultimate bearing capacity gained with S63 and S64 is plotted in Figure 4 together with equation 4 and equation 5. The critical friction angle of the sand used in the test is reported in Larsen (2008) to be equal to $\phi_{cr} = 31°$. According to Bolton (1986) that would give a peak friction angle, ϕ_{peak}, of 39.6°. In Figure 4, it can be seen that equation 4 captures very well the bearing capacities trend with an unexpectedly high value of the friction angle, ϕ'= 45°. Equation 5, with the empirical parameter c proposed by Larsen (2008) and a friction angle close to the critical one (ϕ'= 39°), predicts the result of test S63 but overestimates the bearing capacity of test S64.

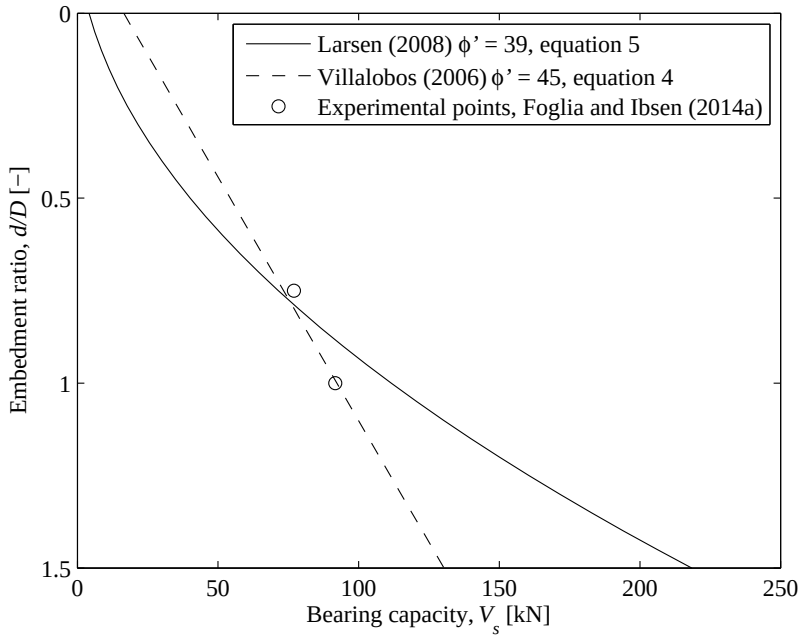

Figure 4: Bearing capacity of bucket foundations estimated with two different methods and experimental results

3 Bearing capacity under general loading

3.1 Flat footings

While most onshore foundations are characterised by predominant vertical loading, V, offshore foundations must withstand general loading with significant components of, horizontal load, H, and moment, M. Well-established design criteria for onshore foundations are not always suitable for offshore systems. For instance, the ultimate bearing capacity of shallow foundations for onshore systems is often unlikely to occur. Conversely, the ultimate bearing capacity of offshore structures (and particularly that of offshore wind turbines) could be breached owing to exceptionally large overturning moments, and cannot therefore be overlooked.

Following the classic bearing capacity theory, when a shallow foundation is subjected to general loading conditions, an array of empirically derived coefficients reduces V_{u}. For flat footings on sand under pure vertical loading, equation 1 becomes:

$$\frac{V_{\mathrm{u}}}{A} = 0.5\gamma' D N_\gamma s_\gamma \tag{6}$$

If the foundation is subjected to general loading, the effect of M is taken care of by reducing the foundation area as a function of the eccentricity induced by the overturning moment ($e = M/V$). Besides, the effect of the horizontal load is introduced through the inclination factor i_γ. As a result of that, the ultimate vertical load of flat foundations on sand under general loading is calculated as:

$$\frac{V_{\mathrm{gu}}}{A'} = 0.5\gamma' D N_\gamma s_\gamma i_\gamma \tag{7}$$

where A' is the effective foundation area calculated as a function of e. A number of authors attempted the assessment of the i_γ coefficient by using analytical and empirical methods. Gottardi (1992) conducted a detailed review of the different expressions proposed in literature. The most used coefficients in engineering practice are those of Meyerhof (1953) and Brinch Hansen

(1970). According to Meyerhof (1953) the inclination factor can be written as:

$$i_\gamma = \left(1 - \frac{\theta}{\phi'}\right)^2 \tag{8}$$

where θ is the angle of inclination of the resultant force, $\theta = arctan(H/V)$. The expression of Brinch Hansen (1970) for i_γ, does not include the friction angle and is written as:

$$i_\gamma = \left(1 - 0.7\frac{H}{V}\right)^5 \tag{9}$$

Similarly, DNV (2014) expresses i_γ as:

$$i_\gamma = \left(1 - \frac{H}{V}\right)^2 \tag{10}$$

Note that Meyerhof (1953) includes the friction angle in the definition of the inclination factor. By using these traditional approaches, the non-linearity of the geotechnical problem, which is rather significant for general loading, is simplistically considered through a superposition of different effects. To reflect properly the non-linearity of the system and consider directly the interaction between V,H and M, interaction diagrams (or failure envelopes) were conceived. Interaction diagrams encompass a region of the three-dimensional load space within which the foundation does not violate the failure criterion. Roscoe and Schofield (1956) and Butterfield and Ticof (1979) were pioneers of this technique which is used today as fundamental element for macro-models (Gottardi et al., 1999; Cremer et al., 2001; Houlsby and Cassidy, 2002; Bienen et al., 2006).

Expressions of the $H - V$ interaction from the inclination factors of Meyerhof (1953), Brinch Hansen (1970) and DNV (2014) can be simply obtained by including i_γ in the bearing capacity formula and expressing H as a function of V (Gottardi, 1992; Byrne, 2000). In Figure 5 the experimentally deduced interaction diagrams of Butterfield and Gottardi (1994) and Houlsby and Cassidy (2002) (Model C) are plotted together with the classic bearing capacity methods.

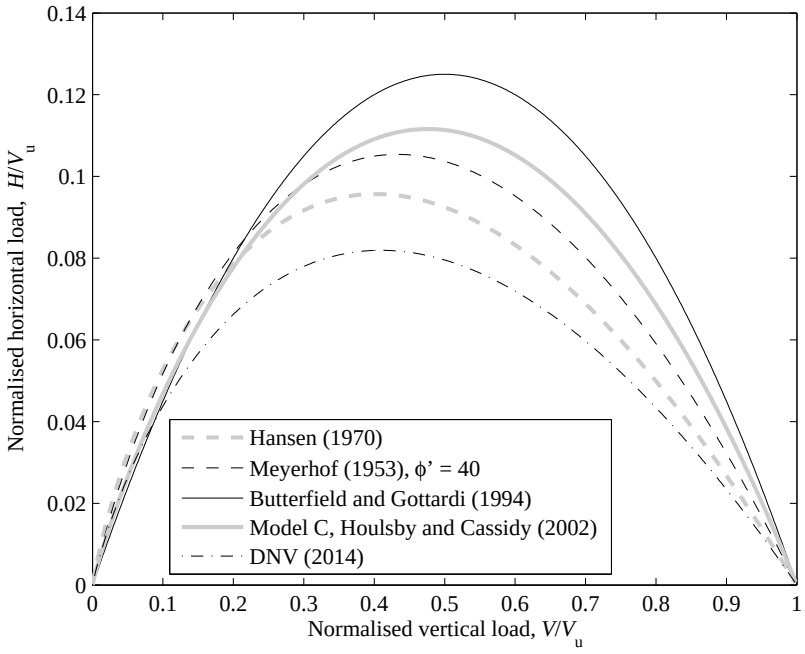

Figure 5: Comparison of different interaction diagrams for flat footings in the normalised load plane

As similarly pointed out by Byrne (2000), the classic methods of Meyerhof (1953) and Brinch Hansen (1970) are conservative for $V/V_{\mathrm{u}} > 0.3$. More importantly, the four envelopes are alike for $V/V_{\mathrm{u}} < 0.3$. Note that this is also the region of the load space relevant for offshore wind turbines. It is also worth to note that the DNV (2014) method gives the most conservative failure envelope and agrees with the other curves only for $V/V_{\mathrm{u}} < 0.1$.

Even though the interaction diagrams appear to agree with the traditional methods in the region of interest, their importance is undeniable. In fact, they form the base of macro-models and are thereby essential to model sophisticated problems regarding the interaction between soil, foundation and superstructure. An analogue plot to Figure 5 could be obtained also for M. Though, the envelopes of Meyerhof (1953), Brinch Hansen (1970) and DNV (2014) would be equal as they all use the same approach to account for the presence of M.

Failure envelopes have been lately incorporated in the API standards (API, 2011). Other well-known failure envelopes for shallow foundations are: Saleçon and Pecker (1995), for footings on clay; Martin and Houlsby (2000), for spudcan foundations on clay; Byrne and Houlsby (2001), for footings on carbonate sand; Randolph and Puzrin (2003), for circular foundations on clay (upper bound solution); Bienen et al. (2006), for footings in six degrees of freedom.

3.2 Skirted foundations

The same principle explained for flat footings is applicable to skirted foundations as well. When a skirted foundation on sand is subjected to general loading, the sustainable vertical load, V_{gs}, can be evaluated as:

$$\frac{V_{\text{gs}}}{A'} = qN_q i_q s_q d_q + 0.5\gamma' D N_\gamma i_\gamma s_\gamma d_\gamma \tag{11}$$

According to Meyerhof (1953) the inclination factor, i_q, can be written as:

$$i_q = \left(1 - \frac{\theta}{90^\circ}\right)^2 \tag{12}$$

The equation of Brinch Hansen (1970) for i_q is:

$$i_q = \left(1 - 0.5\frac{H}{V}\right)^5 \tag{13}$$

The DNV (2014) recommends that i_q is calculated according to:

$$i_q = \left(1 - \frac{H}{V}\right)^4 \tag{14}$$

Since the surcharge component increases the degree of non-linearity of the problem, closed analytical solutions for H to plot the interaction diagram for the methods of Meyerhof (1953), Brinch Hansen (1970) and DNV (2014), cannot be obtained for skirted foundations. Numerical solutions are however obtainable and these are shown in Figure 6 together with the experimentally derived failure envelope of Ibsen et al. (2014).

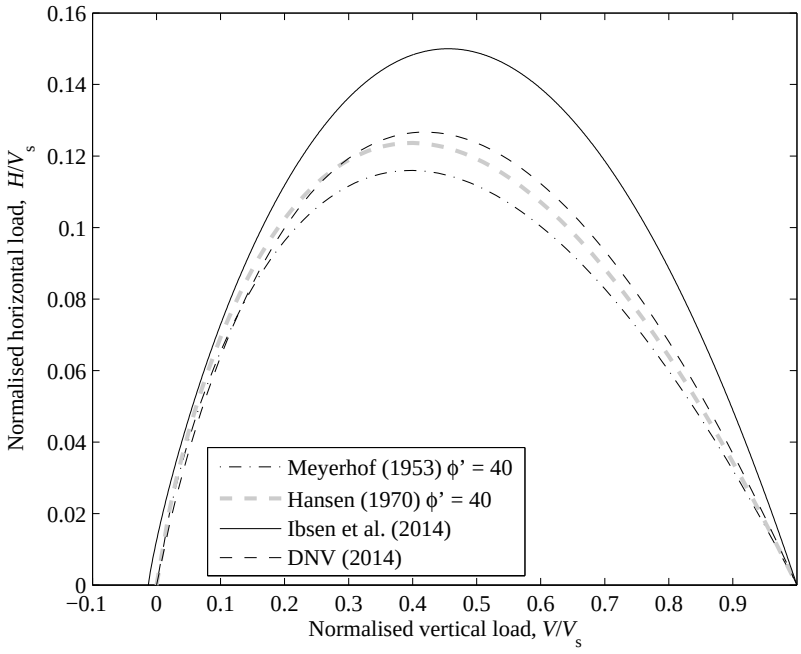

Figure 6: Comparison of different interaction diagrams for skirted foundations in the normalised load plane

A yielding surface for bucket foundations was experimentally investigated by Villalobos (2006) (see also Villalobos et al. (2009)). The ellipsoid extrapolated by Villalobos (2006) has equation:

$$f = \left(\frac{H}{V_0 h_0}\right)^2 + \left(\frac{M}{DV_0 m_0}\right)^2 - 2e_0 \frac{H}{V_0 h_0}\frac{M}{DV_0 m_0} - \beta_{12}^2 \left(\frac{V}{V_0} + t_0\right)^{2\beta_1} \left(1 - \frac{V}{V_0}\right)^{2\beta_2} \quad (15)$$

where V_0 is the preconsolidation vertical load, t_0 is the tension parameter ($t_0 = V/V_0$), h_0, m_0, e_0, β_1 and β_2 are the non-dimensional parameters and β_{12} is defined as:

$$\beta_{12} = \frac{(\beta_1 + \beta_2)^{(\beta_1+\beta_2)}}{\beta_1^{\beta_1}\beta_2^{\beta_2}(t_0+1)^{(\beta_1+\beta_2)}} \quad (16)$$

Ibsen et al. (2014) (see also Larsen, 2008) proposed a failure envelope on the base of the yielding surface of Villalobos (2006). The failure envelope of Ibsen et al. (2014) has the form of equation 15 but with V_s instead of V_0. In this report we are interested in the ultimate resistance of the foundation and the envelope proposed by Ibsen et al. (2014) is therefore used.

Note that, in the legend of Figure 6, the friction angle is indicated also for Brinch Hansen (1970). This is because the d_γ proposed by Brinch Hansen (1970) depends on ϕ'. Instead, as mentioned earlier, depth factors are not included in the formulation of DNV (2014). In Figure 6 it is seen that, for skirted foundations, the three classic bearing capacity approaches give a rather similar representation of the failure load. In a similar fashion to flat footings, the failure envelope derived experimentally gives the largest prediction of bearing capacity. As in Figure 5, in the relevant region for offshore wind turbines, all the methods predict a similar bearing capacity. The classic methods seem to be particularly conservative for $0.3 < V/V_\mathrm{s} < 0.9$.

Eight monotonic tests until failure of a bucket foundation with $d/D = 1$ and $D = 300$ mm, are presented in Foglia et al. (2014). The tests were conducted with $V/V_\mathrm{s} = 0.0026$ and with five different $M/(HD)$ ratios. The failure points of this test series are represented in Figure 7 together with the interaction diagram of Ibsen et al. (2014).

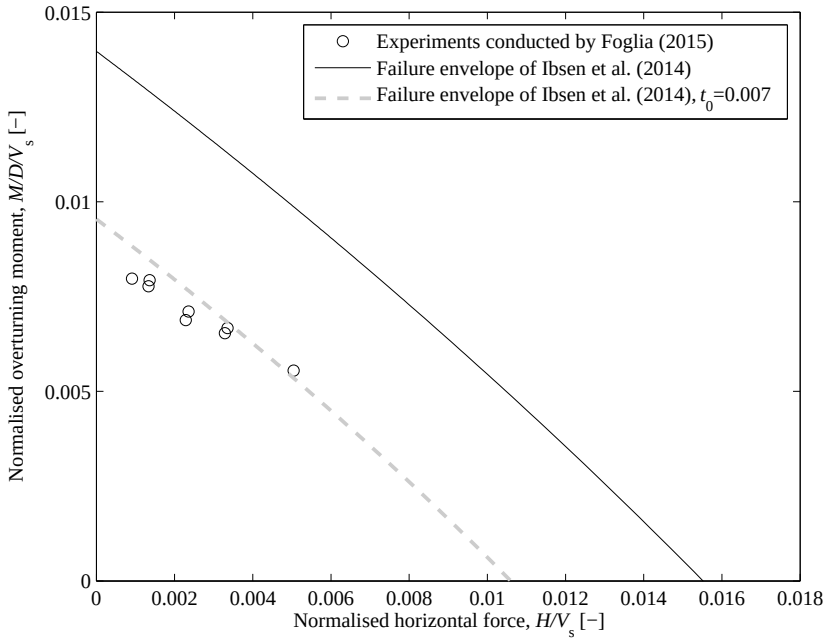

Figure 7: Experimental results of a bucket foundation $(d/D = 1)$ against the original and the modified interaction diagram of Ibsen et al. (2014)

The experimental points are overestimated by the failure envelope. This is attributed to the fact that the failure envelope of Ibsen et al. (2014) was calibrated only over tests with $V/V_{\mathrm{s}} = 0.5$. As shown in Foglia et al. (2014), by setting $t_0 = 0.007$ the curve matches well the experimental results. The choice of adapting the failure surface by changing $t_0 = 0.007$ is not randomly made. t_0 is in fact a rather straightforward parameter to be evaluated as explained in Foglia et al. (2014).

Recently, another interaction diagram on the ($M - H$) load plane has been numerically derived in Achmus et al. (2013a). The numerical simulations were calibrated against large scale tests. According to Achmus et al. (2013a) the normalised ultimate horizontal load in very dense sand can be expressed by:

$$\left(\frac{H_{\mathrm{u}}}{\gamma' d^2 D}\right) = -0.011 \left(\frac{d}{d_{\mathrm{ref}}}\right) (M'_{\mathrm{u}})^2 - 0.43 \left(\frac{d}{d_{\mathrm{ref}}}\right)^{0.2} M'_{\mathrm{u}} + 14.1 \left(\frac{d_{\mathrm{ref}}}{d}\right)^{0.6} \tag{17}$$

where d_{ref} is a reference embedment length equal to 1 m and M'_{u} is expressed by:

$$M'_{\mathrm{u}} = \left(\frac{M_{\mathrm{u}}}{\gamma' d^3 D}\right) \left(\frac{d}{d_{ref}}\right)^{0.8} \tag{18}$$

In a similar way, H'_u is defined as:

$$H'_{\mathrm{u}} = \left(\frac{H_{\mathrm{u}}}{\gamma' d^2 D}\right) \left(\frac{d}{d_{ref}}\right)^{0.6} \tag{19}$$

The failure envelope expressed by equations 17-19 can be compared with the envelope of Ibsen et al. (2014). In order to obtain M'_{u} and H'_{u} values from the failure criteria of Ibsen et al. (2014), it is necessary to estimate the vertical bearing capacity of the bucket foundation, V_{s}. The foundation considered for the calculation has $D = 16$ m, $d = 12$ m and is subjected to $V = 20$ MN. V_{s} is calculated with the software ABC in a non-cohesive soil with $\gamma' = 10$ kN/m and for three values of the friction angle. The comparison is shown in Figure 8.

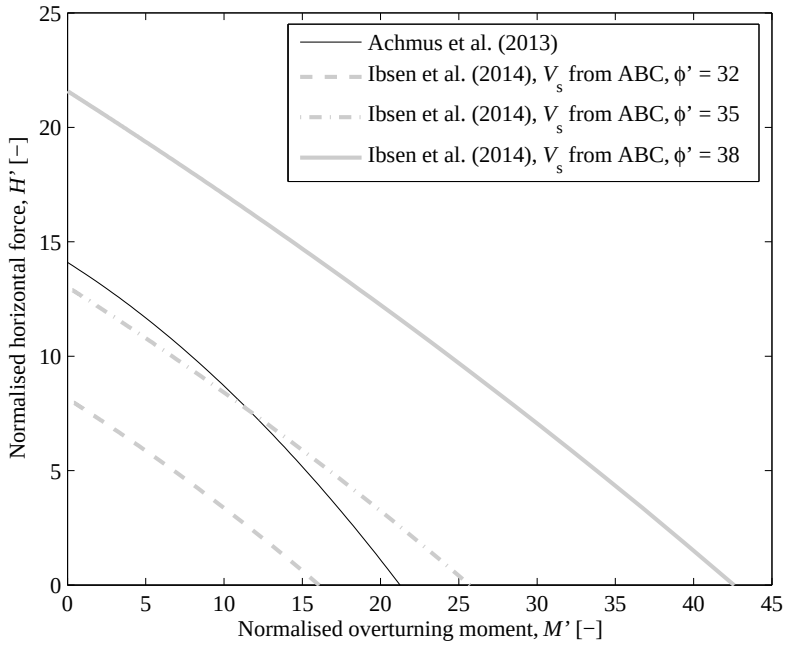

Figure 8: Interaction diagrams of Ibsen et al. (2014) against failure criteria of Achmus et al. (2013a)

Note that the axes of Figure 8 are H' and M'. These are defined as equations 18 and 19 but with H and M instead of H_{u} and M_{u}. The curves shown in Figure 8 from Ibsen et al. (2014) are quite influenced by the choice of V and by the type of soil. In spite of this, it is remarkable that for $\phi' = 35°$ the two methods give similar predictions.

Beside the failure envelope, Achmus et al. (2013a) formulated an expression for the initial stiffness. Furthermore, the numerical simulations revealed an interesting feature of the bearing behaviour: when a bucket foundation approaches failure, a gap between lid and soil occurs. This detachment between soil and structure induces the skirt to bear all the load. The latter information is crucial and would technically implicate that the traditional bearing capacity methods are inadequate instruments to evaluate the capacity of bucket foundations under predominant general loading. Nevertheless, from Figure 6 it is clear that these methods give a fairly similar

result to small-scale experiments.

3.3 Additional literature

Failure envelopes Other failure envelopes for skirted foundation can be found in: Mangal (1999), exploration of the foundation behaviour in partially drained conditions; Bransby and Randolph (1998), Bransby and Yun (2009), Gourvenec (2007) and Gourvenec and Barnett (2011), investigation on combined loading of bucket foundations in undrained condition with numerical and analytical methods; Cassidy et al. (2006), development of a plasticity model for skirted foundations in clay.

Monopod bucket foundations for offshore wind turbines Since the monopod bucket foundation has been considered a cost-competitive option for offshore wind turbine sub-structures (Ibsen, 2008), great attention has been given to the cyclic lateral response of skirted foundations. The main publications on this topic are: Kelly et al. (2006), field tests compared with $1g$ laboratory tests; Achmus et al. (2013b), numerical simulations; Zhu et al. (2013) and Foglia and Ibsen (2014b), $1g$ physical models. Interesting are also the contour diagrams for suction bucket under lateral loading foundations in silt extrapolated by Watson and Randolph (2006) on the base of centrifuge experiments.

Tensile capacity, offshore wind turbines Jacket sub-structures supporting offshore wind turbines can be founded on driven piles or bucket foundations. The load transferred to the foundations is in this case axial, in tension and compression. Bucket foundations for jacket sub-structures have been widely investigated. Feld (2001) performed small-scale $1g$ tensile loading tests with different loading rates. These tests were compared to numerical models and a simple analytical model. The tensile capacity was found to be greatly influenced by the loading rate. Byrne and Houlsby (2002) undertook $1g$ cyclic and monotonic tensile loading tests. To model

the appropriate drainage time, a viscous pore fluid was chosen to saturate the soil sample. The experiments revealed that the rate-dependency becomes significant only at large displacements. Centrifuge tests exploring monotonic and cyclic uplift of bucket foundations were carried out by Senders (2008) who also developed a theoretical model to calculate the pull-out resistance. Interestingly, he observed that unless the cyclic magnitude exceeds the frictional resistance, cyclic degradation does not occur. Very recently, Thieken et al. (2014) have reported a number of numerical simulations of bucket foundations under transient tensile loading. In terms of rate-dependency and sustained loading (equivalent to cyclic loading in this case), the simulations corroborated what was found experimentally by previous studies. Thieken et al. (2014) also found that, as opposite to the drained up-lift capacity (frictional resistance), lid and skirt are equally involved in the partially undrained resistance. Pullout field tests on clay and on sand are respectively presented in Houlsby et al. (2005) and Houlsby et al. (2006).

Bucket foundations for oil and gas platforms Bucket foundations have been mostly used as foundations for jacket structures supporting oil and gas platforms or as anchoring systems for tension leg platforms or floating platforms. Bucket foundations for floating platforms and tension leg platforms are often named suction anchors as their embedment length is larger than the diameter.

According to the type of sub-structure or mooring system (jacket, catenary, taut line) the foundations are subjected to different loading conditions. For jackets and for mooring systems in vertical configuration, the tensile loading governs the foundation design. Experimental tests on tensile loading were overtaken for example by: Wang et al. (1977), breakout capacity in three different soils; Steensen-Bach (1992), monotonic loading in clay and sand; Andersen et al. (1992), pull-out capacity method based on laboratory tests and validated against field tests; Clukey et al. (1995), centrifuge study on monotonic and static tensile resistance in clay; Whittle

et al. (1998), static and sustained loading in clay; El-Gharbawy and Olson (1998), monotonic and cyclic loading in clay.

When floating platforms are connected to the seabed through taut lines, the suction anchor is subjected to combined horizontal load and vertical load in tension. Instead, in case catenary moorings are adopted, the suction anchors have to withstand horizontal load only. Early studies on these issues are Hogervost (1980) and Larsen (1989). More recently, Andersen et al. (2005) wrote a compendium on design and analysis of suction anchors in clay. Supachawarote et al. (2004) run numerical simulations of suction anchors in clay deriving the failure envelope in the $(V - H)$ load plane identifying the optimum load attachment position.

The knowledge contained in these papers will perhaps turn out to be valuable when designing anchoring systems for floating offshore wind turbines or wave energy devices.

4 Installation

4.1 Bucket installation by suction

The first documents on the installation of bucket foundations have been published more than half a century ago (Goodman et al., 1961; Sato, 1965). One of the first offshore structures supported by skirted foundations is Gullfaks C (Tjelta et al., 1988). This was a very heavy structure to be installed in relatively soft soil. In order to avoid a significant enlargement of the foundation area, concrete skirts of 22 m were provided to the structure. To prove the penetrability of long concrete skirts, large-scale tests of two steel cylinders connected through a concrete panel were performed (Tjelta et al., 1986). To help the consolidation process this structure was provided with an active drainage system consisting of filters mounted on the skirt wall. Information on the monitoring campaign regarding Gulfaks C is given in Tjelta et al. (1992).

As explained in dedicated sections in Lesny (2011) and Randolph and Gourvenec (2011), the installation of bucket foundations can be divided into two main phases. The first phase consists

of self-weight penetration into the superficial layer of the seabed. The penetration achievable during this installation stage depends on the properties of the soil and on the weight of the upper structure. In the second phase, a pumping system pumps out water from inside the bucket creating suction (or under pressure). Frequently, to ensure a fully controlled penetration, the suction is combined with water injection at the skirt tip. A comprehensive study on this technique was undertaken by Cotter (2010). The suction applied within the foundation produces two phenomena: seepage flows around and inside the bucket and differential pressure acting on the lid. In soils with low permeability (fine grained), the decisive effect is the differential pressure. In soils with high permeability, the action of the seepage flows is predominant. Seepage flows are directed towards the lid within the soil plug and towards the skirt tip in the soil surrounding the foundation. In addition, the seepage flows reduce significantly the end bearing resistance of the skirt tip. Evidence of this effect is given for instance in Bye et al. (1995) and Tjelta (1994) where, previous to the installation of the Europipe 16/11-E Riser jacket, field tests on a steel cylinder were performed.

As underlined by Tjelta (2014), many issues could be encountered during the installation of bucket foundations. According to Tjelta (2014), possible problems during the installation phases could relate to soil limitations, structural limitations or pumping system limitations.

Soil limitations are mainly two: soil plug heave and piping channels. When the under pressure is applied to permeable soils, piping channels will occur if the critical hydraulic gradient is exceeded. Soil plug heave, instead, may occur in fine grained soils if the under pressure is larger than the resistance of the soil plug. A simple method to estimate the maximum under pressure allowed before soil plug heave, is described in Randolph and Gourvenec (2011).

Structural limitations concern strength of the top plate, buckling of the shell and buckling of the top plate. The effect of geometric imperfections on buckling is analysed in Madsen et al. (2013).

In Figure 9 a picture of the large-scale installation tests conducted in 2012 in Frederikshavn

Figure 9: Field tests of the installation of a bucket foundation with $d = 4$ m and $D = 4$ m, Frederikshavn 2012. On the right-hand side the pumping system

is illustrated. Note the multi-shield (anti-buckling) shape of the cross section as opposed to standard circular cross sections. Pumping system-related issues can be cavitation of the water and pump leakages. To avoid cavitation, the suction applied does not have to exceed the vapour pressure of the water. The deeper the water the more pressure can be applied before breaching the vapour pressure limit.

Small-scale and real-scale studies addressing installation issues are numerous in literature (Senpere and Auvergne, 1982; Rusaas et al., 1995; Alhayari, 1998; Solhjell et al., 1998; Chen and Randolph, 2004; Tran et al., 2004; Houlsby et al., 2005). A complete procedure for suction-assisted penetration design is described, and proved against real measurement and small-scale tests, in Houlsby and Byrne (2005). Villalobos (2006) examines the penetration of small-scale bucket pointing out the differences in bearing behaviour between jacked and suction installation. For bucket foundations the installation phases are important parts of the design process. Scrupulous installation analysis should be conducted for every new site. Besides, to mitigate the risk, small-scale or large-scale experiments could be considered. A picture of one field test of a

Figure 10: Field tests of installation and bearing capacity of a bucket foundation with $d = 2$ m and $D = 2$ m, Frederikshavn 2002

bucket foundation with diameter 2 m and embedded length 2 m is depicted in Figure 10.

4.2 Bucket installation by pushing

Although penetration by pushing (or jacking) has relatively little applicability to real cases, it is of interest to analyse this phenomenon in the context of small-scale experimental tests. Test C41, presented in Foglia and Ibsen (2014a), is the representative experiment used for the installation comparisons. The bucket used in the test has $D = 300$ mm, $d = 300$ mm and wall thickness, $t = 1.5$ mm.

A straightforward interpretation of the total installation force of the physical experiments, V_{i}, is possible by using a simple linear model. The contribution of the skirt tip end bearing, V_{end}, can be simply superimposed to that of the internal and external frictional resistance acting on the

skirt, V_{skirt}, as follows:

$$V_{\text{i}} = V_{\text{end}} + V_{\text{skirt}} \tag{20}$$

The skirt tip end bearing resistance can be calculated by assuming a footing of width equal to the skirt thickness t, and length equal to $\pi(D + D_i)/2$:

$$V_{\text{end}} = t\pi \frac{(D + D_{\text{i}})}{2} (0.5tN_\gamma\gamma' + h\gamma' N_q) \tag{21}$$

where h is the given penetration depth and D_{i} is the internal diameter of the bucket foundation. Villalobos (2006) calculated V_{end} considering the penetration of two corps into the sand:

$$V_{\text{end}} = t\pi \frac{(D + D_{\text{i}})}{2} (tN_\gamma\gamma' + 2h\gamma' N_q) \tag{22}$$

The difference between the two approaches for the foundation used in test C41, is shown in Figure 11. The plot shows that the choice of how to calculate V_{end} is not negligible. Houlsby and Byrne (2005) also adopted equation 21. V_{skirt} can be calculated by summing the internal and the external shear resistance acting on the skirt wall:

$$V_{\text{skirt}} = D_i\pi \int_0^h \tau_{\text{i}} dz + D\pi \int_0^h \tau_{\text{o}} dz \tag{23}$$

The shear stresses are calculated as:

$$\tau_{\text{i}} = \tau_{\text{o}} = K\sigma'_v tan(\delta) \tag{24}$$

where σ'_v is the vertical earth pressure at the given penetration depth, δ is the interface friction angle taken equal to $\phi'/3$ and K is the passive coefficient of horizontal earth pressure calculated according to Villalobos (2006):

$$K = \frac{2 - cos^2\phi'}{cos^2\phi'} \tag{25}$$

This value of K is derived taking into account the soil arching effect caused by the shear stresses acting on the surface of a skirt penetrating into the soil.

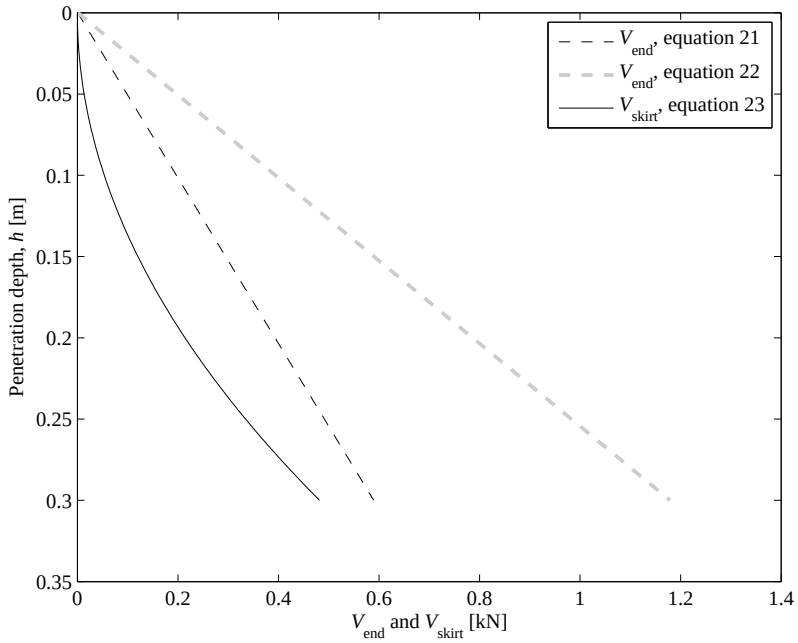

Figure 11: Comparison of the contributions to V_{i}. Calculations performed with $\phi' = 40°$

In Figure 11 it can be seen that, as expected, the frictional force caused by the shear stresses on the skirt surface has a smaller contribution to the penetration resistance than the skirt tip end bearing. Besides, it should be pointed out that the higher the friction angle the larger the discrepancy between V_{end} and V_{skirt}. The installation curve of test C41 against three linear model curves, are shown in Figure 12. The linear model, with an input friction angle of $\phi' = 44$, gives a good estimation until 100 mm of penetration. In general though, the linear model is not able to predict the experimental observations.

Two more advanced non-linear theoretical methods to obtain the jacked penetration curves of bucket foundations are suggested in Houlsby and Byrne (2005). These models have been proven valid by a number of studies and they embrace the effect of increase in stresses due to the frictional forces acting on the skirt during penetration. The first model considers a constant increment of stresses with depth. The second model allows the stresses to vary linearly with

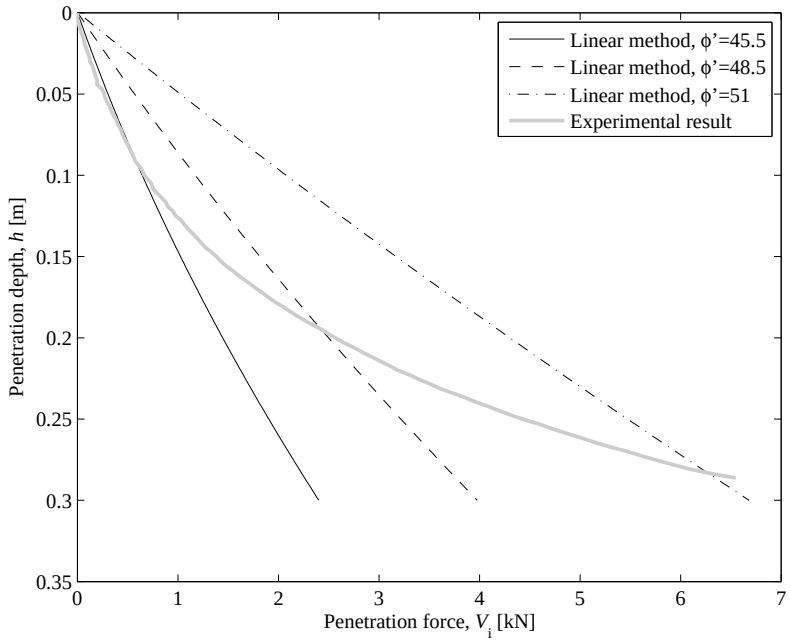

Figure 12: Linear estimation of the penetration resistance with three different friction angles against experimental curve

depth. In the following, these two models are referred to as: non-linear model 1 and non-linear model 2. Further details on the models are not mentioned here. The reader should refer to Houlsby and Byrne (2005) and Villalobos (2006) for theoretical explanations and numerical implementation

Senders (2008) investigated the behaviour of bucket foundations supporting tripods. He conducted centrifuge tests addressing installation and vertical cyclic response of the foundations. Senders (2008) implemented the second non-linear method of Houlsby and Byrne (2005) to interpret centrifuge experimental data. He concluded that with adequate input parameters the method is able to predict the experimental behaviour.

Cotter (2010) conducted numerous installation tests on three different soil samples. He mainly investigated the installation process with respect to the suction needed for the penetration and

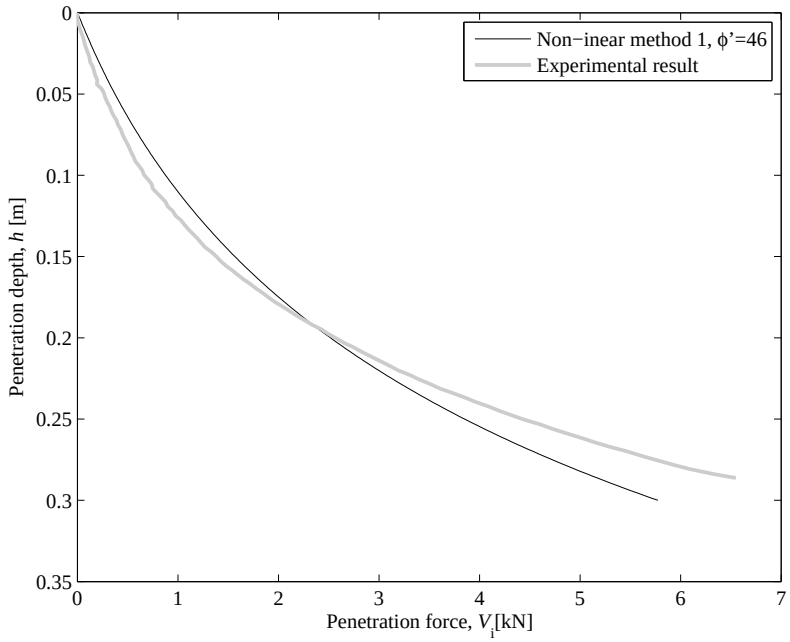

Figure 13: Non-linear model 1 against experimental results

to the skirt tip injection for steering the bucket into the ground. Cotter (2010) chose the second non-linear method of Houlsby and Byrne (2005) to predict the experimental data during self-penetration of the bucket foundation. Also Villalobos (2006) successfully implemented the approaches presented in Houlsby and Byrne (2005). The non-linear models are plotted together with the installation curve of test C41 in Figures 13 and 14. Simulations for several values of ϕ' were run. In the figures the best result achieved for one value of the friction angle is shown. The calculation factors chosen for the simulations were those suggested by the previous studies mentioned above: $m = 2$ (for non-linear model 1), $f_1 = 1$ and $f_2 = 2$ (for non-linear model 2). Note, in Figure 14, a discontinuity in correspondence to $h = 150$ mm owing to a change in the solutions of non-linear model 2 when $h \geq D_{\mathrm{i}}/2f_1$.

The non-linear model 2 interprets the experimental trend better than the linear model. However, non-linear model 1 seems to fit best the experimental observations. Of course, by choosing

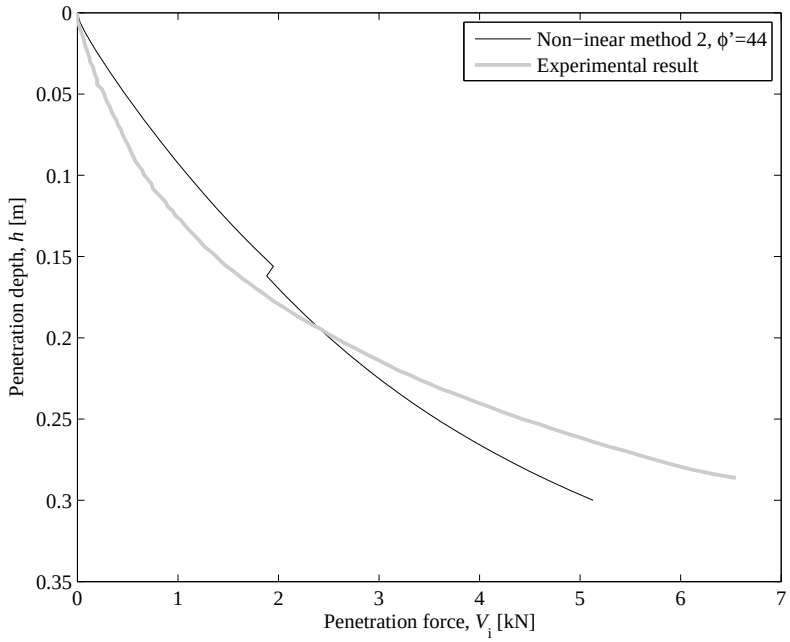

Figure 14: Non-linear model 2 against experimental results

another set of input parameters (K, δ, f_1 and f_2) non-linear model 1 might be able to better interpret the experimental results.

5 Conclusions

The bearing capacity of a flat footing is estimated with seven different methods. The formula given by DNV (2014) seems to give the most conservative estimation. Two methods to estimate the bearing capacity of bucket foundations are compared against experimental results. The method proposed by Villalobos (2006) predicts well the experimental data for a very high value of the friction angle. The method proposed by Larsen (2008), with a friction angle similar to the peak friction angle, predicts one experimental point but seems to overestimate the trend shown by the experimental data.

Interaction diagrams for flat footings are presented and evaluated against classic methods. The

bearing capacity calculated with DNV (2014) gives the smallest prediction. However, in the relevant region for offshore wind turbines, full agreement between the methods is found. Also for skirted foundations, interaction diagrams and classic approaches are compared. Similarly to what observed for flat footings, the largest discrepancy between classic methods and interaction diagrams is seen out of the relevant region for offshore wind turbines. The failure envelope derived by Ibsen et al. (2014) is shown to overestimate the experimental results at small V/V_{s}. The tensile parameter t_0 can however be modified to obtain a better description of the experimental points. The interaction diagram for bucket foundations proposed by Achmus et al. (2013a) is proven to be reasonably in agreement with experimentally derived envelopes and appears thereby to be a powerful preliminary design tool.

Three methods to estimate the jacked installation of bucket foundations are adopted to interpret one experimental curve. As expected, the non-linear models show better prediction abilities than the linear model.

From the literature review of the bucket bearing behaviour it is clear that a large amount of knowledge has been collected on bucket foundation supporting floating structures and substructures with multiple foundations. Only recently, the research focus has turned to monopod bucket foundation.

The authors would like to emphasize that real-scale installation of bucket foundations has been proven over the last 30 years in many soil conditions. Therefore, this design and construction phase should not be an issue any longer. More rational research directions include the behaviour of buckets under predominant overturning moment and the dynamic properties of the foundation. Finally, the monopod bucket foundation concept will have proper industry recognition once its bearing behaviour will be proven in real offshore environment.

Nomenclature

A	area of the foundation
A'	effective area of the foundation
D	foundation width (diameter for circular cross section)
D_{i}	internal diameter of bucket foundations
D_{r}	relative density
H	horizontal load
H'	normalised horizontal load
H'_{u}	normalised ultimate horizontal load
K	coefficient of lateral earth pressure
L	length of the foundation
M	moment
M'	normalised moment
M'_{u}	normalised ultimate moment
N_c, N_q, N_γ	bearing capacity factors
R	outer radius of the bucket
V	vertical load
V_{u}	ultimate vertical load of flat footings
V_{s}	ultimate vertical load of skirted foundations
V_{f}	vertical contribution of the frictional resistance of the skirt
V_{gu}	ultimate vertical load of flat footings under general loading
V_{gs}	ultimate vertical load of skirted foundations under general loading
V_{i}	penetration resistance during jacked installation
V_{end}	contribution of tip end bearing to the installation resistance
V_{skirt}	contribution of the skirt to the installation resistance
V_0	preconsolidation vertical load
c	cohesion
d'	depth pf excavation
d	length of the skirt
d_{ref}	reference skirt length
d_c, d_q, d_γ	depth factors
e	load eccentricity
h	penetration depth
h_0, m_0, t_0, e_0	dimensionless parameters of the failure surface
i_q, i_γ	load inclination factors
m, f_1, f_2	dimensionless parameters of the non linear installation models
q	surcharge
q_u	ultimate bearing capacity of flat footings
s_c, s_q, s_γ	shape factors
t	thickness of the skirt

β_1, β_2, β_{12}	dimensionless parameters of the failure surface
δ	interface friction angle
ϕ'	effective soil friction angle
γ'	effective unit weight of the soil
θ	angle between H and V
τ_{o}	shear stress on the outer skirt
τ_{i}	shear stress on the inner skirt

References

Achmus, M., Akdag, C. T. and Thieken, K. (2013a). Load-bearing behavior of suction bucket foundations in sand. *Applied Ocean Research* 43, 157-165

Achmus, M., Thieken, K., Akdag, C. T., Schröder, C. and Spohn, C. (2013b). Load bearing behaviour of bucket foundations in sand. In *Proceeding of the 3rd International Symposium on Computational Geomechanics (ComGeoIII), Krakov*, 586-597

Alahyari, S. (1998). Innovative developments in suction pile technology. *Offshore Technology Conference (OTC), Houston*, paper 8836

Andersen, K. H., Dyvik, R. and Schrøder, K. (1992). Pull-out capacity analyses of suction anchors for tension leg platforms. In *Procceedings of the International Conference on Behaviour of Offshore Structures (BOSS), London*, Vol. 2

Andersen, K. H., Murff, J. D., Randolph, M. F., Clukey, E. C., Erbrich, C. T., Jostad, H. P., Hansen, B, Aubeny, C., Sharma, P. and Supachawarote, C. (2005). Suction anchors for deepwater applications. In *Proceedings of the International Symposium on Frontiers in Offshore Geotechnics (ISFOG), Perth*, 3-29

API (2011). *Geotechnical and Foundation Design Considerations*. American Petroleum Institute, ISO 19901-4:2003 (Modified)

Bienen, B., Byrne, B. W., Houlsby, G. T. and Cassidy, M. J. (2006). Investigating six-degree-of-freedom loading of shallow foundations on sand. *Géotechnique* 56, No. 6, 367-379

Bolton, M. D. (1986). The strength and dilatancy of sands. Géotechnique 36, No. 1, 65-78 and discussion Géotechnique 37, No. 2, 219-226

Bolton, M. D. and Lau, C. K. (1993). Vertical bearing capacity factors for circular and strip footings on Mohr-Coulomb soil. *Canadian Geotechnical Journal* 30, 1024-1033

Bowles, J. E. (1996) *Foundation analysis and design*. McGraw-Hill

Bransby, M. F. and Randolph, M. F. (1998). Combined loading of skirted foundations. *Géotechnique* 48, No. 5, 637-655

Bransby, M. F. and Yun, G. J. (2009). The undrained capacity of skirted strip foundations under combined loading. *Géotechnique* 59, No. 2, 115-125

Brinch Hansen, J. (1970). A revised and extended formula for bearing capacity. Bulletin No. 28, Danish Geotechnical Institute, Copenhagen, 5-11

Butterfield, R. and Ticof, J. (1979). The use of physical models in design. In *Proceedings of the 7th European Conference on Soil Mechanics, Brighton*, 259-261

Butterfield, R. and Gottardi, G. (1994). A complete three-dimensional failure envelope for shallow footings on sand. *Géotechnique* 44 No. 1, 181-184

Bye, A., Erbrich, C., Rognlien, B., and Tjelta, T. I. (1995). Geotechnical design of bucket foundations. *Proc. of Offshore Technology Conference (OTC), Houston*, paper 7793

Byrne, B. W. and Houlsby, G. T. (1995). Drained behaviour of suction caisson foundations on very dense sand *Offshore Technology Conference (OTC), Houston*, paper 10994

Byrne, B. W. (2000). *Investigations of suction caissons in dense sand*. Ph.D. thesis, Oxford University

Byrne, B. W. and Houlsby, G. T. (2001). Observations of footing behaviour on loose carbonate sands. *Géotechnique* 51, No. 5, 463-466

Byrne, B. W. and Houlsby, G. T. (2002). Experimental investigations of response of suction caissons to transient vertical loading. *Journal of Geotechnical and Geoenvironmental Engi-*

neering 128, No. 11, 926-939

Cassidy, M. J., Randolph, M. F. and Byrne, B. W. (2006). A plasticity model describing caisson behaviour in clay. *Applied Ocean Research* 28, 345-358

CEN (2004). *Eurocode 7*. European committee for standardisation

Chen, W. and Randolph, M. (2004). Radial stress changes around caissons installed in clay by jacking and by suction. In *Proceedings of the International Ocean and Polar Engineering Conference (ISOPE), Toulon*, Vol. 2, 493-499

Clukey, E. C., Morrison, M. J., Garnier, J. and Corté, J. F. (1995). The response of suction caissons in normally consolidated clays to cyclic TLP loading conditions. *Offshore Technology Conference (OTC), Houston*, paper 7796

Cotter, O. (2010).*The installation of suction caisson foundations for offshore renewable energy structures*. Ph.D. thesis, Oxford University

Cremer, C., Pecker, A. and Davenne, L. (2001). Cyclic macro-element for soilstructure interaction: material and geometrical non-linearities. *Journal of Earthquake Engineering* 6, No. 25, 1257-1284

DNV (2014). *Design of Offshore Wind Turbine Structures*. Det Norske Veritas, Offshore standard DNV-OS-J101

El-Gharbawy, S. and Olson, R. (1998). The pullout capacity of suction caisson foundations for tension leg platforms. In *Proceedings of the International Ocean and Polar Engineering Conference (ISOPE),Montreal*, Vol. 1, 531-536

Fang, H.-Y. (1991). *Foundation Engineering Handbook*. Springer

Feld, T. (2001). *Suction buckets, a new innovative foundation concept, applied to offshore wind turbines*. Ph.D. thesis, Aalborg University

Foglia, A. and Ibsen, L. B. (2014a). *Laboratory experiments of bucket foundations under cyclic loading*. DCE Technical report No. 177, Department of Civil Engineering, Aalborg Univer-

sity

Foglia, A. and Ibsen, L. B. (2014b). *Monopod bucket foundations under cyclic lateral loading*. DCE Technical Memorandum No. 49, Department of Civil Engineering, Aalborg University

Foglia, A., Govoni, L., Gottardi, G. and Ibsen, L. B. (2014). *Investigations on macro-element modelling of bucket foundations for offshore wind turbines*. DCE Technical Memorandum No. 48, Department of Civil Engineering, Aalborg University

Goodman, L. J., Lee, C. N. and Walker, F. J. (1961). The feasibility of vacuum anchorage in soil. *Géotechnique* 11, No. 4, 356-359

Gottardi, G. (1992). *Modellazione del comportamento di fondazioni superficiali su sabbia soggette a diverse condizioni di carico*. Ph.D. thesis, Padova University

Gottardi, G., Houlsby, G. T. and Butterfield, R. (1999). Plastic response of circular footings under general planar loading. *Géotechnique* 49, No. 4, 453469

Gourvenec, S. (2007). Failure envelopes for offshore shallow foundations under general loading. *Géotechnique* 57, No. 9, 715728

Gourvenec, S. and Barnett, S. (2011). Undrained failure envelope for skirted foundations under general loading. *Géotechnique* 61, No. 3, 263270

Hogervost, J. R. (1980). Field trials with large diameter suction piles. *Offshore Technology Conference (OTC), Houston*, paper 3817

Houlsby, G. T. and Cassidy, M. J. (2002). A plasticity model for the behaviour of footings on sand under combined loading. *Géotechnique* 52, No. 2, 117-129

Houlsby, G. T. and Martin, C. M. (2003). Undrained bearing capacity factors for conical footings on clay. *Géotechnique* 53, No. 5, 513-520

Houlsby, G. T. and Byrne, B. W. (2005). Design procedures for installation of suction caissons in sand. *Proceedings of the ICE, Geotechnical Engineering* 158, No. 3, 135-144

Houlsby, G. T., Kelly, R. B., Huxtable, J. and Byrne, B. W. (2005). Field trials of suction

caissons in clay for offshore wind turbine foundations. *Géotechnique* 55, No. 4, 287-296

Houlsby, G. T., Kelly, R. B., Huxtable, J. and Byrne, B. W. (2006). Field trials of suction caissons in sand for offshore wind turbine foundations. *Géotechnique* 56, No 1, 3-10

Ibsen, L. B. (2008). Implementation of a new foundations concept for offshore wind farms. *Keynote of the Nordic Geotechnical Meeting (NGM), Sandefjord*

Ibsen, L. B., Larsen, K. A. and Barari, A. (2014). Calibration of Failure Criteria for Bucket Foundations on Drained Sand under General Loading. *Journal of Geotechnical and Geoenvironmental Engineering* 140, No. 7

Larsen, P. C. (1989). Suction anchors as an anchoring system for floating offshore constructions. *Offshore Technology Conference (OTC), Houston*, paper 6029

Larsen, K. A. (2008). *Static behaviour of bucket foundations*. Ph.D. thesis, Aalborg University

Lesny, K. (2011). *Foundations for Offshore Wind Turbines - Tools for Planning and Design*. VGE Verlag GmbH

Kelly, R. B., Houlsby, G. T. and Byrne, B. W. (2006). A comparison of field and laboratory tests of caisson foundations in sand and clay. *Géotechnique* 56, No. 9, 617-626

Madsen, S., Andersen, L. V. and Ibsen, L. B. (2013). Numerical buckling analysis of large suction caissons for wind turbines on deep water. *Engineering structures* 57, 443-452

Mangal, J. K. (2008). *Partially-drained loading of shallow foundations on sand*. Ph.D. thesis, Oxford University

Martin, C. M. and Houlsby, G. T. (2000). Combined loading of spudcan foundations on clay: laboratory tests. *Géotechnique* 50, No. 4, 325-337

Martin, C. M. (2003). User guide for ABC - Analysis of Bearing Capacity. Report No. OUEL 2261/03, Department of Engineering Science, Oxford University

Martin, C. M. (2005). Exact bearing capacity calculations using the method of characteristics. In *Proceedings of the 11th International Conference of IACMAG*, Vol. 4, 441-450

Meyerhof, G. G. (1953). The bearing capacity of foundations under eccentric and inclined loads. In *Proceedings ot the 3rd International Conference in Soil Mechanics and Foundation Engineering*, ICSMFE, vol. 1, 440-445

Meyerhof, G. G. (1963). Some recent research on the bearing capacity of foundations. *Canadian Geotechnical Journal* 1, 16-26

Prandtl, L. (1920). Über die Härte plastischer Körper. Nachrichten Gesellshaft Wissenschaft, Göttingen, math.-phys. Klasse

Randolph, M. F. and Puzrin, A. M. (2003). Upper bound limit analysis of circular foundations on clay under general loading. *Géotechnique* 53, No. 9, 785796

Randolph, M. F. and Gourvenec, S. (2011). *Offshore geotechnical engineering*. Spon press

Roscoe, K. H. and Schofield, A. N. (1956). The stability of short pier foundations in sand. *British Welding Journal*. August, 343-354

Rusaas, P., Giske, S. R., Aas-Jakobsen, A., Barret, G., Christiansen, P. E. and Baerheim, M. (1995). Design, operation planning and experience from the marine operations for the europipe jacket with bucket foundations. *Offshore Technology Conference (OTC), Houston*, paper 7794

Saleçon, J. and Pecker, A. (1995). Ultimate bearing capacity of shallow foundations under inclined and eccentric loads. Part I: purely cohesive soil. *European Journal of Mechanics - A/Solids* 14, No. 3, 349-375

Sato, H. (1965). New type breakwater constructed by pressed down p.c. cylinders. *International Navigation Congress, Stockholm*

Senders, F. A. (2008). *Suction caissons in sand as tripod foundations for offshore wind turbines*. Ph.D. thesis, The University of Western Australia

Senpere, D. and Auvergne, G. A. (1982). Suction anchor piles - a proven alternative to driving or drilling. *Offshore Technology Conference (OTC), Houston*, paper 4206

Solhjell, E., Sparrevik, P., Haldorsen, K. and Karlsen, V. (1998). Comparison and back calculation of penetration resistance from suction anchor installation in soft to stiff clay at the Njord and Visund fields in the North Sea. *Offshore Site Investigations and Foundations Behaviour (SUT), London*

Steensen-Bach, J. O. (1992). Recent model tests with suction piles in clay and sand. *Offshore Technology Conference (OTC), Houston*, paper 6844

Supachawarote, C., Randolph, M. F. and Gourvenec, S. (2004). Inclined pull-out capacity of suction caissons. In *Proceedings of the International Ocean and Polar Engineering Conference (ISOPE), Toulon*, Vol. 2, 500-506

Terzaghi, K. (1943). *Theoretical soil machanics*. John Wiley and sons

Thieken, K., Achmus, M and Schröder, C. (2014). *On the behavior of suction buckets in sand under tensile loads*. *Computers and Geotechnics* 60, 88-100

Tjelta, T. I., Guttormsen, T. R. and Hermstad, J. (1986). Large-scale penetration test at a deepwater site. *Offshore Technology Conference (OTC), Houston*, paper 5103

Tjelta, T. I., Skotheim, A. A. and Svanø, G. (1988). Foundation design for deepwater gravity base structure with long skirts on soft soils. In *Procceedings of the International Conference on Behaviour of Offshore Structures (BOSS), Trondheim* Vol. 1, p. 173

Tjelta, T. I., Janbu, N. and Grande, L. (1992). Observations on drainage control effects on Gullfaks C gravity structure. Norwegian University of Science and Technology, Department of Geotechnical Engineering

Tjelta, T. I. (1994). Geotechnical aspects of bucket foundations replacing piles for the Europipe 16/11-E jacket. *Offshore Technology Conference (OTC), Houston*, paper 7397

Tjelta, T. I. (2014). 25 Years Experience with Suction Techniques in Oil & Gas. Presentation at The Universal Foundation Technical Workshop, Hamburg 25th 26th February 2014

Tran, M. N., Randolph, M. F. and Airey, D. W. (2004). Experimental study of suction installa-

tion of caissons in dense sand. In *Proceedings of the International Conference on Offshore Mechanics in Artic Engineering (OMAE), Vanvouver*, paper No. OMAE2004-51076

Vaitkunaite, E., Ibsen, L. B., and Nielsen, B. N. (2014). New Medium-Scale Laboratory Testing of Bucket Foundation Capacity in Sand. In *Proceedings of the International Ocean and Polar Engineering Conference (ISOPE) Busan*, Vol. 2, 514-520

Vesić, A. S. (1973). *Analysis of ultimate loads of shallow foundations*. *JSMFD*, ASCE 99, 45-73

Villalobos, F. A. (2006). *Model testing of foundations for offshore wind turbines*. Ph.D. thesis, Oxford University

Villalobos, F. A., Byrne, B. W. and Houlsby, G. T. (2009). An experimental study of the drained capacity of suction caisson foundations under monotonic loading for offshore applications. *Soils and Foundations* 49, No. 3, 477488

Wang, M. C., Demars, K. R. and Nacci, V. A. (1977). Breakout capacity of model suction anchors in soil. *Canadian Geotechnical Journal* 14, 246-257

Watson, P. G. and Randolph, M. F. (2006). A centrifuge study into cyclic loading of caisson foundations. *In proceedings of the 6th International Conference on Physical Modelling in Geotechnics (ICPMG), Hong Kong*, vol. 1, 693-699

Whittle, A. J., Germaine, J. T. and Cauble, D. F. (1998). Behavior of miniature suction caissons in clay. *Offshore site investigation and foundation behaviours (SUT), London* 279-300

Zhu, B., Byrne, B. W. and Houlsby, G. T. (2013). Long-term lateral cyclic response of suction caisson foundations in sand. *Journal of Geotechnical and Geoenvironmental Engineering* 139, No. 1, 73-83

Paper II

Title:

A preliminary study on bucket foundations under transient lateral loading

Authors:

Foglia, A., Ibsen, L. B., Nielsen, S. K. and Mikalauskas, L.

Year of publication:

2013

Published in:

The Proceedings of The Twenty-third International Offshore and Polar Engineering Conference (ISOPE), Anchorage, Alaska, USA, June 30-July 5, 2013 (corrected version)

Number of pages:

7

A Preliminary Study on Bucket Foundations under Transient Lateral Loading

Aligi Foglia, Lars Bo Ibsen, Søren Kjær Nielsen
Department of Civil Engineering, Aalborg University
Aalborg, Denmark

Linas Mikalauskas
Lic Engineering A/S
Hellerup, Denmark

ABSTRACT

This study aims at investigating the behaviour of monopod bucket foundations through a 1*g* physical model. The foundations are installed in dense water-saturated sand and are subjected to lateral load. The response of bucket foundations in different drainage conditions is explored by running tests with different loading rates. Particular focus is given to the response of the foundation under transient loading (simulating a 50 year wave or emergency stop of a wind turbine). Important knowledge on the pore pressure development within and around the foundation during loading is obtained.

KEY WORDS: Bucket foundation; dense sand; loading rate; rapid loading.

INTRODUCTION

Bucket foundations

Offshore wind farms will play a significant part in the European energy market of the coming years. Today, the main challenge faced by the offshore wind market is to reduce the costs of turbine support structures. The monopod bucket foundation is one possible solution to this problem.
This kind of sub-structure is made of steel and does not need any transition piece between the foundation and the turbine tower. The foundation is an upside-down bucket with diameter, *D*, and length of the skirt, *d*. A typical real-scale foundation has a diameter of 12-18 m and an embedment ratio, *d*/*D*, of 0.5-1.
Conventional foundation types such as gravity based foundations, monopiles and spread-out foundations have been successfully used the last ten years in spite of high manufacturing and installation costs.
The monopod bucket foundation is installed by suction assisted penetration, and, given proper soil conditions and water depths, has the potential to become a cost-effective foundation for offshore wind turbines.
The bucket foundation (also referred as to suction caisson or suction bucket) has been used several times as embedded shallow foundation for offshore oil and gas facilities. Tjelta (1995) is an interesting document on the issues encountered when installing a 4 legs jacket structure supported by bucket foundations.
The loading conditions of offshore wind turbines differ considerably from those of oil and gas platforms. New design drivers are therefore needed, and, throughout the last decade, a number of studies have been conducted to explore the behavioural pattern of response of bucket foundations for offshore wind turbines (Villalobos, 2009; Larsen, 2008). The first bucket foundation supporting a wind turbine was installed in 2002 a few meters offshore in Frederikshavn, Denmark (Ibsen, 2008).
The design criteria for bucket foundations are based on those for shallow foundations. Typically, although offshore environment is characterized by partially drained conditions, the bucket foundation design is driven by the drained capacity.
Sea states include wind waves and swells which act on offshore structures as a cyclic series of fluctuating pressure. In shallow water depth, breaking waves can heavily impact the structure in a very short time frame. Within the in-service design situation, extreme events such as freak waves (Haver and Andersen 2000) and emergency stops of the rotor, have to be considered. Designing a bucket foundation to withstand extreme events by adopting the drained parameters may be too conservative. This article addresses this issue by exploring the response of the bucket foundation in different drainage conditions. The method used is a 1*g* small-scale physical model.

Transient loading

According to Byrne (2000), a transient load can be defined as that load whose loading rate has an influence on the soil/structure interaction. This can be the case for both monotonic and cyclic loading. Theoretically, the loading rate influences the structure behaviour only in case the soil is saturated with a fluid. Offshore soil conditions are always water-saturated, however, relatively few experimental studies have been conducted on the loading rate dependency of offshore shallow foundations.
A fundamental work on transient loading is Vesić et al. (1965). Several vertical loading tests of footings on dry and saturated sand were conducted at different loading rates, and, the bearing capacity found was compared to the static one. Rather surprisingly they found that in both cases the bearing capacity decreased for displacement rates in the range 0.003-0.3 mm/s. Instead, for displacement velocities faster than 3 mm/s the dry samples reached the static ultimate capacity whereas the saturated samples presented significantly increased ultimate resistance.
Mangal and Houlsby (1999) demonstrated that for shallow foundations the interaction diagrams for combined loading are transient-dependent.
Houlsby et al. (2005) found that the tensile capacity of bucket foundations depends markedly on the pulling out rate.
Byrne and Houlsby (2002) and Byrne and Houlsby (2004) run several

cyclic loading tests in oil saturated sand and found that the loading rate has an impact on the bucket behaviour only at small displacements.
Rapid loading element tests were conducted for instance by Ibsen and Lade (1998) where samples were brought to cavitation-failure.
From the mentioned literature it is clear that a transient effect, even though small, exists and that is generally beneficial to the bearing capacity of a shallow foundation.
The reason for this effect is quite well expressed in studies such as Bye et al. (1995) and Vesić et al. (1965). When loading rates are large enough, the water does not have time to migrate through the pores of the soil and transient undrained condition occurs. Fully undrained conditions would not allow any volumetric change and, in dense sand, this would cause negative pore water pressure (suction, or under pressure). At this state, as long as the water flow attempts to reestablish the pressure equilibrium, the bearing capacity increases dramatically. In some cases it is even likely that the ultimate strength is dictated by the cavitation of the pore fluid.
This article intends to give an insight into the response of bucket foundation structures when subjected to single extreme events characterized by a high loading rate. This is accomplished by testing a small-scale bucket foundation under lateral loading applied at different velocities. The study presents the results of 8 tests. In particular, the case of rapid loading is focused on. The most important model innovation is the possibility of tracing the patterns of pore pressure development inside and along the skirt by means of 8 pore pressure transducers. A scaling law for the pore pressure distribution around and inside the foundation is proposed and important information on the drainage conditions during loading are achieved. The patterns of displacement as well as the load-displacement curves are presented and commented upon.

A SCALING LAW FOR PORE PRESSURE DEVELOPMENT DURING TRANSIENT LOADING

Single gravity physical models can give qualitative information on geotechnical problems. Expressing the quantities involved with non-dimensional groups is fundamental to generalize results and to identify the governing variables of a given phenomenon. In this study we are primarily interested in the pore pressure, Δp, developed underneath and around a bucket foundation, under lateral loading. A simple way of interpreting the results of this experimental campaign is proposed in the following.
The response of a geotechnical structure is the result of the interaction between soil, foundation and environmental loading. Δp [FL^{-2}] is expected to be a function of the displacement rate, v[LT^{-1}], the soil permeability, k [LT^{-1}], the drainage length, L [L] and the unit weight of the pore fluid, γ_w [FL^{-3}]:

$$\Delta p = f\left(k, v, L, \gamma_w\right) \tag{1}$$

The drainage length is assumed to be proportional to the skirt length and diameter:

$$L \propto (d, D) \tag{2}$$

A non-dimensional pore pressure development can thus be expressed by a dimensionless group as follows:

$$\frac{\Delta p}{\gamma_w D} = g\left(\frac{vd}{kD}\right) \tag{3}$$

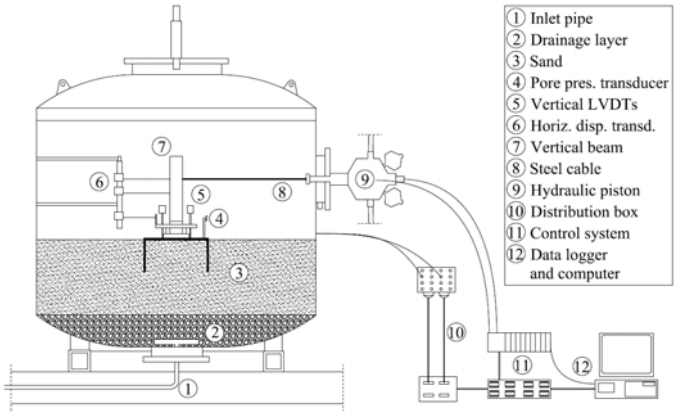

Figure 1. Drawing of the test setup. Tank, instrumented bucket, hydraulic piston and data sampling system.

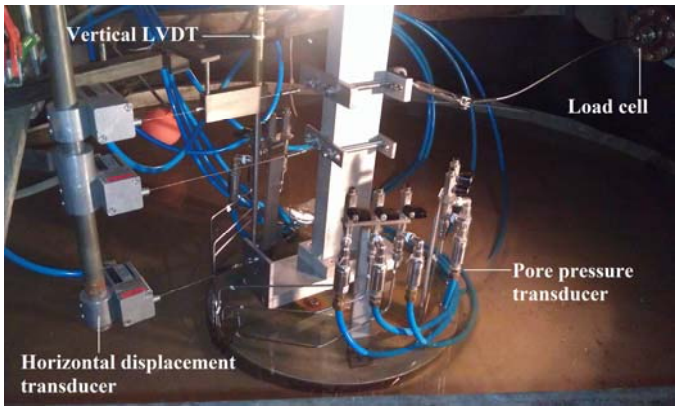

Figure 2. Picture of the test setup. Displacement, pore pressure and force transducers.

Table 1. Properties of Aalborg University Sand No. 1.

Property	Value
d_{50}, [mm]	0.14
$C_u = d_{60} / d_{10}$	1.78
Specific grain density d_s	2.64
Maximum void ratio e_{min}	0.86
Minumum void ratio e_{min}	0.55

Where g is an unknown function which can be found by conducting small-scale experiments.
Obviously, the pore pressure measured in laboratory tests is much smaller than that developed in full-scale. However, if the dimensional analysis is successful, the non-dimensional pore water pressure pattern should resemble the one of full-scale systems.

EXPERIMENTAL SETUP

The testing equipment is sketched in Fig.1. It consists of a pressure tank, an instrumented foundation, a hydraulic piston, a data logger, a control system and a computer. The pressure tank has a diameter of 2100 mm and a height of 2166 mm. The tank contains a soil layer of 730 mm which lies over a drainage layer of 90 mm. The soil is Aalborg University sand No. 1, its properties are listed in Table 1. A permeability study of the sand used was carried out by Sjelmo (2012). In that study, an expression of the permeability, as a function of the

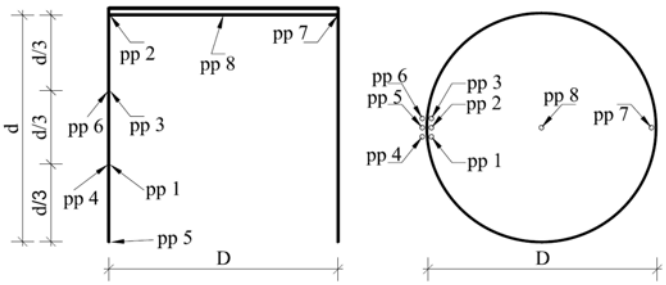

Figure 3. Vertical and horizontal section of the bucket foundation with position of the pore pressure transducers. Horizontal displacement applied from left to right.

Table 2. Test program. Bucket A has d = 0.25 m and D = 0.5; bucket B has d = 0.5 m and D = 0.5.

Test number	Bucket type	Displacement rate v [mm/s]
1	A	0.01
2	A	0.1
3	A	1.0
4	A	10.0
5	B	0.01
7	B	0.1
8	B	1.0
9	B	10.0

void ratio, was derived.

Two bucket foundations were used in the experiments. Bucket A has D = 500 mm and d/D = 0.5 while bucket B has D = 500 mm and d/D = 1. The foundations were instrumented with 8 pore pressure transducers, and five displacement transducers. Two displacement transducers were linear variable differential transformers (LVDTs). The LVDTs were placed vertically on the lid. The remaining three displacement transducers were mounted on an independent frame and horizontally connected to the structure. A picture of the instrumented foundation after a test is illustrated in Fig. 2. A drawing that shows the position of the pore pressure transducers is depicted in Fig. 3.

The displacement transducers recordings are corrected and computed to give rotational displacement, θ, vertical displacement, w, and horizontal displacement, u. The sign convention used is that put forward by Butterfield et al. (1997). The load reference point is the center of the bucket lid, on the soil side.

On the lid a vertical beam was mounted. The beam was connected to the hydraulic piston with a steel cable with an eccentricity of 480 mm from the bucket lid. To measure the lateral force, F, caused by the applied displacement, a load cell was fit between the cable and the piston.

TEST DESCRIPTION AND TESTING PROGRAM

Before each test the soil sample was prepared in a systematic manner to ensure uniform and consistent conditions. Firstly, water was let in the tank by applying an upward gradient of 0.9. By doing this, the sample was loosened up and brought to zero-condition. Secondly, the sample was mechanically vibrated to recreate dense conditions. Thirdly, a series of small-scale cone penetration tests (CPTs) was conducted with three purposes: test the soil uniformity, ensure the test repeatability and calculate the soil parameters. The relative density was found ranging from 78 % to 89 % with an average of 84 %.

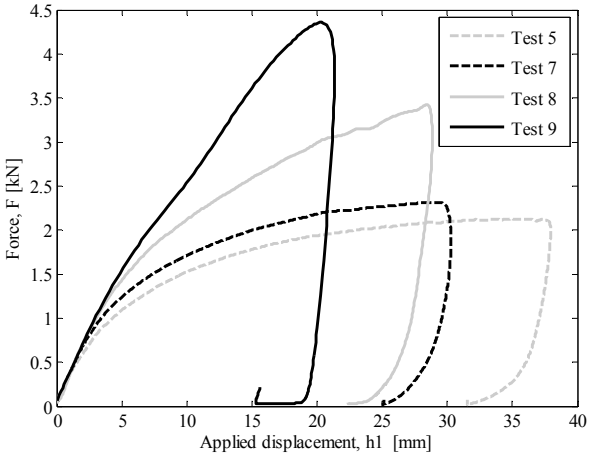

Figure 4. Force against applied displacement of bucket B.

The foundation was driven into the soil by means of a hydraulic jack. To prevent pressure within the bucket to occur, one air valve on the lid was open during penetration and sealed afterwards. Once the installation was complete, the piston was connected to the loading beam and the pressure inside the tank was set to 200 kPa. Such a choice was made to ensure that the water pressure did not exceed the cavitation limit at any time during the test.

The test was carried out by applying a designated displacement to the loading piston and thereby to the point of load application. The designated displacement of the piston was 40 mm. In each test the displacement velocity was set as listed in Table 2. The horizontal displacement transducer mounted at the same height of the load application point measured the exact displacement experienced by the structure during the test, namely the applied displacement. The displacement measured by this transducer, *h1*, indicates whether or not the test was properly controlled. The deflection due to the bending moment of the vertical bar is neglected.

During the test, the foundation was subjected to monotonically increasing horizontal and moment loading and constant vertical loading (only the weight of the foundation and equipment).

The non-dimensional group normally used to represent the vertical load of a foundation is $V / (\gamma' D^3)$, where γ' is the effective unit weight of the soil and V the vertical load. This ratio equals 0.43 and 0.54 respectively for bucket A and bucket B. Nowadays a typical wind turbine structure would have this ratio between 0.1 and 1. In contrast, a bucket foundation for oil and gas facilities would have in general $V / (\gamma' D^3) >$ 3 (Randolph and Gourvenec, 2011). This clarifies also why offshore wind turbine structures need other design drivers than those traditionally used for offshore oil and gas platforms.

PRESENTATION OF RESULTS

Bearing behaviour and displacement trajectories

An essential graph to understand the experiments is illustrated in Fig. 4 for bucket B, and, in Fig. 5, for bucket A. These figures show the horizontal force exerted by the piston against *h1*. It can be observed that none of the tests reaches the 40 mm of horizontal displacement the actuator was designed for. This is likely to be due to the limited capacity of the hydraulic piston to exert large forces with fast loading rate. In other words, the designated displacement could not be mobilised and the tests cannot be entirely compared to each other.

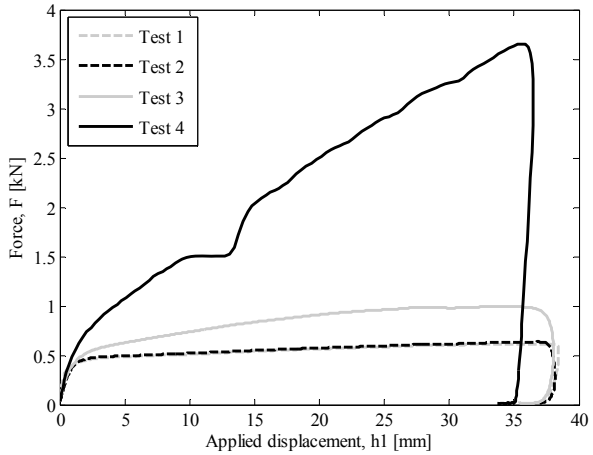

Figure 5. Force against applied displacement of bucket A.

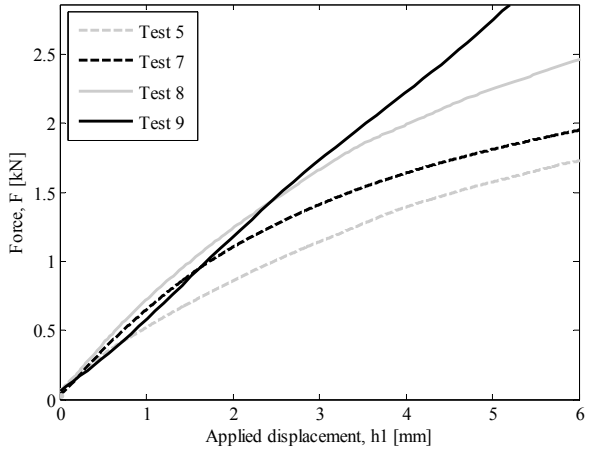

Figure 6. Magnified view of Fig. 4.

However, it is noticeable that all the curves reach 20 mm of horizontal displacement, and, therefore, the tests can be examined with some restrictions. Seemingly, the experiments were not fully controllable after the first 20 mm of horizontal displacement. The presentation and the discussion of the results will be limited only to the comparable part of the experiments. Note that most of the following graphs will be plotted with the applied displacement, *h1*, on the x-axis.

Not unexpectedly, Figs. 4~5 indicate that the loading rate has an effect on the lateral response of the foundations tested. Every test presents a dramatic reduction of the stiffness after a few millimetres of displacement applied (from 1.5 to 2.5 mm). This stiffness reduction is pronounced in tests 1, 2, 3, 5, 7 and 8. For both buckets, it is impressive how the fastest tests do not show any stiffness reduction after the very first millimetres of displacement. Furthermore, it is worth noting that the foundation, at the end of test 4, is subjected to a force which is four-fold that seen in test 3. The same difference was expected also between tests 8 and 9, though much less displacement could be applied to them.

It is of great interest to consider the initial stiffness since that is the part of the load-displacement curve that is relevant for real environmental loading. A magnified view of the initial stiffness region of the *h1-F* graph for bucket B is illustrated in Fig. 6. The graph shows that the loading rate does not seem to have relevant influence on the initial stiffness.

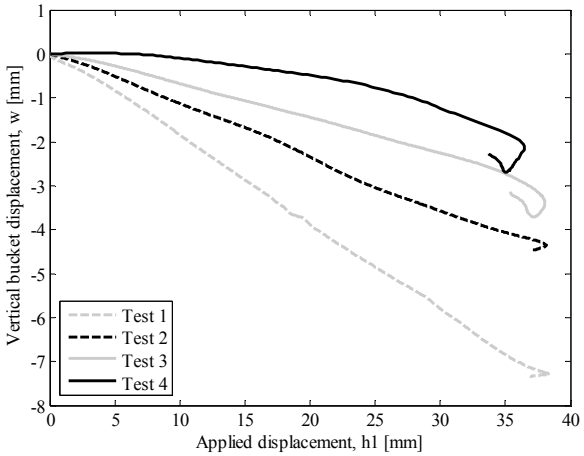

Figure 7. Vertical displacement of bucket A against the applied displacement.

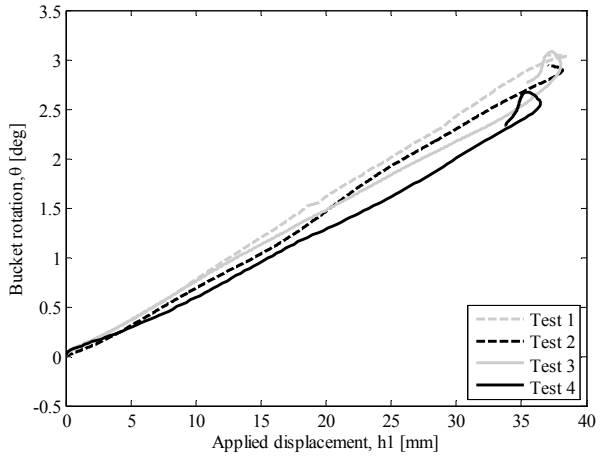

Figure 8. Rotational displacement of bucket A against the applied displacement.

The displacement trajectories presented in the following show curves that refer to bucket A. Bucket B was found to behave qualitatively in the same manner. The analysis of the pattern of displacements reveals that only the vertical displacement, *w*, is influenced by the loading rate. In Fig. 7, the *h*1-*w* curve, is illustrated. *w* is largest for the slowest test, test 1, and decreases consistently for increasing loading rates. The plot of the rotational displacement, θ, against *h1* is depicted in Fig. 8. No significant discrepancy is found between the curves. The same trend was shown by the horizontal displacement, *u*.

Pore pressure

According to the loading rate the pore pressure pattern changes significantly among the tests. A typical record of a pore pressure transducer against the actuator movement is illustrated in Fig. 9. For clarity, the pore pressure response of tests 4 and 9, is separately plotted in Figs. 10~11. It is immediately apparent that in the tests conducted with the smallest loading rate the pore pressure is negligible for both buckets. Note that the curves of tests 1 and 5 cannot be distinguished since they are superimposed. For tests 2, 7, 3 and 8, the load is partly

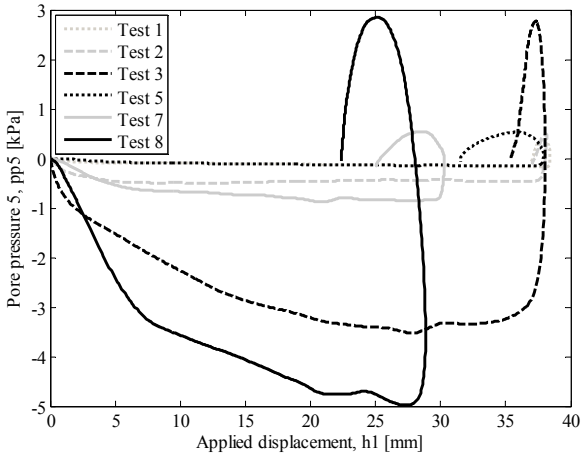

Figure 9. Pore pressure measurements of pp 5.

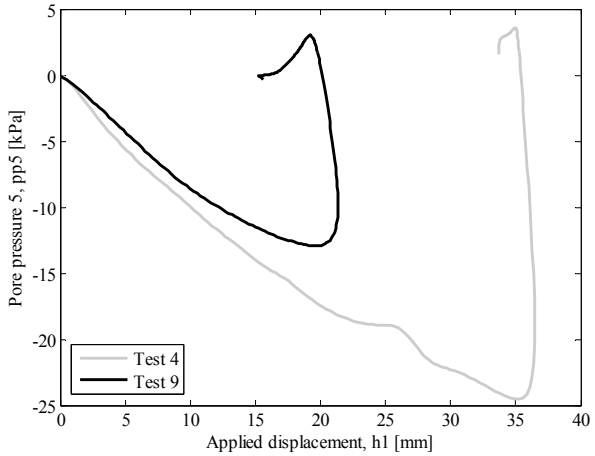

Figure 10. Pore pressure measurements of pp 5 for the tests with largest loading rate.

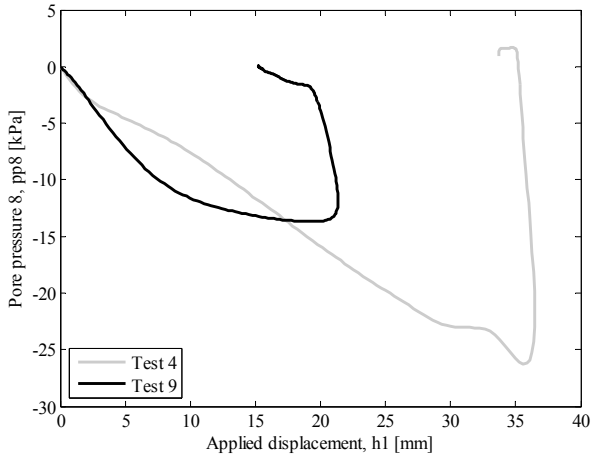

Figure 11. Pore pressure measurements of pp 8 for the tests with largest loading rate.

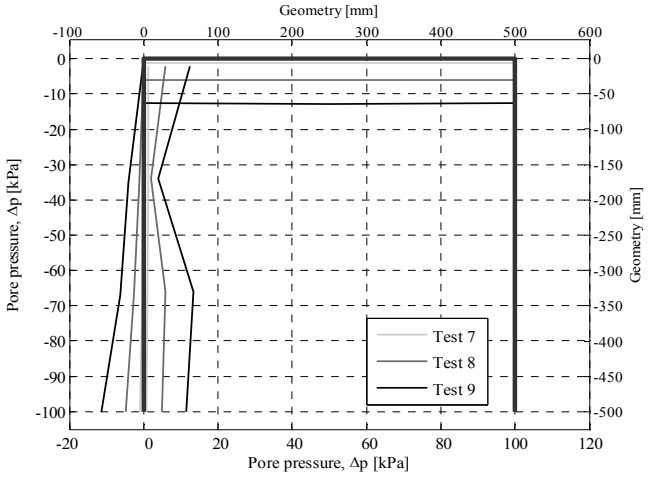

Figure 12. Pore pressure profile along the skirt and underneath the lid of bucket B. Horizontal displacement applied from left to right.

transmitted to the water and the pore pressures are larger for bucket B. This can be attributed to an increase in the drainage path due to a longer skirt (Eq. 3). Also, it is singular how in the first 2.5 mm of applied displacement, the pore pressure recorded underneath bucket A was larger than that of bucket B (see Fig. 9 test 3 against 8 and 2 against 7).

Considering now the fastest tests, namely tests 4 and 9, it appears that for both foundations the pore pressure develops differently to the other tests. Fig 10 shows the pore pressure of the skirt tip (pp5) while Fig 11 shows the pore pressure of the centre of the bucket lid (pp8). The transducers placed on the lid, pp 2, pp 8 and pp 7 show a larger pressure for bucket B in the beginning which is matched by that of bucket A during the test. Instead, the external transducers along the skirt, pp 4, pp 5 and pp 6, follow the same trend in both buckets with the pore pressure underneath bucket A slightly greater. More importantly, for both buckets, the tests conducted at the fastest displacement rate present no flattening part. The pore pressure for these tests seems to increase indefinitely (as the load does) and thus the condition within the tests can be said to be substantially undrained.

A sketch of the pore pressure profile is illustrated in Fig. 12. Across the diameter the pore fluid response seems to have equal magnitude. Rather curiously, a discontinuity in the pore pressure profile underneath the foundation was seen for the fastest tests in both buckets. A transducer failure is to be excluded since the readings of the two buckets were recorded by different transducers. To be excluded is also a non-uniform soil condition. Although some doubts remain on the origin of this phenomenon, it is most likely a consequence of the drainage condition.

INTERPRETATION OF THE RESULTS

For offshore wind energy converters, one of the conditions for which the serviceability limit is breached, is the excessive tilt of the structure (DNV, 2011). Excessive tilt leads to a change in the acting forces that might compromise the wind generator performance or cause degenerative settlements. An attempt to scale up the rotation of small-scale experiment of bucket foundations was made by Kelly et al. (2006). When applying such scaling to the tests presented here, the rotation measured in small-scale, θ_S, is approximately the 20 % of the large-scale rotation, θ_L, of a standard foundation. Now, considering a large-scale tilting limit $\theta_{LT} = 0.5°$ the small-scale limit would be $\theta_{ST} = 0.1°$ (according to Kelly et al., 2006). By examining Fig. 8, this

corresponds to approximately *h1* = 2 mm. It can be observed that, by setting this value of θ_{ST}, the loading rate does not influence markedly the behaviour of the two buckets tested (cf. Figs. 4~6). It should also be emphasized that for bucket B, the loading rate independency holds for a larger displacement (see Fig. 4 against Fig. 5).

Furthermore, test 1 and 2 present exactly the same *H-h1* curve but a fairly dissimilar trend of *w*. This means that even though the loading rate produces no effects on the load-displacement behaviour, it may affect the trajectory of the vertical displacement.

Turning now to the interpretation of the pore pressure, the dimensionless pore pressure measured inside the bucket against the dimensionless group derived in Eq. 3 is plotted in Fig. 13. The values of Δp / ($\gamma_w D$) in circles and crosses refer to all the tests performed and to two pore pressure transducers. Even though the features of the experiments change considerably, this representation of the results gives a fairly consistent distribution of Δp / ($\gamma_w D$). This means that the proposed non-dimensional groups is a good means by which the pore pressure development of different bucket foundations, subjected to various loading rate, may be represented.

A power law in the form:

$$\frac{\Delta p}{\gamma_w D} = g\left(\frac{vd}{kD}\right) = a\left(\frac{d}{kT_L}\right)^n \tag{4}$$

is fitted to the experimental points as a preliminary interpretation of the results. The parameters of Eq. 4 may be properly calibrated by including all the pore pressure readings and by conducting new tests with buckets of various sizes. These findings could be used to validate numerical results of water pressure development of a bucket foundation under lateral monotonic loading.

CONCLUSIONS AND FUTURE WORK

From the tests result it is evident that a bucket foundation under fast monotonic loading has enhanced bearing capacity at large displacements. A striking finding of this study, though not new, is that the loading rate produces no marked influence on the initial stiffness. As demonstrated in the results interpretation, within the serviceability design, the loading rate effect might be negligible. Consequently, the effect of the loading rate should be considered only when designing a foundation to withstand extreme environmental conditions.

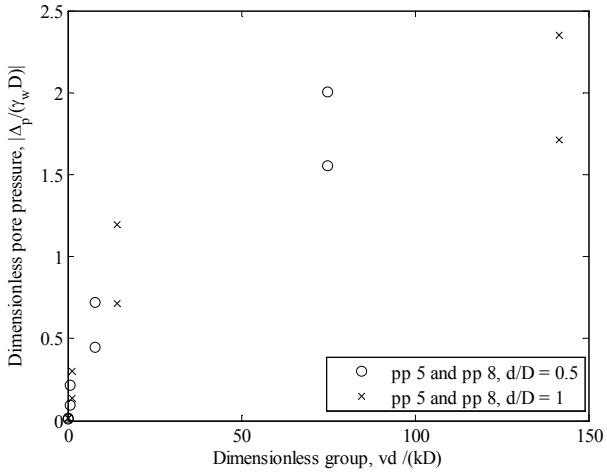

Figure 13. Experimental data plotted in non-dimensional form. Bucket A and B, pp 5 and 8, four different loading rates.

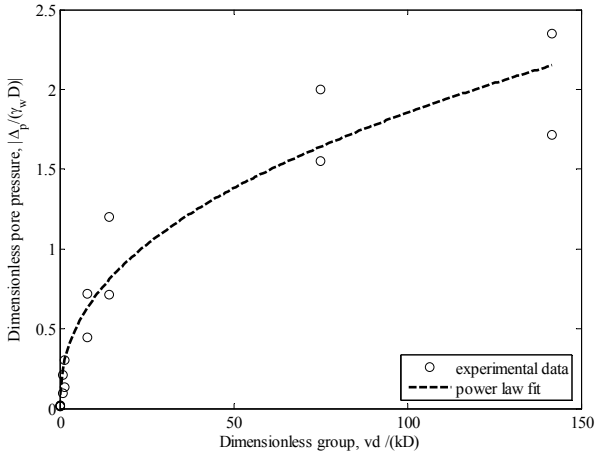

Figure 14. Experimental data and fitting function.

To interpret the pore pressure development, a simple dimensionless group was derived as a function of drainage length, loading rate and soil permeability. The simple interpretation of the pore pressure development has been shown to be somewhat successful. Some unexpected results from the pore pressure, such as the discontinuity in the internal pressure profile, remain unclear.

Scaling laws that address drainage patterns should be more deeply investigated and large-scale tests shall be performed in order to prove whether the patterns found in small-scale resemble those of large-scale foundations. It is deemed that by improving both the experimental rig and the comprehension of the model, extraordinary results may be obtained. The actuator capacity should be enhanced to cope with large foundation capacities encountered at fast loading rate. Besides, to have a full picture of the pore pressure distribution, pore pressure transducers should be placed also on the bucket front, and not only on the back. An extensive testing program undertaken with an improved experimental setup will be essential to complete the observations outlined in this study.

ACKNOWLEDGEMENTS

The experiments presented in this paper were carried out in cooperation with Mr. Åsmund Sjelmo. His contribution to this study is acknowledged.

REFERENCES

Bye A, Erbrich C, Rognlien B and Tjelta TI (1995). "Geotechnical design of bucket foundations," *Proc. 27th Annual Offshore Technology Conference* OTC, Huston, Texas, pp 869-883.

Byrne MW (2000). "Investigations of suction caissons in dense sand," PhD Thesis, Oxford University.

Byrne BW and Houlsby GT (2002). "Experimental investigations of the response of suction caissons to transient vertical loading," *Journal of Geotechnical and Geoenvironmental Engineering ASCE*, Vol. 11, pp 926-939.

Byrne BW and Houlsby GT (2004). "Experimental investigations of the response of suction caissons to transient combined loading," *Journal of Geotechnical and Geoenvironmental Engineering ASCE*, Vol. 3, pp 240-253.

Butterfield R, Houlsby GT, and Gottardi G (1997). "Standardized sign conventions and notation for generally loaded foundations,"

Geotechnique, Vol 47, Nr. 2, pp 79-90.

DNV (2011). *Offshore standard: Design of offshore wind turbine structures*, Det Norske Veritas, DNV-OS-J101.

Haver S and Andersen OJ (2000). "Freak waves: rare realizations of a typical population or typical realizations of a rare population?," *Proc. 10th International Offshore and Polar Engineering Conference*, ISOPE Seattle, USA, pp 123-130.

Houlsby GT, Kelly RB and Byrne BW (2005). "The tensile capacity of suction caissons in sand under rapid loading" *Proc. Frontiers in Offshore Geotechnics*, ISFOG, Taylor and Francis Group, pp 405-410.

Ibsen LB (2008). "Implementation of a new foundations concept for offshore wind farm," *Nordic Geotechnical meeting*, Sandefjord, Norway.

Ibsen LB and Lade PV (1998). "The strength and deformation characteristics of sand beneath vertical breakwaters subjected to wave loading," Aalborg University Geotechnical Engineering Papers, Soil Mechanics Paper No. 23.

Kelly RB, Houlsby GT and Byrne BW (2006). "A comparison of field and laboratory tests of caisson foundations in sand and clay," *Geotechnique*, Vol 56, Nr. 9, pp 617-626.

Larsen KA (2008). "Static behaviour of bucket foundations," PhD Thesis, Aalborg University.

Mangal JK and Houlsby GT (1999). "Partially-drained loading of shallow foundations on sand," *Proc. 31st Annual Offshore Technology Conference* OTC, Huston, Texas.

Randolph M and Gourvenec S (2011). "Offshore geotechnical engineering," Spon Press.

Sjelmo A (2012). "Soil-structure interaction in cohesionless soils due to monotonic loading," MSc Thesis, Aalborg University.

Tjelta TI (1995). "Geotechnical experience from the installation of the Europipe jacket with bucket foundations," *Proc. 27th Annual Offshore Technology Conference* OTC, Huston, Texas, pp 897-905.

Vesić AS, Banks DC and Woodard JM (1965). "An experimental study of dynamic bearing capacity of footings on sand" *Proc. 6th Int. Conf. on Soil Mech. And Foundation Eng.*, Montreal, 2 pp 209-213.

Villalobos FA (2006). "Model testing of foundations for offshore wind turbines," PhD Thesis, Oxford University.

Paper III

Title:

Monopod bucket foundations under cyclic lateral loading

Authors:

Foglia, A. and Ibsen, L. B.

Year of publication:

2014

Published in:

DCE Technical Memorandum No. 49, Department of Civil Engineering, Aalborg University.

A journal publication based on this Technical Memorandum can be found under:

Foglia, A. and Ibsen, L. B. (2016). Monopod Bucket Foundations Under Cyclic Lateral Loading. *International Journal of Offshore and Polar Engineering* 26, No. 2.

Number of pages:

16

Monopod bucket foundations under cyclic lateral loading

Abstract

The monopod bucket foundation can be a cost-reducing sub-structure for offshore wind turbines. To avoid problems during the turbine operation, the long-term effect of cyclic loading must be considered in the design of the foundation. In this paper a 1*g* testing rig is adopted to extend the knowledge on bucket foundations under lateral cyclic loading. The test setup is described in detail and a comprehensive experimental campaign is presented. The foundation is subjected to cyclic overturning moment, cyclic horizontal loading and constant vertical loading, acting on the same plane for thousands of cycles. Three buckets with different embedment ratios are tested. The data interpretation is focused on the long-term permanent rotation of the foundation and, particularly, on understanding how the controlling variables influence the potential for rotation accumulation. New and more general parameters of an empirical model predicting the long-term plastic rotation are proposed on the base of the experimental results.

List of notation

γ'	effective unit weight of the sand
D_r	relative density of the sand
D	foundation diameter
d	foundation embedment (skirt length)
t	wall thickness
f_L	cyclic loading frequency
N	number of cycles
H	horizontal load acting on the load reference point
h	eccentricity of the horizontal load
M	overturning moment acting on the load reference point $M = hH$
M_R	ultimate monotonic moment
M_{max} , M_{min}	maximum and minimum cyclic overturning moment
H_{max} , H_{min}	maximum and minimum horizontal load
V	vertical load acting on the load reference point
θ_N	rotational displacement of the foundation after N cycles
θ_0	rotational displacement of the foundation at $N = 1$
θ_s	rotational displacement of the foundation under monotonic loading when $M = M_{max}$
θ_T	rotation tolerance
θ_f	rotational displacement at the end of a cyclic test
$\tilde{\theta}_N$	normalised accumulated rotation
ζ_b	cyclic loading magnitude ratio, $\zeta_b = M_{max} / M_R$
ζ_c	cyclic loading ratio, $\zeta_c = M_{min} / M_{max}$
T_b, T_c, α	parameters of the empirical model

1. Introduction

To make offshore wind competitive in the energy market, cost-effective solutions for foundations and installation technologies must be developed. The monopod bucket foundation, given the right soil profile, can be a cost-reducing sub-structure for offshore wind turbines. This steel structure includes a bucket foundation and a conical shaft. The shaft is the interface between the support structure and the turbine tower. As opposed to monopile foundations, no transition piece is needed. The bucket foundation, known also as suction caisson, is a shallow skirted foundation with circular cross section of diameter, D and skirt length, d. This foundation concept has been adopted for decades in the oil and gas industry as an alternative to drilling or driving for anchoring mooring buoys (Senpere and Auvergne, 1982) or as a foundation for jackets (Bye et al., 1995). A picture of a monopod bucket foundation placed on the deck of an installation vessel is shown in Figure 1. This full-scale structure was installed at Dogger Bank, in the British Sector of the North Sea. The dimensions of this structure are: D = 15 m, d = 7.5 m and wall thickness, t = 30 mm.

The installation consists of two phases: first, the foundation penetrates the seabed for a few meters by its own weight; second, suction assisted penetration is carried out until the skirt is fully embedded. This installation technology prevents the generation of noises that can be harmful for marine mammals. Furthermore, such installation process can be fully reversed, ensuring the full recovery of the structure at the end of the lifetime. DNV (2011) states that repeated loading may lead to irreversible soil deformation (and thus irreversible foundation displacement) that could jeopardize the turbine operation. When designing in the serviceability limit states (SLS) or in the fatigue limit states (FLS), this is to be accounted for by calculating the cumulative displacement with an adequate method.

Figure 1: Large-scale monopod bucket foundation on the deck of a jackup vessel

Another important consequence of repeated loading is that it may lead to changes in the natural frequency of the system and, in the worst case, trigger resonance.
The offshore environment presents adverse loading conditions, *i.e.* large overturning moment, M, and horizontal load, H, due to the action of waves. The condition is worsened for offshore wind turbines as these are light structures with $M/(VD)$ typically larger than 1.

The drained and undrained response of shallow embedded foundations under general loading is widely explored in literature (Gourvenec, 2007; Villalobos et al., 2009, Barari et al. 2012, Achmus et al. 2013b, Ibsen et al., 2014a, Ibsen et al., 2014b). Andersen (2009) presents a framework to estimate the settlements of shallow foundations subjected to cyclic loading due to storms. A well-established method to predict the response of offshore foundations under long-term cyclic lateral loading (*i.e.* millions of load cycles) does not exist yet. Lately, many research contributions have been given to this issue. Numerical models of monopiles were developed by Achmus et al. (2009) and subsequently by Depina et al. (2013). Monopiles were also tested in single gravity physical models by Peralta (2010) and Taşan et al. (2011). Centrifuge modelling has also been attempted. Watson and Randolph (2006) carried out an experimental campaign testing a bucket foundation and deriving fatigue contours for few hundreds of cycles. More recently Klinkvort and Hededal (2013), Garnier (2013) and Kirkwood and Haigh (2014) run lateral cyclic loading centrifuge tests on monopiles. Achmus et al. (2013a) run numerical simulations of bucket foundations under cyclic loading investigating the effect of load magnitude, relative density and embedment ratio, d/D.
Comprehensive state of the art studies on cyclic loading of offshore foundations are Jardine et al. (2012), Randolph (2012) and Andersen et al. (2013).

This paper deals with the issues related to permanent displacements of bucket foundations engendered by cyclic loading. In particular, the accumulation of rotational displacement is addressed, as recommended by standards (DNV, 2011) and industry practice. A similar study on this issue has been conducted by Zhu et al. (2013). They performed tests on dry loose sand with a bucket of D = 200 mm, and d/D = 0.5 under two different vertical loads. The experimental data was interpreted with the empirical model proposed in LeBlanc et al. (2010) and the parameters of the model were found independent of the vertical load applied.
The main objective of this study is to generalise the method to buckets with three different embedment ratios. A comprehensive experimental campaign concerning bucket foundations subjected to lateral cyclic loading is presented. The physical model design is thoroughly described and the experimental results are interpreted. The effect of loading frequency and relative density on the pattern of response is addressed. The post-cyclic behaviour and the robustness of the foundation in terms of cyclic loading are also investigated. In order to add practical value to the study, cyclic capacity curves are constructed and used in a design case.

2. Physical model design

2.1 Scope and aims of the modelling

Conducting geotechnical experiments in 1g is a delicate issue and, when designing the experimental setup, all the choices must be choices of meaning. The geotechnical system taken as prototype to resemble in

small-scale experiments is a bucket foundation supporting a 5 MW wind turbine installed in dense silica sand. The diameter of the foundation is D = 15 m while the moment to horizontal load ratio is $M/(HD)$ = 2. The scale of the model is 1:50.

In general, when the results of small-scale experiments are to be scaled up, adequate scaling laws are required. In this work, rather than scaling up results directly to prototype scale, the intention is to capture general behavioural patterns of the foundation. To recreate similar responses in two different scales, non-dimensional groups are to be retained between small-scale and prototype-scale. Three simple dimensionless groups were considered in this study: $M/(HD)$, t/D and $V/(\gamma' D^3)$ where γ' is the effective unit weight of the sand and V is the vertical loading. In real-scale wind turbine structures V includes the self-weight of the foundation and the weight of the whole superstructure. A realistic ratio $V/(\gamma' D^3)$ for large-scale bucket foundations supporting wind turbines ranges between 0.1 and 1. The typical value of t/D lies in the range 0.002 – 0.003. As these groups were to be conserved, the physical model was designed accordingly. For the entire experimental campaign $M/(HD)$ was set to 1.98 while $V/(\gamma' D^3)$ was between 0.73 and 0.89, depending on the bucket tested. The non-dimensional group t/D was 0.005 for all the buckets. Although the latter exceeds the maximum value suggested by industry practice, it is deemed that this group would affect the model accuracy only in case of differences in order of magnitude.

Since the pore pressure development is not of primary interest in this study, the loading frequency was not scaled and only tests conducted in substantially drained conditions were interpreted with the empirical model. The drainage condition of the tests was evaluated on the base of the findings of Foglia et al. (2013) as explained further in the paper.

It is well-known that realistic shear strength of the soil in 1*g* models can be achieved by increasing the void ratio of the soil we would have in large-scale. In so doing the path toward the critical state line of the soil in small-scale would resemble that in large-scale and dilation would be suppressed (Cerato and Lutenegger, 2007, LeBlanc et al., 2010, Wood, 2004). However, here the aim is not to scale up the ultimate capacity and the stiffness of the monotonic behaviour. If serviceability and fatigue limit state design situations are investigated, the load magnitudes involved are limited and no dilation is likely to occur. Thus, it is argued that preparing the sand at very low D_r would result in samples more prone to disturbance and, more importantly, would lead to overly conservative results in terms of permanent displacements as a result of an unrealistic potential for compaction. For this reason, in an attempt to better capture the displacements accumulation, the relative density of the prototype-scale is conserved in small-scale. The samples were densely packed also to obtain general failure of the foundation and gain thereby a clear reference failure moment from the monotonic tests.

The aim of this experimental campaign was to extend the previous analysis of Zhu et al. (2013) by changing some essential features of the model. The novel analysis concerns buckets of three different bucket geometries, the effect of loading frequency and the post-cyclic behaviour. Besides, the soil sample is water saturated, densely packed and the foundations tested are 100 mm larger in diameter.

2.2 Description of the model

The experimental rig used to carry out the testing program was designed and constructed at Aalborg

University. The system was designed on the base of the rig employed by LeBlanc et al. (2010). A sketch of the equipment is illustrated in Figure 2. A sand box (1600 x 1600 x 1150 mm) and a loading frame are the main components of the setup. The sand box is made of steel and is equipped with a drainage layer at the bottom. The drainage system consists of perforated pipes, 100 mm of drainage material (gravel) and sheets of geotextile dividing the layers. The pipes let the water evenly within the sand container. The water is provided by a tank and the water gradient is regulated with valves. The loading frame surrounds the sand box and provides a firm support to the equipment for monotonic and cyclic loading. Two screw jacks are mounted on the sides of the loading frame, one for lateral monotonic loading and the other for the foundation installation. To apply cyclic loading to the foundations, the rig is integrated with a loading beam hinged on one side of the box, four pulleys, three weight-hangers, few meters of steel wire and additional steel frame. An electric motor capable of exerting constant rotational motion is mounted on the hinged beam. The cyclic loading is induced to the system by applying a rotational motion to weight-hanger 1 which in turn cause the hinged beam to oscillate in the vertical direction.

The foundation is subjected to cyclic loading through a vertical beam bolted on the bucket lid which is directly connected to the system with two wires, one on each side. The features of the cyclic loading applied can be adjusted by changing the set of weights on the weight-hangers. Three foundations with diameter, D = 300 mm, and embedment ratios equals to 1, 0.75 and 0.5, were tested. Throughout the paper the buckets will be addressed by using their embedment ratio (d/D = 1, d/D = 0.75 and d/D = 0.5). The skirts of the foundations have all the same wall thickness, t = 1.5 mm. This particular thickness was chosen in order to ensure a fully rigid response of the foundations during any loading phase. The foundations are instrumented with three linear variable differential transformers (LVDTs). Two load cells are mounted on the vertical bar to record the net load applied to the foundation. A PC-based data acquisition system is used to transfer data from the measurement devices to the computer. The data sampling frequency is set to 2 Hz. The soil used for conducting the experimental program is Aalborg University Sand No. 1 (*cf.* Table 1 for properties). The reference system taken for forces and displacements is that proposed by Butterfield et al. (1997).

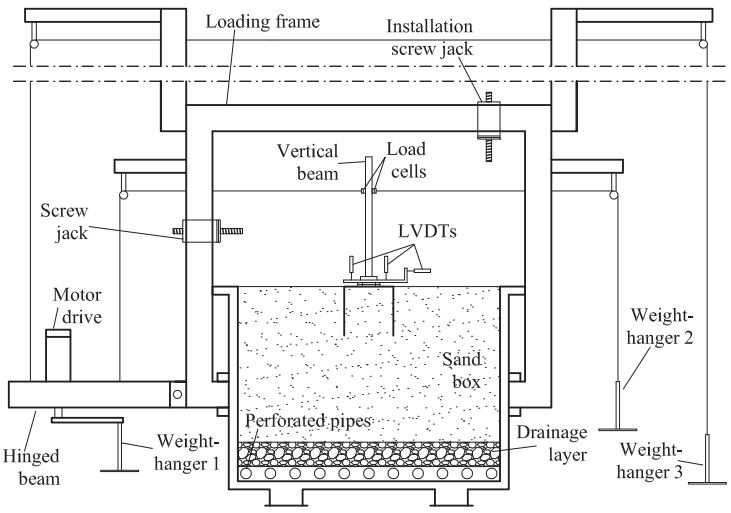

Figure 2: Schematic illustration of the testing rig

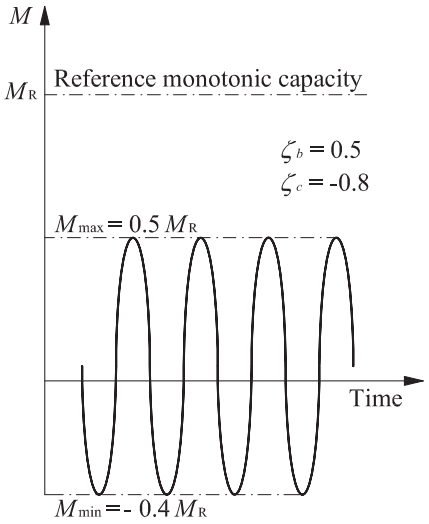

Figure 3: Example of biased two-way cyclic loading

Each cyclic test was carried out in four stages: sample preparation, installation, cyclic loading test and post-cyclic monotonic test. To ensure repeatability, a systematic sample preparation procedure was carried out before each test. A gradient close to the critical one was applied to the sample. Thereafter, mechanical vibration of the sand was performed. After vibrating, the uniformity and the compaction state of the sample were assessed by analysing small-scale cone penetration tests (CPT) performed in three different positions. The sample had a high compaction state, average D_r = 89 %. The bucket was installed in the middle of the sand box by means of a screw jack with a penetration rate of 0.02 mm/s. The foundation was installed by pushing rather than by applying suction. This has certainly an effect on the foundation capacity (Villalobos, 2006). However, the potential for rotational displacement accumulation should not be significantly affected as it is normalised with the monotonic reference rotation (see the next section).

Three air valves placed on the lid were let open during the penetration. Once the installation stage was complete, the installation rig was dismantled and the air valves were sealed to ensure full contact between soil and bottom lid during the test. The vertical beam was then bolted on the bucket lid and connected to the system. The number of cycles applied was between $1 \cdot 10^4$ and $5 \cdot 10^4$. At the end of the cyclic stage the cyclic equipment was meticulously substituted with the monotonic one to run the post-cyclic test. Cyclic loading tests were load-controlled. With respect to the load reference point the foundation was subjected to sinusoidal cyclic horizontal load, $H_{\min} \leq H \leq H_{\max}$, sinusoidal cyclic overturning moment, $M_{\min} \leq M \leq M_{\max}$, and constant vertical load, V (self-weight of the foundation and weight of the vertical beam).

The reference monotonic tests were controlled by designating a displacement rate to the point of load application. Foglia et al. (2013) conducted test of bucket foundations controlled in the same manner. The foundations were instrumented with eight pore pressure transducers placed under the lid and along the skirt. Four different displacement rates were tested. Tests carried out with displacement rate in the range 0.01 – 0.1 mm/s were found to be in substantially drained conditions. Based on this finding, the reference monotonic experiments were designed as displacement-controlled quasi-static tests with a displacement rate imposed by the actuator of 0.011 mm/s.

Table 1. Properties of Aalborg University Sand No. 1

Property	Value	Unit
Grain diameter corresponding to 50 % passing	0.14	[mm]
Uniformity coefficient	1.78	[-]
Specific grain density	2.64	[-]
Maximum dry unit weight	17.03	[kN/m^3]
Minimum dry unit weight	14.19	[kN/m^3]

2.3 Experimental program

Before describing all the phases of the experimental program, it is necessary to outline the key elements of the empirical model used to analyse the data (LeBlanc et al., 2010). The object of the empirical model is the relationship between the normalised accumulated rotation, $\tilde{\theta}_{\mathrm{N}}$, and the number of cycle N:

$$\tilde{\theta}_{\mathrm{N}} = \frac{\theta_{\mathrm{N}} - \theta_0}{\theta_{\mathrm{s}}} = T_b(\zeta_b, R_d) T_c(\zeta_c) N^{\alpha} \quad (1)$$

where θ_{N} is the accumulated rotation at cycle of number N, θ_0 is the rotation at the first cycle, θ_{s} is the rotation of the monotonic test at $M = M_{\max}$ and T_b, T_c and α are the parameters of the model. T_b and T_c depend on the cyclic loading features ζ_b and ζ_c which are defined as follows:

$$\zeta_b = \frac{M_{\max}}{M_{\min}}, \zeta_c = \frac{M_{\min}}{M_{\mathrm{R}}} \quad (2)$$

A graphical representation of the two ratios is given in Figure 3.

The model is defined by means of the boundary condition T_c (ζ_c = 0) = 1.

The experimental campaign comprises seven test series. Each of them was conducted with clear intention and with great attention to details. Table 2 (see at the end of the paper), lists all the tests of the experimental campaign.

In Series 1, 5 and 6, ζ_c was set to 0 and thereby the parameters T_b could be deduced for the three buckets. In Series 2, ζ_b was set to approximately 0.37 to obtain the parameter T_c. In Series 3 the robustness of the foundation against cyclic loading was addressed by conducting tests at increasing ζ_b. Series 4 was devoted to investigate the influence of the loading frequency on the cyclic behaviour. Series 0 includes the three monotonic reference tests.

Technical problems denied the post-cyclic stages of C47 and C39 to be performed.

3. Results

3.1 Presentation of typical results

Selected results are presented in order to give an insight into the general behavioural patterns of bucket foundations under lateral cyclic loading. It is common practice to present the results of small-scale experiments in non-dimensional form. However, in this section qualitative and scaling-independent results are shown. Thus, it was deliberately chosen to present the results without scaling.

Figure 4 shows how the rotational displacement accumulates for two tests and a magnified view of few cycles. Even though cyclic amplitude and mean value are very dissimilar in magnitude, the accumulation rate appears fairly comparable. In Figure 5, the three monotonic reference tests are plotted. Test S30 developed a clear general failure mechanism, with a noticeable peak in moment capacity followed by a softening branch. Tests S57 and S48, did not show a distinct peak in moment capacity. Instead, a plateau followed by a moderate negative gradient took place. Although the relative density is very high, the general failure of the system occurs only for the foundation with the largest embedment ratio. This kind of response could be seen in analogy with the findings of Vesić (1973), who investigated how the failure mechanism of shallow foundations under pure vertical loading changes as a function of D_r and d/D. M_{R} was taken as the maximum moment reached during the test. In the same graph, the points corresponding to the first cycle of all the cyclic tests of d/D = 1 are depicted. All the points, except for those of the two tests with highest moment (C39 and C40), lie along the monotonic curve. This proves the substantially drained condition of these tests. The two tests that deviate from the monotonic test had most likely too high loading rate to remain substantially

drained. Though, it should be emphasised that the tests which underwent partly drained conditions are not taken into consideration when interpreting the data with the empirical model.

It is worth to notice that also the tests conducted at different loading frequencies (squares on Figure 5) follow the fully drained response. Even further in the tests, no significant and consistent alteration of the behaviour in terms of displacements was found between the tests of Series 4.

In Figure 6, the rate of displacement accumulation in terms of rotation (*i.e.* the permanent rotation accumulated every ten cycles, θ_{N+10} - θ_N) is plotted against N for three tests of series 2. In general, when the rate of accumulation grows with the number of cycles, cyclic progressive failure occurs. This is not the case for the tests shown in Figure 6. The plot shows a significant rotational displacement accumulation within the first hundreds of cycles, followed by a plastic adaptation in which the rate of accumulation gradually decreases until reaching a negligible value. As expected, the larger the ζ_b the more number of cycles are required for the accumulation rate to reduce.

In Figure 7, the ultimate post-cyclic moment against the rotation at failure of all the tests of d/D = 1 is plotted. The large majority of the points exceeds the reference moment (test S30). On average, the post-cyclic capacity is 10.5 % larger than the reference capacity.

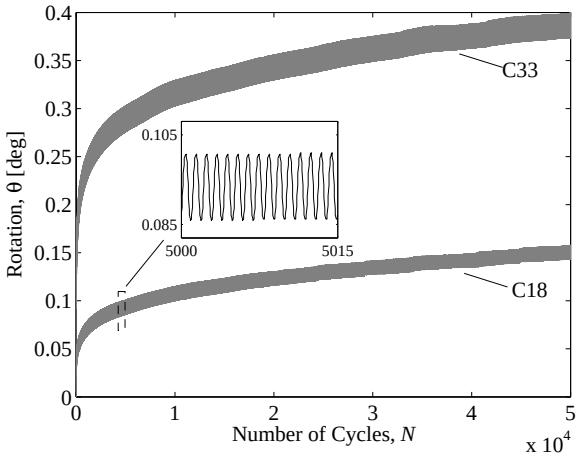

Figure 4: Rotational displacement accumulation for two different tests and magnified view of few cycles

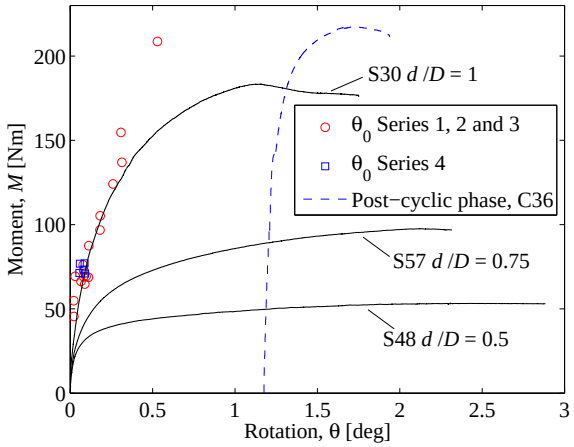

Figure 5: Reference monotonic tests S30, S48 and S57, post-cyclic phase of C36 and points relative to the maximum rotation of the first cycle

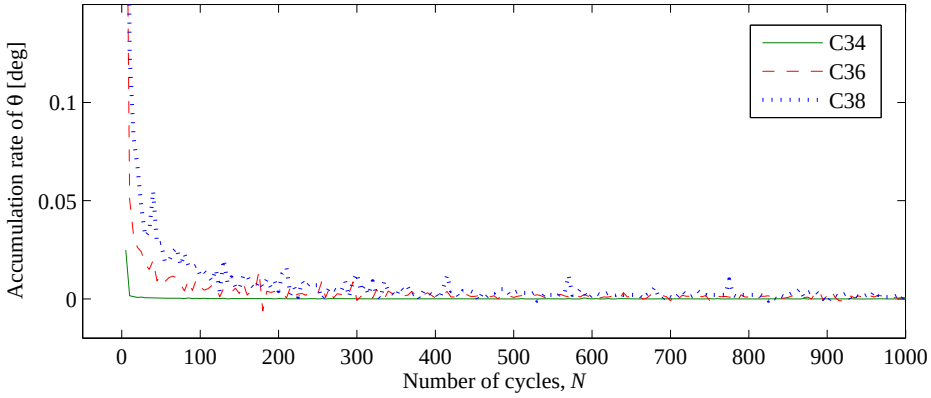

Figure 6: Accumulation rate of the rotational displacement of tests C34, C36 and C38 for the first 1000 cycles

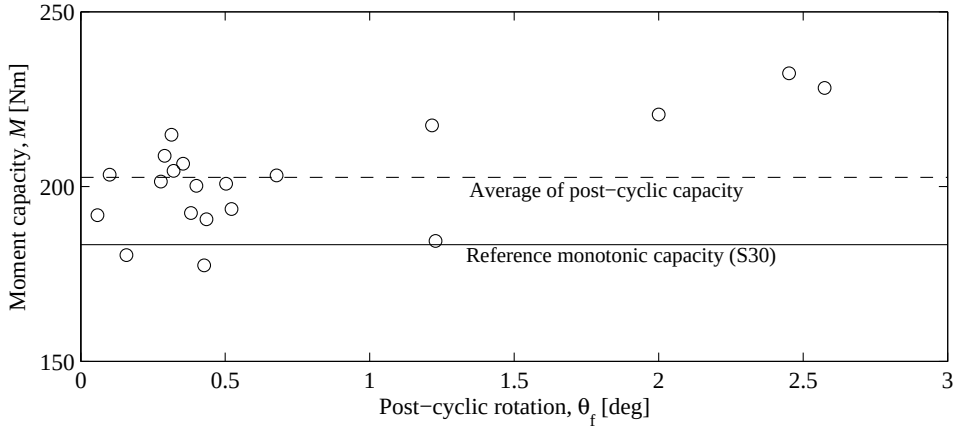

Figure 7: Post-cyclic moment capacity for series 1, 2 ,3 and 4 compared to the monotonic capacity

The same observation can be made in Figure 5 on the *M*-θplane where the post-cyclic phase of test C36 is plotted. The post-cyclic curve has higher initial stiffness and capacity than the reference monotonic curve. The failure mechanism is brittle as for the monotonic test.

3.2 Interpretation of the results

Equation 1 is used to fit all the tests run in substantially drained conditions. In general, the exponent α has the tendency to reduce as *T* increases. This suggests that when a foundation system accumulated significant rotational displacement in the beginning, it has less potential for accumulation further in the test. This is in accordance to what pointed out by Achmus et al. (2013a) where the ratio θ_N/θ_0 was found to have a higher rate for low values of ζ_b. A clear dependency of α on the test features could not be detected and, therefore, a constant exponent was used to analyse the data. When fitting all the drained tests until *N* = 10000 with Eq. (1), the average α turns out to be 0.189 with a standard deviation of 0.034. The value of α differs significantly from that of Zhu et al. (2013) and this is to be ascribed to the different relative density of the sands.

The results of series 1, 5 and 6 are presented in Figure 8. The points extrapolated using three different bucket geometries seem to follow the same trend. This indicates that the parameter T_b does not depend on the embedment ratio. This observation contrasts with Achmus et al. (2013b) who found the accumulated rotation to be slightly higher for *d*/*D* = 0.5. An interpolating curve in the form of a power law was chosen to fit the data:

$$T_b = 2.41\zeta_b^{1.64} \tag{3}$$

In Figure 8, the fit proposed by Zhu et al. (2013) is also plotted. The discrepancy between the two trends proves the T_b-dependency on the relative density. The same pattern (*i.e.* T_b reducing for looser compaction states) was found by LeBlanc et al. (2010). Recently, T_b was found dependent on the particle size in a study conducted by Abadie and Byrne (2014). However, the uncoupled effect of these two properties of the system has not been identified yet. The experimental points of series 2, together with the fit deduced by Zhu et al. (2013), are shown in Figure 9.

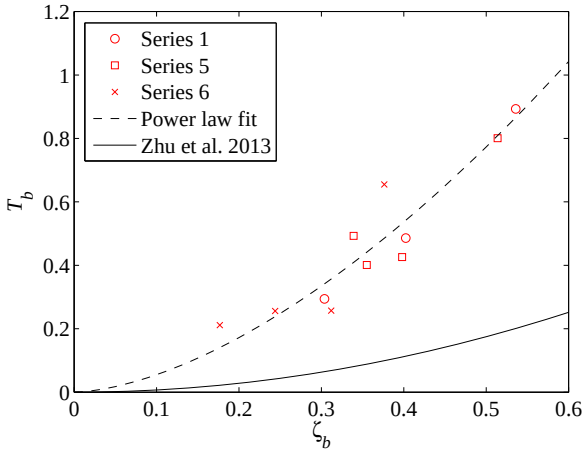

Figure 8: T_b parameter: Zhu et al., 2013, experimental points of this work and relative fit

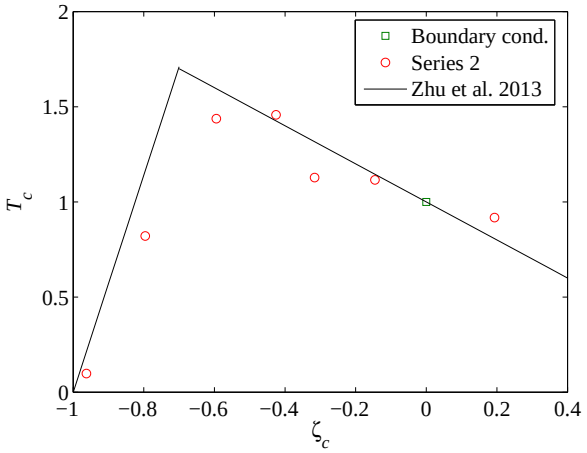

Figure 9: T_c parameter: Zhu et al., 2013 and experimental points of this work

Despite the significantly different embedment ratio and relative density, the experimental points match the fit. It can be concluded that T_c depends neither on the embedment ratio, nor on the relative density. The tests of Series 2 also support the idea that T_c peaks in correspondence to a biased two-way loading configuration. Interestingly, Kirkwood and Haigh (2014) attributed this phenomenon to the reduction of locked in stresses occurring in presence of biased two-way loading conditions.

4. Implication to foundation design

From the observations on the post-cyclic behaviour (Figure 5 and Figure 7) two distinct implications emerge. Firstly, since the foundation was pre-subjected to cyclic M and H the yielding surface expanded and therefore it is not surprising that the initial stiffness increases. Secondly, and perhaps more importantly, the failure envelope seems to increase when a foundation is pre-subjected to cyclic loading.

In the following, an example of how to put into practice the empirical model is given. As explained earlier in the paper, no direct result of the tests is scaled up by means of scaling laws. Instead, it is assumed that when the dimensionless groups of large-scale systems are similar to those used in the experimental campaign, the general relationship found in small-scale between monotonic and cyclic response is applicable in large-scale.

The example consists in a preliminary estimation of the long-term accumulated rotation of a bucket foundation supporting a 5 MW wind turbine. The estimation is preliminary in the sense that it is based only on the empirical model which would need to be validated against real-scale measurements over many years of turbine operation. As substantially drained conditions are considered, it is reasonable to assume $\theta_0 = \theta_s$.

The features of the bucket foundation are D = 15 m, d/D = 0.75 and t = 30 mm. The foundation is subjected to general loading: constant vertical loading, V = 35 MN, cyclic overturning moment and cyclic horizontal loading. A one-way loading configuration (ζ_c = 0) is chosen and the analysis evaluates both SLS and FLS design cases. According to LeBlanc et al. (2010), typical design cases for offshore wind turbines are for SLS, $N = 10^2$ and $\zeta_b = 0.473$, whereas for FLS, $N = 10^7$ and $\zeta_b = 0.295$.

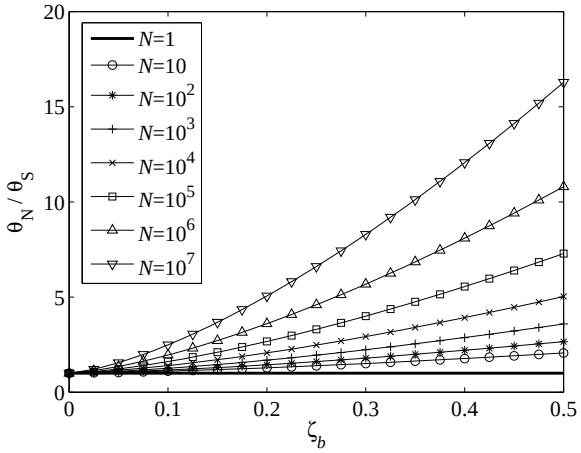

Figure 10: Normalised accumulated rotation as a function of the number of cycles and ζ_b

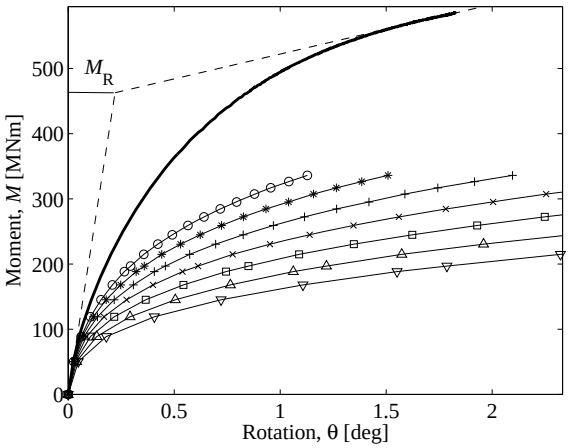

Figure 11: Cyclic capacity curves as opposed to monotonic capacity curves

By simply combining Equations 1 and 3 the accumulated rotation as a function of loading configuration and number of cycle can be evaluated:

$$\frac{\theta_N}{\theta_s} = 1 + \left(2.41\zeta_b^{1.64}\right) I_c N^{0.189} \tag{4}$$

A design graph relevant to the loading case in object, and based on Equation 4, is illustrated in Figure 10. To use Figure 10 in the design case, it is necessary to evaluate the monotonic $M - \theta$ curve in some manner. For this purpose, a drained numerical simulation is performed with the software Plaxis 3D. The Hardening Soil Model is used to run the drained simulation. Typical dense silica sand parameters are adopted. The ultimate moment capacity is defined by the intersection between the tangents to the initial and final points of the curve (M_R = 462.74 MNm). Equation 4 can be used to estimate the accumulated displacements for SLS design, $\theta_{N,\ SLS}$ = 0.506, and FLS design $\theta_{N,\ FLS}$ = 0.749. Some authors adopt a very stringent 0.5º as maximum rotation criterion justifying such a choice as the limit recommended by DNV (2011). However, DNV (2011) suggests this value in the context of a mere example and, in some cases, this stringent limit might lead to over-conservative design. The rotation tolerance relative to the normal operation of the wind turbine should instead be defined by the turbine manufacturer and the contractors on a case by case basis.

In order to have a graphical understanding of the secant stiffness degradation due to repeated loading, cyclic capacity curves can be constructed on the base of Equation 4 and the monotonic M-θ curve. This can be accomplished by simply calculating θ_N for different values of N and ζ_b. The cyclic capacity curves are plotted in Figure 11 as opposed to the monotonic curve. The legend of Figure 10 applies also to Figure 11. By entering the graph with the appropriate N and ζ_b, $\theta_{N,\ SLS}$ and $\theta_{N,\ FLS}$ can be graphically found.

5. Limitations of the physical model

The lateral cyclic loading is applied in terms of sinusoidal and continuous M and H.

In reality, environmental loads do not fluctuate regularly about a mean value. Imposing sinusoidal M

and *H* on the foundation is, in fact, unrealistic and leads inevitably to conservative prediction of displacements (Byrne, 2000). If realistic displacements are to be predicted, a relationship between real wave load patterns and equivalent sinusoidal load should be established.

Offshore environment is featured by a combination of waves, wind and currents, that results in a multi-directional load configuration (Fraunhofer IWES, 2009). Regardless, the geotechnical system considered in this paper has three degrees of freedom and the three loading components act in a single plane. Interestingly, Rudolph et al. (2014) investigated the cyclic behaviour of monopiles subjected to changing direction cyclic loading and found an amplification factor of 45% in 1*g* tests and 63% in centrifuge. In-plane loading conditions seem to have a beneficial effect on the accumulated displacements and therefore reduce the conservatism of the model.

In addition, the simplified method proposed does not account for the varying loading features of the cyclic load. However, this is important when real load time series are considered. In case a more sophisticated estimation of the accumulated displacements is needed, loading packages with different loading features could be included in the model, perhaps on the base of previous studies such as Peralta (2010) and LeBlanc et al. (2010b).

The empirical model is based on 1*g* tests only. Thus, it should be corroborated with centrifuge experiments or large-scale tests before using it with confidence in real design cases.

6. Conclusions

Bucket foundations have been extensively used and yet their behaviour under cyclic lateral loading is not fully explored. This paper presents a physical model and a comprehensive experimental campaign. The data analysis is focused on the long-term accumulated displacement and, particularly, on the rotational displacement. Some conclusions can be drawn about the general response of bucket foundations under cyclic loading.

The accumulation rate of the rotational displacement (calculated every ten cycles) is seen to reduce to negligible values within the first few hundreds of cycles, regardless of the load magnitude. The permanent displacement is not influenced by the loading frequency in the range tested (between 0.025 and 0.1 Hz). Post-cyclic curves are found different from the pure monotonic curves in terms of initial stiffness and ultimate capacity. This implies that, as expected, cyclic loading-induced permanent displacements affect the elasto-plastic proprieties of the geotechnical system.

The experimental data is also interpreted with an existing empirical model and new parameters are extrapolated. It is remarkably important to emphasise that the three bucket geometries tested seem to respond equally to cyclic loading. This means that, in the range of embedment ratio tested (0.5, 0.75 and 1) all the bucket geometries are equally influenced by cyclic loading. On the base of the empirical model, cyclic capacity curves are constructed and employed in a practical example.

Table 2. List of the experiments

Series 0	d/D	fL [Hz]	ζ_b	ζ_c
S30	1	-	-	-
S57	0.5	-	-	-
S48	0.75	-	-	-
Series 1				
C16	1	0.1	0.403	-0.047
C17	1	0.1	0.536	0.027
C18	1	0.1	0.304	-0.042
Series 2				
C20	1	0.1	0.358	-0.595
C22	1	0.1	0.383	0.193
C23	1	0.1	0.381	-0.426
C24	1	0.1	0.367	-0.963
C32	1	0.1	0.421	-0.146
C33	1	0.1	0.382	-0.316
C47	1	0.1	0.378	-0.796
Series 3				
C34	1	0.1	0.252	-0.604
C35	1	0.1	0.484	-0.543
C36	1	0.1	0.583	-0.563
C37	1	0.1	0.687	-0.578
C38	1	0.1	0.758	-0.583
C39	1	0.1	0.856	-0.588
C40	1	0.1	1.155	-0.469
Series 4				
C41	1	0.1	0.400	-0.514
C42	1	0.05	0.420	-0.500
C44	1	0.03	0.389	-0.598
C45	1	0.2	0.387	-0.479
C46	1	0.025	0.419	-0.500
Series 5				
C50	0.5	0.1	0.355	-0.054
C53	0.5	0.1	0.514	-0.049
C54	0.5	0.1	0.339	0.019
C55	0.5	0.1	0.398	0.040
Series 6				
C58	0.75	0.1	0.177	0.089
C59	0.75	0.1	0.244	0.055
C60	0.75	0.1	0.312	-0.055
C61	0.75	0.1	0.376	-0.053

References

Abadie CN and Byrne BW (2014) Cyclic loading response of monopile foundations in cohesionless soils. In *Proceedings of the 8th International Conference of Physical Modelling in Geotechnics (ICPMG)* (Gaudin C and White DJ (eds)). Taylor & Francis Group, London, UK, pp. 779-784.

Achmus M, Kuo Y-S and Abdel-Rahman K (2009) Behavior of monopile foundations under cyclic lateral load. *Computer and Geotechnics* **36(5)**: 725-735, http://dx.doi.org/10.1016/j.compgeo.2008.12.003

Achmus M, Thieken K, Akdag CT, Schröder C and Spohn C (2013a) Load bearing behaviour of bucket foundations in sand. In *Proceedings of the 3rd International Symposium on Computational Geomechanics (ComGeoIII)*, Krakow, Poland.

Achmus M, Akdag CT and Thieken K (2013b) Load-bearing behavior of suction bucket foundations in sand. Applied Ocean Research **43**: 157-165, http://dx.doi.org/10.1016/j.apor.2013.09.001

Andersen KH (2009) Bearing capacity under cyclic loading – offshore, along the coast, and on land. The 21st Bjerrum Lecture presented in Oslo, 23 November 2007. *Canadian Geotechnical Journal* **46(5)**: 513-535, http://dx.doi.org/10.1139/T09-003

Andersen KH, Puech AA and Jardine RJ (2013) Cyclic resistant geotechnical design and parameters selection for offshore engineering and other applications. In *Proceedings of TC 209 Workshop – Design for cyclic loading: piles and other foundations* (*ISSMGE)*, Paris, France, pp. 9-43.

Barari A and Ibsen LB (2012) Undrained response of bucket foundations to moment loading. *Applied ocean research* **36**: 12-21*,* http://dx.doi.org/10.1016/j.apor.2012.01.003

Butterfield R, Houlsby GT and Gottardi G (1997) Standardised sign conventions and notation for generally loaded foundations. *Géotechnique* **47(5)**: 1051-1054*,* http://dx.doi.org/10.1680/geot.1997.47.5.1051

Bye A, Erbrich C, Rognlien B and Tjelta TI (1995) Geotechnical design of bucket foundations. In *Proceedings of the Offshore Technology Conference (OTC)*, Houston, Texas, pp. 869-883.

Byrne BW (2010) *Investigations of suction caissons in dense sand*. Ph.D thesis, Oxford University, UK.

Cerato AB and Lutenegger AJ (2007) Scale effects of shallow foundation bearing capacity on granular material. *Journal of Geotechnical and Geoenvironmental Engineering* **133(10)**: 1192-1202, http://dx.doi.org/10.1061/(ASCE)1090-0241(2007)133:10(1192)

Depina I, Le TMH, Eiksund G and Benz T (2013) Cyclic behaviour of laterally loaded piles in soils with variable properties. In *Proceeding of the Twenty-third International Offshore and Polar Engineering (ISOPE)*, Anchorage, Alaska, USA, pp. 583-588.

DNV (Det Norske Veritas) (2011) DNV-OS-J101: Offshore standard: design of offshore wind turbine structures. DNV, Oslo, Norway.

Fraunhofer IWES (2010) Wind energy report Germany 2009 – Offshore. Fraunhofer IWES, Fassel, Germany.

Foglia A, Ibsen LB, Nielsen SK and Mikalauskas, L (2013). A preliminary study on bucket foundations under transient lateral loading. In *Proceeding of the Twenty-third International Offshore and Polar Engineering (ISOPE)*, Anchorage, Alaska, USA, pp. 465-471.

Garnier J (2013) Advances in lateral cyclic pile design: Contribution of the SOLCYP project. In *Proceedings of TC 209 Workshop – Design for cyclic loading: piles and other foundations (ISSMGE)*, Paris, France, pp. 59-68.

Gourvenec S (2007) Failure envelopes for offshore shallow foundations under general loading. *Géotechnique* **57(9)**: 715-728, http://dx.doi.org/10.1680/geot.2007.57.9.715

Ibsen LB, Barari A and Larsen KA (2014a) Adaptive plasticity model for bucket foundations. *ASCE Journal of Engineering Mechanics* **140(2)**: 361-373, http://dx.doi.org/10.1061/(ASCE)EM.1943-7889.0000633

Ibsen LB, Larsen KA and Barari A (2014b) Calibration of failure criteria for bucket foundations on drained sand under general loading. *Journal of Geotechnical and Geoenvironmental Engineering* **140(2)**, http://dx.doi.org/10.1061/(ASCE)GT.1943-5606.0000995

Jardine RJ, Andersen K and Puech A (2012) Cyclic loading of offshore piles: potential effects and practical design. Keynote Paper of the *7th International Conference on Offshore Site Investigations and Geotechnics*, Society for Underwater Technology, London, UK, pp. 59-100.

Kirkwood PB and Haigh SK (2014) Centrifuge testing of monopiles subject to cyclic lateral loading. In *Proceedings of the 8th International Conference of Physical Modelling in Geotechnics (ICPMG)* (Gaudin C and White DJ (eds)). Taylor & Francis Group, London, UK, pp. 827-831.

Klinkvort RT and Hededal O (2013). Lateral response of monopile supporting an offshore wind turbine. *Geotechnical Engineering* **166(2)**: 147-158, http://dx.doi.org/10.1680/geng.12.00033

LeBlanc C, Byrne BW and Houlsby GT (2010a). Response of stiff piles in sand to long-term cyclic lateral loading. *Géotechnique* **60(2)**: 79:90, http://dx.doi.org/10.1680/geot.7.00196

LeBlanc C, Byrne BW and Houlsby GT (2010b). Response of stiff piles to random two-way lateral loading. *Géotechnique* **60(9)**: 715:721, http://dx.doi.org/10.1680/geot.09.T.011

Peralta KP (2010) *Investigations on the behaviour of large diameter piles under long-term lateral cyclic loading in cohesionless soil*. Ph.D thesis, Leibniz University, Germany.

Randolph MF (2012) Offshore design approaches and model tests for sub-failure cyclic loading of foundations. In *Mechanical Behaviour of Soils under Environmentally-Induced Cyclic Loading* (di Prisco C and Wood DM (eds)). Springer, New York, USA.

Rudolph C, Grabe J and Bienen B (2014) Response of monopiles under cyclic lateral loading with a varying loading direction. In *Proceedings of the 8th International Conference of Physical Modelling in Geotechnics (ICPMG)* (Gaudin C and White DJ (eds)). Taylor & Francis Group, London, UK, pp. 453-458.

Senpere D and Auvergne A (1982) Suction anchor piles – a proven alternative to driving or drilling. In *Proceedings of the Offshore Technology Conference (OTC)*, Houston, Texas, pp. 483-493.

Taşan HE, Rackwitz F and Savidis S (2011) Experimentelle untersuchungen zum verhalten von zyklisch horizontal belasteten monopiles. Bautechnik **88(2)**: 102-112, http://dx.doi.org/ 10.1002/bate.201110010

Vesić, A.S. (1973). Analysis of ultimate loads of shallow foundations. *Journal of the Soil Mechanics and Foundations Division,* American Society of Civil Engineers 99(1): 45-73.

Villalobos FA (2006) *Model testing of foundations for offshore wind turbines*. Ph.D thesis, Oxford University, UK.

Villalobos FA, Byrne BW and Houlsby GT (2009) An experimental study of the drained capacity of suction caisson foundations under monotonic loading for offshore applications. *Soils and foundations* **49(3)**: 477-488.

Watson PG and Randolph MF (2009) A centriguge study into cyclic loading of caisson foundations. In *Proceedings of the 6th International Conference of Physical Modelling in Geotechnics (ICPMG)* (Ng CWW et al. (eds)). Taylor & Francis Group, London, UK, pp. 693-700, http://dx.doi.org/10.1201/NOE0415415866.ch99

Wood DM (2004) Geotechnical Modelling. CRC Press.

Zhu B, Byrne BW and Houlsby GT (2013) Long-term lateral cyclic response of suction caisson foundations in sand. Journal of Geotechnical and Geoenvironmental Engineering **139(1)**: 73-83, http://dx.doi.org/10.1061/(ASCE)GT.1943-5606.0000738

Paper IV

Title:

Investigations on macro-element modelling of bucket foundations for offshore wind turbines

Authors:

Foglia, A., Govoni, L., Gottardi, G. and Ibsen L. B.

Year of publication:

2014

Published in:

Technical Memorandum No. 48, Department of Civil Engineering, Aalborg University.

A journal publication based on this Technical Memorandum can be found under:

Foglia, A., Gottardi, G., Govoni, L., Ibsen, L.B. (2015). Modelling the drained response of bucket foundations for offshore wind turbines under general monotonic and cyclic loading. *Applied Ocean Research* 52, 80-91.

Number of pages:

37

Investigations on macro-element modelling of bucket foundations for offshore wind turbines

Aligi Foglia[1], Laura Govoni[2], Guido Gottardi[2], Lars Bo Ibsen[1]

[1]Department of Civil Engineering, Aalborg University
[2]DICAM, University of Bologna

In this report a macro-element model for bucket foundations is formulated and validated against small-scale experimental results. The topics investigated are the response of the foundation under general monotonic loading and the long-term accumulated displacements under cyclic loading. The macro-model for shallow foundations proposed by Nova and Montrasio (1991) is modified to comply with the response of skirted foundations for offshore wind turbines under general loading. On the base of di Prisco et al. (2003a), the constitutive relationship is modified to account for cyclic loading. The validation of the macro-model against the physical experiments shows promising results.

1 Introduction

Offshore wind turbines (OWTs) are light and dynamically sensitive structures. This determines a unique loading condition which consists of large cyclic overturning moment M, relatively large cyclic horizontal load H and small vertical load V. The design of these structures is mostly driven by the dynamic properties of the system and by the long-term response under cyclic loading in terms of stiffness and accumulated displacements (Haigh, 2014). This report deals with

the substantially drained response of bucket foundations under monotonic and cyclic loading. More specifically, a macro-model to evaluate the response of bucket foundations supporting OWTs, is formulated. This chapter includes a literature review and a description of the contribution of the paper. The chapter "Physical modelling" presents the experiments used to calibrate the parameters of the model. The chapter "Analytical modelling" describes the analytical models used and shows comparisons with the experimental results.

1.1 Literature review

Through macro-element modelling, preliminary estimations of the response of a geotechnical system can be obtained. This technique is applicable to many kinds of geotechnical problems but its primary and best-known application is on shallow foundations. In Wood (2012) three different applications of macro-element modelling are thoroughly described. Generally speaking, a macro-model consists of three elements: geotechnical structure, surrounding soil and displacement or load field applied to the system, *cf.* Figure 1. For shallow foundations, the concept has perhaps its origin with Roscoe and Schofield (1956). During the last decades, the theory of plasticity has been employed by a number of researchers to investigate the response of shallow foundations under general loading. The main objective of these studies has been to overcome the traditional semi-empirical method to calculate the bearing capacity in favor of a new approach capable of capturing the non-linearity of the problem and suitable for numerical simulations. An early study on interaction diagrams is Butterfield and Ticof (1979). Subsequently, Nova and Montrasio (1991) derived a model for strip footing. Gottardi and Butterfield (1993, 1995) carried out important studies on shallow footings, addressing failure surfaces and displacement patterns under general planar loading. Martin (1994) conceived Model B for spudcans on clay. Gottardi et al. (1999) developed the basis for Model C (footings on sand) which was then completed by Houlsby and Cassidy (2002). Byrne and Houlsby (2001) extrap-

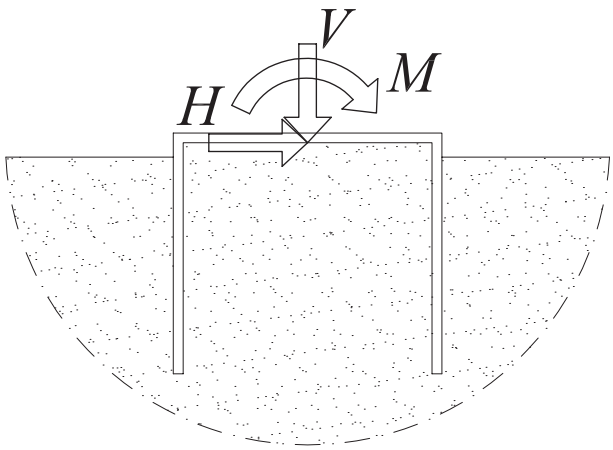

Figure 1: Fundamental macro-element components: foundation, surrounding soil and three-dimensional load field

olated the yielding surfaces for footings on carbonate sands. Bienen et al. (2006) explored the behaviour of footings in six degrees of freedom (6-DOF). To calibrate a macro-model, physical experiments are essential. Often, in order to extrapolate the necessary model parameters, loading paths that do not resemble possible real loading conditions must be carried out. 1g physical models have been by far used to obtain the model parameters. Recently, also centrifuge tests have been conducted on this purpose. To a large extend centrifuge data corroborated the findings of single gravity modelling (Govoni et al., 2011; Zhang et al., 2014).

Of current interest is cyclic macro-modelling. The majority of the studies on cyclic macro-modelling concerns structures under seismic excitations. In the last decade, many contributions have been given to this research topic. A comprehensive and very informative document on this theme is di Prisco (2012). Cremer et al. (2001) describe a macro-element formulation for a shallow foundation in plain strain. They suggest a multi-surface plasticity model and take into account the non-linearity of the material and the non-linearity due to the partial uplift of the footing. Chatzigogos et al. (2011) developed further the work of Cremer et al. (2001) and conceived a bounding surface hypoplastic model. Nguyen-Sy (2006) derived a hyperplastic model (Houlsby and Puzrin, 2007) and applied it to bucket foundations. di Prisco et al. (2003a,

2003b) integrated the Nova and Montrasio (1991) model with a boundary surface model to represent cyclic loading. An application of the latter is presented in di Prisco et al. (2006). Buscarnera et al. (2010) used the same model to calculate the accumulated displacement of onshore wind turbine on gravity based foundation under wind loading. Kafle and Wuttke (2013) slightly modified the model of Nova and Montrasio (1991) and di Prisco et al. (2003a) to predict the response of a footing on unsaturated soil. Salciarini and Tamagnini (2009) proposed a hypoplastic macrolement for surface footings. The same model was then expanded to 6-DOF in Tamagnini et al. (2013).

1.2 Outline of the study

The aim of this study is to show that experimental results of bucket foundations under monotonic and cyclic loading can be interpreted by means of a macro-element model. Prior to model the cyclic loading response, it is fundamental to have a reliable and consistent description of the monotonic behaviour. The model chosen for interpreting the monotonic experiments is the Nova and Montrasio (1991) model (NMM). This choice is driven by the possibility of modelling long-term cyclic loading as elucidated in di Prisco et al. (2003a, 2003b) and Buscarnera et al. (2010). In order to have satisfying match with the experimental data, the NMM is necessarily modified. A simplified version of the boundary surface model proposed by (di Prisco et al., 2003a) is incorporated into the modified NMM to model the cyclic loading response. The macro-model simulates satisfactorily the physical response. Particularly, the comparison with four experimental cyclic tests is encouraging and reveals that certain features of the cyclic behaviour can be replicated by the macro-model.

It should be said upfront that a rigorous extrapolation of the model parameters is beyond the scope of this work. Regardless, the results achieved are meaningful and clearly highlight the potential of the model.

2 Physical modelling

A large number of single gravity tests of bucket foundations were carried out at Aalborg University to explore the cyclic lateral response of the foundation in dense saturated sand (Foglia et al., 2014). Based on the experimental results, the empirical model predicting the long-term accumulated rotation proposed by LeBlanc et al. (2010) was calibrated for dense saturated sand and extended to three different embedment ratios, $d/D = 0.5$, $d/D = 0.75$ and $d/D = 1$ where d is the embedment length and D the diameter of the foundation. In this study a more sophisticated interpretation based on the macro-element philosophy is proposed. In this section a selected series of tests which are necessary to the model formulation is presented. Nine monotonic tests and four cyclic loading tests are chosen to extrapolate some of the model parameters and to validate the model. All the experiments are listed in Table 1 where M_{R} is the moment capacity and M_{max} and M_{min} are the maximum and the minimum moment applied in a cyclic loading test. Eight monotonic tests (S13, S19, S25, S26, S27, S28, S29 and S30) are constant V tests with five different $M/(HD)$ ratios. One monotonic test (S64) is a pure vertical loading test until failure. The cyclic loading tests are constant V tests with $M/(HD) = 1.987$. The three different loading paths are represented on the three two-dimensional load planes, $(M/D - V)$, $(M/D - H)$ and $(H - V)$, in Figure 2. The tests were conducted with two different rigs but with the same bucket foundation and on the same sand, Aalborg University Sand No. 1 (*cf.* Table 2 for the index properties of the sand). The bucket foundation tested is made of steel and has the following features: outer diameter, $D = 300$ mm, length of the skirt, $d = 300$ mm, wall thickness, $t = 1.5$ mm, lid thickness, $t_l = 11.5$ mm and self-weight, $W = 125$ N. The cyclic tests and all the monotonic tests except for S64, were conducted with the experimental rig described in detail in Foglia et al. (2014). The size of the sand sample is 1600 x 1600 x 1150 mm; a picture of the setup is shown in Figure 3.

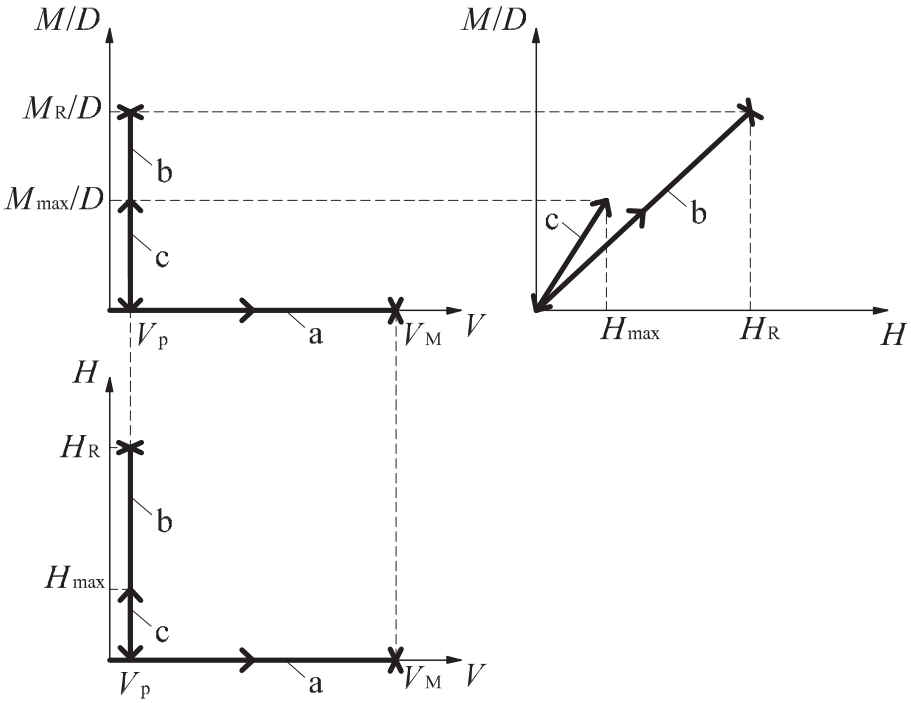

Figure 2: The three loading paths a, b and c on the three two-dimensional load planes: a) monotonic V test until failure; b) monotonic constant V test until failure, with constant $M/(HD)$; c) cyclic constant V test until failure, with constant $M/(HD)$

Table 1: Selected experimental tests for the model calibration and validation

Test name	$M/(HD)$ [-]	V [N]	M_{max}/M_R [-]	M_{min}/M_{max} [-]
S13	3.010	241	-	-
C16	1.987	241	0.403	-0.047
C18	1.987	241	0.299	-0.042
S19	1.987	241	-	-
C20	1.987	241	0.353	-0.595
S25	1.100	241	-	-
S26	5.820	241	-	-
S27	8.748	241	-	-
S28	5.819	241	-	-
S29	3.010	241	-	-
S30	1.987	241	-	-
S33	1.987	241	0.377	-0.316
S64	Pure vertical loading test			

Table 2: Index properties of Aalborg University sand No. 1

Property	Value	Unit
Grain diameter corresponding to 50% passing	0.14	[mm]
Uniformity coefficient	1.78	[-]
Specific grain density	2.64	[-]
Maximum void ratio	0.86	[-]
Minimum void ratio	0.55	[-]

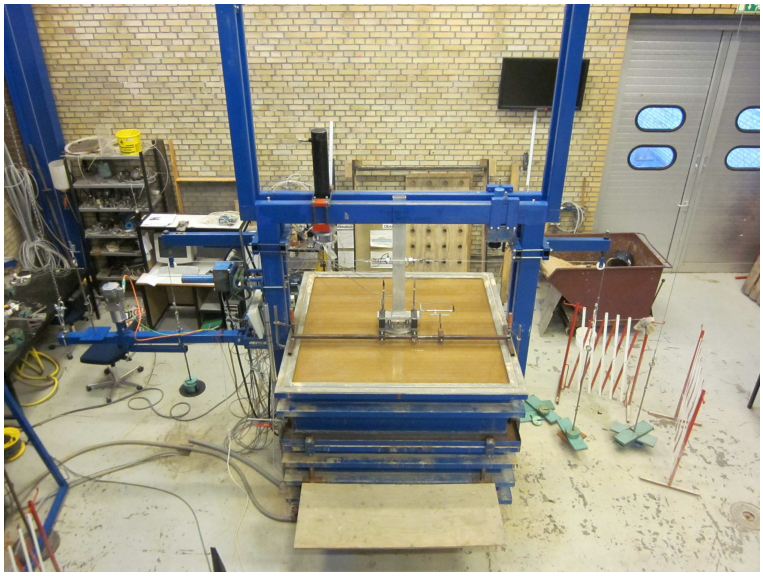

Figure 3: Picture of the experimental rig adopted to perform all the tests except for S64

The vertical load acting on the foundation during the tests includes the buoyant self-weight of the bucket and the weight of the measuring system mounted on the foundation. V is for each test equal to 241 N. The monotonic tests were displacement controlled tests until failure. One example of load-displacement curves for each $M/(HD)$ ratio is illustrated in Figure 4. The cyclic tests were load controlled with loading frequency $f_l = 0.1$ Hz and number of cycles $N = 5 \cdot 10^4$. Figures 5 and 6 depict the first 100 cycles of test C16.

A second testing rig, with a much more powerful actuator and a larger sand sample, was employed to run the pure vertical loading test until failure, test S64. This testing rig was designed to test bucket foundations with $D = 1000$ mm. A detailed description of the laboratory setup

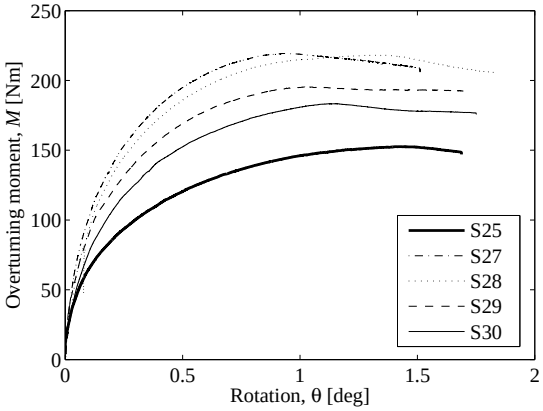

Figure 4: Example of monotonic tests, $M - \theta$ curves of 5 tests with different $M/(HD)$ ratio

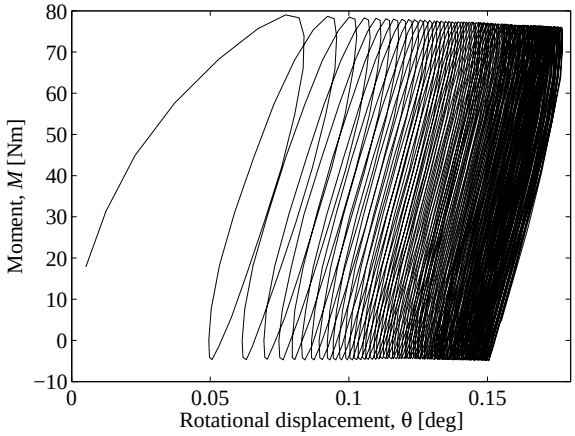

Figure 5: Experimental $M-\theta$ curve, test C16, first 100 cycles

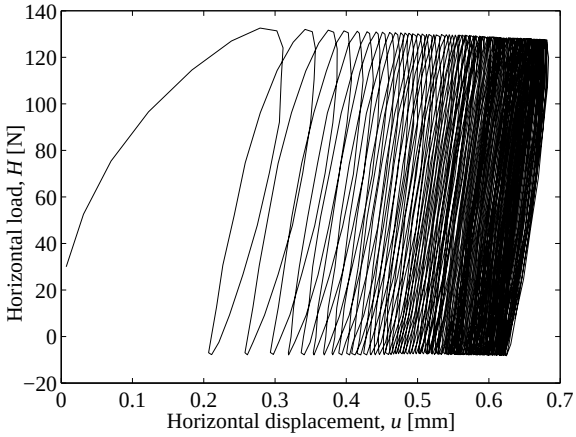

Figure 6: Experimental $H-u$ curve, test C16, first 100 cycles

is available in Vaitkunaite et al. (2014). In test S64, a local shear failure of the soil can be observed, *cf.* section 3.1.2.

The bearing capacity of the foundation is obtained as $V_{\mathrm{M}} = 91.66$ kN. Throughout the report a ratio $V/V_{\mathrm{M}} = 0.0026$ is used for the simulations and the interaction diagram comparisons. For both the laboratory setups, the sample was prepared by mechanical vibration of the soil. This technique allowed to have dense or very dense samples. The relative density D_r, is calculated by interpreting small scale cone penetration test data with an empirical correlation. The average

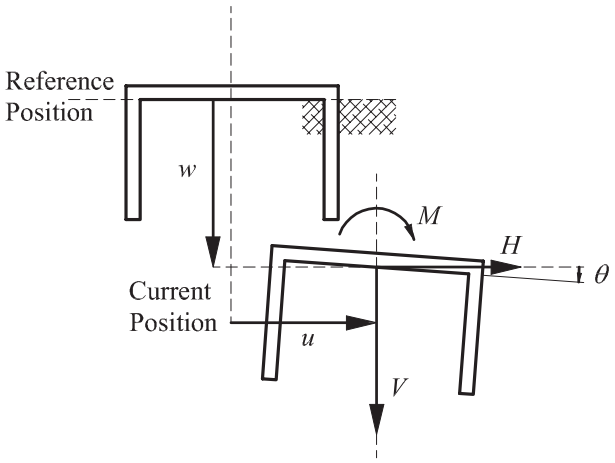

Figure 7: Sign conventions, after Butterfield et al. (1997)

D_r of the selected tests is 88.25%.

The sign convention for loads (V, H, M) and displacements (w, u, θ) is chosen according to the unified and consistent system proposed by Butterfield et al. (1997). Figure 7 depicts the sign conventions.

3 Analytical modelling

In this chapter the models used to interpret the experimental data are described. The calibration of some of the parameters is carried through on the base of the available experimental data. All assumptions and uncertainties are pointed out. Some points of discussion on the calibration of the parameters and on the model architecture are put forward.

3.1 Monotonic loading

3.1.1 Model architecture

The macro-element model of Nova and Montrasio (1991) is based on the classic framework of elasto-plasticity and was conceived to predict the mechanical response of a strip footing on a homogeneous soil layer under combined planar loading. The validity of the model was

then extended to different shallow foundations by Montrasio and Nova (1997), and to strip foundation under cyclic loading by di Prisco et al. (2003a). The model consists of five elements: elastic matrix, yielding surface, plastic potential, hardening law and flow rule. Following the rules of strain-hardening models the elements are combined to form the flexibility matrix $\boldsymbol{C}$, which relates the vector of normalised incremental displacements $d\boldsymbol{q}$, to the vector of normalised incremental forces $d\boldsymbol{Q}$:

$$d\boldsymbol{q} = \boldsymbol{C} d\boldsymbol{Q} \tag{1}$$

where $\boldsymbol{q}$ is the generalised vector of normalised displacements whereas $\boldsymbol{Q}$ is the generalised vector of normalised loads. $\boldsymbol{q}$ and $\boldsymbol{Q}$ are defined as:

$$\boldsymbol{q} = \begin{pmatrix} \eta \\ \varepsilon \\ \zeta \end{pmatrix} = V_{\mathrm{M}} \begin{pmatrix} w \\ \mu u \\ \psi D \theta \end{pmatrix} \tag{2}$$

$$\boldsymbol{Q} = \begin{pmatrix} \xi \\ h \\ m \end{pmatrix} = \frac{1}{V_{\mathrm{M}}} \begin{pmatrix} V \\ H/\mu \\ M/(\psi D) \end{pmatrix} \tag{3}$$

where μ and ψ are constitutive dimensionless parameters of the model.

Elasticity matrix The elasticity matrix, $\boldsymbol{K}_e$, is defined as:

$$\boldsymbol{K}_e = \mathrm{diag}(k_V, k_H, k_M) \tag{4}$$

Its elements are evaluated according to Doherty and Deeks (2003). To calculate the components of $\boldsymbol{K}_e$, an elastic modulus, $E = 25$ MPa, and a Poisson ratio, $\nu = 0.2$, are assumed.

Yielding surface The original yielding surface of the NMM is:

$$f = \left(\frac{H}{V_{\mathrm{M}}\mu}\right)^2 + \left(\frac{M}{D V_{\mathrm{M}} \psi}\right)^2 - \left(\frac{V}{V_{\mathrm{M}}}\right)^2 \left(1 - \frac{V}{V_{\mathrm{M}} \rho_c}\right)^{2\beta} \tag{5}$$

where ρ_c is the hardening parameter, V_{M} the bearing capacity of the foundation and β a constitutive parameter of the model. By substituting the load components according to eq. 3, eq. 5

becomes:

$$f = h^2 + m^2 - \xi^2 \left[1 - \left(\frac{\xi}{\rho_c}\right)\right]^{2\beta} \tag{6}$$

In the three-dimensional load space $(V - H - M/D)$ the yielding surface is an ellipsoid while in the three-dimensional normalised load space $(\xi - h - m)$ the yielding surface becomes a spheroid.

When using the strain-hardening plasticity frameworks it is typical to normalise the loads by V_0 which is the maximum vertical load ever applied to the foundation (Villalobos et al., 2009; Houlsby and Cassidy, 2002; Gottardi et al., 1999). This is apparently not the case in eq. 5. It should be clear though that $\rho_c = V_0/V_{\mathrm{M}}$ and, therefore, by simply substituting V_{M} with V_0/ρ_c, eq. 5 becomes normalised by V_0.

To include the contribution of the skirt to the resistance, eq. 5 is modified similarly to Villalobos et al. (2009):

$$f = \left(\frac{H}{V_{\mathrm{M}}\mu}\right)^2 + \left(\frac{M}{DV_{\mathrm{M}}\psi}\right)^2 - \left(\frac{V}{V_{\mathrm{M}}} + t_0\rho_c\right)^2 \left(1 - \frac{V}{V_{\mathrm{M}}\rho_c}\right)^{2\beta} \tag{7}$$

It is worth noting that by including t_0 in the formulation, the model has no longer a closed form solution.

Equation 7 differs from that of Villalobos et al. (2009) in three aspects. First, it is expressed by means of V_{M} and not V_0. Second, there is no term relative to the eccentricity of the surface in the $(H - M/D)$ load plane. The third and most substantial difference is that t_0 is not a function of V_0 and is defined as $V_{\mathrm{tM}}/V_{\mathrm{M}}$ where V_{tM} is the drained pull out resistance of the foundation.

V_{M} was found experimentally with test S64. To calculate V_{tM} a failure model in tension must be chosen. A pertinent failure model in tension is that in which the bucket foundation and the soil plug are involved in the pull out. As a result of that, the contributions of the pull out drained resistance are three: the buoyant weight of the foundation W'_{f}, the buoyant weight of the soil

plug W'_{p} and the tangential forces acting on the outer skirt. V_{tM} can then be expressed as follows:

$$V_{\mathrm{tM}} = 2\pi r_{\mathrm{o}} \int_0^d \tau_{\mathrm{o}} dx + W'_{\mathrm{f}} + W'_{\mathrm{p}} \tag{8}$$

where r_{o} is the outer radius of the foundation and τ_{o} is the shear stress along the wall. Obviously, V_{tM} (and thus t_0) is influenced by the choice of the soil-steel interface angle and the coefficient of lateral earth pressure. After scrupulous consideration and comparison with Villalobos (2006) a value of $t_0 = 0.007$ was taken. A more detailed discussion on t_0 is given in section 3.1.4.

The choice of using equation 7 is justified by the following observation. Standard dimensions of bucket foundations for real-scale OWTs are listed in Table 3 together with the load conditions suggested by Byrne (2013) and Lesny (2011). In Table 3, h is the load eccentricity, the subscripts "*w*" stands for waves and currents and the subscript "*wi*" stands for wind. To calculate the range of $M/(HD)$, the maximum M is divided by the minimum values of (HD) whereas the minimum M is divided by the maximum values of (HD). It should be mentioned though that most likely the real load paths will lie in the middle of the range and not in the region around the boundaries. In Figure 9 the loading path range for bucket foundations supporting OWTs is plotted together with the failure envelopes of Villalobos et al. (2009) and Nova and Montrasio (1991). To plot the envelope of Villalobos et al. (2009) the parameters of Ibsen et al. (2014), calibrated with small scale tests until failure, are adopted (except for t_0 which is set equal to 0.007). The parameters used to plot the envelope of the NMM are derived in section 3.1.2. In Figure 9 it is seen that in the sector of interest for OWTs the two envelopes give a fairly similar representation of the ultimate resistance. For the sake of completeness, it is worth to mention that the discrepancy between the two failure envelopes is exacerbated in the second quadrant. However, the load path is unlikely to lie on the second quadrant, unless V acts on the foundation with a large horizontal eccentricity.

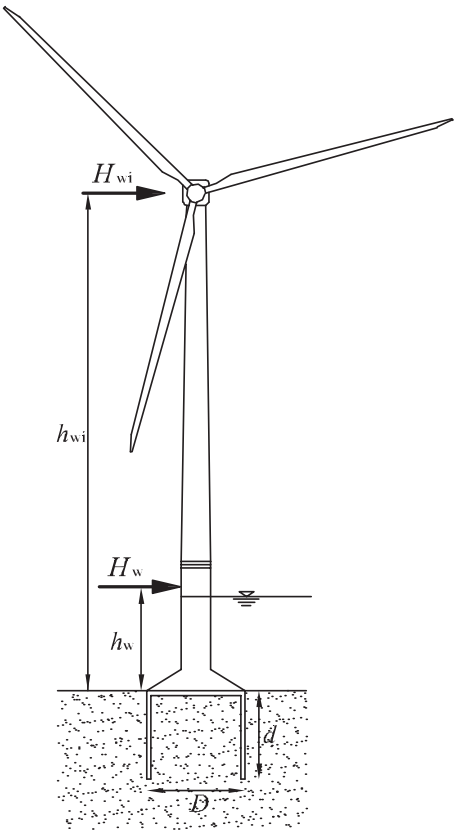

Figure 8: Sketch of an OWT

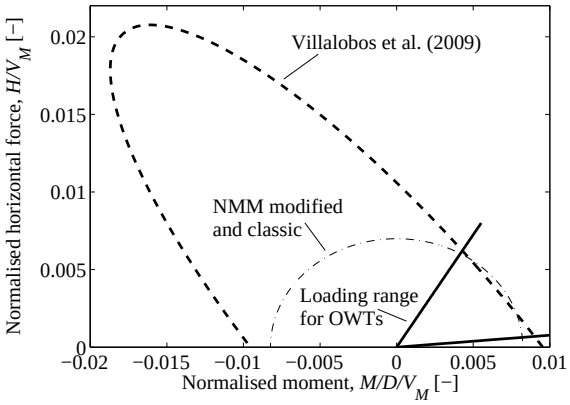

Figure 9: Benchmark of failure envelopes

Table 3: Range of features of a bucket foundation supporting a standard offshore wind turbine, (Byrne, 2011; Lesny, 2011)

Value	Unit	Maximum	Minimum
H_w	[MN]	10	3
H_{wi}	[MN]	2	1
h_w	[m]	40	20
h_{wi}	[m]	120	90
D	[m]	18	14
M	[MNm]	640	150
H	[MN]	12	4
V	[MN]	35	6
$M/(HD)$	[-]	11.43	0.69

Plastic potential In analogy with the yielding surface, the plastic potential differs from the original model only by the inclusion of the parameter t_0:

$$g = (\lambda h)^2 + (\chi m)^2 - (\xi + t_0\rho_g)^2 \left[1 - \left(\frac{\xi}{\rho_g}\right)\right]^{2\beta} \tag{9}$$

In eq. 9 ρ_g is a fictitious variable whereas λ and χ are constitutive dimensionless parameters.

Hardening law The hardening law is the rule by which the evolution of the hardening parameter, $d\rho_c$, is defined as a function of the increment of plastic displacements, $d\boldsymbol{q}_p$:

$$d\rho_c = (1-\rho_c)\frac{R_0}{V_{\mathrm{M}}}\left(d\eta + \frac{\alpha\,|d\varepsilon|}{\mu} + \frac{\gamma\,|d\zeta|}{\psi}\right) \tag{10}$$

In eq. 10, α and γ are constitutive dimensionless parameters while R_0 is the initial stiffness of the $V-w$ curve extrapolated in section 3.1.2. A discussion on the hardening law is proposed in section 3.1.5.

Flow rule The flow rule is consistent with the original model, and more generally, with the standard theory of plasticity. When the conditions $f=0$ and $df=0$ are fulfilled, the incremental plastic displacements $d\boldsymbol{q}_p$ can be expressed by:

$$d\boldsymbol{q}_p = \Lambda\frac{\partial g}{\partial \boldsymbol{Q}} \tag{11}$$

where Λ is the plastic multiplier.

3.1.2 Calibration of the modified NMM

Failure envelope (μ, ψ and β) The monotonic tests were run until failure of the geotechnical system. Thus, the yielding surface extrapolated is a failure surface ($\rho_c = 1$). Tests exploring the yielding surfaces were not possible with any of the experimental rig available. Hence, it is a fundamental assumption of the model that each and every yielding surface differs from the failure surface only in size, *i.e.* by the value of ρ_c. Moreover, to calibrate the failure envelope the variety of experiments was limited to only constant V tests with five different $M/(HD)$ ratios. This gives however sufficient information on the region of the load space ($V-H-M/D$) of interest for OWTs, *i.e.* V/V_{M} very close to the origin of the axes and loading paths with no change in V. The original (eqs. 5 and 6) and the modified (eq. 7) failure envelopes are calibrated with the same set of experimental data. Figure 10 shows two failure

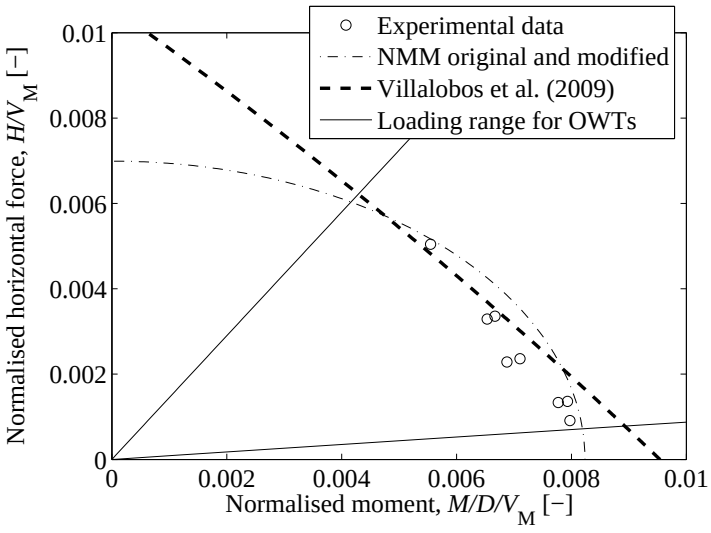

Figure 10: Calibration of the failure envelope of original and modified NMM on the base of experimental data

envelopes with the experimental points and the load range for OWTs in the normalised load plane ($H/V_{\mathrm{M}} - M/(DV_{\mathrm{M}})$) at $V/V_{\mathrm{M}} = 0.0026$. The two envelopes are that of Villalobos et al. (2009) with the parameters of Ibsen et al. (2014) and that of the modified NMM. The original NMM is calibrated in order to be equal to the modified NMM at $V/V_{\mathrm{M}} = 0.0026$. The purpose of that is to underline how essential the inclusion of t_0 is in the formulation of the model when trying to fit the experimental load-displacement curves with the two models, *cf.* section 3.1.3. Since the number of failure points is scarce, no best fit of the data is attempted. Rather, a conservative fit which encompasses all the experimental points is adopted. The parameter β is set equal to 0.95 as suggested in literature by Montrasio and Nova (1997). Appropriate values of μ and ψ for the modified yielding surface are 0.73 and 0.86 respectively.

$\mathbf{R_0}$ and $\mathbf{V_M}$ The bearing capacity of the foundation, V_{M}, and the initial vertical stiffness, R_0, can be extrapolated from the $V - w$ curve of test S64. Such curve is shown in Figure 11. The value of V at the end of the skirt penetration (point A in Figure 11) is the result of the

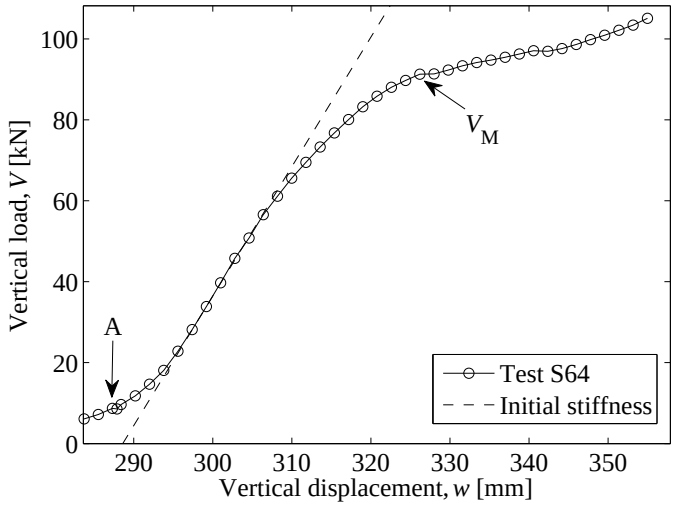

Figure 11: Experimental $V - w$ curve, and fit of the initial stiffness

reaction vertical forces due to tip end bearing and wall friction. By fitting with a straight line the initial points of the curve, R_0 is evaluated as 3202 kN/m. Strictly speaking, this value of R_0 is not accurate. To gain the exact value of R_0 the foundation should be unloaded as soon as full penetration is achieved and then re-loaded. During test S64 no unloading phase was performed after full penetration of the foundation. Nevertheless, the precision of R_0 is considered sufficient for the scope of the paper.

In Figure 11 a local shear failure of the soil can be observed in correspondence to an abrupt change in stiffness ($w = 326.2$ mm). V_{M} is taken equal to 91.66 kN.

α, γ, λ and χ As elucidated in Nova and Montrasio (1991), to calibrate the parameters of the potential and of the hardening rule, pure H and pure M tests are necessary. Although, when the load eccentricity ratio $M/(HD)$ exceeds a certain value, the behaviour of the foundation is no longer significantly affected by the increase of vertical eccentricity (see test S27 and S28 in Figure 4). This applies to both load-displacement curves and displacement trajectory curves. Evidence of such response is given in Figure 12, where the standard NMM with standard

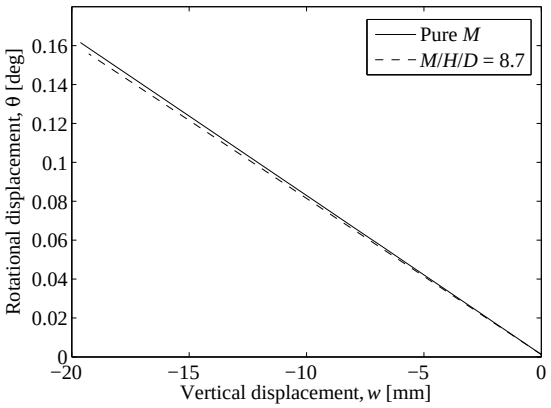

Figure 12: Displacement trajectory of a pure *M* test and a $M/(HD) = 8.7$ test simulated with the original NMM

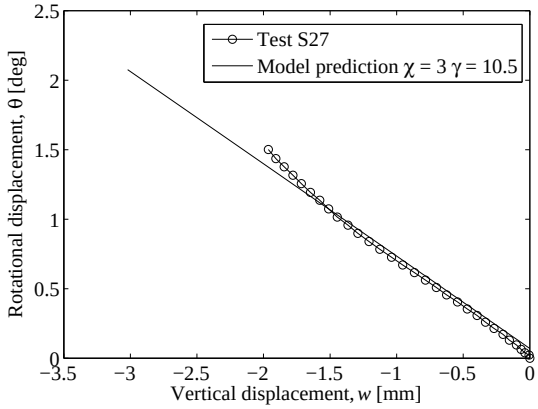

Figure 13: Displacement trajectory of test S27 against model prediction to extrapolate χ and γ

parameters is used to predict a pure M ($M/(HD) = \infty$) test and a test with $M/(HD)$ = 8.7. The two trajectories match very well, meaning that the test with $M/(HD)$ = 8.7 (test S27), can be used instead of a pure M test to calibrate χ and γ. Two parameters that give a reasonable fit of the $\theta - w$ trajectory are χ = 10.5 and γ = 3 (*cf.* Figure 13).

The other two parameters, namely α and λ, are evaluated by conducting a parametric study trying to match the load-displacement curves and the displacement trajectories of the available tests. Appropriate values for α and λ are 11 and 10.5 respectively.

3.1.3 Model validation

The parameters of the original NMM are evaluated with the same procedure explained in section 3.1.2 for the modified NMM. As shown in Figure 14, by using the original NMM, the load-displacement curves achieved cannot simulate the experimental data. By adopting the modified version of the NMM, both load-displacement curves and displacement trajectories curves are reasonably well predicted (*cf.* Figure 15 - Figure 30). As expected, not all tests are equally well represented by the model. Nonetheless, it is partly reassuring to note that the largest deviation

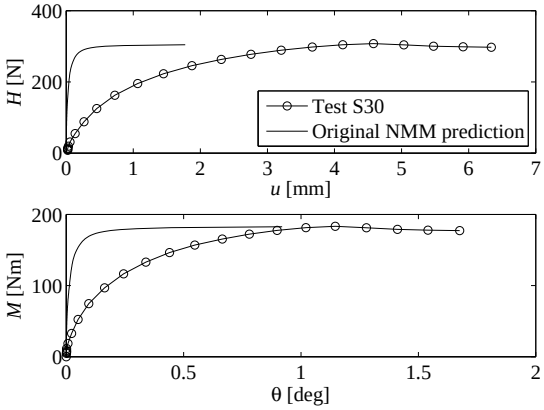

Figure 14: Original NMM prediction of test S30

between analytical and experimental results is found in those curves which are most affected by the parameters gained by trial and error procedure (u-w trajectories of Figure 24 and Figure 26). Also the M-θ curves of the same tests (Figure 23 and Figure 25) are overpredicted by the model. The displacement trajectory θ-w, which was more rationally calibrated, appears to be consistent throughout the entire tests series. This observation however, does not exclude a possible weak point of the model when dealing with the prediction of the u-w trajectories.

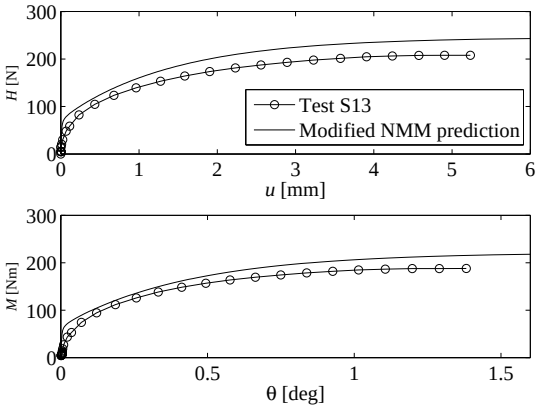

Figure 15: Modified NMM prediction of test S13, load-displacement curves

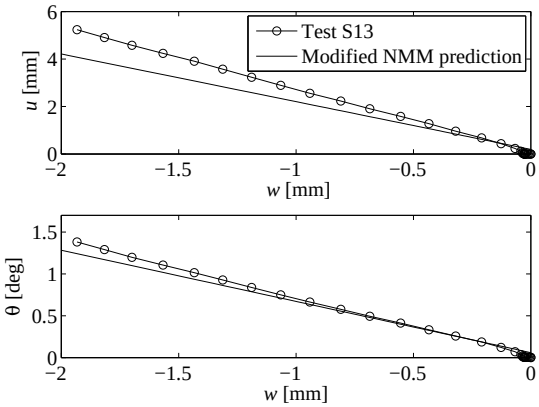

Figure 16: Modified NMM prediction of test S13, displacement trajectories

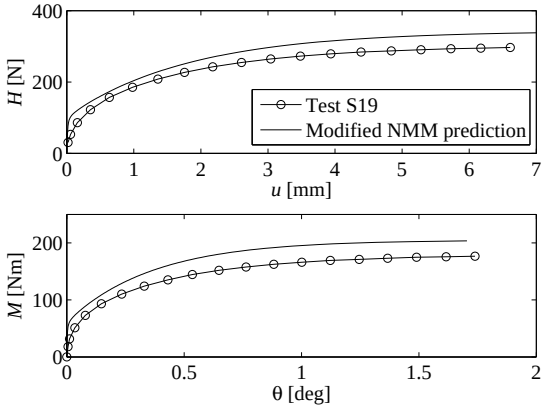

Figure 17: Modified NMM prediction of test S19, load-displacement curves

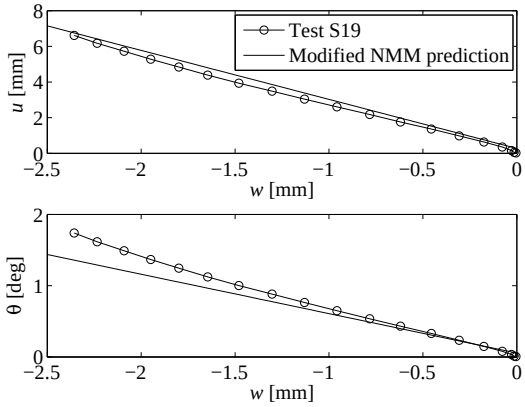

Figure 18: Modified NMM prediction of test S19, displacement trajectories

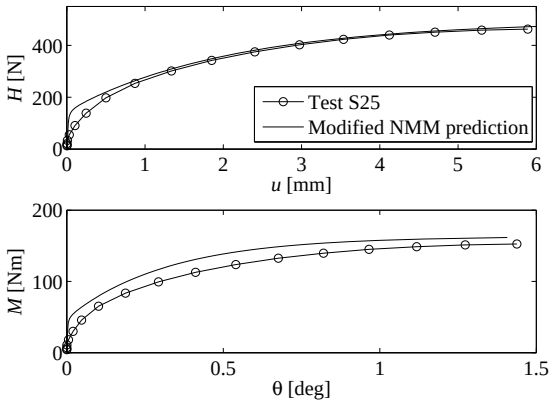

Figure 19: Modified NMM prediction of test S25, load-displacement curves

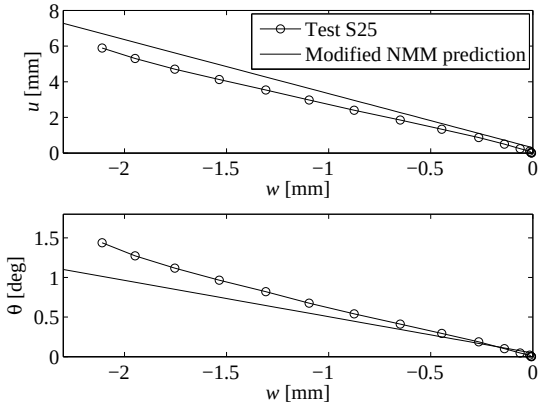

Figure 20: Modified NMM prediction of test S25, displacement trajectories

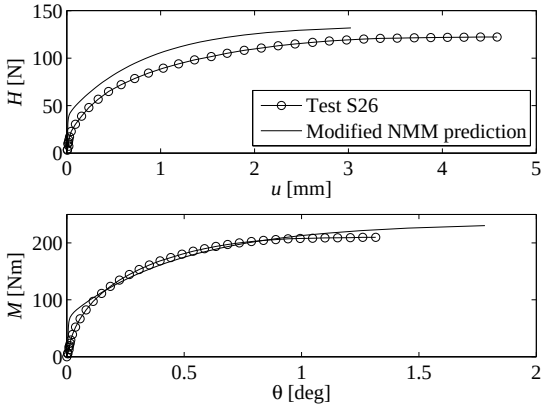

Figure 21: Modified NMM prediction of test S26, load-displacement curves

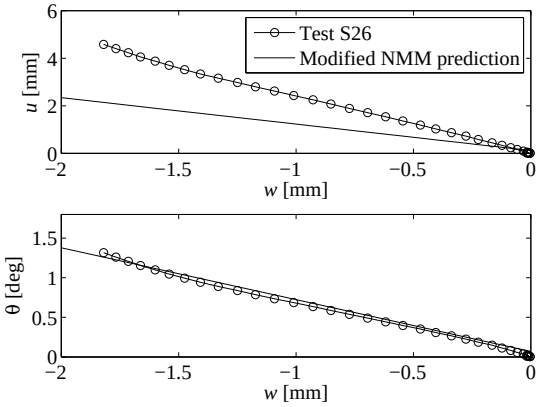

Figure 22: Modified NMM prediction of test S26, displacement trajectories

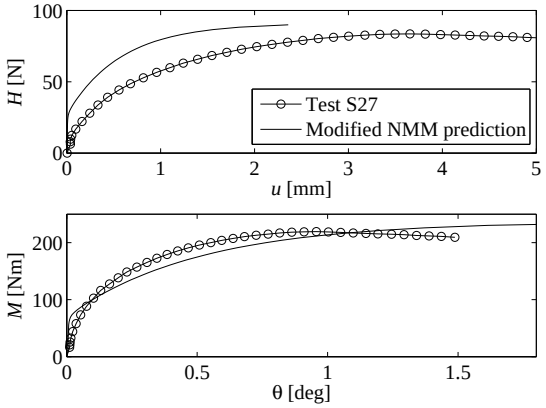

Figure 23: Modified NMM prediction of test S27, load-displacement curves

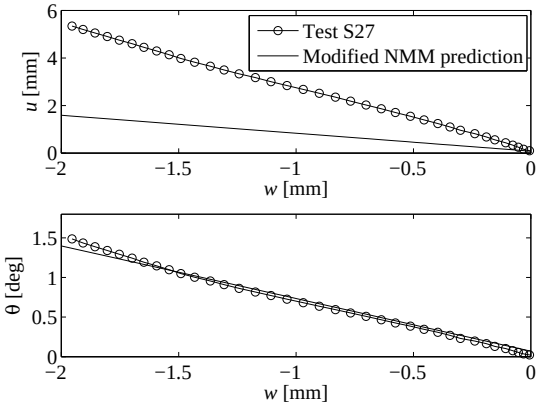

Figure 24: Modified NMM prediction of test S27, displacement trajectories

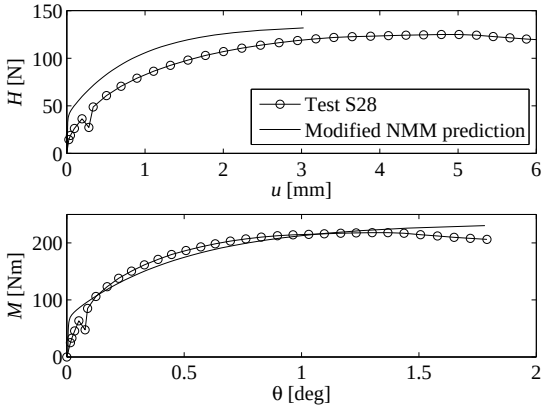

Figure 25: Modified NMM prediction of test S28, load-displacement curves

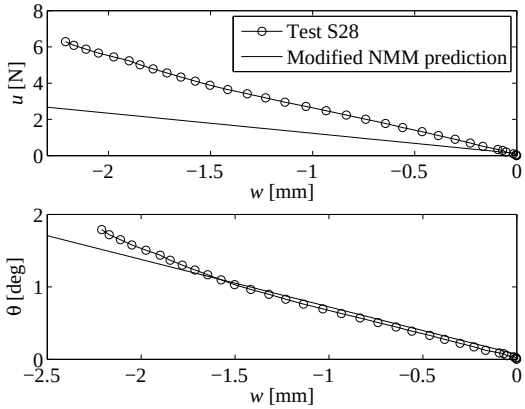

Figure 26: Modified NMM prediction of test S28, displacement trajectories

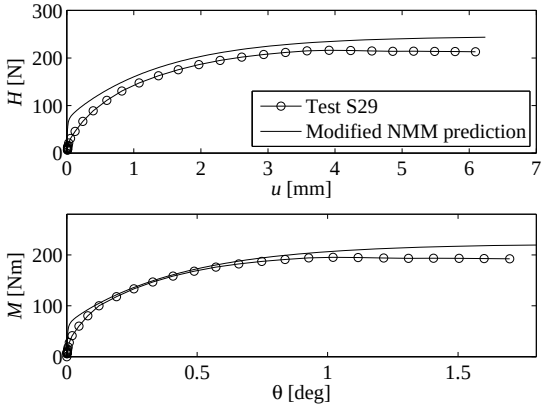

Figure 27: Modified NMM prediction of test S29, load-displacement curves

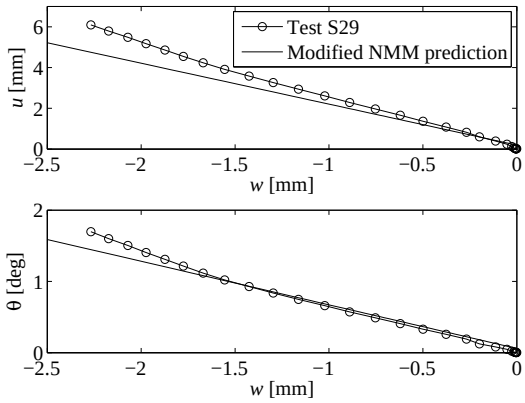

Figure 28: Modified NMM prediction of test S29, displacement trajectories

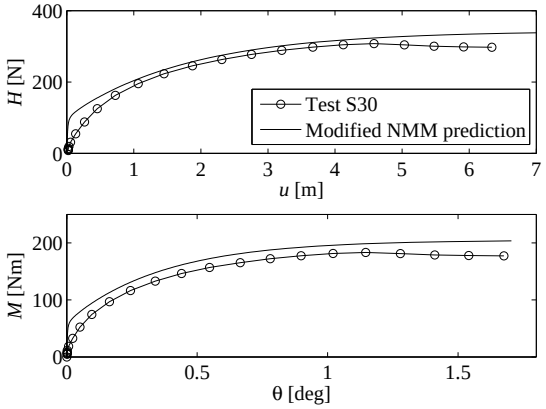

Figure 29: Modified NMM prediction of test S30, load-displacement curves

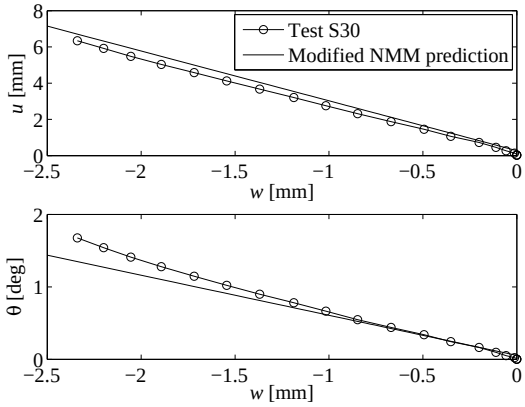

Figure 30: Modified NMM prediction of test S30, displacement trajectories

The incapability of the original NMM to reproduce the experimental results is attributed to the radically different way in which the yielding surface expands in the two models during monotonic loading. As shown in Figure 31, when using the original NMM, there is no gradual transition from one yielding surface to the other. All the yielding surfaces tend to collapse onto one envelope. When including t_0 in the model formulation (see Figure 32), the path towards failure shows a much more gradual evolution of the yielding surface than the original NMM. This observation is true when $V/V_{\mathrm{M}} \approx 0$. In case $V/V_{\mathrm{M}} > 0$, for example for oil and gas platforms, the effect of t_0 would be negligible and the original NMM could perhaps be able to predict the response.

The parameters of the modified NMM used to match the experimental curves are summarised in Table 4.

3.1.4 Discussion on t_0

The tension parameter, t_0, was introduced for the first time by Villalobos (2006) as a function of V_0 ($t_0 = V_{\mathrm{tM}}/V_0$). t_0 was essential to his study to define a yielding surface capable to describe loads in tension. This surface was then employed in a hyperplastic macro-model by Nguyen-

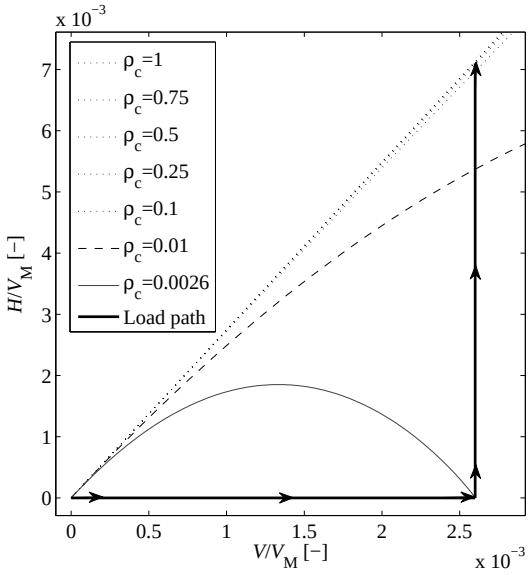

Figure 31: Yielding surface evolution for the original NMM

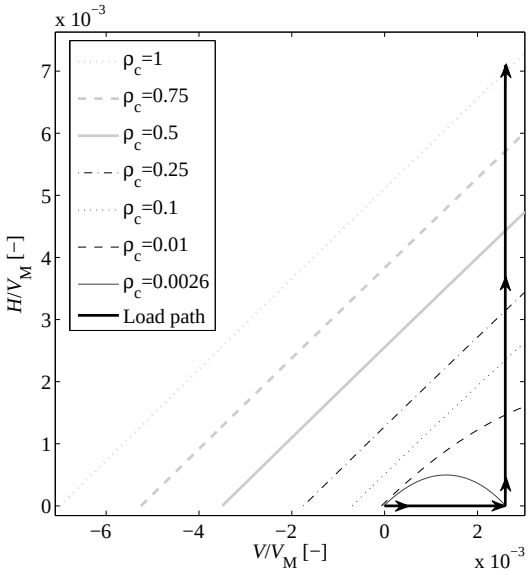

Figure 32: Yielding surface evolution for the modified NMM

Table 4: Parameters of the modified NMM

μ [-]	ψ [-]	β [-]	α [-]	γ [-]	χ [-]	λ [-]	t_0 [-]	V_{M} [kN]	R_0 [kN/m]
0.73	0.86	0.95	11	10.5	3	3.5	0.007	91.66	3202

.

Sy (2006). To not overcomplicate the model Nguyen-Sy (2006) set t_0 constant. In the model presented here, t_0 is also kept constant but is calculated with the ultimate bearing capacity V_{M} instead of V_0. As a result, the value of t_0 evaluated in this work is one order of magnitude smaller than that of Villalobos (2006) and Nguyen-Sy (2006). Letting t_0 vary according to the development of the yielding has not been attempted here but would perhaps be of interest.

3.1.5 Discussion on the hardening law

All the tests carried out at such a small value of V/V_{M} showed uplift ($w < 0$) instead of settlement ($w > 0$). It should be clarified that this kind of behaviour cannot be an artefact of the experimental rig since the same finding is reported in Villalobos et al. (2009). The theory

behind the macro-element approach defines each yielding surface as uniquely associated with a value of the hardening parameter. This is properly elucidated, and put into concrete, in Gottardi et al. (1999) who plotted back-calculated $V - w_{\mathrm{p}}$ curves from radial displacement and constant V tests against the hardening law (where w_{p} is the irreversible vertical displacement). Obviously, the same procedure would not be possible here since the hardening law involves all three components of the plastic displacement. A hardening law merely based on a compressive $V-w$ curve would be not theoretically compatible with loading paths close to the axes origin as there, for bucket foundations, uplift instead of settlement occurs. In the opinion of the authors this aspects should be further investigated.

3.2 Cyclic loading

In this section a simplified version of the boundary surface model developed by di Prisco et al. (2003a) is presented (see also di Prisco et al., 2003b; di Prisco et al., 2006; Buscarnera et al., 2010). Originally, the model in question was designed to simulate the response of shallow foundations subjected to a planar earthquake excitation. The version of the model presented here is conceived to reproduce the behaviour of foundations under sinusoidal M and H with constant V. As a result of that, the model is simplified and some of its elements are neglected. The constitutive parameters are estimated by trial and error against the experimental results.

3.2.1 Model architecture

Let us assume that a point of the load space Q (ξ_{Q}, h_{Q}, m_{Q}) represents the current load state. Boundary surface models define the amount of cyclic displacement for each load step as a function of the distance between Q and an image point, I (ξ_{I}, h_{I}, m_{I}), that lies on a defined boundary surface (see Figure 33). In the model presented here, the boundary surface coincides with the yielding surface while the image point is identified with an appropriate mapping rule

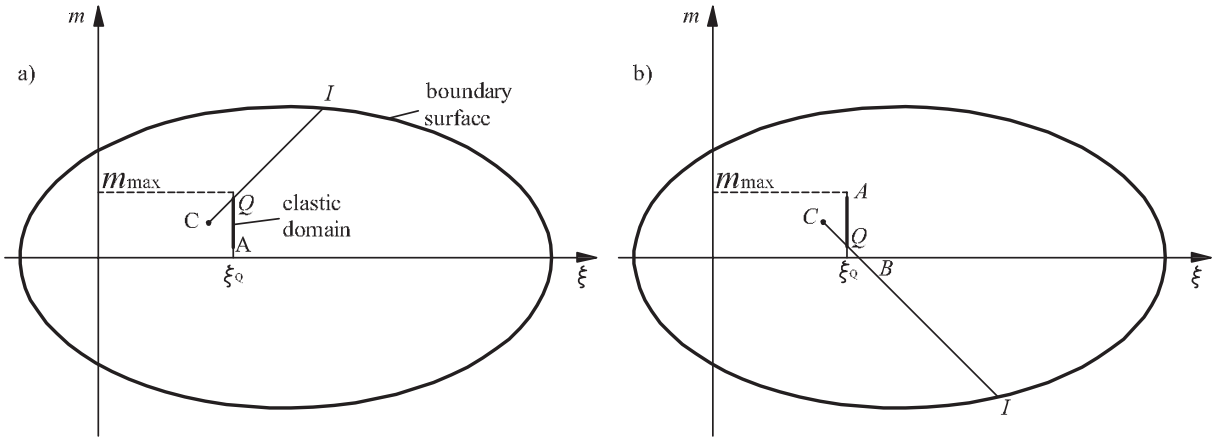

Figure 33: Sketch of the mapping rule for the definition of δ, a) $dm > 0$, $m_{\mathrm{I}} > 0$ and $m_{\mathrm{Q}} > 0$; b) $dm < 0$, $m_{\mathrm{I}} < 0$ and $m_{\mathrm{Q}} > 0$. Elastic domain and boundary surface in bold solid line

explained in the following. The model is integrated into the NMM framework by means of the matrix $\mathbf{\Phi}$ which is incorporated into the flow rule as follows:

$$d\boldsymbol{q}_p = \Lambda \mathbf{\Phi} \frac{\partial g}{\partial \boldsymbol{Q}} \tag{12}$$

The matrix $\mathbf{\Phi}$ is diagonal and its elements are defined as:

$$\Phi_{ii} = exp\left(-\alpha_i \sqrt{\frac{\delta \rho_c}{\xi}}\right) exp\left(-\beta_i \rho_k\right) \tag{13}$$

where α_i and β_i are constitutive parameters, ρ_k is a variable updated as ρ_c (eq. 10) and δ is a function of the distance between the current load state Q and the image point on the boundary surface, I. To describe how the mapping rule works, a sketch of the normalised load plane ($m - \xi$) is illustrated in Figure 33. For simplicity, a two dimensional load path with $0 < m_{\mathrm{Q}} < m_{\mathrm{max}}$ is chosen. An elastic domain in which no irreversible displacements can occur, is defined by means of the segment AQ which is a portion of the total load path. In this study it was deliberately chosen to set the elastic domain equal to the 75% of the total load path. According to the sign of dm, the point C (ξ_{C}, h_{C}, m_{C}), which is necessary to discover the position of I, has coordinates:

$$\xi_{\mathrm{C}} = \xi_{\mathrm{Q}} - QA/2 \tag{14}$$

$$m_{\mathrm{C}} = \begin{cases} m_{\mathrm{Q}} - QA/2 & \text{for } dm > 0 \\ m_{\mathrm{Q}} + QA/2 & \text{for } dm < 0 \end{cases} \tag{15}$$

The straight line connecting C to Q identifies the image point I on the boundary surface. The point of intersection between the line CI and the ξ axis is named B. The variable δ is defined as follows:

$$\delta = \begin{cases} CB + \phi BI & \text{for } m_{\mathrm{I}} < 0 \text{ and } m_{\mathrm{Q}} > 0 \\ CB + \phi BI & \text{for } m_{\mathrm{I}} > 0 \text{ and } m_{\mathrm{Q}} < 0 \\ CI & \text{for } m_{\mathrm{I}} < 0 \text{ and } m_{\mathrm{Q}} < 0 \\ CI & \text{for } m_{\mathrm{I}} > 0 \text{ and } m_{\mathrm{Q}} > 0 \end{cases} \tag{16}$$

where ϕ is a constitutive dimensionless parameter of the model. The second condition of equation 16 never occurs within the loading paths modelled in this study. Nevertheless, it is included for the sake of completeness.

The original boundary surface model of di Prisco et al. (2003a) includes a further element, namely the memory surface. Since the loading conditions are such that M and H are periodic with constant amplitude, the memory surface is not necessary to the model definition.

The boundary surface model presented introduces 7 new non-dimensional parameters. As yet, it is unclear how to calibrate these parameters in a systematic way. However, in the following section, the results of a parametric study aimed at fitting the experimental long-term rotation and horizontal displacement of the foundation is shown.

3.2.2 Model validation

In Figures 34 and 35 the load-displacement curves of test C16 evaluated with the model are shown. By comparison with Figures 5 and 6, it can be observed that some features of the cyclic behaviour are properly simulated by the model: after each load cycle, the displacement components accumulate, the accumulation rate decreases and the area of the hysteresis loops becomes smaller. On the other hand, the model is unable to reproduce the increase in tangent stiffness as a function of *N* and the overlapping of hysteretic loops. The change in stiffness can be incorpo-

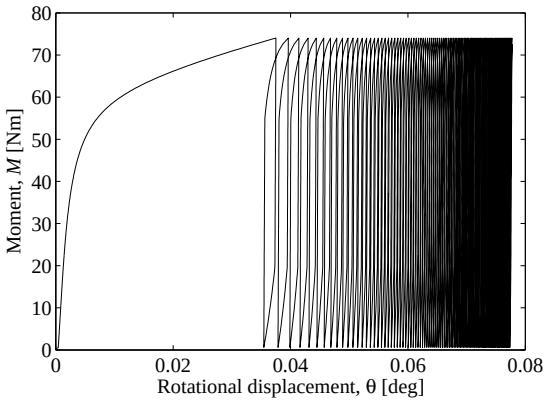

Figure 34: $M - \theta$ curve of the model simulating test C16, first 100 cycles

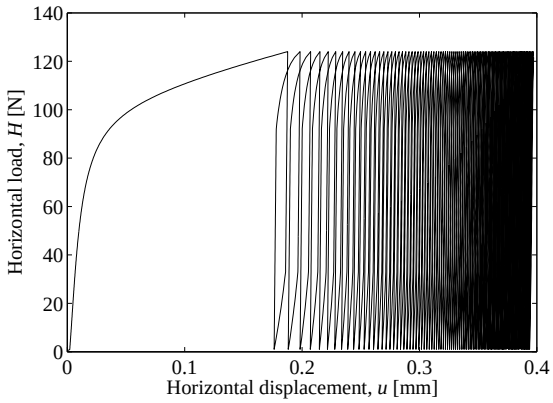

Figure 35: $H - u$ curve of the model simulating test C16, first 100 cycles

rated into the model by deriving an experimentally based updating rule for $\boldsymbol{K}_e$. However, this was not attempted in the present study as the long-term accumulated displacements, rather than the change in unloading-reloading stiffness, was the main aim of the modelling. Figures 36-45 compare the experimental results with the model simulations. In order to neutralise the inaccuracy of the monotonic response and thereby analyse the cyclic modelling independently of the monotonic behaviour, the long-term accumulated displacements of experimental and analytical results are compared in terms of normalised displacements. The normalised rotation is defined as $(\theta_{\mathrm{N}} - \theta_0)/\theta_0$, where θ_{N} is the rotational displacement at cycle N and θ_0 is the rotational displacement at the first load cycle. The same definition applies to the normalised horizontal displacement, but with u instead of θ. Note that for the analytical model, $\theta_0 = \theta_s$ and $u_0 = u_s$, where the subscript "s"indicates the displacements on the monotonic curve corresponding to M_{max}. The experimental tests, even though were performed in substantially drained condition, do not strictly satisfy this condition.

The parameters governing the cyclic behaviour are determined by trial and error from the four experimental cyclic tests. The macro-model appears to have good prediction abilities of the normalised accumulated displacements u and θ.

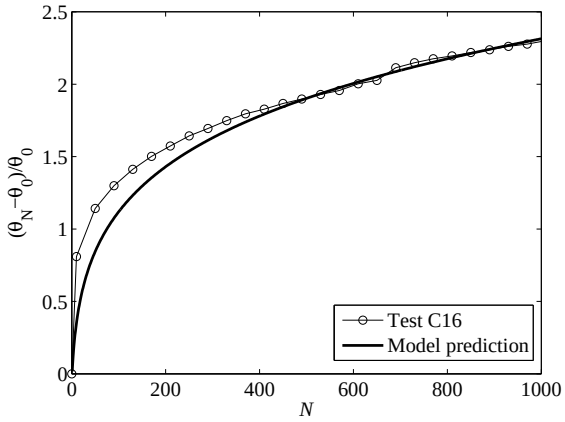

Figure 36: Accumulated rotational displacement of the first 1000 cycles, experimental and analytical results for test C16

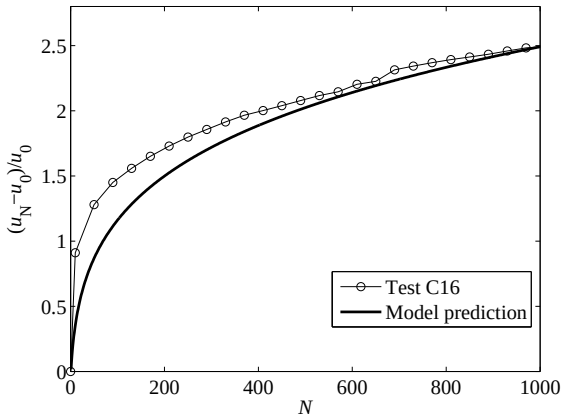

Figure 37: Accumulated horizontal displacement of the first 1000 cycles, experimental and analytical results for test C16

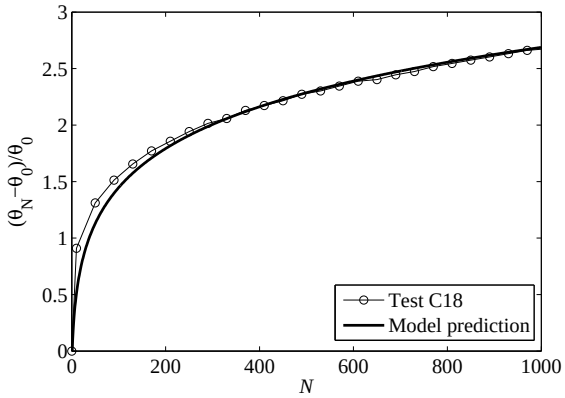

Figure 38: Accumulated rotational displacement of the first 1000 cycles, experimental and analytical results for test C18

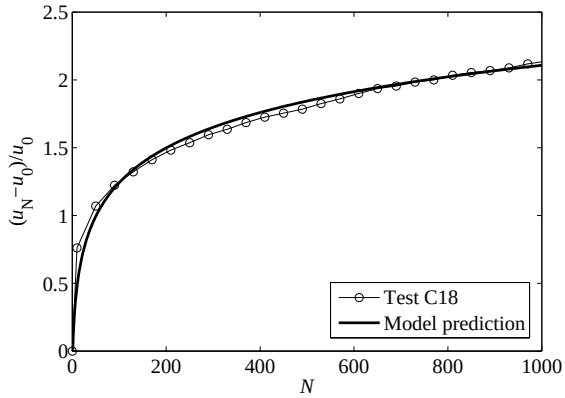

Figure 39: Accumulated horizontal displacement of the first 1000 cycles, experimental and analytical results for test C18

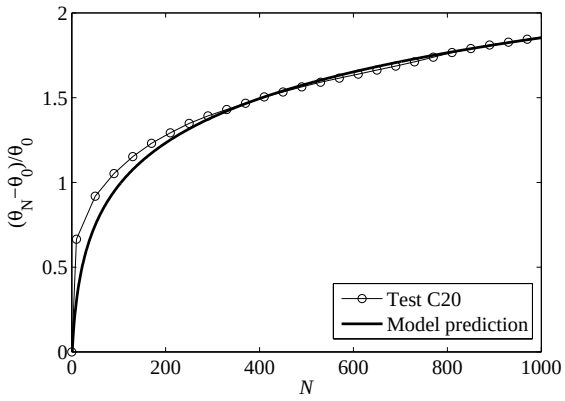

Figure 40: Accumulated rotational displacement of the first 1000 cycles, experimental and analytical results for test C20

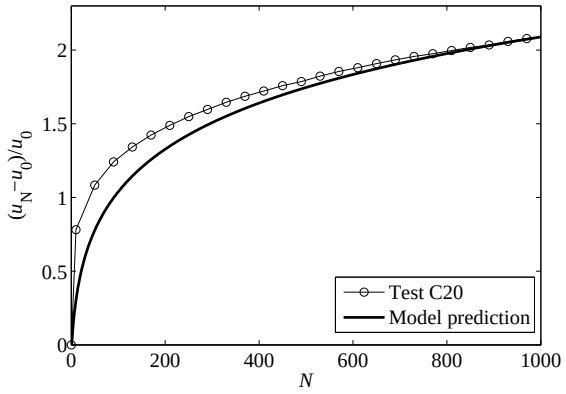

Figure 41: Accumulated horizontal displacement of the first 1000 cycles, experimental and analytical results for test C20

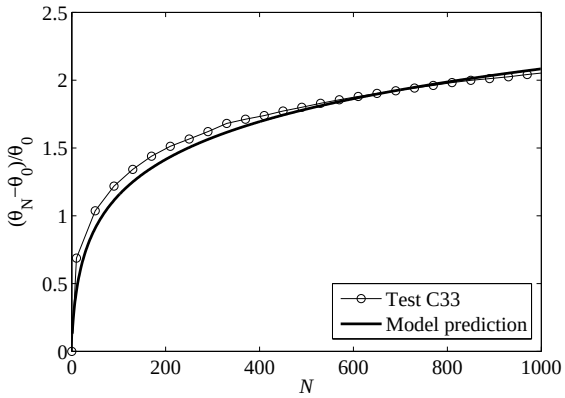

Figure 42: Accumulated rotational displacement of the first 1000 cycles, experimental and analytical results for test C33

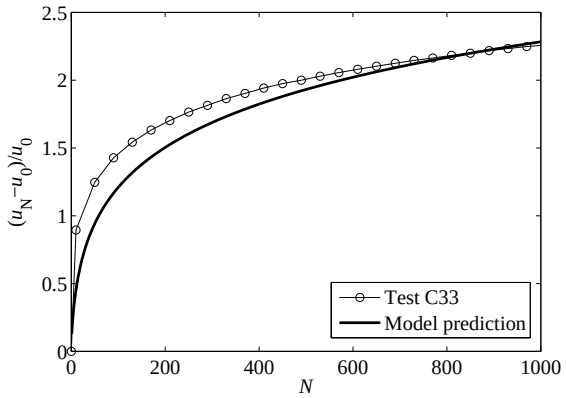

Figure 43: Accumulated horizontal displacement of the first 1000 cycles, experimental and analytical results for test C33

To achieve a proper quantitative match of the experimental results, the cyclic parameters related to u and θ have necessarily to be changed for each simulation. The parameters used in the simulations are listed in Table 5. Figure 44 shows how the parameters vary as a function of the cyclic loading magnitude ratio, $M_{\text{max}}/M_{\text{R}}$. A clear decreasing trend of the parameters for increasing $M_{\text{max}}/M_{\text{R}}$ can be observed. By including more tests in the analysis, also the dependency of the parameters on the cyclic loading ratio, $M_{\text{min}}/M_{\text{max}}$, might be obtained. By slightly adjusting the

parameters, the displacements at number of cycles larger than 1000 can also be predicted (*cf.* Figures 45 and 46).

The reason of the variability of the parameters of the boundary surface model is to be found in how the mapping rule is defined. It is likely that a more sophisticated mapping rule would be able to capture the normalised displacements avoiding the dependency of the parameters on the loading path.

Table 5: Parameters of the boundary surface model

Test	α_V	α_H	α_M	β_V	β_H	β_M	ϕ
C16	350	5	5	70	6	6	0.01
C18	350	14	14	70	43	39	0.01
C20	350	13	13	70	27	29	0.01
C33	350	7	7	70	16	17	0.01

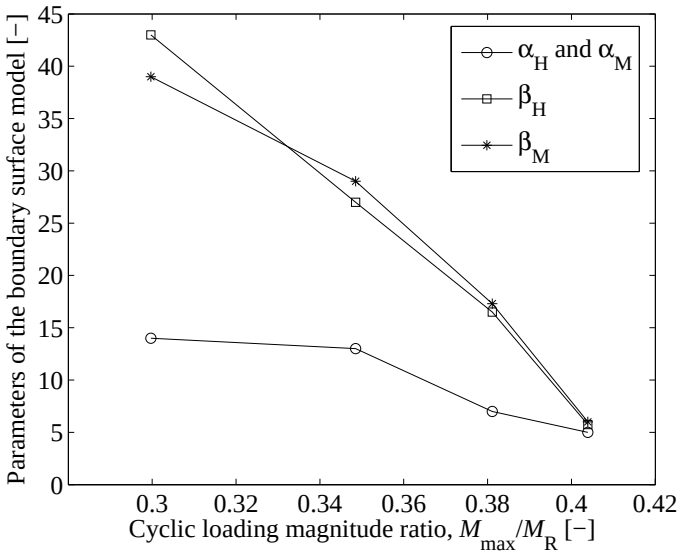

Figure 44: Parameters of the boundary surface model as a function of the cyclic loading magnitude ratio

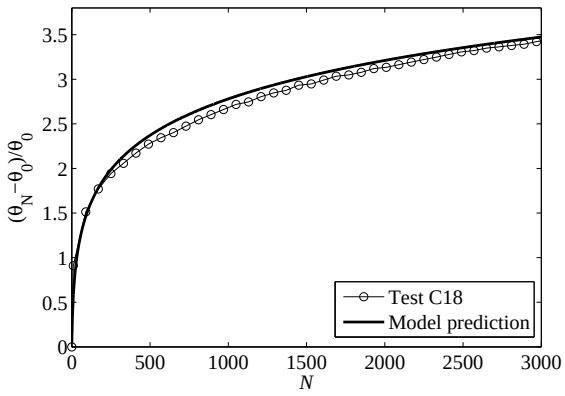

Figure 45: Rotational accumulated displacement of the first 3000 cycles, experimental and analytical results for test C18

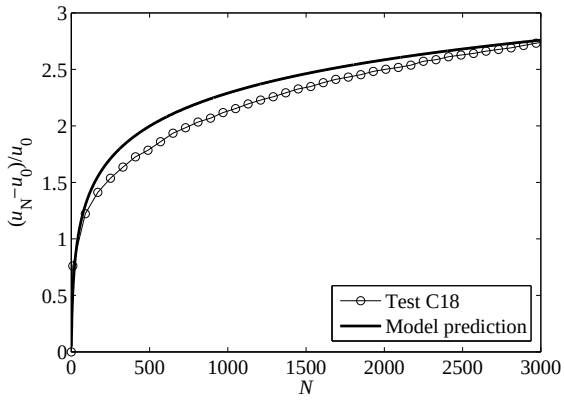

Figure 46: Horizontal accumulated displacement of the first 3000 cycles, experimental and analytical results for test C18

4 Conclusions and future work

In this work the possibility of interpreting experimental tests of bucket foundations under monotonic and cyclic loading with a macro-element model is explored. The problem investigated concerns monopod bucket foundations supporting offshore wind turbines. The well-known model of Nova and Montrasio (1991) is slightly modified and used to interpret a series of monotonic experimental tests. To account for cyclic loading, the model is integrated with a simplified version of the boundary surface model of di Prisco et al. (2003a). Both monotonic and cyclic experimental data are fairly well predicted by the analytical simulations.

Some aspects of the modelling should be further investigated. As emphasised in one of the put forward discussions, the expression of an appropriate hardening law is not an easy task due to the uplift event occurring under general loading at $V/V_{\mathrm{M}} \approx 0$. This issue should be properly addressed. Furthermore, as pointed out in Byrne (2000) and Larsen (2008), close to the origin of the load space the failure locus can be approximated as linear. This could probably be included in the model and reduce the complexity of the approach. Regarding the cyclic

loading modelling, the parameters of the boundary surface model were found to be affected by the loading path. As a result of that, the analysis of additional cyclic loading tests would be necessary to provide the functions related to the parameters. Another way to generalise the model would be to attempt a modification of the mapping rule. Furthermore, the combination of different load packages would be a crucial feature to be included in the model to obtain more realistic responses. Finally, since the model is validated against small-scale experiments, its applicability to real design situations is to be excluded until centrifuge tests or large-scale tests will corroborate the findings of this study.

Abbreviations

OWTs	offshore wind turbines
NMM	Nova and Montrasio (1991) model

Nomenclature

d	length of the skirt
f	yielding function
g	plastic potential
f_l	loading frequency
h	load eccentricity
k_V,k_H,k_M	components of $\boldsymbol{K}_e$
$\boldsymbol{q}$	vector of normalised displacements
r_o	outer radius of the foundation
t	wall thickness
t_l	lid thickness
u	horizontal displacement
u_0	horizontal displacement of the first cycle
u_s	horizontal displacement on the monotonic curve corresponding to M_{max}
w	vertical displacement
w_p	plastic vertical displacement
A,Q,I,C,B	points of the normalised load space used for the mapping rule description
$\boldsymbol{C}$	flexibility matrix

D	foundation diameter
D_{r}	relative density
E	elastic modulus
H	horizontal load
$\boldsymbol{K}_e$	elasticity matrix
$\boldsymbol{Q}$	vector of normalised loads
V	vertical load
V_{M}	bearing capacity of the foundation
V_{tM}	tensile capacity
V_0	preconsolidation vertical load
M_{R}	monotonic moment capacity
M_{max}, M_{min}	maximum and minimum cyclic moment
N	number of cycles
W	self-weight of the foundation
W'_{f}	buoyant weight of the foundation
W'_{p}	buoyant weight of the soil
α_V,α_H,α_M,β_V,β_H,β_M,ϕ	parameters of the boundary surface model
μ,ψ,β,λ,χ,α,γ,R_0,t_0	parameters of the modified NMM
ε	normalised horizontal displacement
ζ	normalised rotational displacement
η	normalised vertical displacement
θ	rotational displacement
θ_0	rotational displacement of the first cycle
θ_s	rotational displacement on the monotonic curve corresponding to M_{max}
ξ	normalised vertical load
δ	variable governing the mapping rule
ν	poisson ratio
ρ_c	hardening parameter
ρ_g	fictitious variable of the plastic potential
ρ_k	updating variable of the boundary surface model
τ_o	shear stresses acting over the skirt
Λ	plastic multiplier
$\boldsymbol{\Phi}$	matrix governing the cyclic displacements accumulation
Φ_{ii}	components of $\boldsymbol{\Phi}$

References

Bienen, B., Byrne, B. W., Houlsby, G. T. and Cassidy, M. J. (2006). Investigating six-degree-of-freedom loading of shallow foundations on sand. *Géotechnique* 56, No. 6, 367-379

Buscarnera, G., Nova, R., Vecchiotti, M., Tamagnini, C. and Salciarini, D. (2010). Settlement analysis of wind turbines. In *Soil-Foundation-Structure Interaction*, Orense et al. (Eds). CRC Press

Butterfield, R. and Ticof, J. (1979). The use of physical models in design. In *Proceedings of the 7th European Conference on Soil Mechanics*, Brighton, 259-261

Butterfield, R., Houlsby, G. T. and Gottardi, G. (1997). Standardized sign conventions and notation for generally loaded foundations. *Géotechnique* 47, No. 5, 1051-1054

Byrne, B. W. (2000). *Investigations of suction caissons in dense sand*. Ph.D. thesis, Oxford University

Byrne, B. W. and Houlsby, G. T. (2001). Observation of footing behaviour on loose carbonate sand. *Géotechnique* 51, No. 5, 463-466

Byrne, B. W. (2011). *Foundation Design for Offshore Wind Turbines*. Géotechnique lecture

Chatzigogos, C. T., Figini, R., Pecker, A. and Salençon, J. (2011). A macroelement formulation for shallow foundations on cohesive and frictional soils. *International Journal for Numerical and Analytical Methods in Geomechanics* 35, No. 8, 902-931

Cremer, C., Pecker, A. and Davenne, L. (2001). Cyclic macro-element for soil-structure interaction: material and geometrical non-linearities. *International Journal for Numerical and Analytical Methods in Geomechanics* 25, No. 13, 1257-1284

di Prisco, C., Nova ,R. and Sibilia, A. (2003a). Shallow footing under cyclic loading: experimental behaviour and constitutive modeling. In *Geotechnical analysis of seismic vulnerability of historical monuments*, Maugeri M. and Nova R. (Eds). Patron, Bologna

di Prisco, C., Nova, R., Perotti, F. and Sibilia, A. (2003b). Analysis of soil-foundation interaction of tower structures under cyclic loading. In *Geotechnical analysis of seismic vulnerability of historical monuments*, Maugeri M. and Nova R. (Eds). Patron, Bologna

di Prisco, C., Massimino, M. R., Maugeri, M., Nicolosi, M. and Nova, R. (2006). Cyclic numerical analyses of Noto Cathedral: soil-structure interaction modelling. *Rivista Italiana di Geotecnica* 2, 49-63

di Prisco, C. (2012). Cyclic mechanical response of rigid bodies interacting with sand strata. In *Mechanical Behaviour of Soils under Environmentally Induced Cyclic Loads*, di Prisco C. and Wood D. M. (Eds). CISM, Udine

Doherty, J. P. and Deeks, A. J. (2001). Elastic response of circular footings embedded in a non-homogeneous half-space. *Géotechnique* 53, No. 8, 703-714

Foglia, A., Ibsen, L. B., Nicolai, G., and Andersen, L. V. (2014). Observations on bucket foundations under cyclic loading in dense saturated sand. In *Proceedings of the 8th international conference of physical modelling in geotechnics (ICPMG), Perth*, Gaudin C. and White D. (Eds.). CRC Press

Gottardi, G. and Butterfield, R. (1993). On the bearing capacity of surface footings on sand under general planar loads. *Soils and Foundations* 33, No. 3, 68-79

Gottardi, G. and Butterfield, R. (1995). The displacement of a model rigid surface footing on dense sand under general planar loading. *Soils and Foundations* 35, No. 3, 71-82

Gottardi, G., Houlsby, G. T. and Butterfield, R. (1999). Plastic response of circular footings on sand under general planar loading. *Géotechnique* 49, No. 4, 453-469

Govoni, L., Gourvenec, S, and Gottardi, G. (2011). A centrifuge study on the effect of embedment on the drained response of shallow foundations under combined loading. *Géotechnique* 61, No. 12, 1055-1068

Haigh, S. K. (2014). Foundations for offshore wind turbines. In *Proceedings of the 8th Inter-*

national Conference of Physical Modelling in Geotechnics (ICPMG), Perth, Gaudin C. and White D. J. (Eds). CRC Press

Houlsby, G. T. and Cassidy, M. J. (2002). A plasticity model for the behaviour of footings on sand under combined loading. *Géotechnique* 52, No. 2, 117-129

Houlsby, G. T. and Puzrin, A. M. (2007). *Principles of Hyperplasticity*. Springer

Ibsen, L. B., Larsen, K. A. and Barari, A. (2014). Calibration of Failure Criteria for Bucket Foundations on Drained Sand under General Loading. *Journal of Geotechnical and Geoenvironmental Engineering* 140, No. 7

Larsen, K. A. (2008). *Static behaviour of bucket foundations*. Ph.D. thesis, Aalborg University

LeBlanc, C., Byrne, B. W. and Houlsby, G. T. (2010). Response of stiff piles in sand to long-term cyclic lateral loading. *Géotechnique* 60, No. 2, 79-90

Lesny, K. (2011). *Foundations for Offshore Wind Turbines - Tools for Planning and Design*. VGE Verlag GmbH

Kafle, B. and Wuttke, F. (2013). Cyclic macroelement for shallow footing over unsaturated soil. In *Advances in Unsaturated Soils*, Caicedo et al. (Eds). CRC Press

Martin, C. M. (1994). *Physical and numerical modelling of offshore foundations under combined loads*. Ph.D. thesis, Oxford University

Montrasio, L. and Nova, R. (1997). Settlement of shallow foundations on sand: geometrical effects. *Géotechnique* 47, No. 1, 46-60

Nguyen-Sy, L. (2006). *The theoretical modelling of circular shallow foundation for offshore wind turbines*. Ph.D. thesis, Oxford University

Nova, R. and Montrasio, L. (1991). Settlements of shallow foundations on sand. *Géotechnique* 41, No. 2, 243-256

Roscoe, K. H. and Schofield, A. N. (1956). The stability of a short pier foundations in sand. *British Welding Journal*. August, 343-354

Salciarini, D. and Tamagnini, C. (2009). A hypoplastic macroelement model for shallow foundations under monotonic and cyclic loads. *Acta Geotechnica* 4, No. 3, 163-176

Tamagnini, C., Salciarini, D. and Ragni, R. (2013). Implementation of a 6-dof hypoplastic macroelement in a finite element code. In *Proceeding of the International Conference on Computational Geomechanics (Comgeo III), Krakow*

Vaitkunaite, E., Ibsen, L. B., and Nielsen, B. N. (2014). New medium-scale laboratory testing of bucket foundation capacity in sand. In *Proceedings of the Twenty-fourth International Ocean and Polar Engineering Conference (ISOPE), Busan*

Villalobos, F. A. (2006). *Model testing of foundations for offshore wind turbines*. Ph.D. thesis, Oxford University

Villalobos, F. A., Byrne, B. W. and Houlsby, G. T. (2009). An experimental study of the drained capacity of suction caisson foundations under monotonic loading for offshore applications. *Soils and Foundations* 49, No. 3, 477-488

Wood, D. M. (2012). Macroelement modelling. In *Mechanical Behaviour of Soils under Environmentally Induced Cyclic Loads*, di Prisco C. and Wood D. M. (Eds), CISM, Udine

Zhang, Y., Cassidy, M. J., Bienen, B. (2014). A plasticity model for spudcan foundations in soft clay. *Canadian Geotechnical Journal* 51, 629-646

Paper V

Title:

Laboratory experiments of bucket foundations under cyclic loading

Authors:

Foglia, A. and Ibsen L. B.

Year of publication:

2014

Published in:

Technical Report No. 177, Department of Civil Engineering, Aalborg University

Number of pages:

156

Laboratory experiments of bucket foundations under cyclic loading

Aligi Foglia and Lars Bo Ibsen

Department of Civil Engineering, Aalborg University

This report collects information on the experimental campaign concerning bucket foundations under lateral cyclic loading conducted by the authors between 2011 and 2014. The report includes a step by step manual on the test procedures and a number of information and graphs for each experiment. In addition, all the tests performed with the relevant features are listed.

1 General description of the setup

The experimental rig used for all the experiments was designed at Aalborg University on the base of the test setup of LeBlanc (2010). The setup consists of a sand box and a loading frame. The sand box is made of steel, has size 1600x1600x1150 mm and is surrounded by the loading frame. A screw jack is mounted on the horizontal beam of the loading frame and is used for the installation of the foundations. Another screw jack is mounted on the vertical beam of the loading frame and is used to apply monotonic lateral loading. The sand box is provided with a drainage system on the bottom. The drainage system consists of perforated pipes, 100 mm of draining material (gravel), and a sheet of geotextile. The pipes are laid in such a way to let the water evenly within the sand box. The water is provided by a tank and the water gradient is

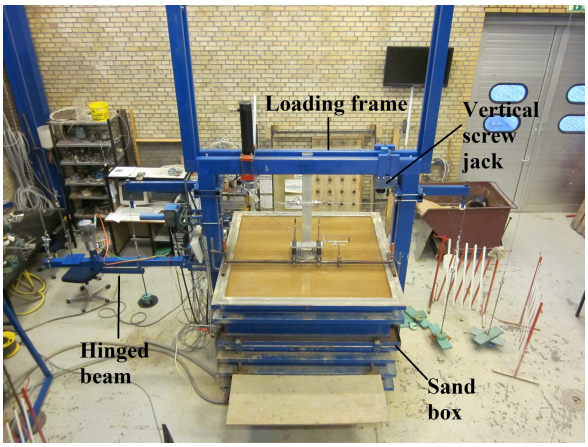

Figure 1: Picture of the rig

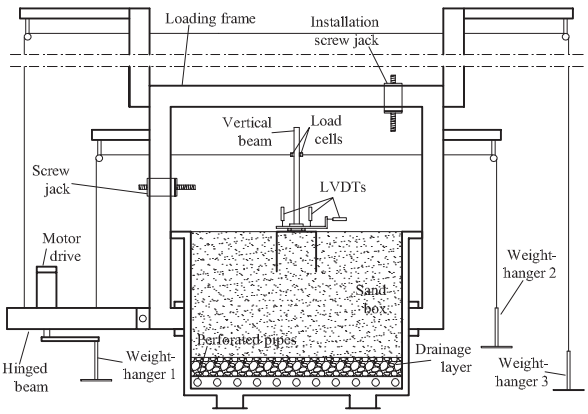

Figure 2: Cross section of the rig

Figure 3: Picture of the foundations used

regulated with valves.

The cyclic loading system consist of a hinged beam with a motor drive and three weight hangers. The cyclic loading is induced to the system by applying a rotational motion to weight-hanger 1 which, in turn, transmits an oscillating motion to the hinged beam. As a result of that, the whole system is caused to undergo cyclic loading. A picture and a sketch of the system are illustrated in Figures 1 and 2. Three foundations with diameter $D = 300$ mm, skirt thickness $t = 1.5$ mm, lid thickness $t_l = 11.5$ mm and embedement ratios 1, 0.75 and 0.5 were adopted to fulfil the experimental program. The three small-scale buckets are depicted in Figure 3.

Table 1: Index properties of Aalborg University sand No. 1

Property	Value	Unit
Grain diameter corresponding to 50% passing	0.14	[mm]
Uniformity coefficient	1.78	[-]
Specific grain density	2.64	[-]
Maximum void ratio	0.86	[-]
Minimum void ratio	0.55	[-]

Figure 4: Power supply

Figure 5: Data acquisition system (Spider 8)

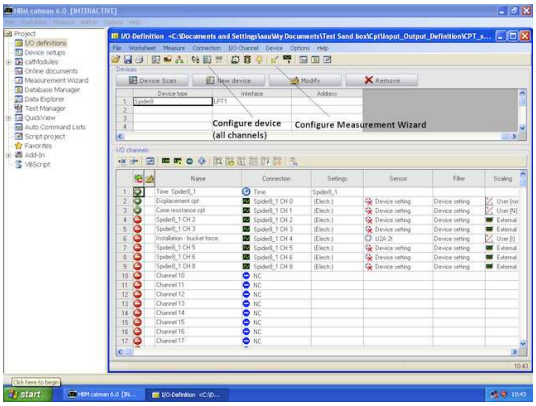

Figure 6: Data sampling software (CATMAN)

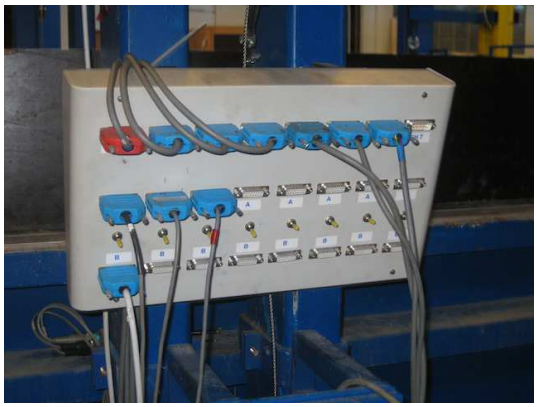

Figure 7: Electric panel

The sand used is Aalborg University sand No. 1. The main properties of the sand are given in Table 1. Addtional information on the sand can be found in Larsen (2008).

To activate the screw jacks and the hydraulic motor (see Chapters 3 and 4) a power supply is used, see Figure 4. If the wires are homopolarly connected to the power supply, a backward

movement of the actuator will be generated. The experimental data is collected by means of a data acquisition system (Spider8) , shown in Figure 5, and a data sampling software (CATMAN), shown in Figure 6. All the transducers are connected to the data acquisition system through an electric panel (Figure 7) placed on one side of the experimental rig.

2 Preparation of the sand sample

In order to ensure the test repeatability, the soil sample is prepared in a systematic manner. The sample preparation procedure is listed in the following steps:

- apply a water gradient close to the critical gradient to loosen up the sand. Open the valve of the water tank until the water reaches the red sign on the piezometer (plastic tube) connected to the sand box. The water level should be approximately 105 cm. Close the water tank valve when the water begins to come out from the sand box

- mount the wooden frame on the sand box. Fix it with clamps to prevent leaks of water during soil vibration, see Figure 8

- add two buckets of clean sand over the soil surface in order to obtain an additional sand layer that will be removed after the vibration of the sand. The sand should be spread as

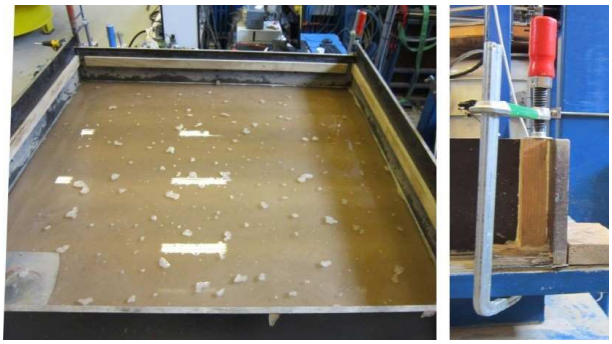

Figure 8: Wooden frame on top of the test sand box on the left-hand side. Particular of one of the clamps fixing the frame on the right-hand side

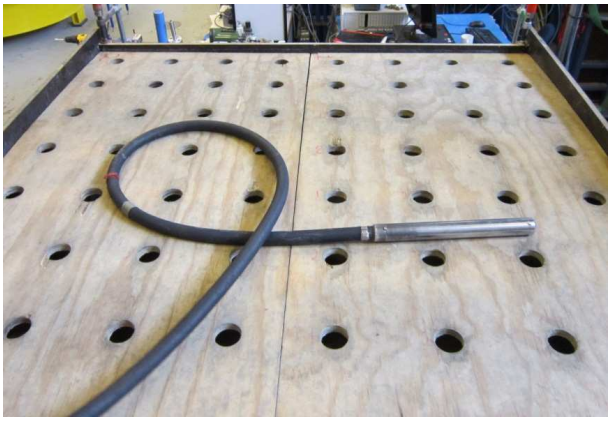

Figure 9: Holed wooden plates with vibration rod on top

even as possible

– fill up the sand box with water from the top until it reaches the cork placed on one side of the wooden frame. Add the water gradually to prevent sand erosion

– place the holed wooden plates on top of the frame, see Figure 9. Each hole on the plate is numbered with 1 or 2. In order to guarantee uniform soil conditions, vibrate first the holes of the same number. Vibrate the remaining holes successively. Start vibrating from one corner, one row of holes after the other

– attach a mark to the vibrator rod so to keep always the same penetration depth. The penetration depth is 80 cm

– after vibrating, remove the clamps and let the water overflowing from the sandbox

– open the valve at the bottom of the sand box for 5 to 10 minutes to reduce the water level and to allow the soil alignment operations. Close the valve when the soil profile is visible

– remove any dirt from the soil surface. Afterwards, align the soil surface with the lath shown in Figure 10. From this step on to avoid any unnecessary contact with the soil

Figure 10: Lath used to smooth the soil surface

– fill up the sandbox with water from the top. The water should flow slowly and hit first a steel plate placed on the corner of the sand box to prevent erosion. Close the water when the water reaches the black line on the sand box edges. The water level should be approximately 5 mm lower than the sand box top

3 Cone penetration test

Small-scale cone penetration tests (CPTs) are necessary to ascertain the uniformity of the sand sample, to check the repeatability of the soil condition and to estimate the soil parameters. The soil parameters are estimated by following the procedure described in Ibsen et al. (2009). It should be emphasised that the relative density calculated with the small-scale CPT is only an estimation based on empirical correlations. Besides, the CPT was re-calibrated several times during the experimental campaign. This causes a significant fluctuation of the relative density estimation throughout the testing programme. In reality, always the same amount of sand in the

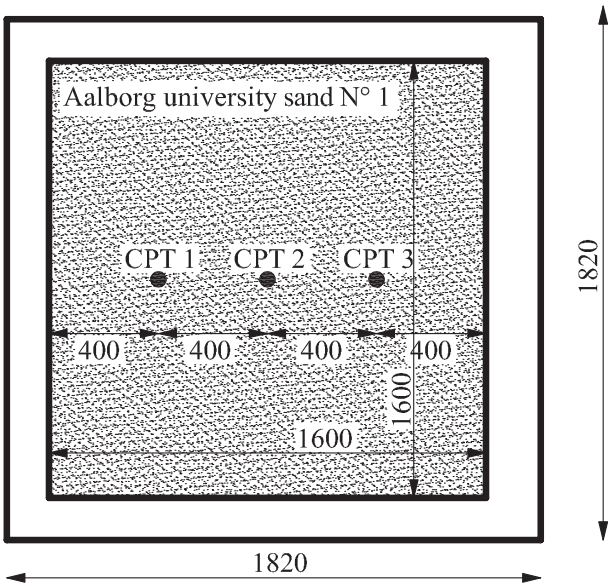

Figure 11: Plan of the sand box with CPT positions. Measures in mm

same volume was used. This means that in spite of the scatter shown by the calculated values, the relative density must have been fairly consistent for the whole experimental programme.
In order to test the soil uniformity the CPTs should be carried out in three different positions of the soil surface . The positions of the CPTs are sketched in Figure 11. The penetration depth is measured with a displacement transducer ASM WS10. Below the CPT procedure is described:

- connect the hydraulic motor (Figure 12) to the screw jack on the loading frame through the two hydraulic cables. Mind the cables far ends, some oil drops might come out and fall over the prepared soil sample

- install the CPT device on the screw jack, see Figure 13. Connect the cable corresponding to the tip resistance to the electric panel

- fix the displacement transducer wire, see Figure 14. Connect the cable corresponding to the penetration depth to the electric panel

- make sure that the signals of penetration resistance and penetration depth are broadcast

Figure 12: Hydraulic motor and cables

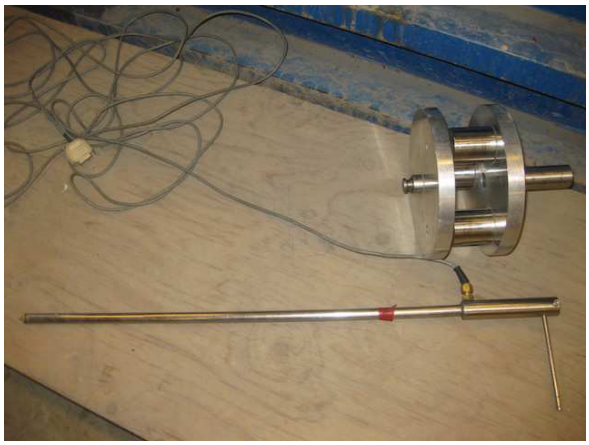

Figure 13: Small-scale CPT device

Figure 14: CPT displacement transducer

to the electric panel

– plug the wires of the hydraulic motor in the power supply

– during penetration, the power supply should be set on the maximum power (20 V). This will ensure a penetration rate of 5 mm/s

The following steps describe the procedure to set up the data recording system before each CPT:

– turn on Spider8 and CATMAN

- open Input/Output (I/O) definitions
- load the (I/O) file from the following folder:
  $C:/MyDocuments/TestSandbox/CPT/InputOutputDefinition/CPTsandbox.IOD$
- click the button *Configure device (all channels)* (Figure 6)
- load the amplifier setup from the following file:
  $C:/MyDocuments/TestSandbox/CPT/SetupAssistant/cptdevicesetup.S8$
- check whether the signals of the needed devices are transmitted (marked in green if so)
- click the button *Configure Measurement Wizard* (Figure 6)
- in the General settings, click the button *Export options* from the Online Data Export menu
- select the following file name:
  $C:/MyDocuments/TestSandbox/ResultsBucket2012$
- create a new folder for a new test and name it "CPTxx", where "xx"is the test name. Open the CPT folder and save the file with the number of the CPT (1 2 or 3)
- from the Configure Measurement Wizard window, click the button *Online Document* and select the following file:
  $C:/MyDocuments/TestSandbox/CPT/Script/cpt.OPG$
- from the Configure Measurement Wizard window, click the button *Start Measurement Wizard*

The recording system is now ready and the CPT can start. To run the test follow the following steps:

– place the CPT device in position 1 (Figure 11)

– turn on the power supply and the hydraulic motor

– lower the CPT device to the point where it touches the water surface by using the control of the hydraulic motor

– tare the recording system in CATMAN by pressing the button *Zero all active channels*

– start recording by pressing the button *Run acquisition* in CATMAN

– penetrate the soil down to a depth of 40 cm

– stop recording by pressing the button *Stop measurement* in CATMAN

– remove the CPT device from the soil by using the control of the hydraulic motor

– turn off the hydraulic motor and quit CATMAN

The entire procedure has to be repeated for the CPT positions 2 and 3. Each CPT record has to be saved in a different file. After carrying out the three CPTs, switch off the power supply and dismantle carefully hydraulic cables and CPT instruments.

4 Installation phase

During the installation process the bucket foundation is instrumented with a load cell (HBM U2B 50 kN) to measure the vertical load, and a displacement transducer (ASM WS10) to measure the penetration depth. The bucket foundation is driven into the soil with the screw jack placed on the loading frame. The installation procedure is described in the following steps:

– place two steel beams on the sand box. These beams support the bucket as illustrated in Figure 15

Figure 15: Bucket on steel beams

Figure 16: Steel pin

– displace the bucket on the steel beams until reaching the centre of the sand box

– place the vertical (or installation) screw jack in the centre of the loading frame. Fix firmly the screw jack to the frame in order to avoid any undesired movement during penetration

– connect the bucket to the screw jack with the steel pin shown in Figure 16

– lift the bucket with the screw jack by using a screwdriver

– remove the supporting beams

– lower the bucket using the screwdriver until it touches the water

– check whether the bucket is placed horizontally with a spirit level, see Figure 17

– use now an electric motor to activate the screw jack and lower thereby the foundation with constant displacement rate of 0.02 mm/s

– the three air valves shown on the right-hand side of Figure 17 have to be opened during penetration

Figure 17: Bucket, air valves and spirit level

– install the steel frame that holds the installation rig bar during penetration to avoid unwanted rotations of the bucket. Mount the displacement transducer for the depth penetration on the magnet support, see Figures 18 and 19

– connect the wires of the vertical load cell and displacements transducer to the electric panel

– make sure that the signals of vertical load cell and displacement transducer are transmitted to the electric panel by checking the Setup Assistant on CATMAN

– install the automatic switch off system on the installation rig bar in order to provide a safety automatic stop of the bucket penetration. Place some wooden blocks on the steel frame to ensure the automatic switch off, see Figure 19

Figure 18: Installation system

Figure 19: System for automatic switch off

Now the installation phase is ready to commence. The following steps summarize the procedure to set up the data recording system before the installation stage:

- turn on Spider8 and CATMAN
- open I/O definitions
- load the I/O file from the following folder:
  $C:/MyDocuments/TestSandbox/Installation/IOdefinition.IOD$
- click the button *Configure device (all channels)* (Figure 6)
- load amplifier setup from the following file:
  $C:/MyDocuments/TestSandbox/Installation/setupassistant.S8$
- check whether the correct signals are broadcast

- click the button *Configure Measurement Wizard* (Figure 6)
- in the General settings, click the button *Export options* from the Online Data Export menu
- select the following file name:
  $C:/MyDocuments/TestSandbox/ResultsBucket2012$
- create a new folder for the new test. Inside the folder create a sub-folder and name it "Installation". Inside this, save the file as "Installation-xx"
- from the Configure Measurement Wizard window, click the button *Online Document* and select the following file:
  $C:/MyDocuments/TestSandbox/Installation/Instscript.OPG$
- from the Configure Measurement Wizard window, click the button *Start Measurement Wizard*

After this, the penetration phase can start. Follow the steps below:

- tare the recording system in CATMAN by pressing the button *Zero all active channels*
- start recording by pressing the button *Run acquisition* in CATMAN
- plug the wires in the power supply in a non-homopolar manner
- turn on the power supply and set it to 20 V
- when the penetration force or the penetration depth is the one desired turn off the power supply
- close the three air valves on the bucket lid
- dismantle cautiously all the installation instruments and disconnect the foundation from the screw jack

5 Cyclic test

Before each test, a vertical tower has to be installed on the foundation. The vertical tower transmits the overturning moment and the horizontal load to the foundation. Two load cells (HBM U2B 50 kN) are fit to the tower at a height (eccentricity of the load) selected by the user. Three LVDTs (HBM W10 TK) measure the displacement of the foundation (see Chapter 7). The following steps describe the cyclic test procedure:

- mount carefully the tower on the bucket foundation installed
- place the steel frame that will hold the three displacement transducers (LVDTs) on the sand box, see Figure 20. Install the three displacement transducers on the steel frame. Make sure that the LVDTs far ends are placed correctly on the tower plates
- connect the LVDTs cables to the electric panel
- make sure that the LVDTs signals are broadcast

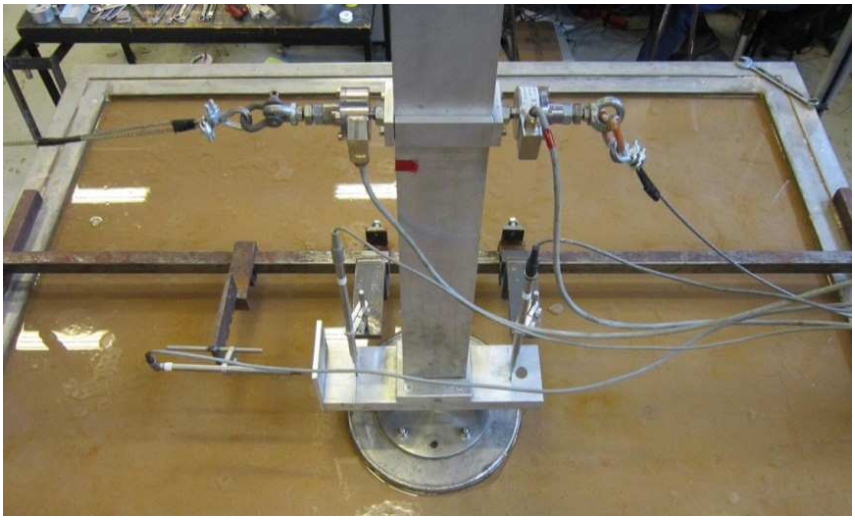

Figure 20: LVDTs mounted on the steel frame, vertical tower above the bucket, load cells and loading cables

Before starting the cyclic test, the data recording system has to be set up by following the procedure below:

- turn on Spider8 and CATMAN
- open I/O definitions
- load the I/O file from the following folder:
  $C:/MyDocuments/TestSandbox/BucketSetup/InputOutput/Bucket2012Trans.IOD$
- click the button *Configure device (all channels)* (Figure 6)
- load the amplifier setup from the following file:
  $C:/MyDocuments/TestSandbox/BucketSetup/SetupAssistant/Bucketsand2011.S8$
- check whether the correct signals are broadcast
- click the button *Configure Measurement Wizard* (Figure 6)
- in the General settings, click the button *Export options* from the Online Data Export menu
- select the following File base name:
  $C:/MyDocuments/TestSandbox/ResultsBucket2012$
- create a new folder inside the folder of the corresponding test and name it “Cyclic”. Create another new folder inside “Cyclic”and name it “MakingO”. Inside this, save the file as “Load”
- from the Configure Measurement Wizard window, click the button *Online Document* and select the following file:
  $C:/MyDocuments/TestSandbox/BucketSetup/Script/cyclicH5.OPG$

Figure 21: Cyclic loading frame

– from the Configure Measurement Wizard window, click the button *Start Measurement Wizard*

After setting up the recording system, the loading system has to be prepared:

– fix the cyclic-loading frame (Figure 21) to the main loading frame and connect the cables of the weight hangers to the load cells on the vertical tower

– make sure the cables are horizontal

– hold the vertical tower in position with clamped wooden blocks

– disconnect the safety cable from the cyclic loading beam (Figure 22)

The cyclic motor can now be started. The cyclic motor is controlled by the software named STARTER. To start such software the following procedure should be followed:

– turn on the cyclic motor and STARTER

– press the *Open project* button and open the file:
$C:/ProgramFiles/SIEMENSstep7/s7proj/project$

Figure 22: Connection between the hinged beam and the safety cable

– open the Project window and select *Connect to target system*

– double click on $S110 - CU305\_D$ from the STARTER main window

– double click on $SERVO - 02$ from the STARTER main window

– select *Commissioning*

– select *Control panel*

– select *Assume control priority!*

– from the Assume Control Priority window, set 1000 ms and press *Accept*

– press *Enables*. Set 150 rounds per minute (rpm). This will in reality correspond to 6 rpm

Before starting the cyclic test, the rig has to be loaded and the cyclic motor activated. The following procedure should be followed:

– tare the recording system in CATMAN by pressing the button *Zero all active channels*

– start recording by pressing the button *Run acquisition* in CATMAN

– put the selected weights on the weight hangers

– tighten the steel cable attached to the hinged beam until CATMAN displays a force of 10N

– click the green button in the window of STARTER to activate the cyclic motor

STARTER is very sensitive and the motor may stop running when using the computer. When the test is to be stopped, click the red button in the window of STARTER, disconnect the target system and quit STARTER. Afterwards, remove the weights. Remember to stop and not to quit the recording session when a post-cyclic test is to be carried out.

6 Post-cyclic test

The post cyclic test is carried out with the screw jack placed on the vertical beam of the loading frame, see Figure 23. Practically speaking, a post-cyclic test is a monotonic test of a bucket that has already accumulated rotation due to cyclic loading. The system is instrumented in the same manner (three LVDTs measuring the displacements and the load cell measuring the applied force). Before starting the cyclic test, the data recording system has to be set up by following the procedure below:

– click the button *Configure Measurement Wizard*

– in the General settings, click the button *Export options* from the Online Data Export menu

– select the following file name:
$C:/MyDocuments/TestSandbox/ResultsBucket2012$

Figure 23: Static loading screw jack

– create a new folder inside the folder with the corresponding test and name it “Post-cyclic”. Inside this folder, save the file as “Post-cyclicxx”

– from the configure Measurement Wizard window, click the button *Start Measurement Wizard*

To ensure fully drained conditions, the post-cyclic tests should be performed with the power supply set to 10V. The post-cyclic test should be stopped when a peak in the load-displacement curve appears. The steps of a post-cyclic test are the following:

– connect vertical tower and screw jack (actuator) with a steel wire

– activate the screw jack by means of a proper electric motor. Before doing that, make sure the static load jack has enough space for spinning back

– start recording by pressing the button *Run acquisition* in CATMAN

– start the power supply and set it to 10 V

– when soil failure has occurred stop recording by pressing the button *Stop measurement* in CATMAN

– invert the wires of the power supply to release the load applied

7 Displacement measurement

The displacements of the bucket foundations are measured by means of two perpendicular plates on which the three LVDTs are placed. Two transducers are placed vertically and one horizontally. The direct measurements do not provide the actual displacement of the foundation. To figure out the displacements, the direct measurements are post-processed. The calculation process is based on that proposed by Larsen (2008). The system is depicted in Figure 24. The sign convention used is that put forward by Butterfield et al. (1997). The convention is illustrated in Figure 25 where, u is the horizontal displacement, w is the vertical displacement, θ is the rotational displacement, V is the vertical load, M is the overturning moment and H is the horizontal load.

The calculation of the displacements, u, w and θ, begins with the definition of the coordinates of the LVDTs at both initial and displaced configuration. Below, the coordinates are specified with respect to the origin of the system which is located on the bottom of the bucket lid, see Figure 24. The subscripts *i* and *d* stand for initial and displaced position.

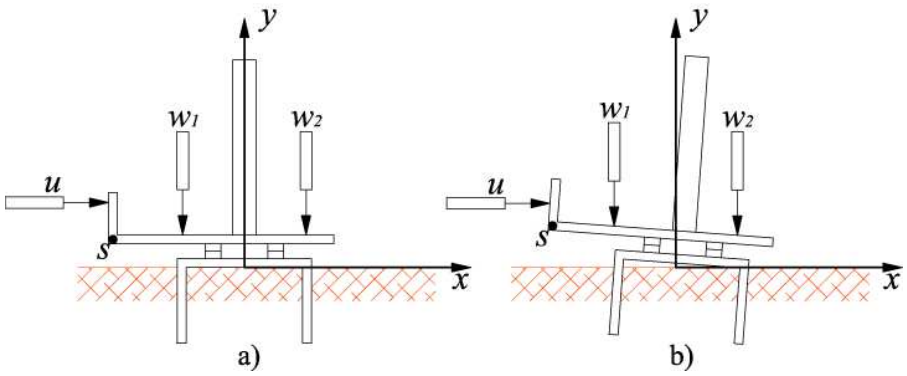

Figure 24: a) initial configuration of the foundation; b) displaced configuration of the foundation. After Larsen (2008)

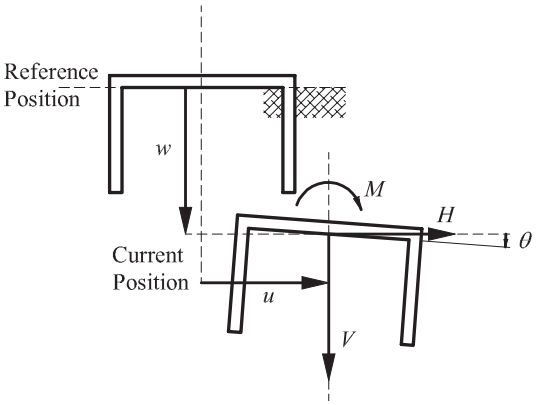

Figure 25: Sign convention for loads and displacements. After Butterfield et al. (1997)

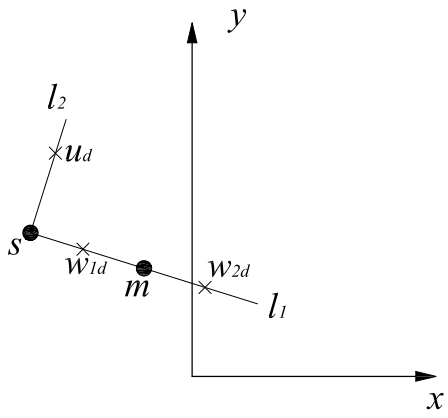

Figure 26: l_1 and l_2 during horizontal loading. After (Larsen, 2008)

The coordinates of the system at the beginning of the experiment can be expressed in mm as:

$$u_{1,i} = (-185, 120);$$

$$w_{1,i} = (-100, 95);$$

$$w_{2,i} = (100, 95);$$

where u_1 refers to the horizontal displacement transducer, w_1 refers to the first vertical displacement transducer and w_2 refers to the second vertical displacement transducer. Obviously, in case the dimension of the perpendicular plates are changed, the numerical value of the coordinates would change accordingly. The procedure though, would remain the same.

When a displacement occurs the coordinates become:

$$u_{1,d} = (-185 + \Delta x, 120);$$

$$w_{1,d} = (-100, 95 + \Delta y1);$$

$$w_{2,d} = (100, 95 + \Delta y2);$$

where Δx is the horizontal transducer measurement, $\Delta y1$ is the measurement of the first vertical transducer and $\Delta y2$ is the measurement of the second vertical transducer.

Note that depending on the displacement induced, the transducer measurements can be either positive or negative with respect to the coordinate system. For instance, according to the system illustrated in Figure 24, the second vertical measurement $\Delta y2$ is negative while the horizontal measurement Δx is positive as well as the first vertical measurement $\Delta y1$.

The horizontal and the vertical displacement of the bucket can be calculated by representing the perpendicular plates with two lines, see Figure 26. These two lines, l_1 and l_2, are expressed with two linear equations:

$$l_1 : \ y = a_1 \cdot x + b_1 \tag{1}$$

$$l_2 : \ y = a_2 \cdot x + b_2 \tag{2}$$

where the angular coefficients a_1 and a_2 and the constants b_1 and b_2 can be deduced for every recording by manipulating transducer coordinates and transducer measurements following equations (3)-(6) shown below. Figure 26 represents the two perpendicular plates in the displaced configuration. In the same figure, the junction of the two plates, s, the midpoint of line l_1, m, and the points of the transducer measurements u_d, $w_{1,d}$ and $w_{2,d}$, are indicated as well.

As it is intuitive, the rotation of the line l_1 is equal to the angular coefficient a_1, which can be calculated with equation 3. Thereof the rotation is simply $\theta = \arctan(a_1)$. Once a_1 is known also a_2 can be calculated in virtue of the perpendicular lines property (equation 4):

$$a_1 = \frac{\Delta y_2 - \Delta y_1}{200} \tag{3}$$

$$a_2 = \frac{-1}{a_1} \tag{4}$$

Now, since the coordinates of the displaced configuration are known, the constants b_1 and b_2 can be calculated as:

$$b_1 = 95 + \Delta y_1 + a_1 \cdot 100 \tag{5}$$

$$b_2 = 120 - (\Delta x - 185) \cdot a_2 \tag{6}$$

Hence, by knowing the constants b_1 and b_2 the coordinates of the junction point *s* can be calculated:

$$x_s = \frac{b_2 - b_1}{a_1 - a_2} \tag{7}$$

$$y_s = a_1 \cdot x_s + b_1 \tag{8}$$

The coordinates of m are necessary to assess the displacement of the bucket foundation reference point. The coordinates of m are calculated as:

$$x_m = x_s + 185 \cdot \cos(\theta) \tag{9}$$

$$y_m = y_s - 185 \cdot \cos(\theta) \tag{10}$$

Finally the horizontal displacement u and the vertical displacement w are obtained with the following relationships:

$$u = x_m - 95 \cdot \sin(\theta) \tag{11}$$

$$w = -(y_m - 95 \cdot \cos(\theta)) \tag{12}$$

In Figure 27 one displacement transducer on the right-hand side and one force transducer (or load cell) on the left-hand side are depicted.

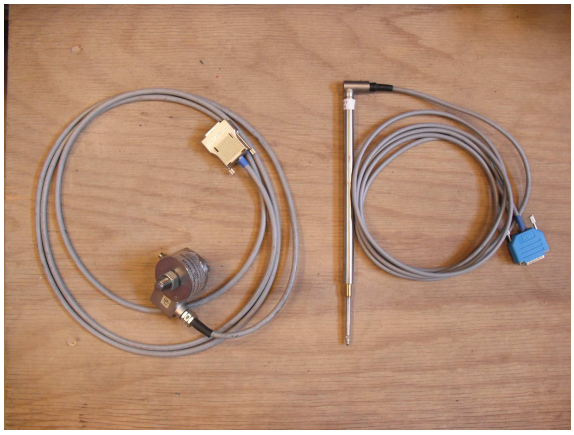

Figure 27: Force and displacement transducer

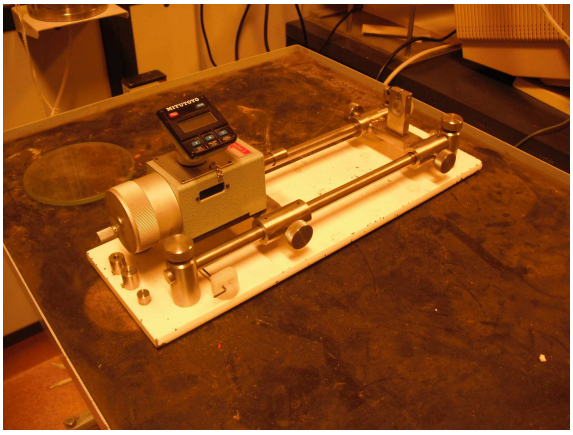

Figure 28: LVDTs calibration rig

Before overtaking the experimental programme all the transducers must be calibrated. The three LVDTs are calibrated by means of the calibration rig depicted in Figure 28.

References

Larsen, K. A. (2008). *Static behaviour of bucket foundations*. Ph.D. thesis, Aalborg University

Butterfield, R., Houlsby, G. T. and Gottardi, G. (1997). Standardized sign conventions and notation for generally loaded foundations. *Géotechnique* 47, No. 5, 1051-1054

LeBlanc, C., Byrne, B. W. and Houlsby, G. T. (2010). Response of stiff piles in sand to long-term cyclic lateral loading. *Géotechnique* 60, No. 2, 79-90

Ibsen, L. B., Hanson, M., Hjort, T. H. and Thaarup, M. (2009). *MC parameter calibration for Aalborg University Sand No. 1*. DCE Technical Report No. 62, Department of Civil Engineering, Aalborg University

Data sheets

The following pages of the report include the list of the tests performed and the essential data sheets of each experimental test.

Legend for tests list and data sheets

D	Diameter of the foundation
d/D	Embedment ratio
M/HD	Ratio between load eccentricity and diameter
Gradient	Water gradient applied before preparing the sample
Dr	Relative density
V max	Maximum vertical load during installation
ζb	Ratio between the maximum cyclic moment and the monotonic failure moment
ζc	Ratio between minimum and maximum cyclic moments
Period	Period of the cyclic loading
No. Cycles	Number of cycles
V	Vertical load during test
θ final	Final accumulated rotation
M max	Post-cyclic maximum moment
θ max	Rotation correspondng to the maximum moment for standard and post-cyclic monotonic tests
V ult	Ultimate vertical load
M1	Mass on the weight hanger 1
M2	Mass on the weight hanger 2
M3	Mass on the weight hanger 3
Mmax	Maximum cyclic moment
Mmin	Minimum cyclic moment

Cyclic tests with constant V and constant M/HD

Test	Loading and foundation geometry			Preparation of the soil sample		Installation phase	Cyclic loading phase						Monotonic post-cyclic phase	
	[mm]	[-]	[-]	[-]	[%]	[N]	[-]	[-]	[sec]	[-]	[N]	[deg]	[Nm]	[deg]
	D	**d/D**	**M/HD**	**Gradient**	**Dr**	**V max**	**ζb**	**ζc**	**Period**	**No. Cycles**	**V**	**θ final**	**M max**	**θ max**
C15	300	1	1.987	-	88.18	-	0.278	-0.846	10	50647	241	0.079	185.4	1.110
C16	300	1	1.987	-	81.57	-	0.403	-0.047	10	50063	241	0.427	177.5	1.995
C17	300	1	1.987	-	79.62	-	0.536	0.027	10	49978	241	1.228	184.4	2.183
C18	300	1	1.987	-	80.71	-	0.304	-0.042	10	50004	241	0.158	180.4	2.222
C20	300	1	1.987	-	82.67	-	0.358	-0.595	10	50049	241	0.435	190.6	1.883
C22	300	1	1.987	-	82.33	-	0.383	0.193	10	50255	241	0.381	192.4	1.542
C23	300	1	1.987	-	86.71	-	0.381	-0.426	10	50209	241	0.503	200.8	2.091
C24	300	1	1.987	-	83.09	-	0.367	-0.963	10	50642	241	0.100	203.4	1.064
C31	300	1	1.987	0.90	91.20	-	0.339	0.036	10	100933	241	0.297	185.9	1.082
C32	300	1	1.987	0.90	92.65	-	0.421	-0.146	10	49959	241	0.522	193.6	1.171
C33	300	1	1.987	0.95	92.09	26967	0.382	-0.316	10	50471	241	0.400	200.2	1.423
C34	300	1	1.987	0.974	92.63	25398	0.252	-0.604	10	10022	241	0.058	191.8	1.447
C35	300	1	1.987	0.974	88.87	25281	0.484	-0.543	10	9976	241	0.678	203.2	1.600
C36	300	1	1.987	0.8	98.79	25149	0.583	-0.563	10	10153	241	1.216	217.5	1.710
C37	300	1	1.987	0.89	99.41	34551	0.687	-0.578	10	10083	241	2.000	220.6	2.376
C38	300	1	1.987	0.817	99.03	25152	0.758	-0.583	10	10016	241	2.574	228.2	2.839
C39	300	1	1.987	1.13	94.68	25668	0.856	-0.588	10	9366	241	3.128	-	-
C40	300	1	1.987	1.06	96.17	25125	1.155	-0.469	10	108	241	2.451	232.4	3.659
C41	300	1	1.987	-	96.39	25731	0.400	-0.522	10	10032	241	0.290	208.8	1.230
C42	300	1	1.987	0.96	96.83	25212	0.420	-0.500	20	10124	241	0.354	206.5	1.488
C44	300	1	1.987	0.956	95.91	27798	0.389	-0.598	30	10148	241	0.277	201.4	1.191
C45	300	1	1.987	-	94.05	25185	0.387	-479	5	10070	241	0.314	214.8	1.66
C46	300	1	1.987	1.06	94.67	25206	0.419	-0.5	40	10031	241	0.321	204.5	1.19
C47	300	1	1.987	1.06	96.9	7659	0.378	-0.796	10	50001	241	0.283	205.5	0.98
C49	300	0.5	1.987	1.08	98.30	14540	0.224	0.037	10	74917	198	0.017	57.37	2.502
C50	300	0.5	1.987	1.08	97.41	14800	0.355	-0.054	10	9953	198	0.0634	56.26	2.52
C51	300	0.5	1.987	1.08	97.76	15200	0.436	-0.040	10	10089	198	0.0888	56.4	2.319
C53	300	0.5	1.987	1.08	92.05	15234	0.514	-0.049	10	16068	198	0.362	57.97	2.486
C54	300	0.5	1.987	0.96	87.55	14301	0.339	0.019	10	16327	198	0.099	46.4	1.778
C55	300	0.5	1.987	0,96	82.55	14325	0.398	0.04	10	15233	198	0.1407	47.3	2.646
C58	300	0.75	1.987	0.96	82.47	19530	0.177	-0.09	10	34459	208	0.03	101.7	2.16
C59	300	0.75	1.987	0.96	82.47	19425	0.244	-0.055	10	9984	208	0.0783	101.2	2.4
C60	300	0.75	1.987	0.96	83.19	19008	0.312	0.0547	10	10058	208	0.0978	103.2	2.27
C61	300	0.75	1.987	0.96	83.41	18116	0.376	0.053	10	18116	208	0.3874	104.5	4.88

Monotonic tests with constant V and constant M/HD

	Loading and foundation geometry			Preparation of the soil sample		Installation phase	Monotonic loading phase		
Test	[mm]	[-]	[-]	[-]	[%]	[N]	[N]	[Nm]	[-]
	D	**d/D**	**M/HD**	**Gradient**	**Dr**	**V max**	**V**	**M max**	**θ max**
S13	300	1	3.010	-	85.3	-	241	189.13	1.92
S19	300	1	1.987	-	81.9	-	241	179,67	2.41
S25	300	1	1.100	-	90.8	-	241	152.59	1.407
S26	300	1	5.820	-	94.09	-	241	213.71	1.32
S27	300	1	8.748	-	94.2	-	241	219.27	0.919
S28	300	1	5.819	-	94.8	-	241	218.09	1.28
S29	300	1	3.010	-	90.52	-	241	195.35	1.02
S30	300	1	1.987	-	92.8	-	241	183.46	1.15
S48	300	0.5	1.987	1.08	94.61	14500	198	53.46	2.3
S52	300	0.5	1.987	1.08	93.55	3639	198	55.18	1.8
S56	300	0.75	1.987	1.08	83.15	4218	208	95.35	2.29
S57	300	0.75	1.987	1.08	83.1	19464	208	97.53	2.12

Pure V monotonic tests

	Foundation geometry		Sample preparation and test phase	
Test	[mm]	[-]	[%]	[kN]
	D	**d/D**	**Dr**	**V ult**
S63	300	0.75	77.97	76.97
S64	300	1	77.39	91.66

Test equipment	Blue sandbox
User	Aligi
Test name	S13
Date	-

Bucket

Diameter [mm]	300
Embedment ratio	1

Test

Static or cyclic test	static
Moment arm [mm]	0.903

General Comments

CPT 1 was not carried out properly

Soil Preparation & Installation Phase

Gradient applied

-

Cone Penetration Resistance

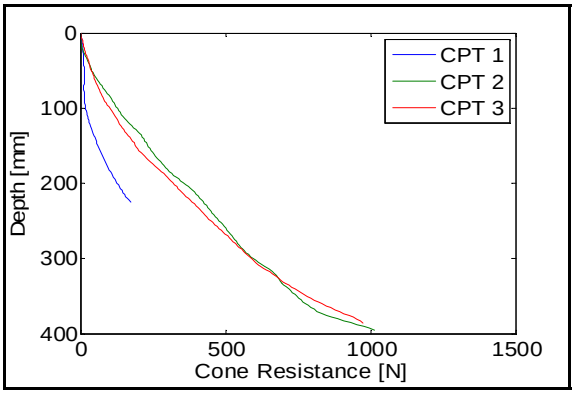

Installation Phase

Relative density [%]

cpt 1	cpt 2	cpt 3	Average
-	86.33	84.27	85.30

Maximum installation force [N]	-
Penetration depth [mm]	-

Horizontal and Vertical displacement-Rotation

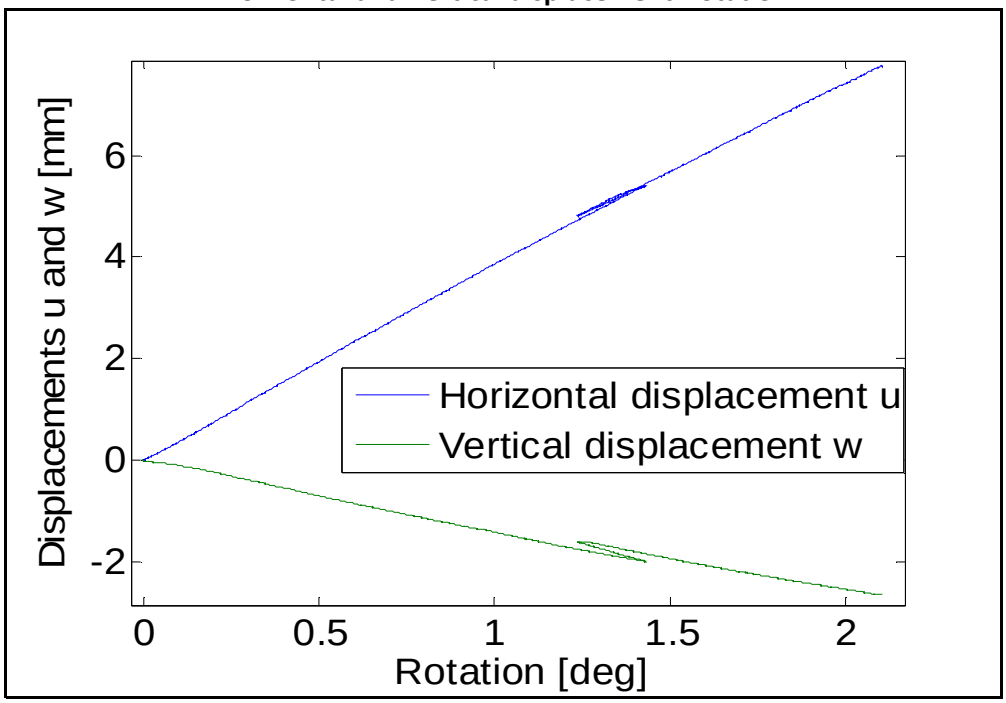

Moment-Rotation

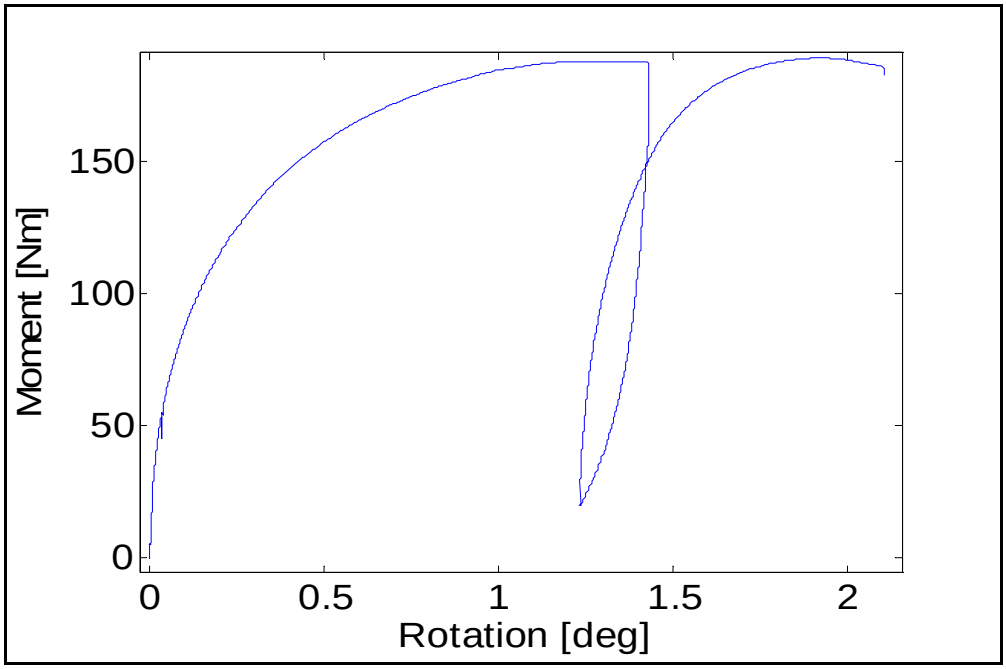

Maximum moment [Nm]	189.13
Rotation at maximum moment [deg]	1.92

Test equipment	Blue sandbox
User	Aligi & Matthias
Test name	C15
Date	07/05/2012

Bucket

Diameter [mm]	300
Embedment ratio	1

Test

Static or cyclic test	cyclic
Moment arm [mm]	596

General Comments

None

Soil Preparation and Installation Phase

Gradient applied

-

Cone Penetration Resistance

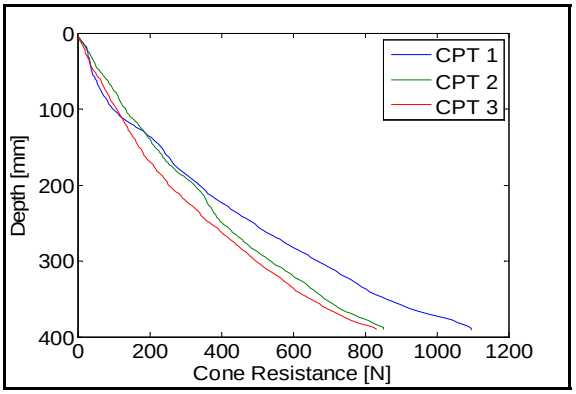

Installation Phase

Relative density [%]

cpt 1	cpt 2	cpt 3	Average
91.63	87.86	85.05	88.18

Maximum installation force [N]	-
Penetration depth [mm]	-

Cyclic Test Phase

Masses on the weight hangers [Kg]

M1	M2	M3
9.775	14.61	33

Number of cycles	50647
Loading period [s]	10

LVDTs-Time, Rotation-Time

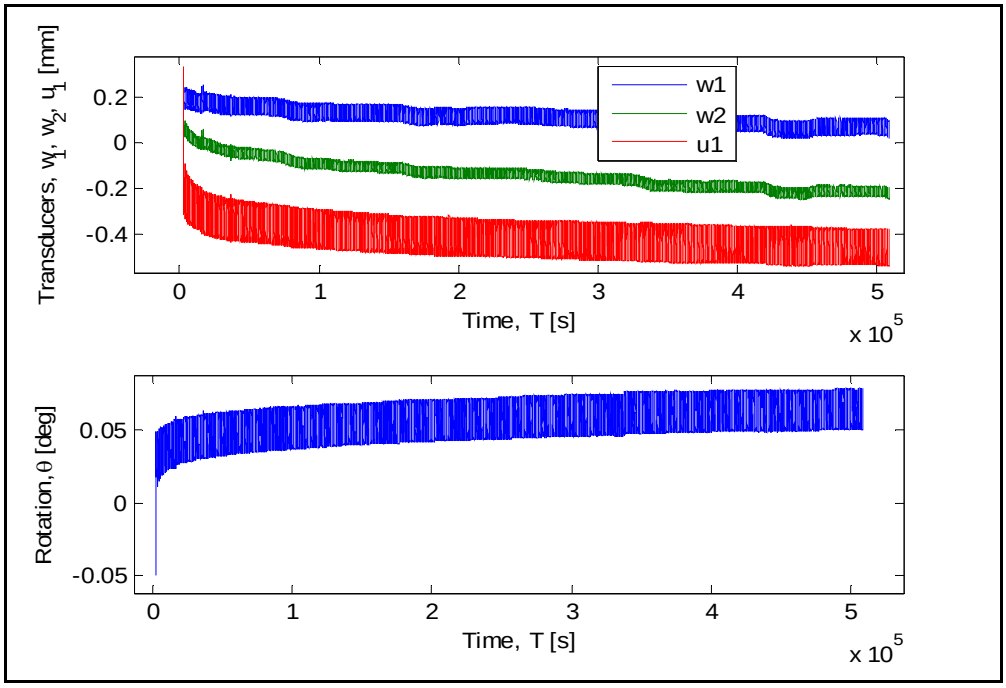

Horizontal Load-Time, Moment-Rotation

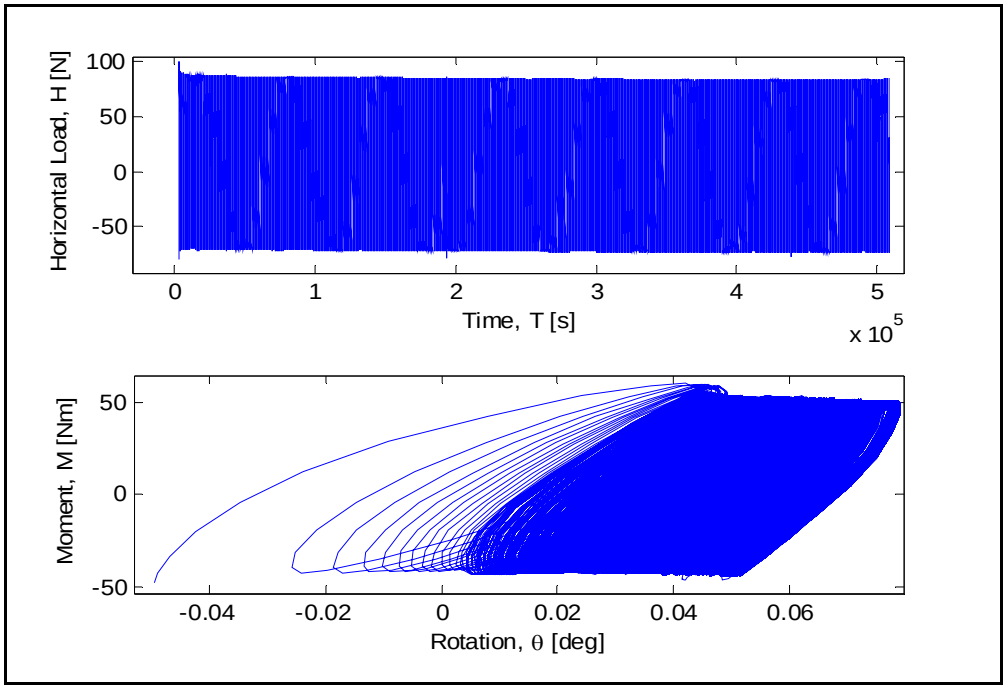

Maximum accumulated rotation [deg] 0.079

Maximum and minimum moment [Nm]

Mmax	Mmin
50.98	-43.14

ζb	ζc
0.278	-0.846

Post-Cyclic Phase

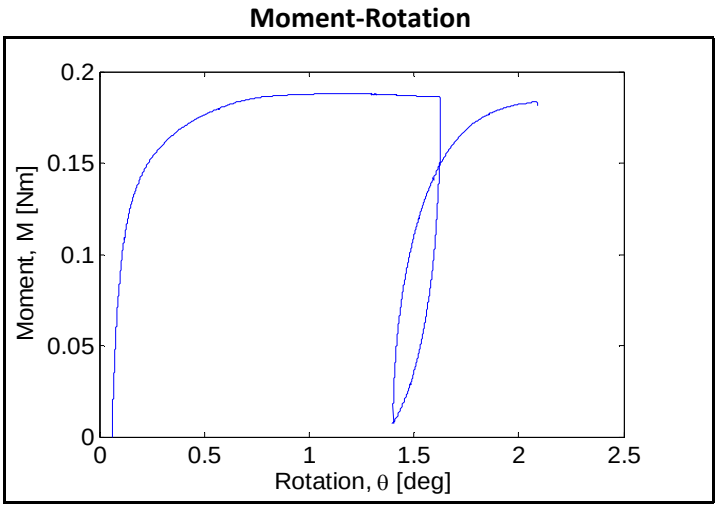

Maximum moment [Nm]	185.41
Rotation at maximum moment [deg]	1.11

Test equipment	Blue sandbox
User	Aligi & Matthias
Test name	C16
Date	23/05/2012

Bucket

Diameter [mm]	300
Embedment ratio	1

Test

Static or cyclic test	cyclic
Moment arm [mm]	596

General Comments

None

Soil Preparation and Installation Phase

Gradient applied

-

Cone Penetration Resistance

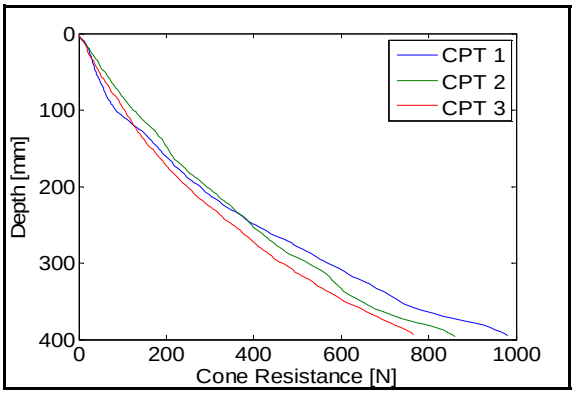

Installation Phase

Relative density [%]

cpt 1	cpt 2	cpt 3	Average
82.49	82.78	79.43	81.57

Maximum installation force [N]	-
Penetration depth [mm]	-

Cyclic Test Phase

Masses on the weight hangers [Kg]

M1	M2	M3
7.775	5.61	33

Number of cycles	50063
Loading period [s]	10

LVDTs-Time, Rotation-Time

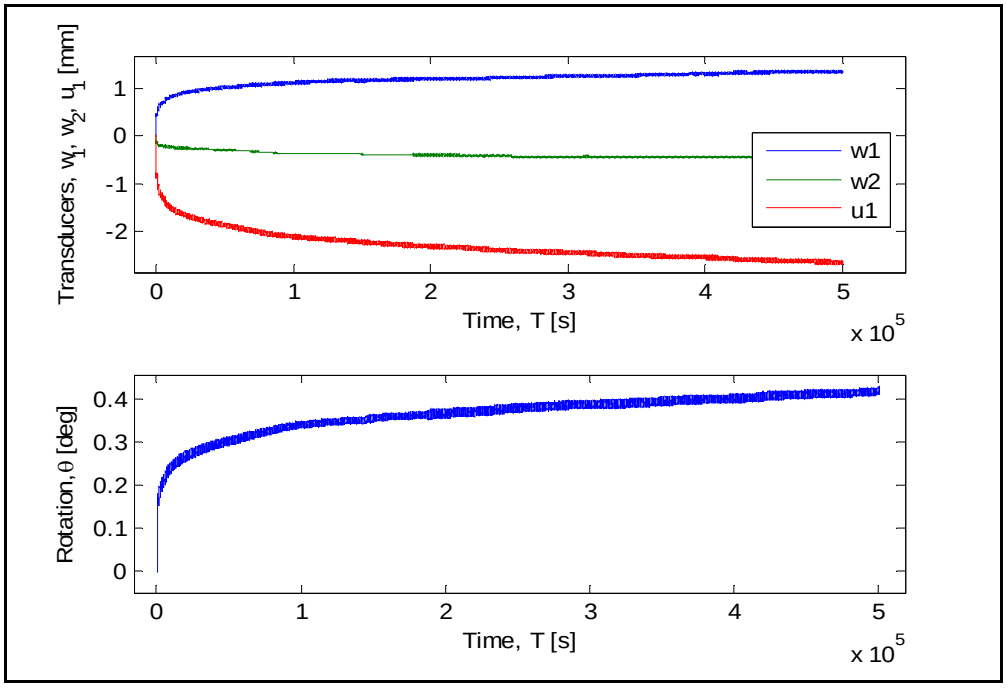

Horizontal Load-Time, Moment-Rotation

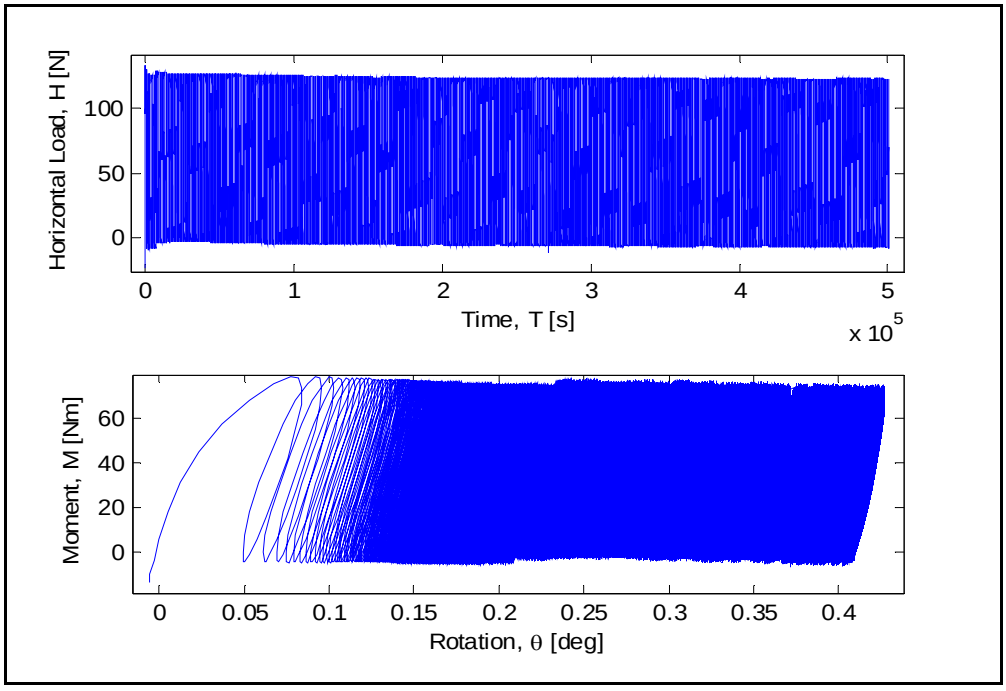

Maximum accumulated rotation [deg] | 0.4271

Maximum and minimum moment [Nm]

Mmax	Mmin
73.82	-3.47

ζb	ζc
0.403	-0.047

Post-Cyclic Phase

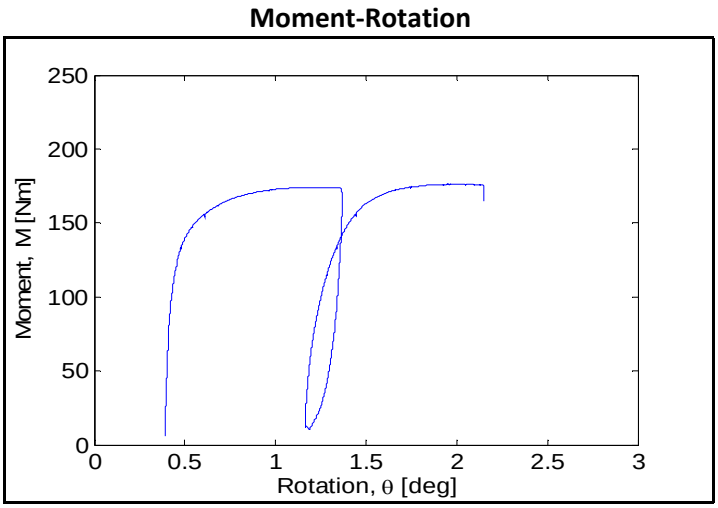

Maximum moment [Nm]	177.46
Rotation at maximum moment [deg]	1.995

Test equipment	Blue sandbox
User	Aligi & Matthias
Test name	C17
Date	30/05/2012

Bucket

Diameter [mm]	300
Embedment ratio	1

Test

Static or cyclic test	cyclic
Moment arm [mm]	596

General Comments

None

Soil Preparation and Installation Phase

Gradient applied

-

Cone Penetration Resistance

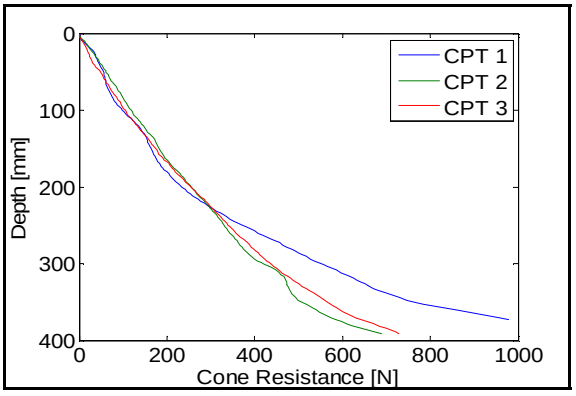

Installation Phase

Relative density [%]

cpt 1	cpt 2	cpt 3	Average
81.02	78.82	79.04	79.62

Maximum installation force [N]	-
Penetration depth [mm]	-

Cyclic Test Phase

Masses on the weight hangers [Kg]

M1	M2	M3
9.775	6.11	33

Number of cycles	49978
Loading period [s]	10

LVDTs-Time, Rotation-Time

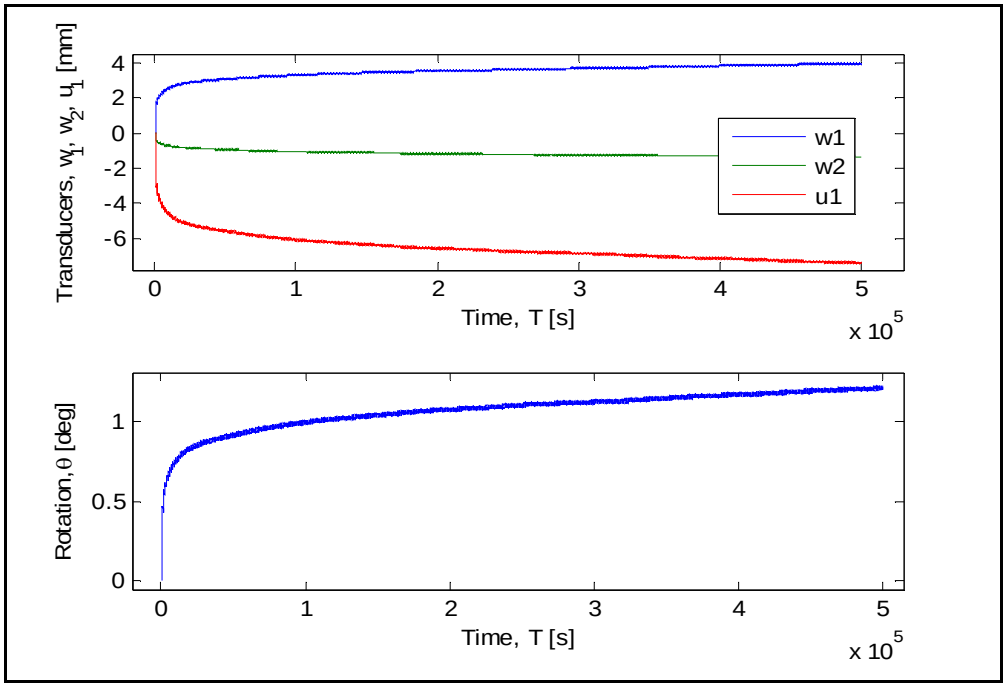

Horizontal Load-Time, Moment-Rotation

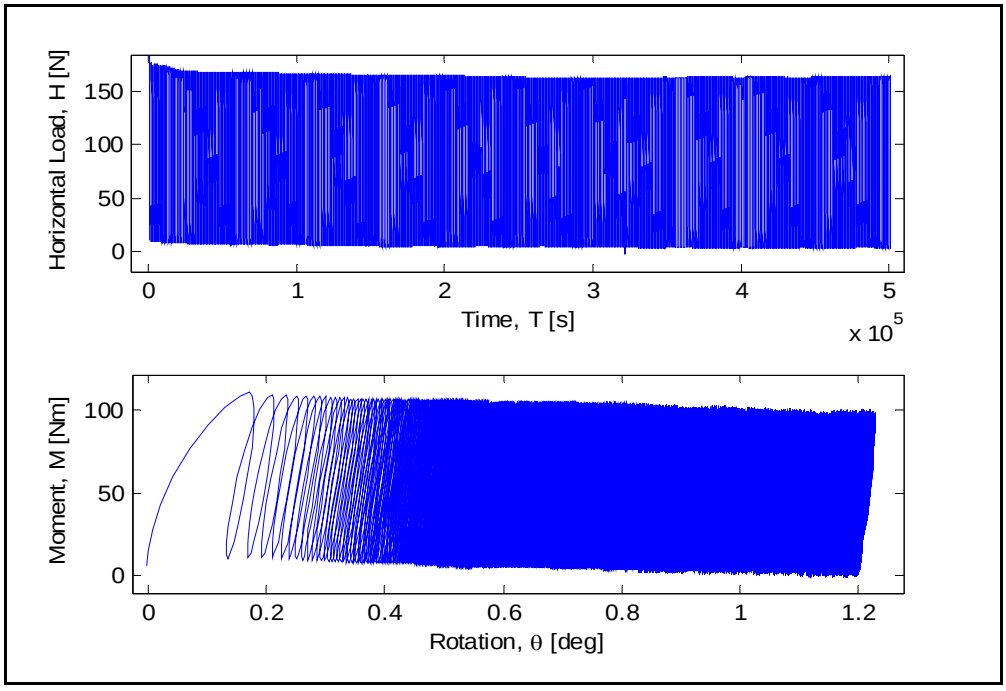

Maximum accumulated rotation [deg]	1.228

Maximum and minimum moment [Nm]

Mmax	Mmin
98.26	2.66

ζb	ζc
0.536	0.027

Post-Cyclic Phase

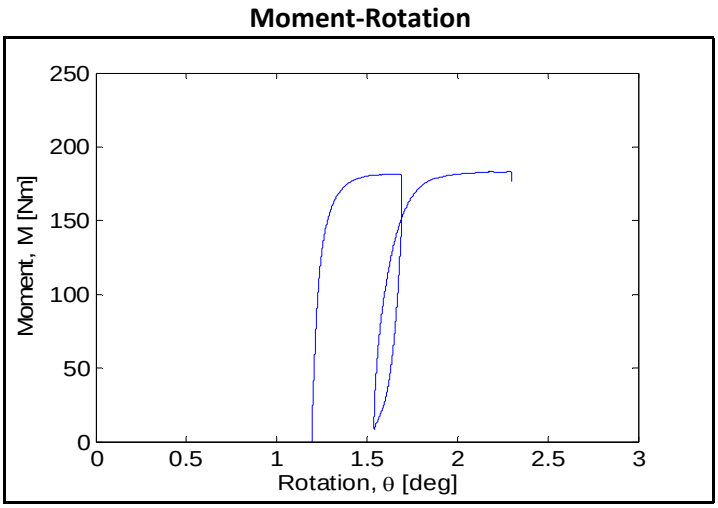

Maximum moment [Nm]	184.43
Rotation at maximum moment [deg]	2.183

Test equipment	Blue sandbox
User	Aligi & Matthias
Test name	C18
Date	07/06/2012

Bucket

Diameter [mm]	300
Embedment ratio	1

Test

Static or cyclic test	cyclic
Moment arm [mm]	596

General Comments

None

Soil Preparation and Installation Phase

Gradient applied

-

Cone Penetration Resistance

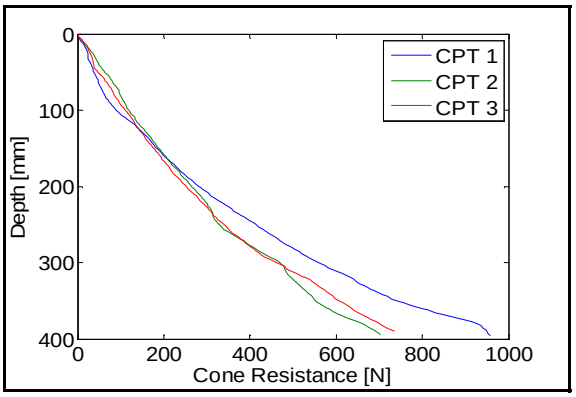

Installation Phase

Relative density [%]

cpt 1	cpt 2	cpt 3	Average
82.68	79.81	79.63	80.71

Maximum installation force [N]	-
Penetration depth [mm]	-

Cyclic Test Phase

Masses on the weight hangers [Kg]

M1	M2	M3
5.775	7.11	33

Number of cycles	50004
Loading period [s]	10

LVDTs-Time, Rotation-Time

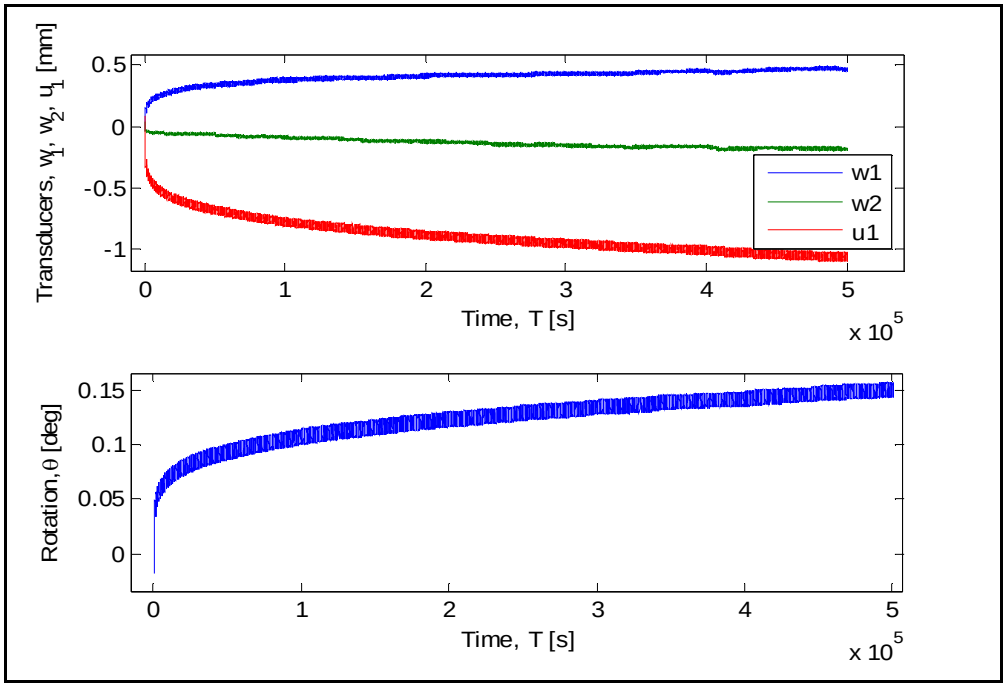

Horizontal Load-Time, Moment-Rotation

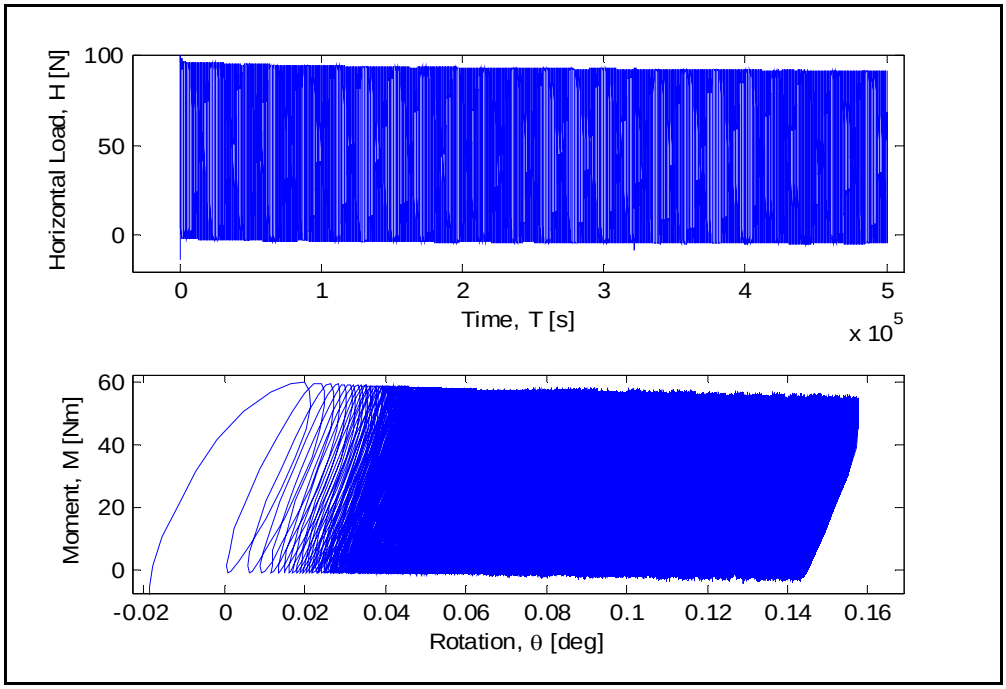

Maximum accumulated rotation [deg] | 0.158

Maximum and minimum moment [Nm]

Mmax	Mmin
55.71	-2.33

ζb	ζc
0.304	-0.042

Post-Cyclic Phase

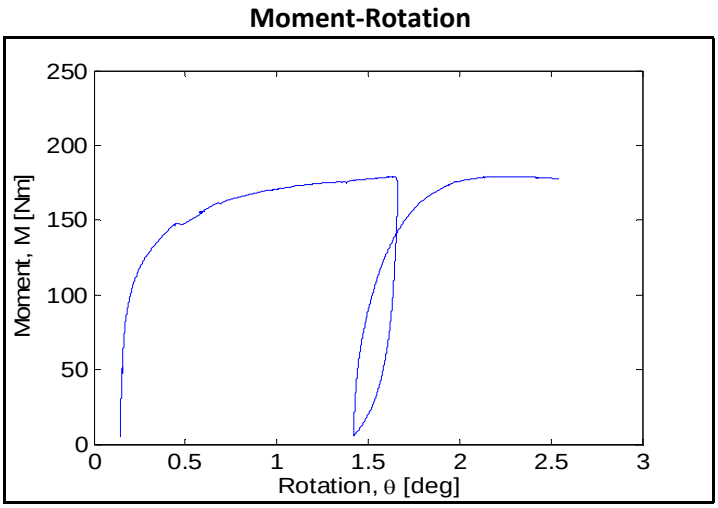

Maximum moment [Nm]	180.4
Rotation at maximum moment [deg]	2.222

Test equipment	Blue sandbox
User	Aligi
Test name	S19
Date	-

Bucket

Diameter [mm]	300
Embedment ratio	1

Test

Static or cyclic test	static
Moment arm [mm]	0.596

General Comments

None

Soil Preparation & Installation Phase

Gradient applied

-

Cone Penetration Resistance

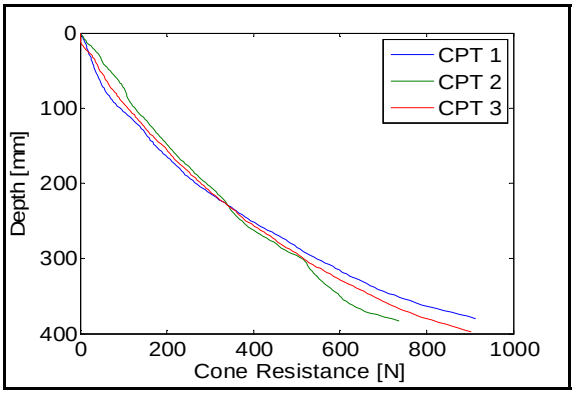

Installation Phase

Relative density [%]

cpt 1	cpt 2	cpt 3	Average
81.77	81.88	82.08	81.91

Maximum installation force [N]	-
Penetration depth [mm]	-

Horizontal and Vertical displacement-Rotation

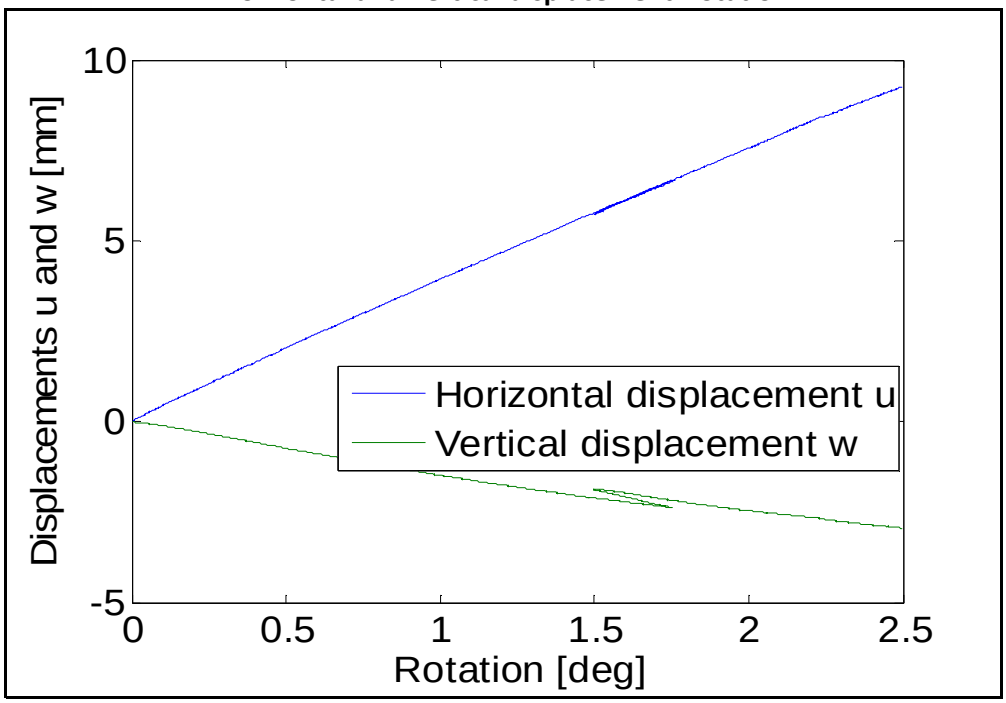

Moment-Rotation

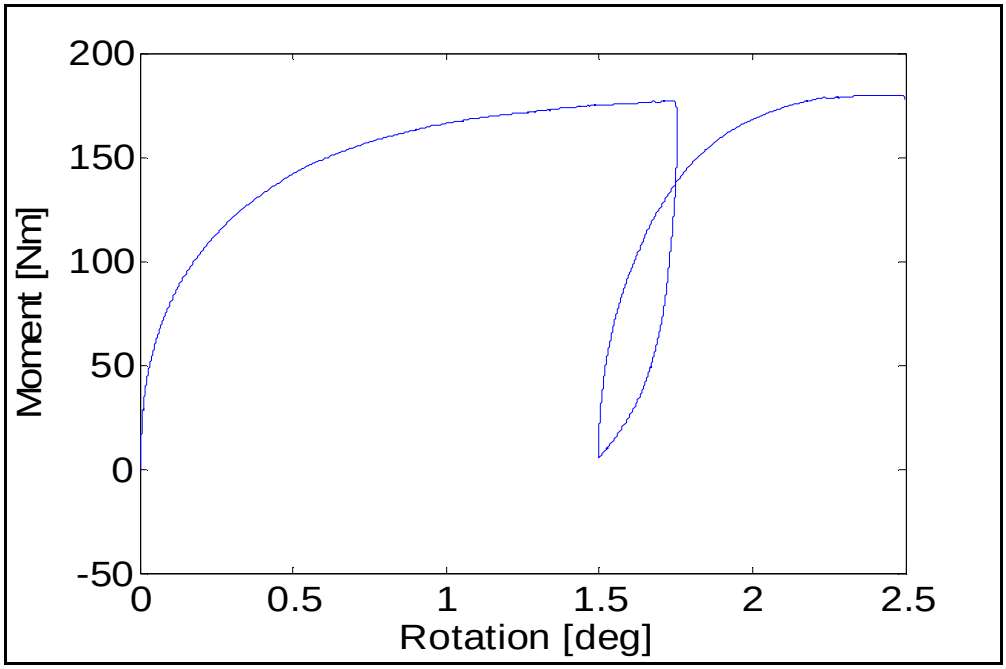

Maximum moment [Nm]	179.67
Rotation at maximum moment [deg]	2.41

Test equipment	Blue sandbox
User	Aligi & Matthias
Test name	C20
Date	14/06/2012

Bucket	
Diameter [mm]	300
Embedment ratio	1
Test	
Static or cyclic test	cyclic
Moment arm [mm]	596

General Comments

There was a mistake when recording the post-cyclic test. Only the moment-rotation curve of the test can be relied on. *u* and *w* cannot be trusted.

Soil Preparation and Installation Phase

Gradient applied

-

Cone Penetration Resistance

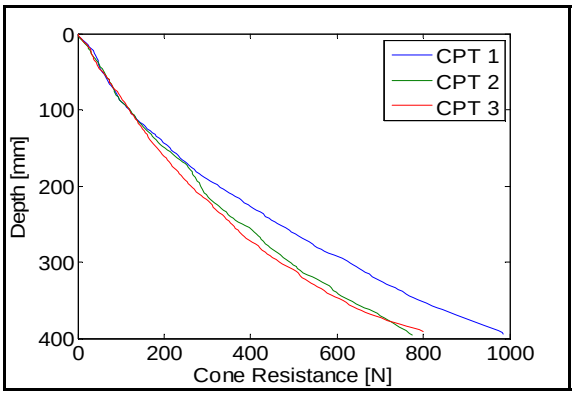

Installation Phase

Relative density [%]

cpt 1	cpt 2	cpt 3	Average
86.65	81.82	80.53	82.67

Maximum installation force [N]	-
Penetration depth [mm]	-

Cyclic Test Phase

Masses on the weight hangers [Kg]

M1	M2	M3
10.575	14.61	33

Number of cycles	50049
Loading period [s]	10

LVDTs-Time, Rotation-Time

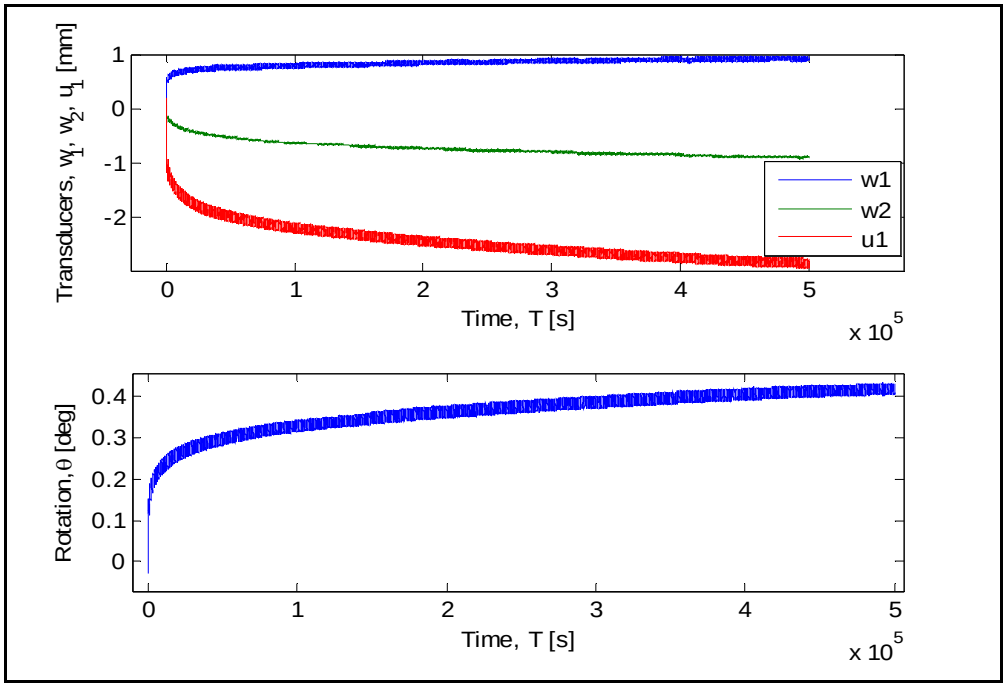

Horizontal Load-Time, Moment-Rotation

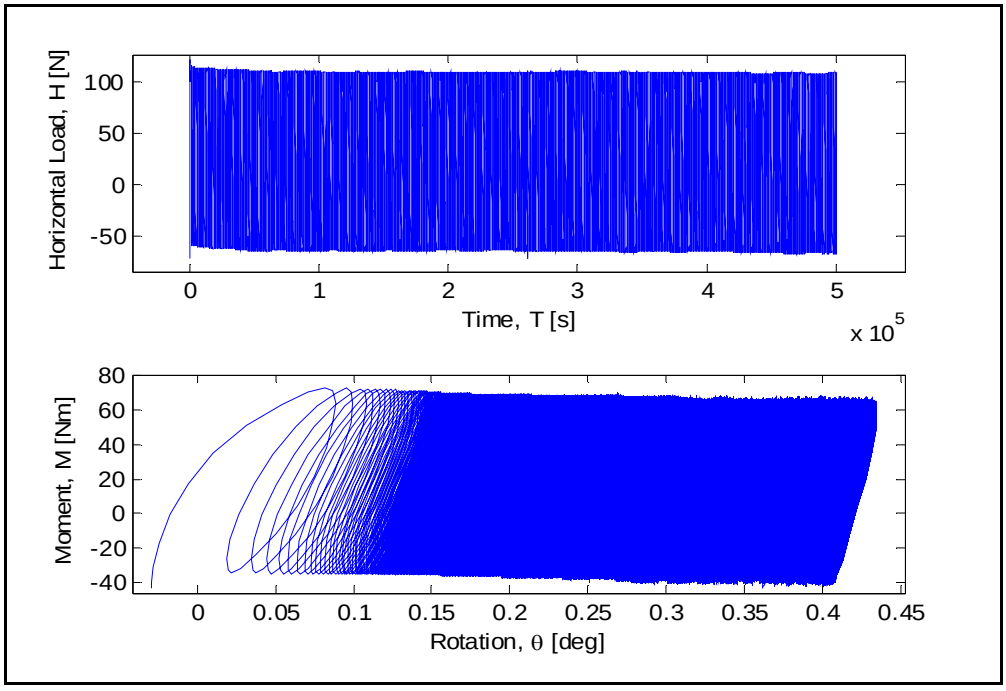

Maximum accumulated rotation [deg]	0.435

Maximum and minimum moment [Nm]

Mmax	Mmin
65.7	-39.07

ζb	ζc
0.358	-0.595

Post-Cyclic Phase

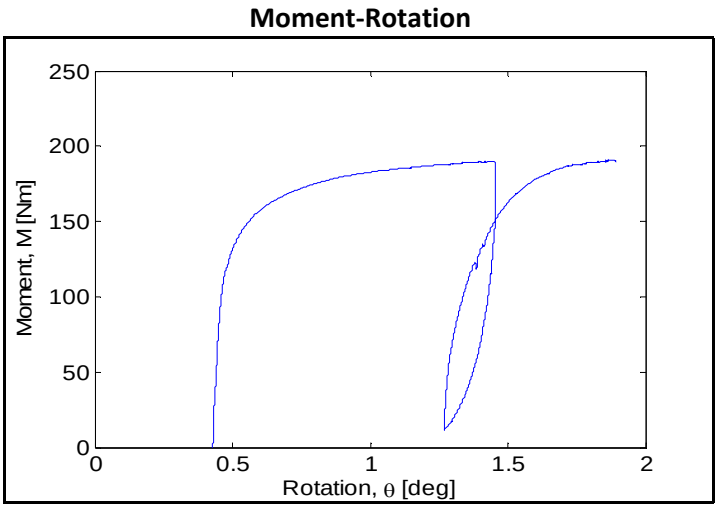

Maximum moment [Nm]	190.64
Rotation at maximum moment [deg]	1.883

Test equipment	Blue sandbox
User	Aligi & Matthias
Test name	C22
Date	28/06/2012

Bucket

Diameter [mm]	300
Embedment ratio	1

Test

Static or cyclic test	cyclic
Moment arm [mm]	596

General Comments

None

Soil Preparation and Installation Phase

Gradient applied

-

Cone Penetration Resistance

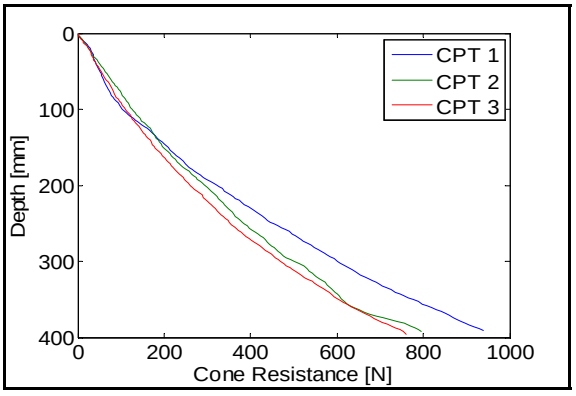

Installation Phase

Relative density [%]

cpt 1	cpt 2	cpt 3	Average
84.77	82.11	80.11	82.33

Maximum installation force [N]	-
Penetration depth [mm]	-

Cyclic Test Phase

Masses on the weight hangers [Kg]

M1	M2	M3
5.275	4.61	33

Number of cycles	50255
Loading period [s]	10

LVDTs-Time, Rotation-Time

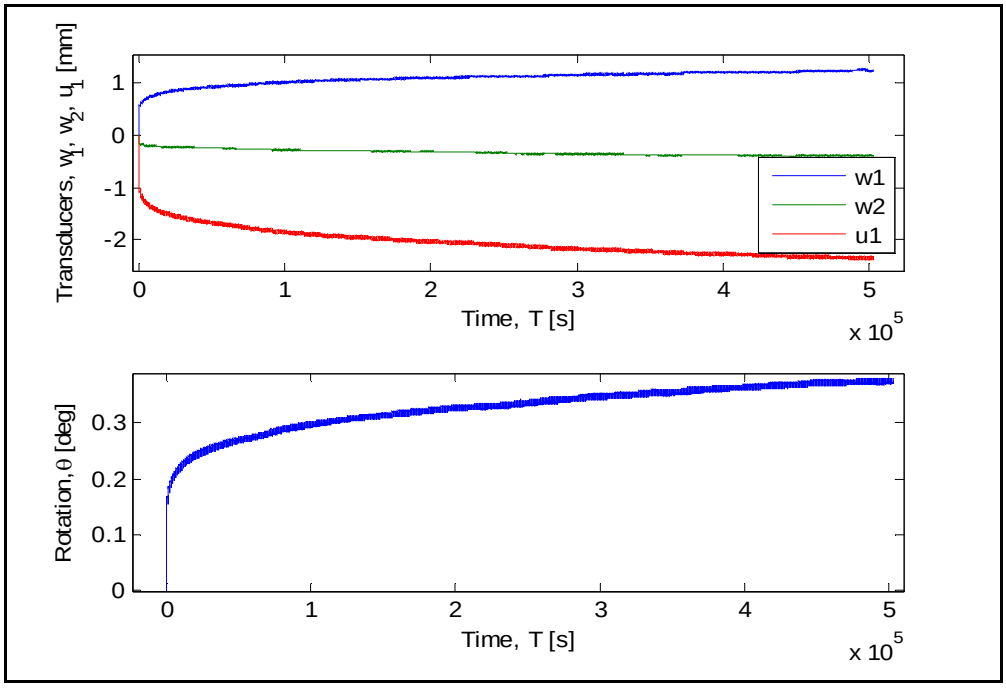

Horizontal Load-Time, Moment-Rotation

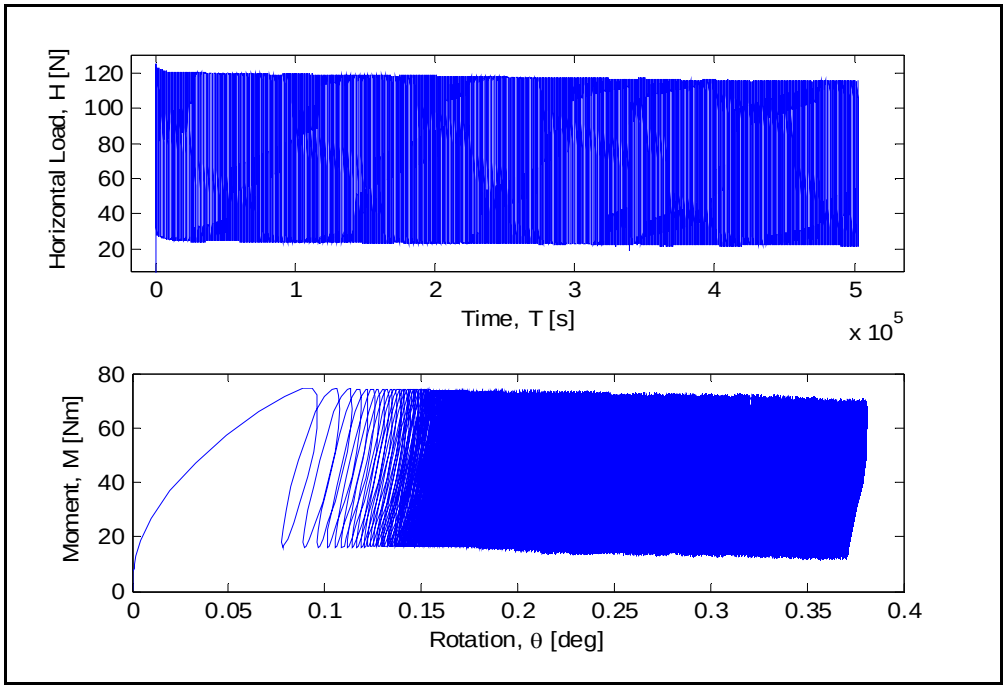

Maximum accumulated rotation [deg]	0.381

Maximum and minimum moment [Nm]

Mmax	Mmin
70.26	13.58

ζb	ζc
0.383	0.193

Post-Cyclic Phase

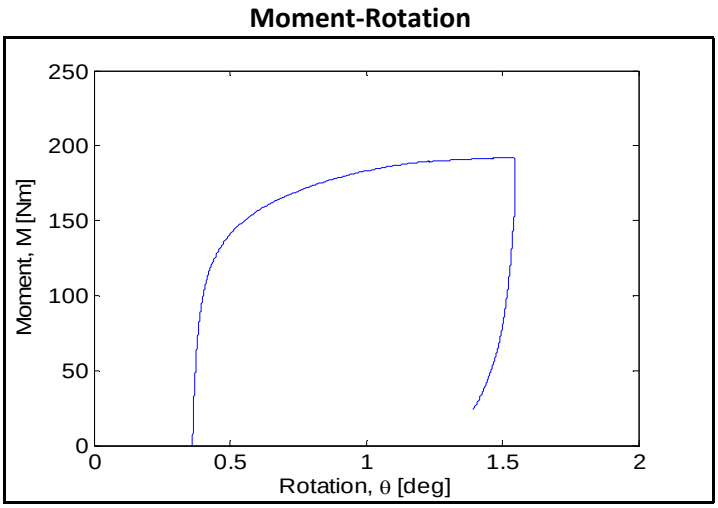

Maximum moment [Nm]	192.4
Rotation at maximum moment [deg]	1.542

Test equipment	Blue sandbox
User	Aligi & Matthias
Test name	C23
Date	05/07/2012

Bucket

Diameter [mm]	300
Embedment ratio	1

Test

Static or cyclic test	cyclic
Moment arm [mm]	596

General Comments

None

Soil Preparation and Installation Phase

Gradient applied

-

Cone Penetration Resistance

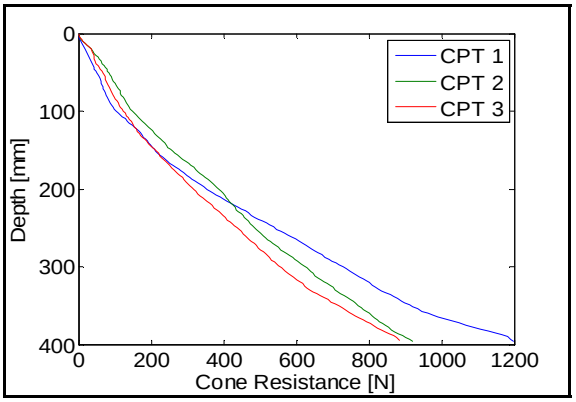

Installation Phase

Relative density [%]

cpt 1	cpt 2	cpt 3	Average
88.09	87.78	84.25	86.71

Maximum installation force [N]	-
Penetration depth [mm]	-

Cyclic Test Phase

Masses on the weight hangers [Kg]

M1	M2	M3
9.775	11.61	33

Number of cycles	50209
Loading period [s]	10

LVDTs-Time, Rotation-Time

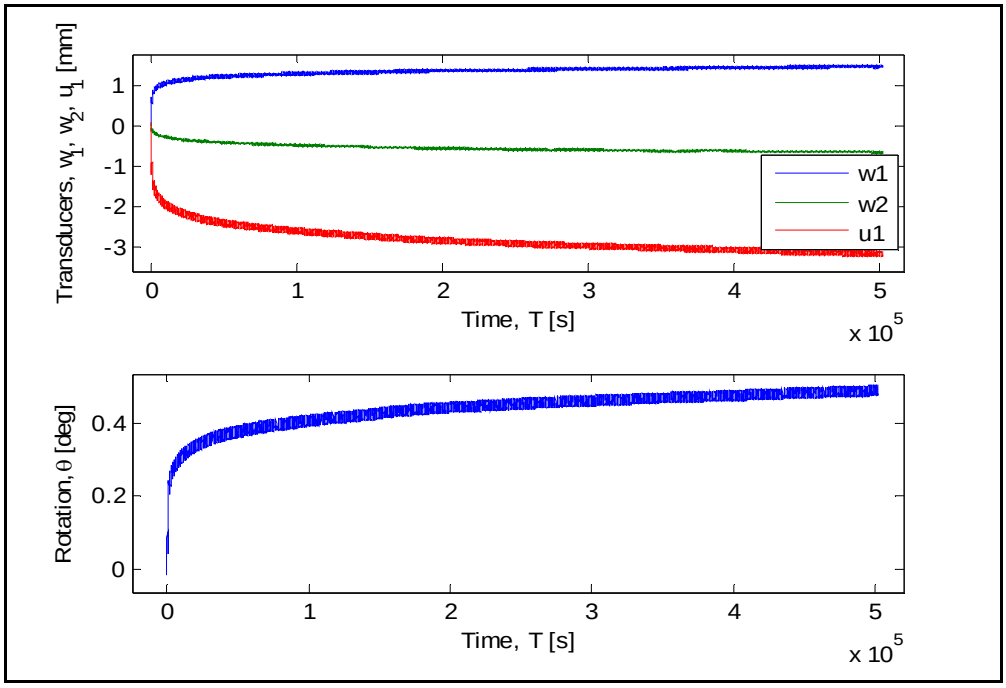

Horizontal Load-Time, Moment-Rotation

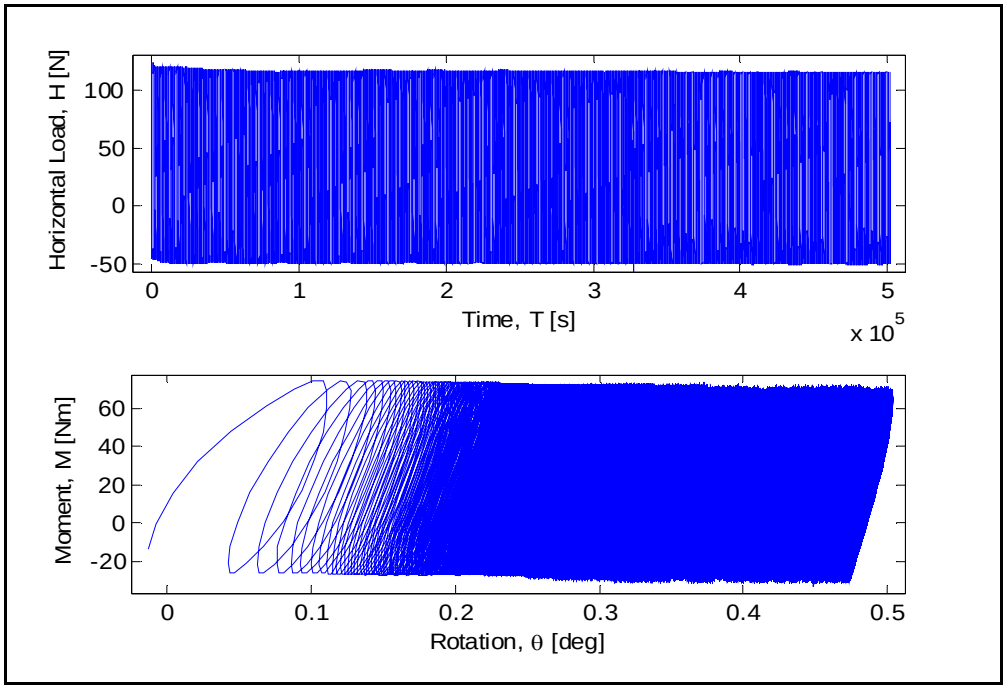

Maximum accumulated rotation [deg] 0.503

Maximum and minimum moment [Nm]

Mmax	Mmin
69.84	-29.73

ζb	ζc
0.381	-0.426

Post-Cyclic Phase

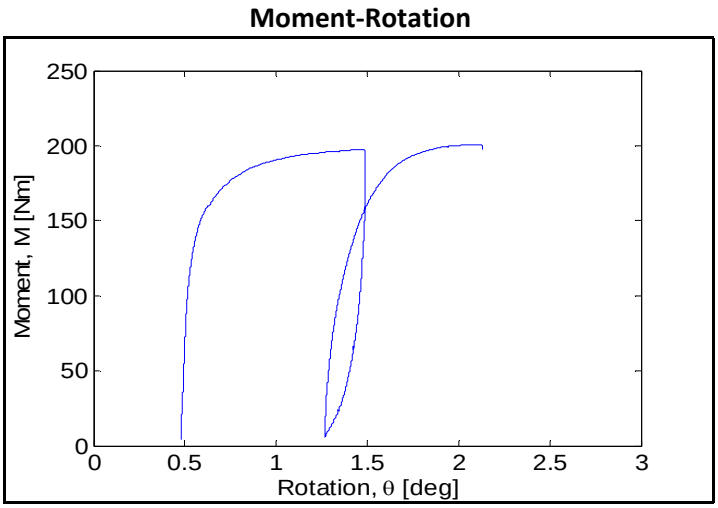

Maximum moment [Nm]	200.8
Rotation at maximum moment [deg]	2.091

Test equipment	Blue sandbox
User	Aligi & Matthias
Test name	C24
Date	12/07/2012

Bucket

Diameter [mm]	300
Embedment ratio	1

Test

Static or cyclic test	cyclic
Moment arm [mm]	596

General Comments

None

Soil Preparation and Installation Phase

Gradient applied

-

Cone Penetration Resistance

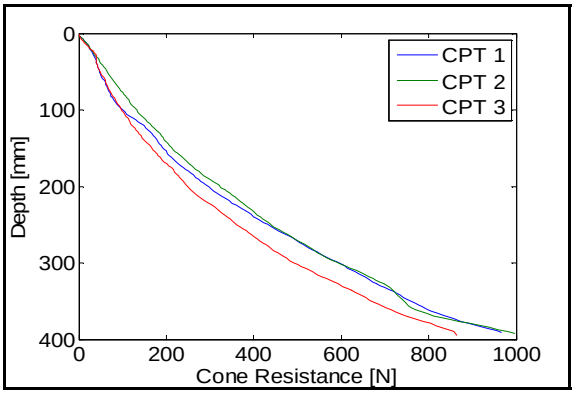

Installation Phase

Relative density [%]

cpt 1	cpt 2	cpt 3	Average
83.8	85.23	80.24	83.09

Maximum installation force [N]	-
Penetration depth [mm]	-

Cyclic Test Phase

Masses on the weight hangers [Kg]

M1	M2	M3
13.575	23.11	33

Number of cycles	50642
Loading period [s]	10

LVDTs-Time, Rotation-Time

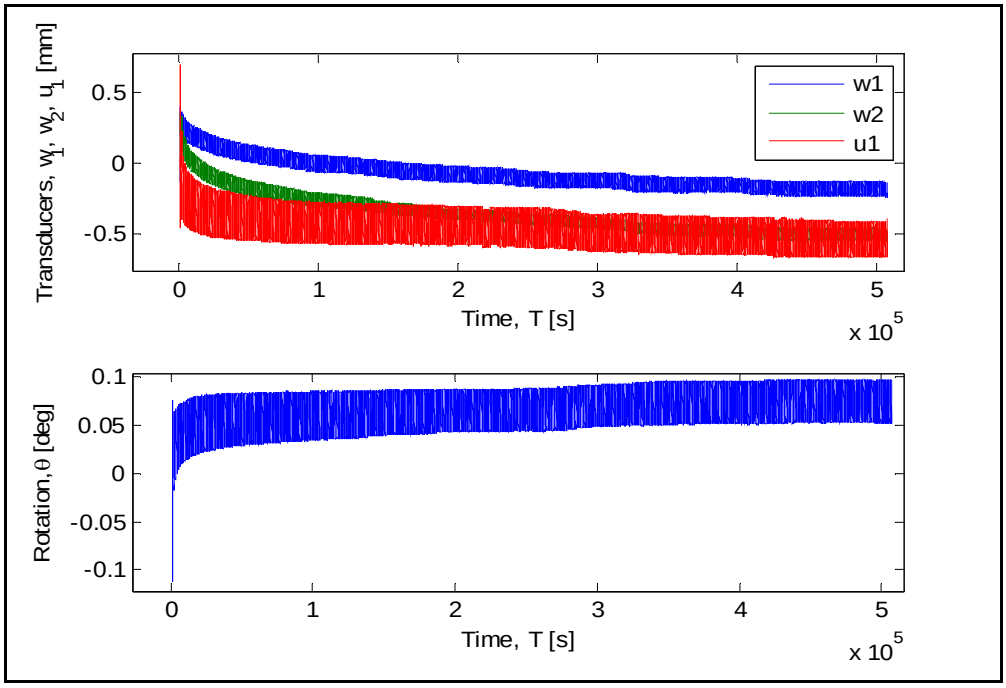

Horizontal Load-Time, Moment-Rotation

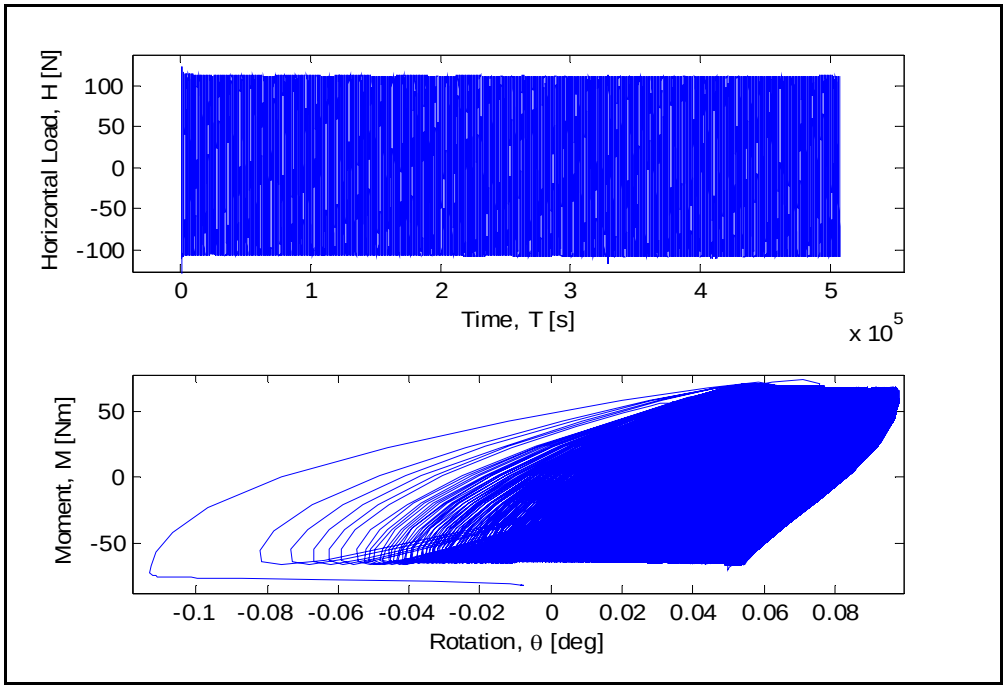

Maximum accumulated rotation [deg]	0.1

Maximum and minimum moment [Nm]

Mmax	Mmin
67.28	-64.77

ζb	ζc
0.367	-0.963

Post-Cyclic Phase

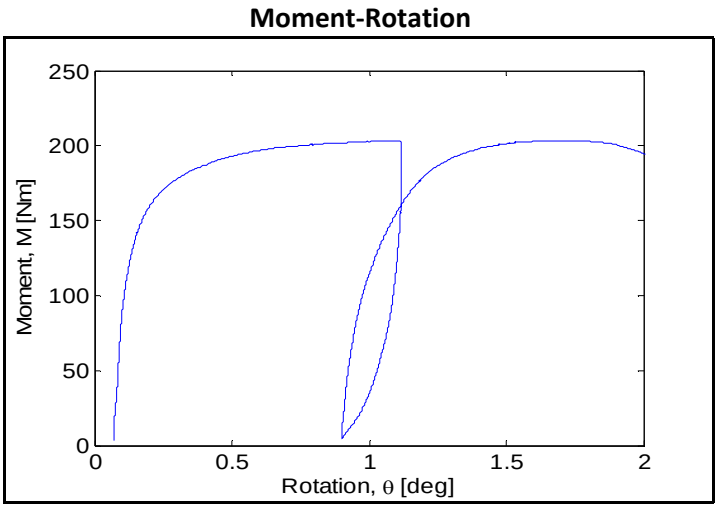

Maximum moment [Nm]	203.4
Rotation at maximum moment[deg]	1.064

Test equipment	Blue sandbox
User	Aligi
Test name	S25
Date	-

Bucket

Diameter [mm]	300
Embedment ratio	1

Test

Static or cyclic test	static
Moment arm [mm]	0.33

General Comments

None

Soil Preparation & Installation Phase

Gradient applied

-

Cone Penetration Resistance

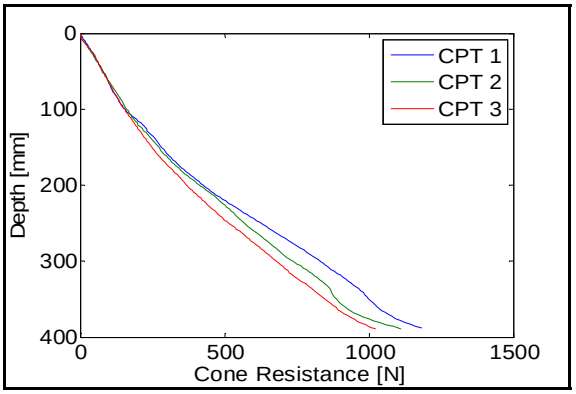

Installation Phase

Relative density [%]

cpt 1	cpt 2	cpt 3	Average
92.8	90.88	88.72	90.80

Maximum installation force [N]	-
Penetration depth [mm]	-

Horizontal and Vertical displacement-Rotation

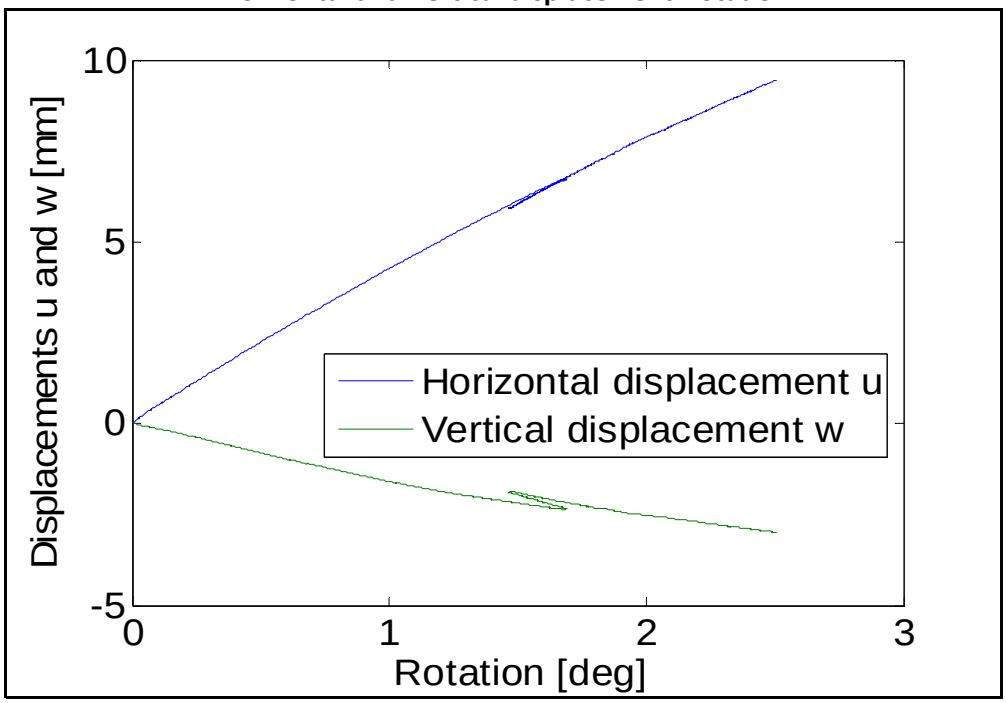

Moment-Rotation

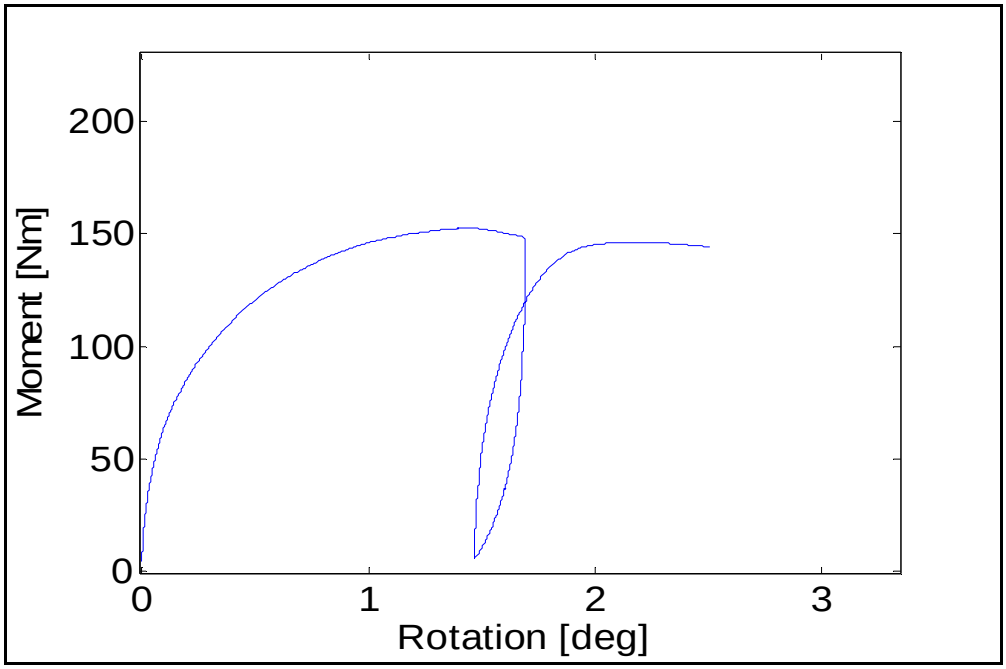

Maximum moment [Nm]	152.59
Rotation at maximum moment [deg]	1.407

Test equipment	Blue sandbox
User	Aligi
Test name	S26
Date	-

Bucket	
Diameter [mm]	300
Embedment ratio	1
Test	
Static or cyclic test	static
Moment arm [mm]	1.746

General Comments

None

Soil Preparation & Installation Phase

Gradient applied

-

Cone Penetration Resistance

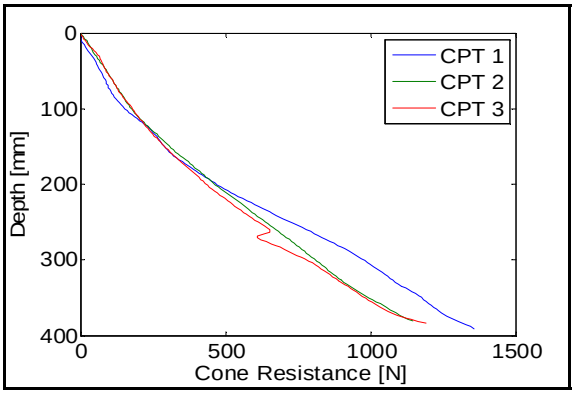

Installation Phase

Relative density [%]

cpt 1	cpt 2	cpt 3	Average
95.79	93.75	92.72	94.09

Maximum installation force [N]	-
Penetration depth [mm]	-

Horizontal and Vertical displacement-Rotation

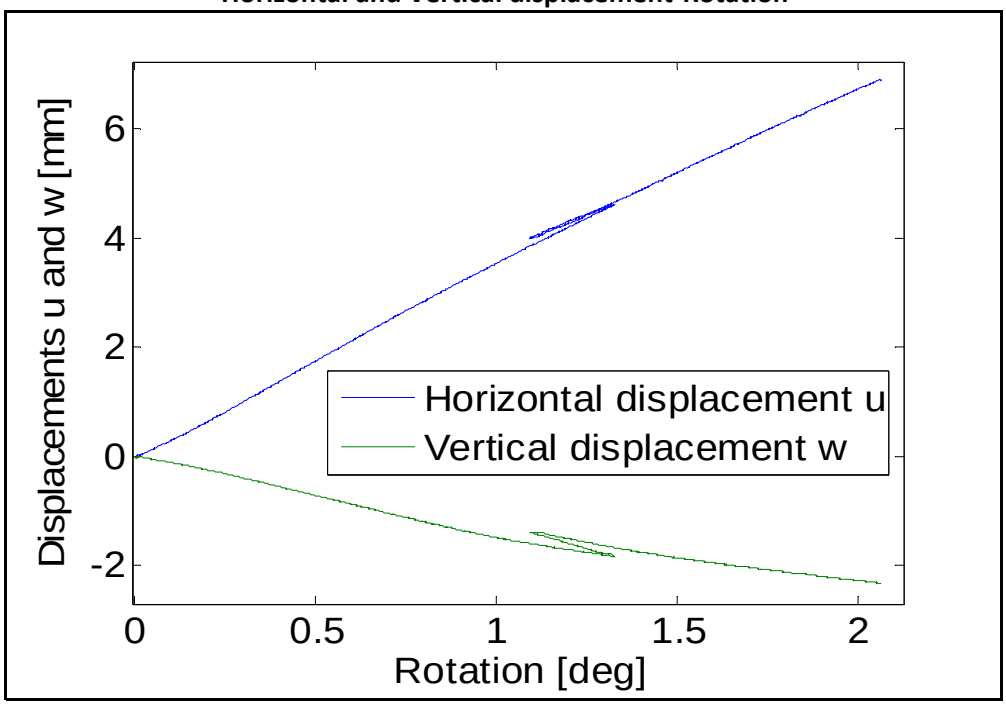

Moment-Rotation

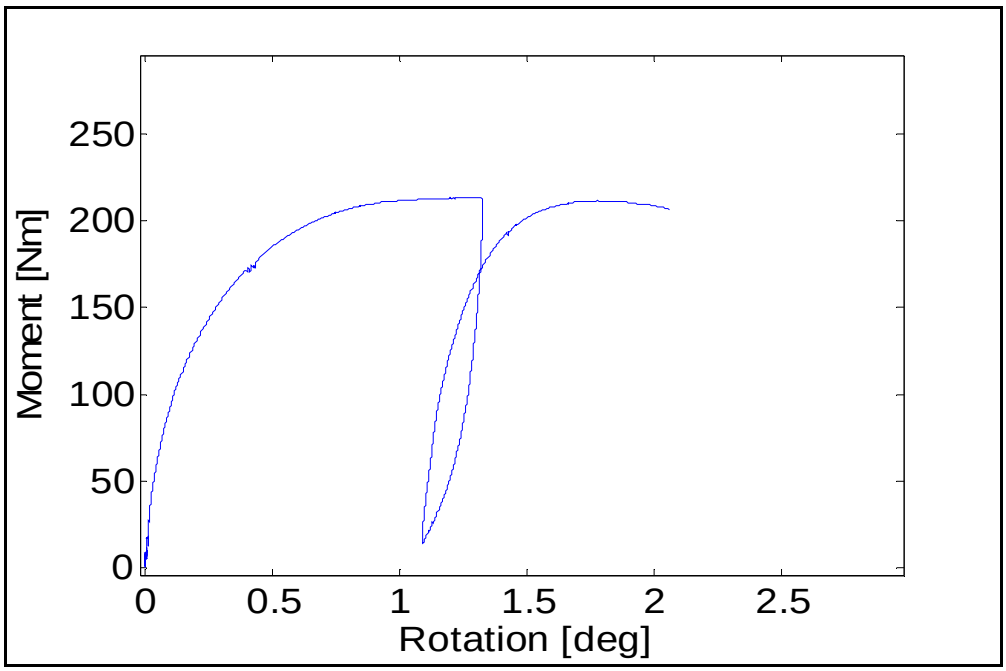

Maximum moment [Nm]	213.71
Rotation at maximum moment [deg]	1.32

Test equipment	Blue sandbox
User	Aligi
Test name	S27
Date	-

Bucket

Diameter [mm]	300
Embedment ratio	1

Test

Static or cyclic test	static
Moment arm [mm]	2.62

General Comments

None

Soil Preparation & Installation Phase

Gradient applied

-

Cone Penetration Resistance

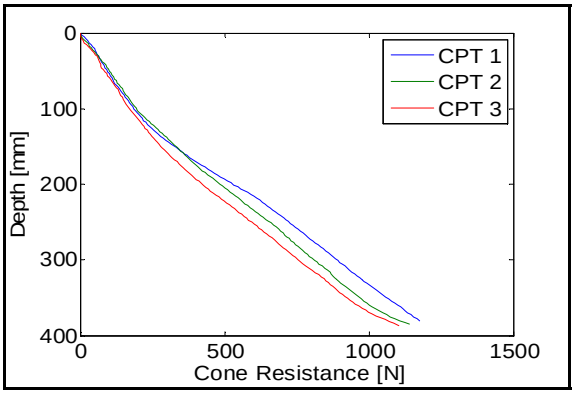

Installation Phase

Relative density [%]

cpt 1	cpt 2	cpt 3	Average
96.2	94.61	91.8	94.20

Maximum installation force [N]	-
Penetration depth [mm]	-

Horizontal and Vertical displacement-Rotation

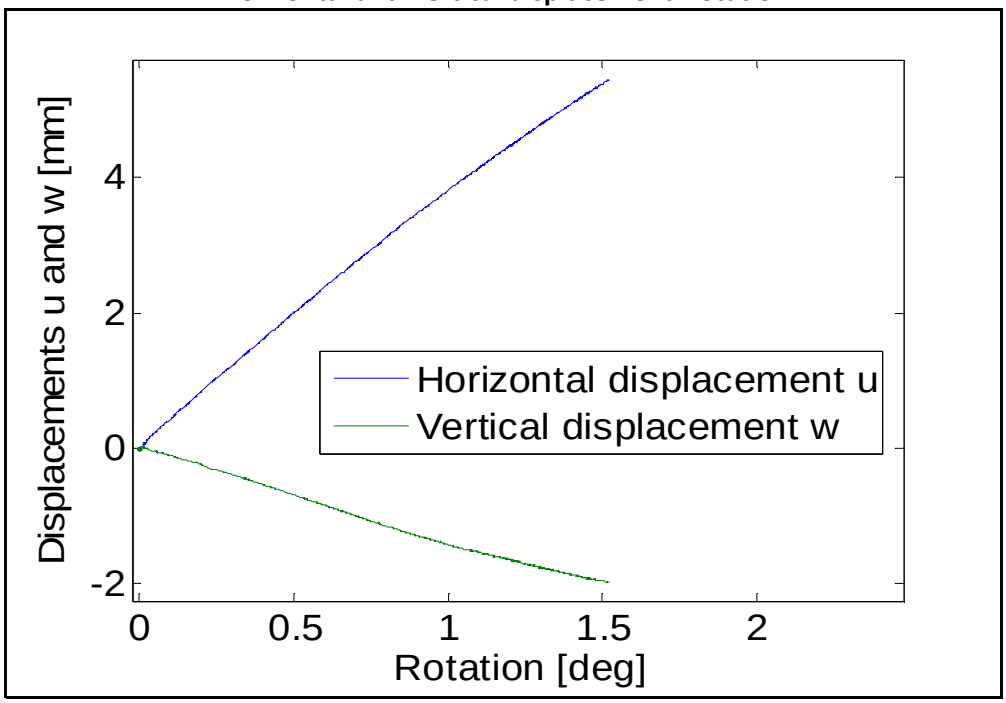

Moment-Rotation

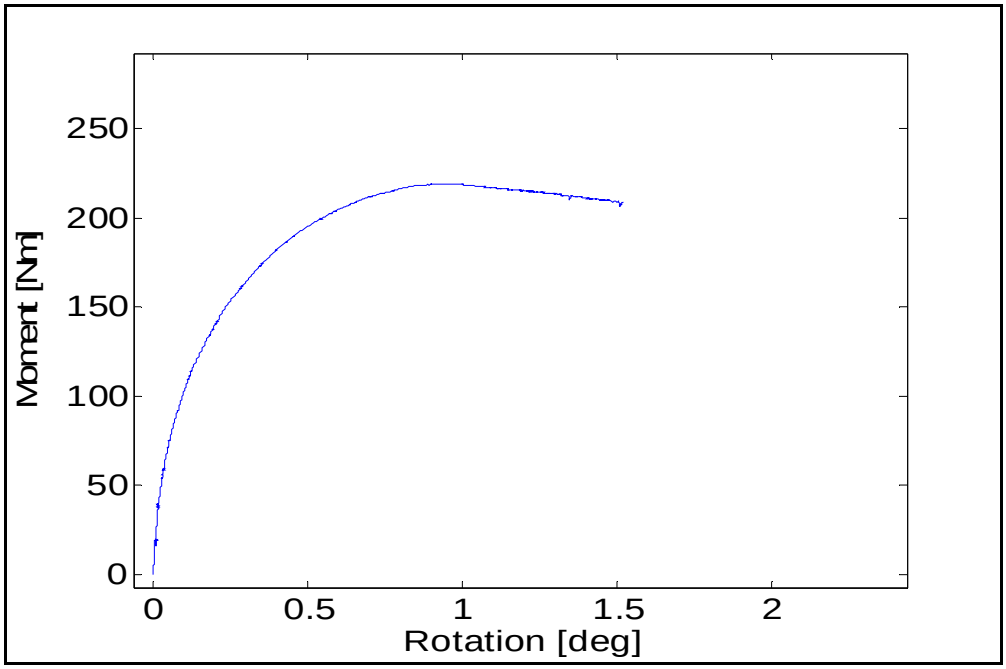

Maximum moment [Nm]	219.27
Rotation at maximum moment [deg]	0.919

Test equipment	Blue sandbox
User	Aligi
Test name	S28
Date	-

Bucket	
Diameter [mm]	300
Embedment ratio	1
Test	
Static or cyclic test	static
Moment arm [mm]	1.74

General Comments

None

Soil Preparation & Installation Phase

Gradient applied

-

Cone Penetration Resistance

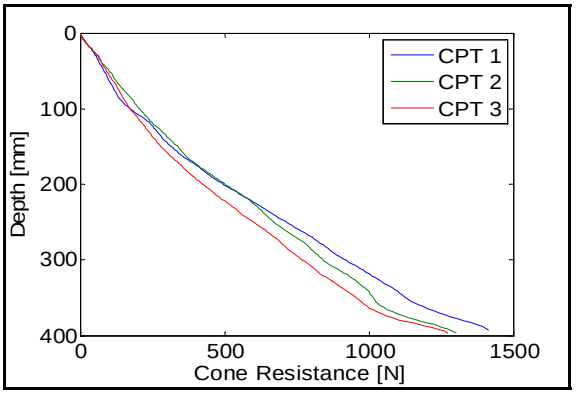

Installation Phase

Relative density [%]

cpt 1	cpt 2	cpt 3	Average
96.38	95.69	92.34	94.80

Maximum installation force [N]	-
Penetration depth [mm]	-

Horizontal and Vertical displacement-Rotation

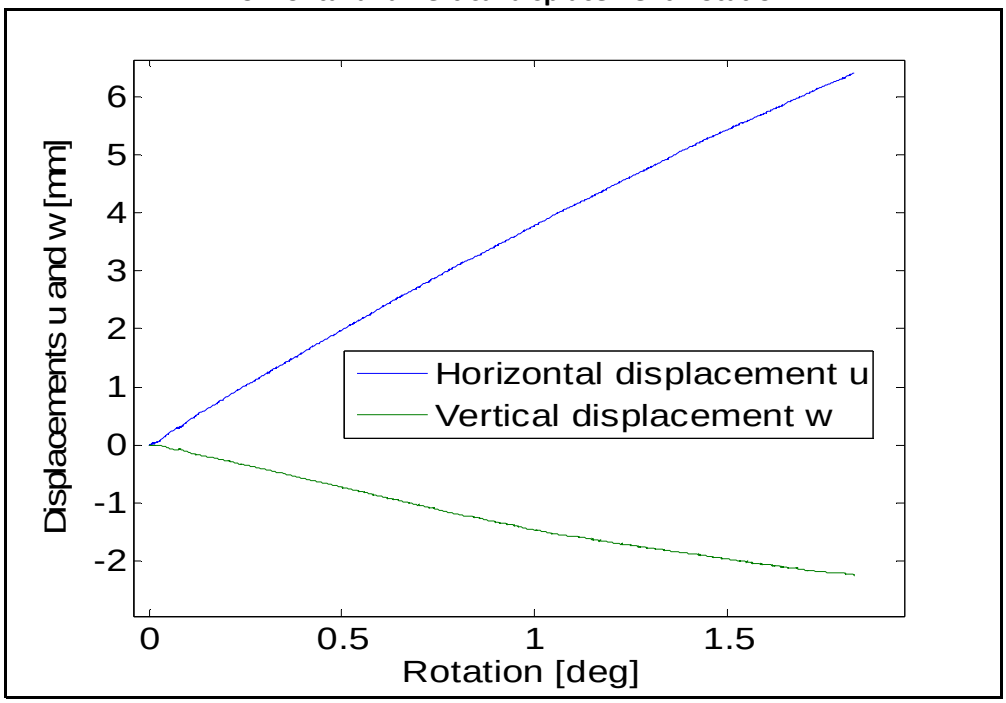

Moment-Rotation

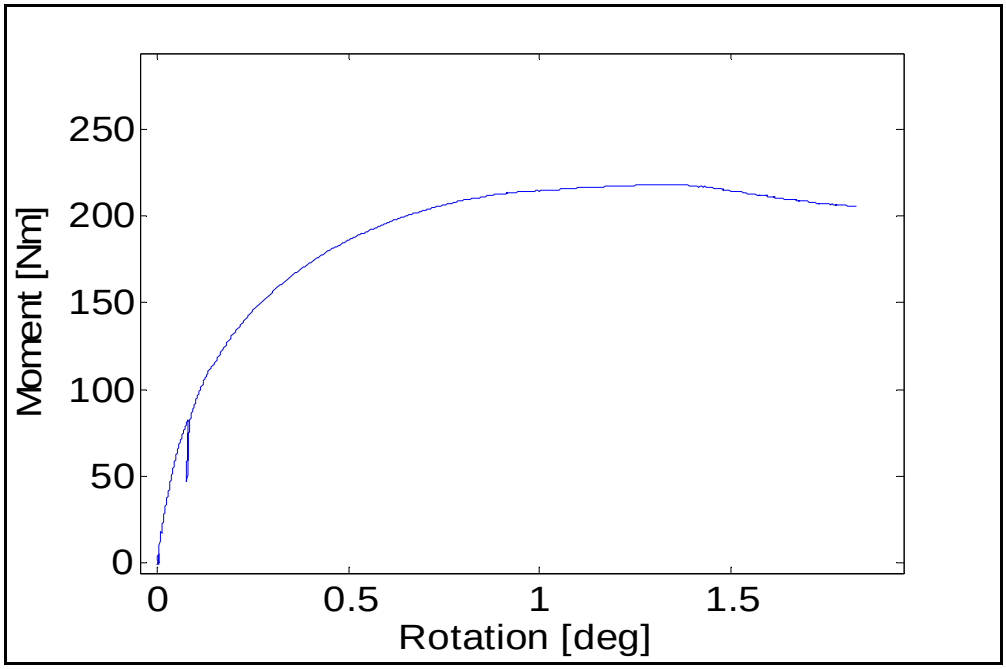

Maximum moment [Nm]	218.09
Rotation at maximum moment [deg]	1.28

Test equipment	Blue sandbox
User	Aligi
Test name	S29
Date	-

Bucket	
Diameter [mm]	300
Embedment ratio	1
Test	
Static or cyclic test	static
Moment arm [mm]	0.903

General Comments

None

Soil Preparation & Installation Phase

Gradient applied

-

Cone Penetration Resistance

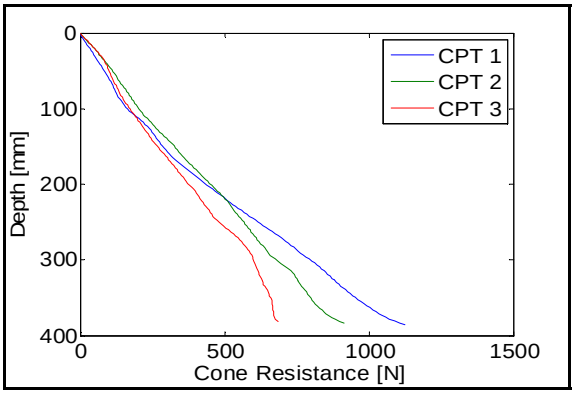

Installation Phase

Relative density [%]

cpt 1	cpt 2	cpt 3	Average
92.81	91.74	87.2	90.58

Maximum installation force [N]	-
Penetration depth [mm]	-

Horizontal and Vertical displacement-Rotation

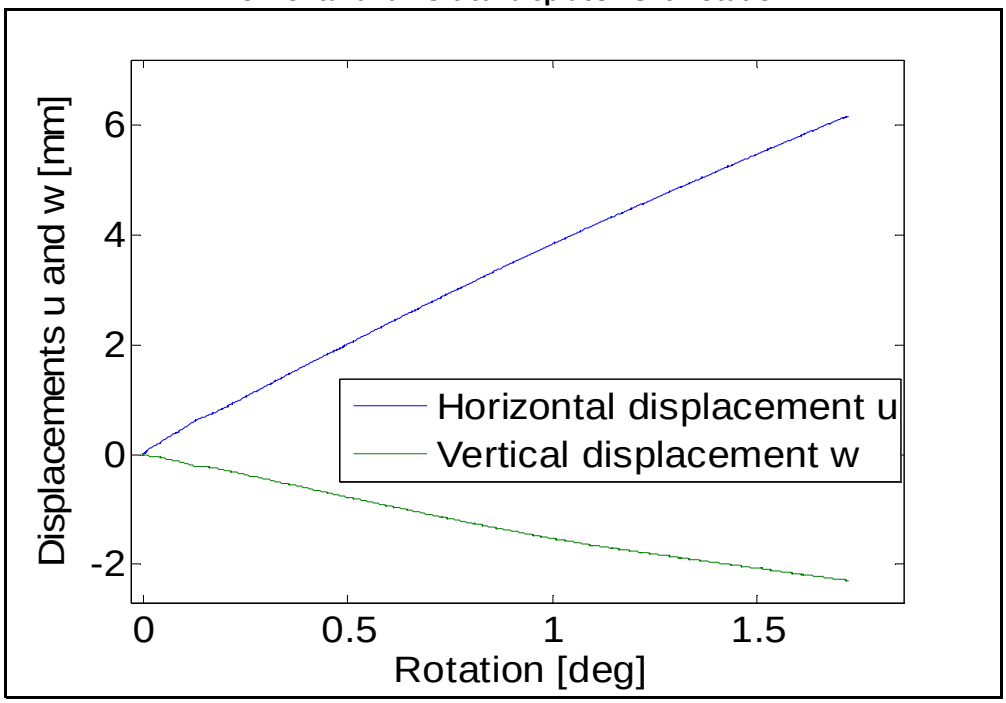

Moment-Rotation

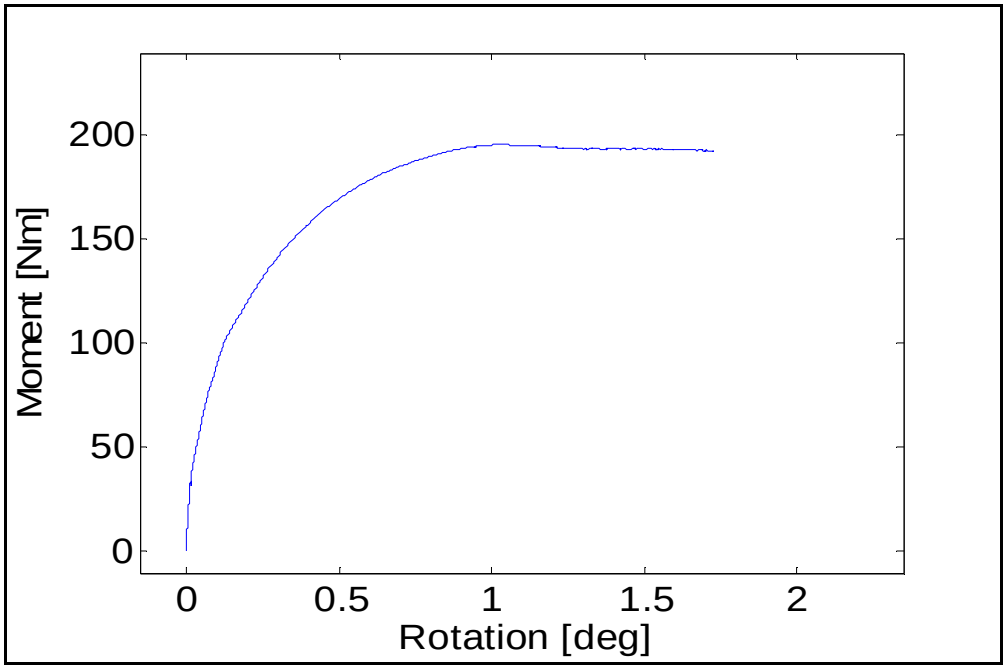

Maximum moment [Nm]	195.35
Rotation at maximum moment [deg]	1.02

Test equipment	Blue sandbox
User	Aligi
Test name	S30
Date	-

Bucket

Diameter [mm]	300
Embedment ratio	1

Test

Static or cyclic test	static
Moment arm [mm]	0.596

General Comments

None

Soil Preparation & Installation Phase

Gradient applied

-

Cone Penetration Resistance

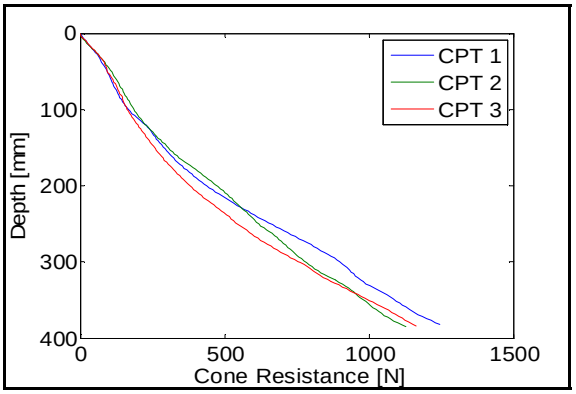

Installation Phase

Relative density [%]

cpt 1	cpt 2	cpt 3	Average
94.31	93.58	90.79	92.89

Maximum installation force [N]	-
Penetration depth [mm]	-

Horizontal and Vertical displacement-Rotation

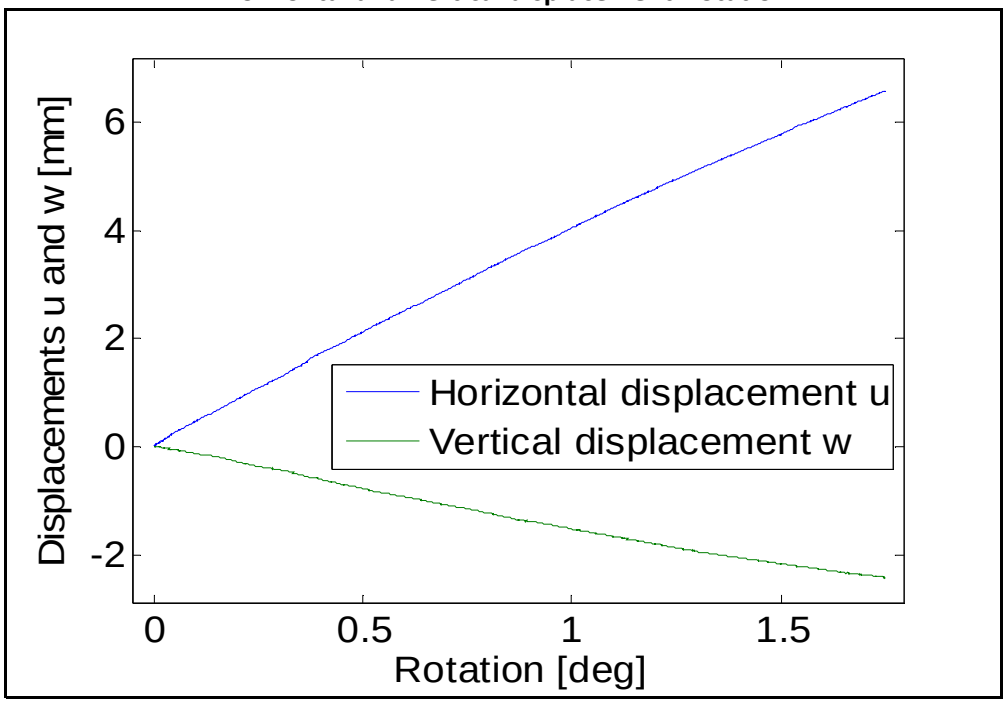

Moment-Rotation

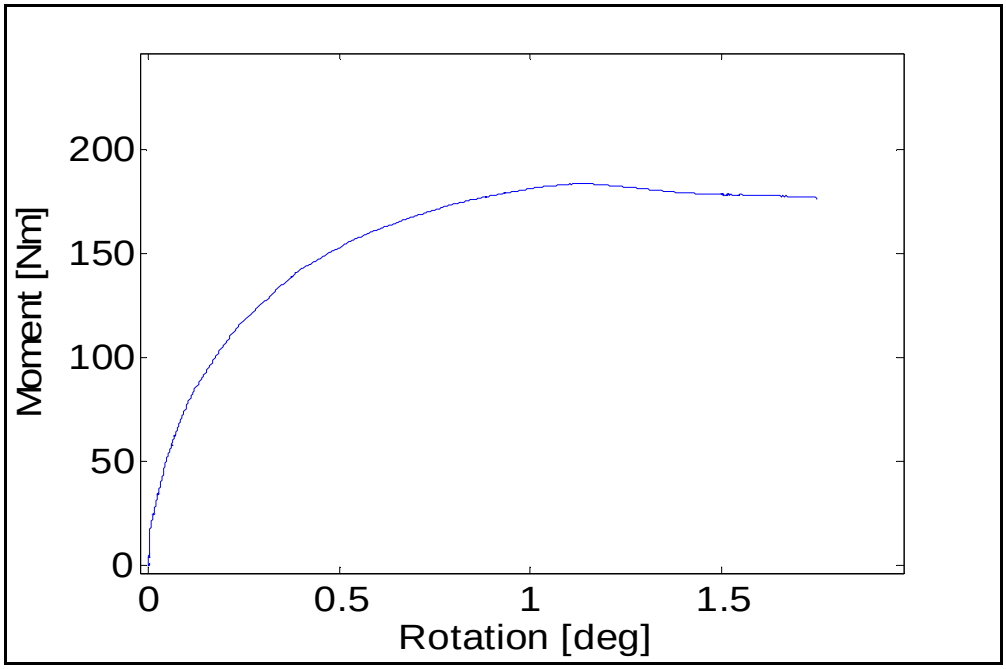

Maximum moment [Nm]	183.46
Rotation at maximum moment [deg]	1.15

Test equipment	Blue sandbox
User	Aligi & Giulio
Test name	C31
Date	29/08/2012

Bucket

Diameter [mm]	300
Embedment ratio	1

Test

Static or cyclic test	cyclic
Moment arm [mm]	596

General Comments

Test 31 was performed to check the repeability of test 18.
The test was stopped and adjusted after few cycles for a mistake in setting the weights.

Soil Preparation and Installation Phase

Gradient applied

0.90

Cone Penetration Resistance

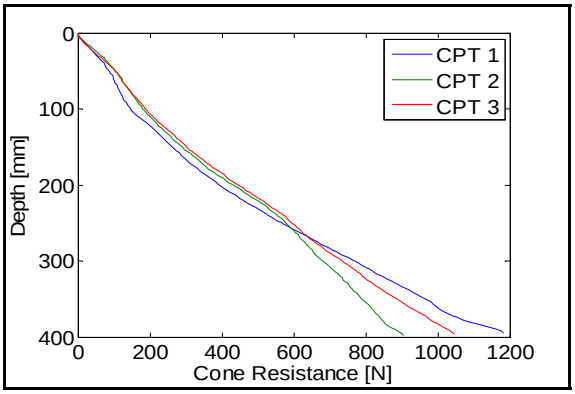

Installation Phase

Relative density [%]

cpt 1	cpt 2	cpt 3	Average
90.82	90.57	92.22	91.2

Maximum installation force [N]	-
Penetration depth [mm]	-

Test Phase

Masses on the weight hangers [Kg]

M1	M2	M3
5.775	7.11	33

Number of cycles	100933
Loading period [s]	10

LVDTs-Time, Rotation-Time

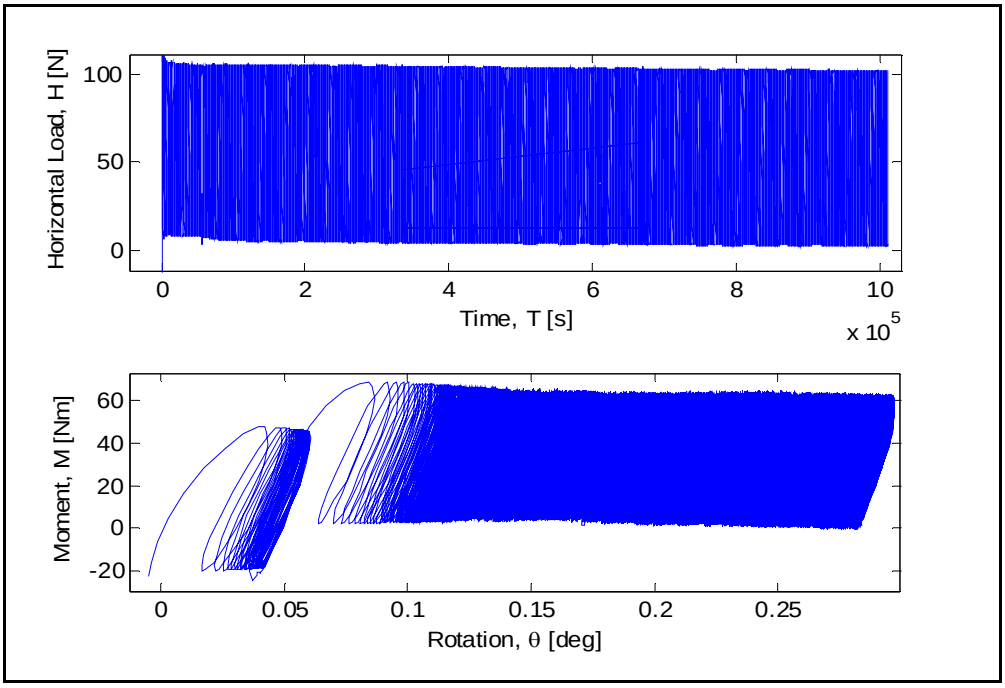

Horizontal Load-Time, Moment-Rotation

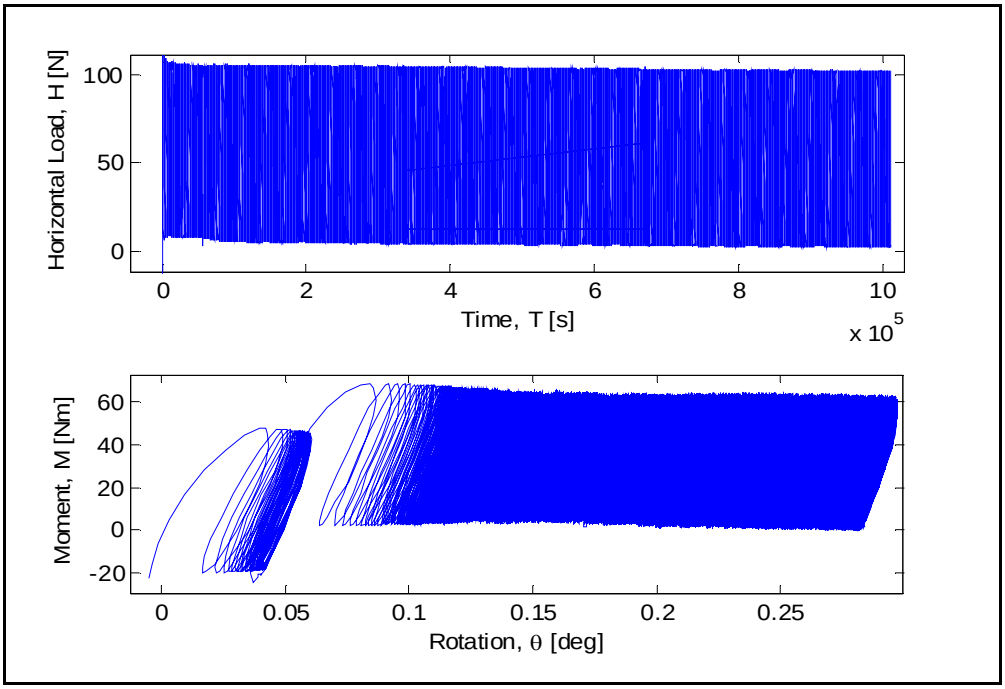

Maximum accumulated rotation [deg]	0.297

Maximum and minimum moment [Nm]

Mmax	Mmin
62.16	2.26

ζb	ζc
0.34	0.036

Post-Cyclic Phase

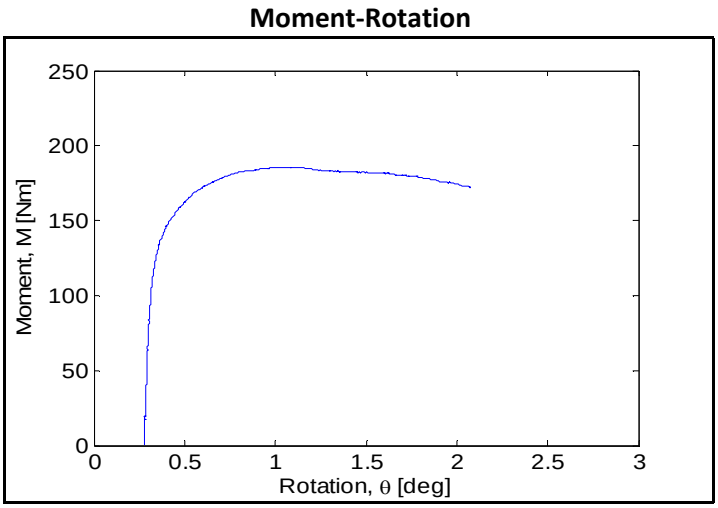

Maximum moment [Nm]	185.9
Rotation at maximum moment [deg]	1.082

Test equipment	Blue sandbox
User	Giulio & Aligi
Test name	C32
Date	12/09/2012

Bucket

Diameter [mm]	300
Embedment ratio	1

Test

Static or cyclic test	cyclic
Moment arm [mm]	596

General Comments

The installation force was measured in this test for the first time. The result was not satisfying.
The record stopped by itself for only 20 collecting folders were set.

The LVDTs were changed to W10TK 46, 45, 47

Soil Preparation and Installation Phase

Gradient applied

0.90

Cone Penetration Resistance

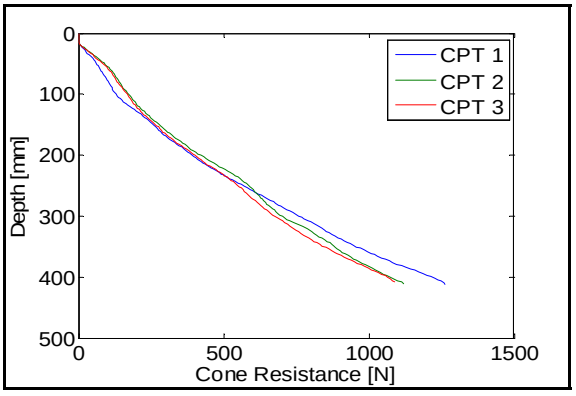

Installation Phase

Relative density [%]

cpt 1	cpt 2	cpt 3	Average
93.33	92.72	91.88	92.65

Maximum installation force [N]	-
Penetration depth [mm]	-

Cyclic Test Phase

Masses on the weight hangers [Kg]

M1	M2	M3
8.775	8.41	33

Number of cycles	49959
Loading period [s]	10

LVDTs-Time, Rotation-Time

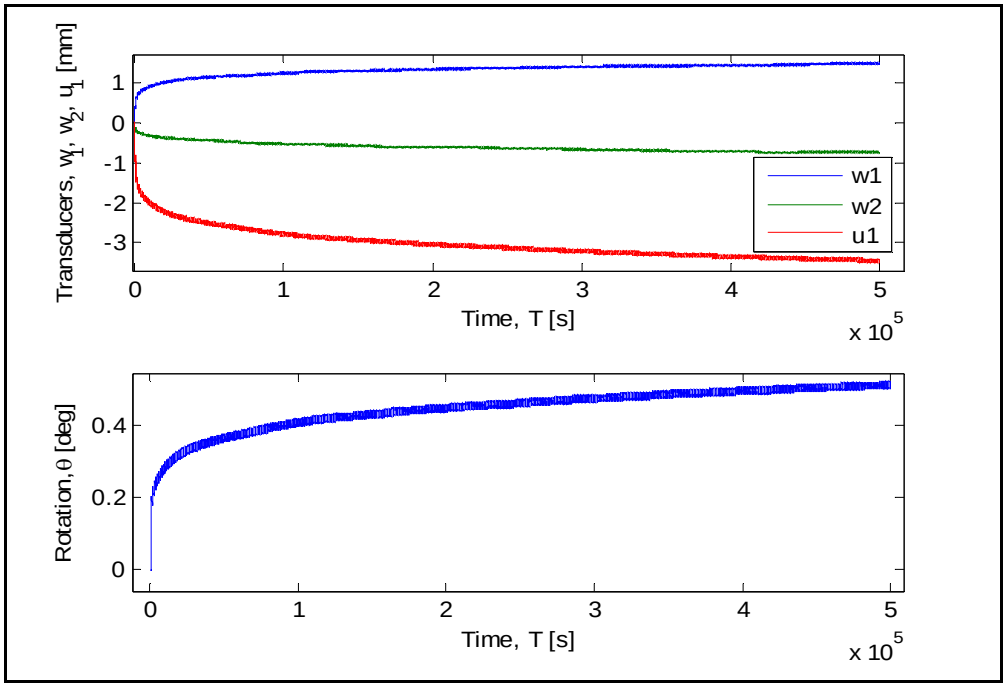

Horizontal Load-Time, Moment-Rotation

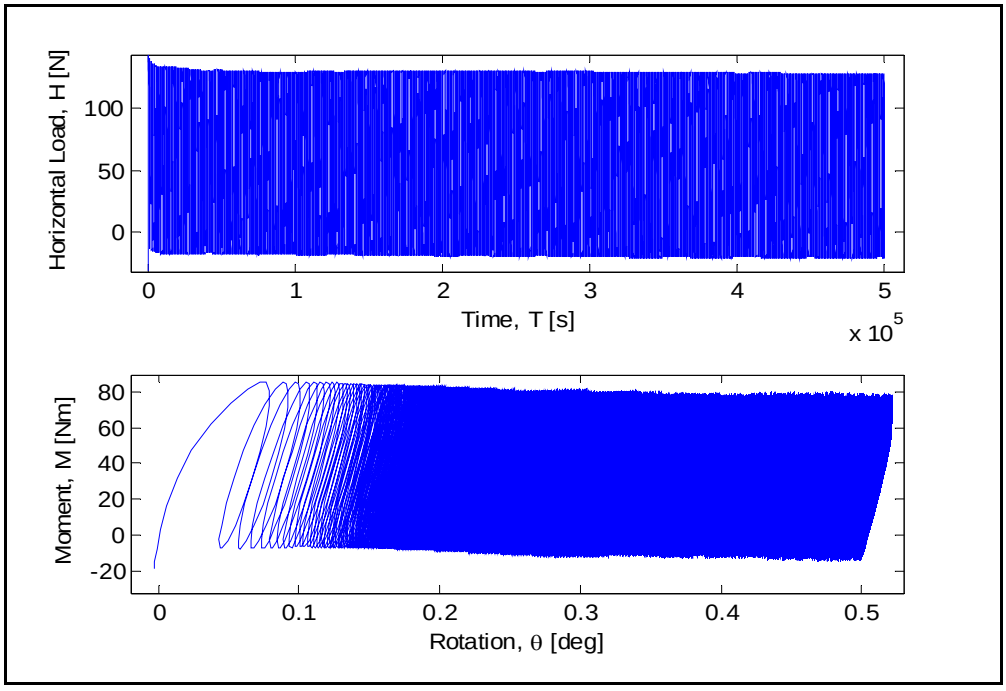

Maximum accumulated rotation [deg] 0.522

Maximum and minimum moment [Nm]

Mmax	Mmin
77.21	-11.48

ζb	ζc
0.421	-0.149

Post-Cyclic Phase

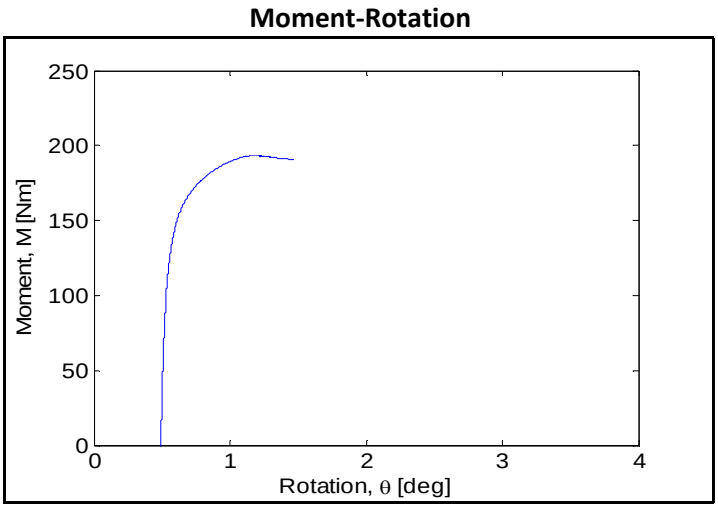

Maximum moment [Nm]	193.6
Rotation at maximum moment [deg]	1.171

Test equipment	Blue sandbox
User	Giulio & Aligi
Test name	C33
Date	19/09/2012

Bucket

Diameter [mm]	300
Embedment ratio	1

Test

Static or cyclic test	cyclic
Moment arm [mm]	596

General Comments

In this test the installation force was correctly measured for the first time.

Soil Preparation and Installation Phase

Gradient applied

0.95

Cone Penetration Resistance

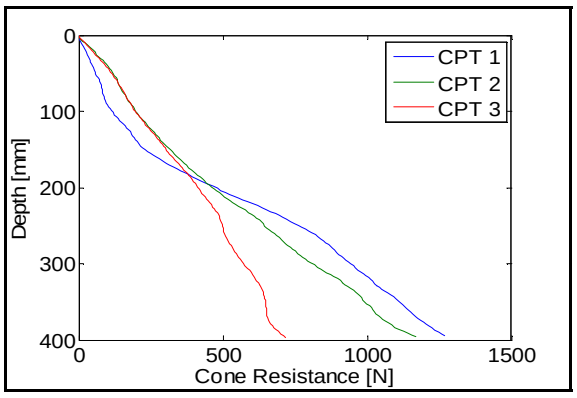

Installation Phase

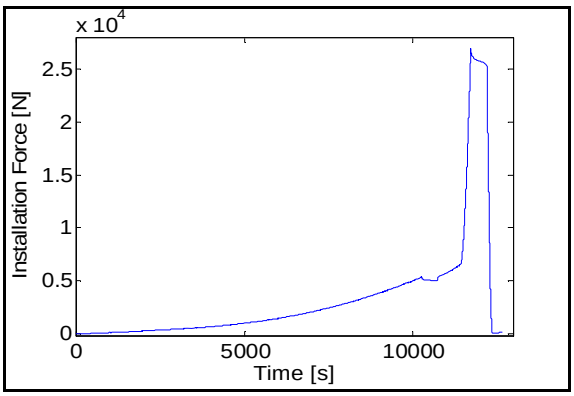

Relative density

cpt 1	cpt 2	cpt 3	Average
93.68	94.25	88.36	92.09

Maximum installation force [N]	26967
Penetration depth [mm]	-

Cyclic Test Phase

Masses on the weight hangers [Kg]

M1	M2	M3
9.075	10.51	33

Number of cycles	50471
Loading period [s]	10

LVDTs-Time, Rotation-Time

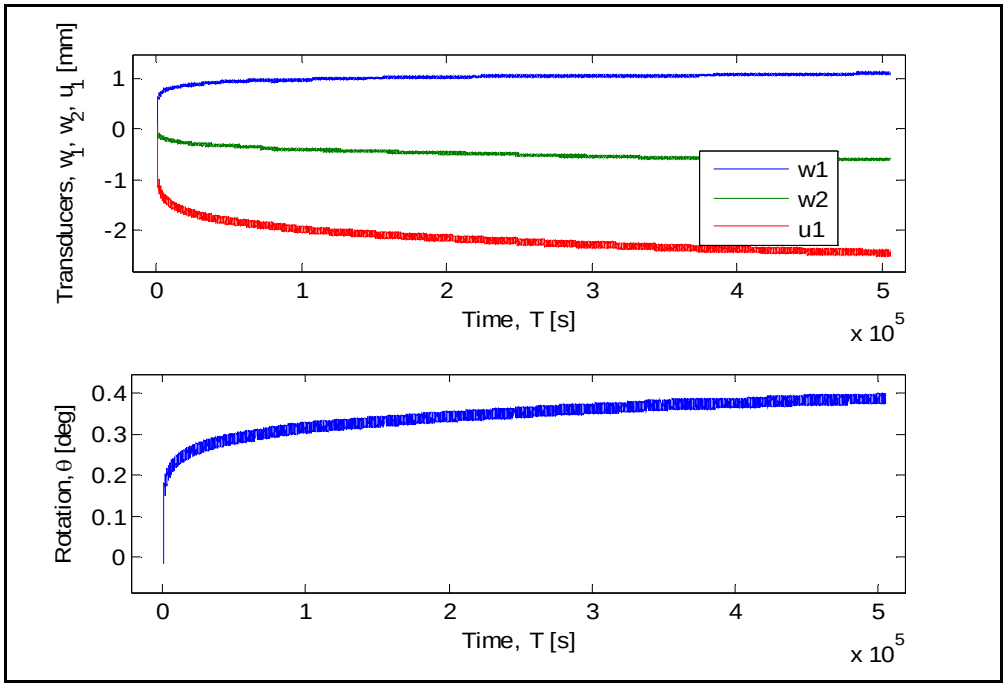

Horizontal Load-Time, Moment-Rotation

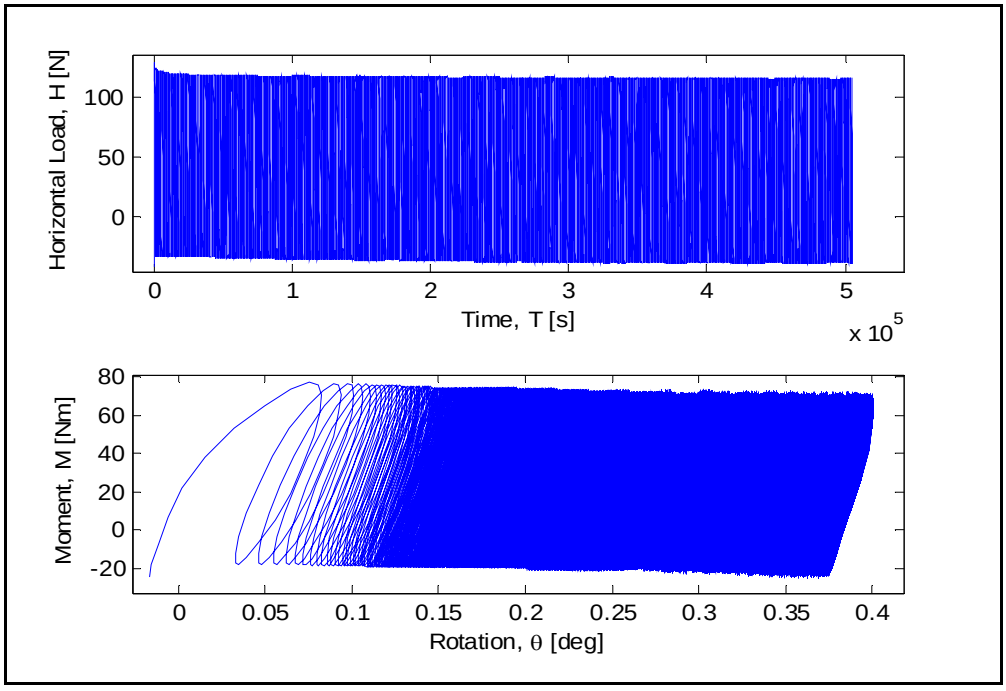

Maximum accumulated rotation [deg]	0.4

Maximum and minimum moment [Nm]

Mmax	Mmin
70.13	-22.16

ζb	ζc
0.383	-0.316

Post-Cyclic Phase

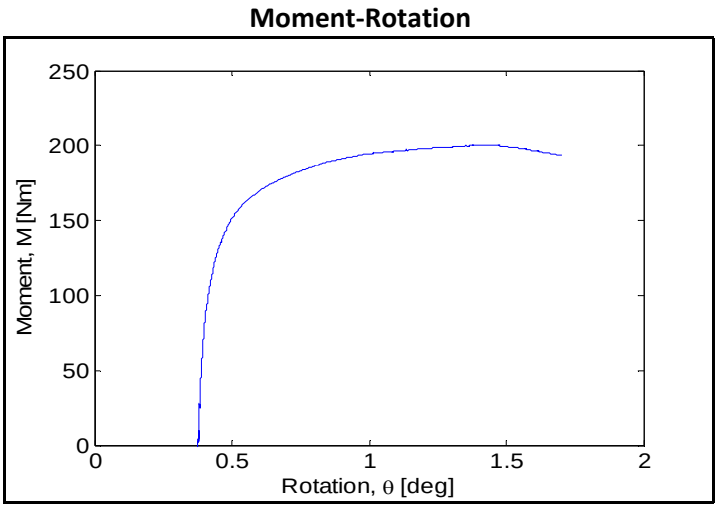

Failure moment [Nm]	200.2
Rotation at failure [deg]	1.423

Test equipment	Blue sandbox
User	Giulio & Aligi
Test name	C34
Date	27/09/2012

Bucket

Diameter [mm]	300
Embedment ratio	1

Test

Static or cyclic test	cyclic
Moment arm [mm]	596

General Comments

None

Soil Preparation and Installation Phase

Gradient applied

0.974

Cone Penetration Resistance

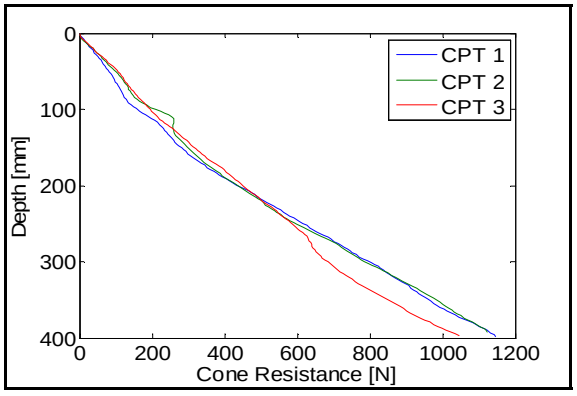

Installation Phase

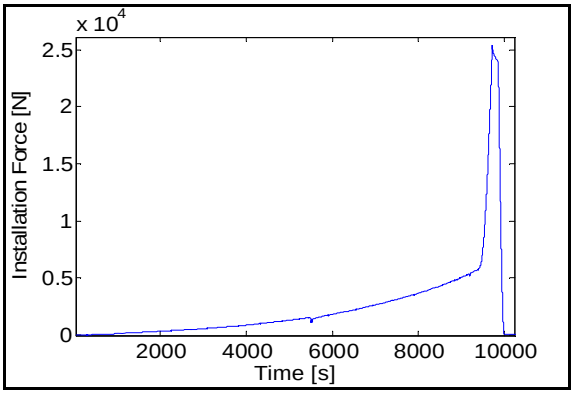

Relative density [%]

cpt 1	cpt 2	cpt 3	Average
92.46	93.42	92	92.63

Maximum installation force [N]	25398
Penetration depth [mm]	-

Cyclic Test Phase

Masses on the weight hangers [Kg]

M1	M2	M3
7.275	10.61	33

Number of cycles	10022
Loading period [s]	10

LVDTs-Time, Rotation-Time

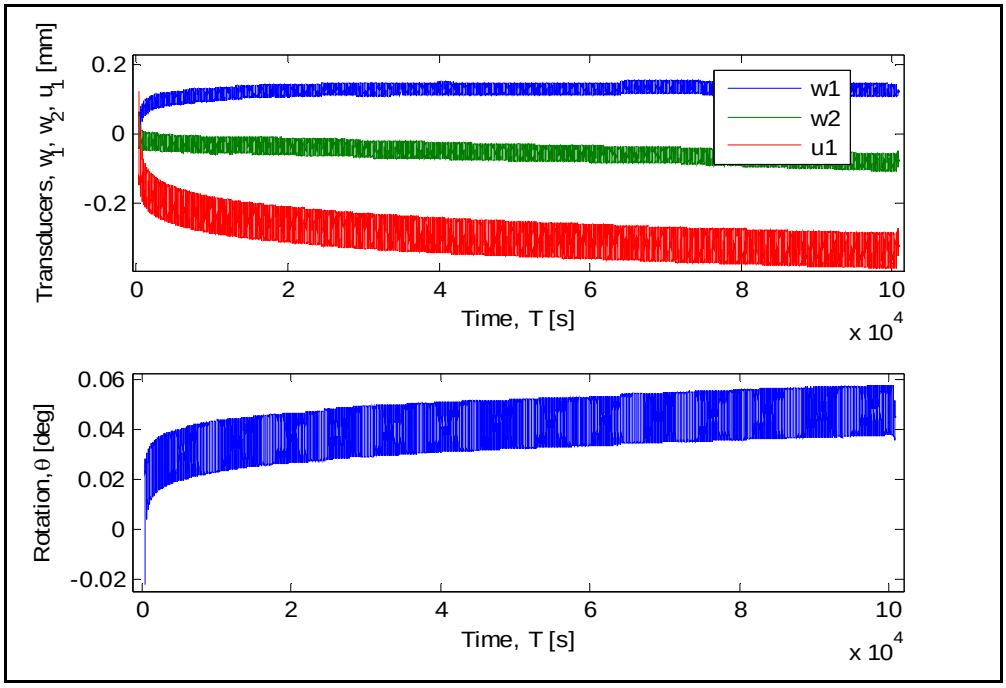

Horizontal Load-Time, Moment-Rotation

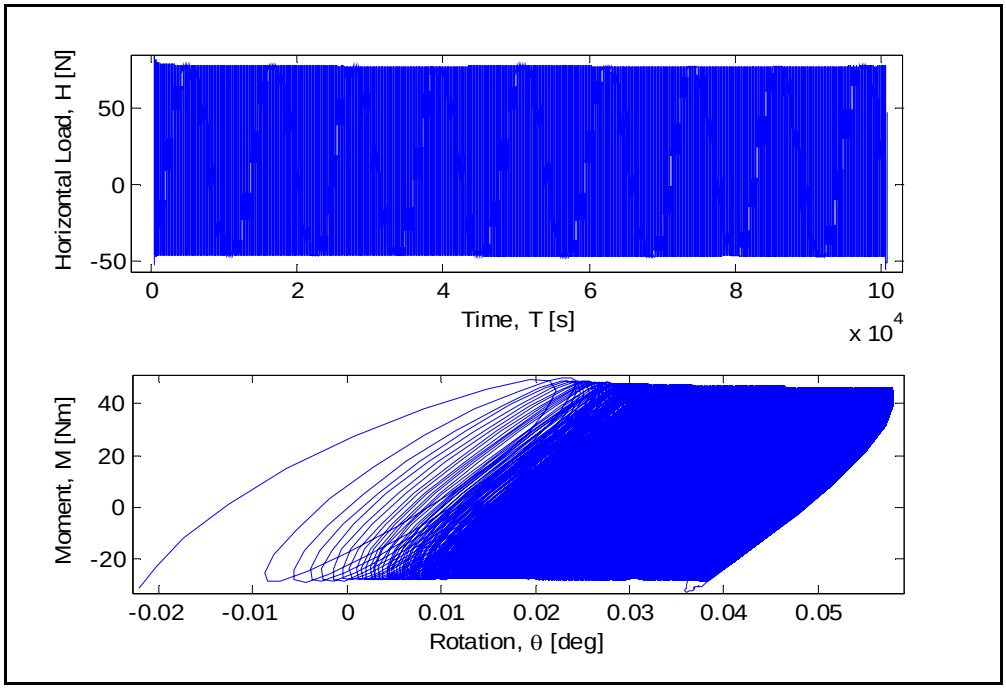

Maximum accumulated rotation [deg] | 0.058

Maximum and minimum moment [Nm]

Mmax	Mmin
46.18	-27.9

ζb	ζc
0.252	-0.6

Post-Cyclic Phase

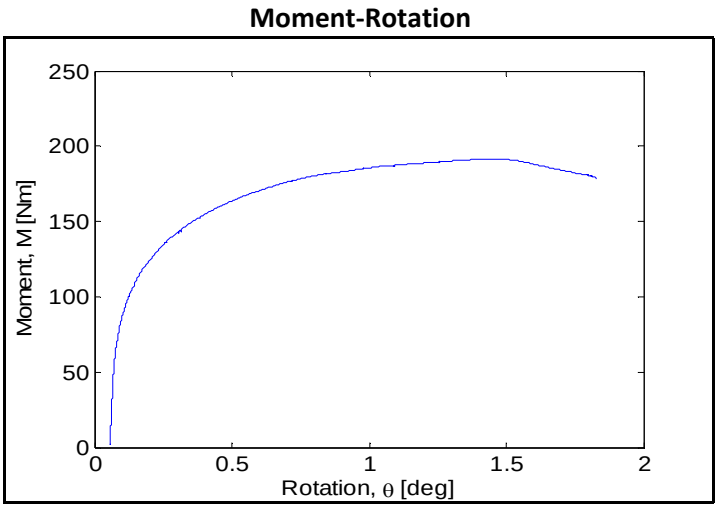

Maximum moment [Nm]	191.8
Rotation at maximum moment [deg]	1.447

Test equipment	Blue sandbox
User	Giulio & Aligi
Test name	C35
Date	02/10/2012

Bucket

Diameter [mm]	300
Embedment ratio	1

Test

Static or cyclic test	cyclic
Moment arm [mm]	596

General Comments

None

Soil Preparation and Installation Phase

Gradient applied

0.974

Cone Penetration Resistance

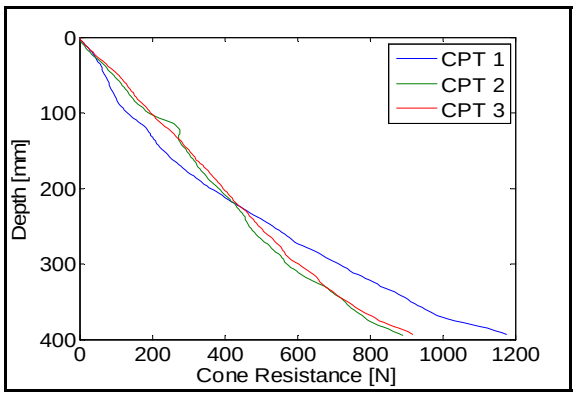

Installation Phase

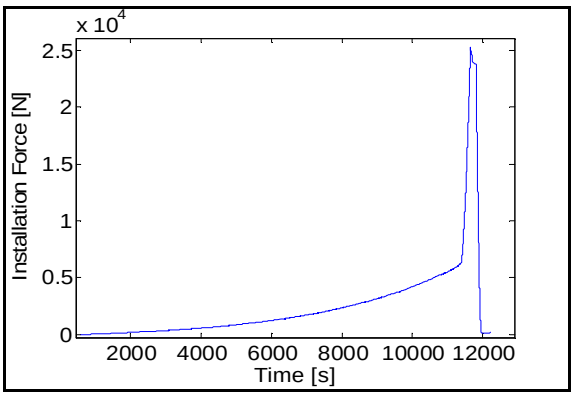

Relative density [%]

cpt 1	cpt 2	cpt 3	Average
88.79	88.6	89.21	88.87

Maximum installation force [N]	25281
Penetration depth [mm]	-

Cyclic Test Phase

Masses on the weight hangers [Kg]

M1	M2	M3
13.375	19.21	33

Number of cycles	9976
Loading period [s]	10

LVDTs-Time, Rotation-Time

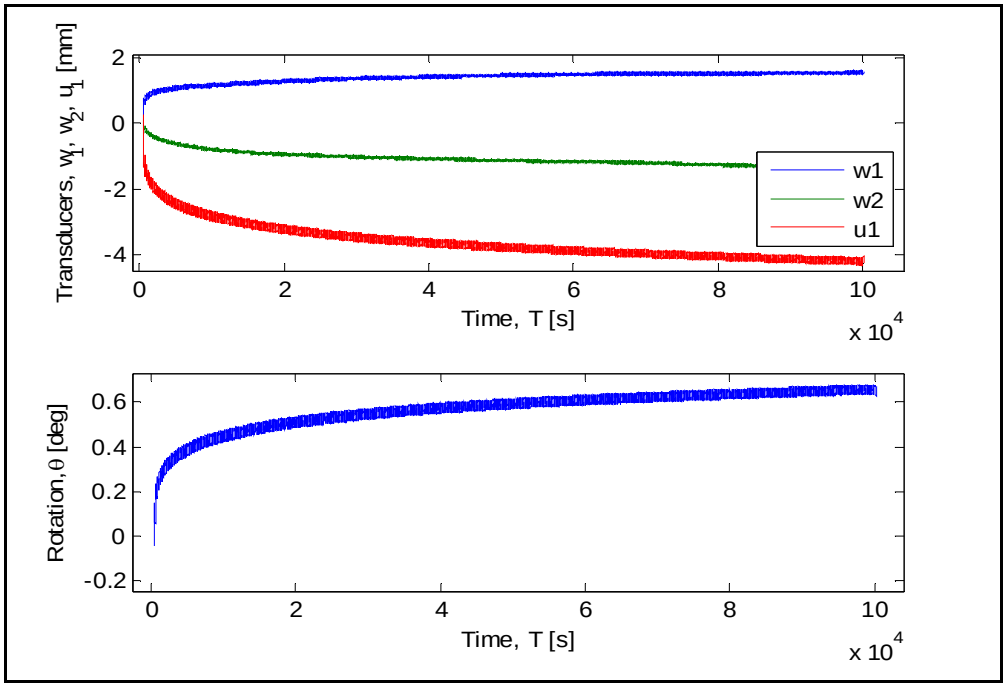

Horizontal Load-Time, Moment-Rotation

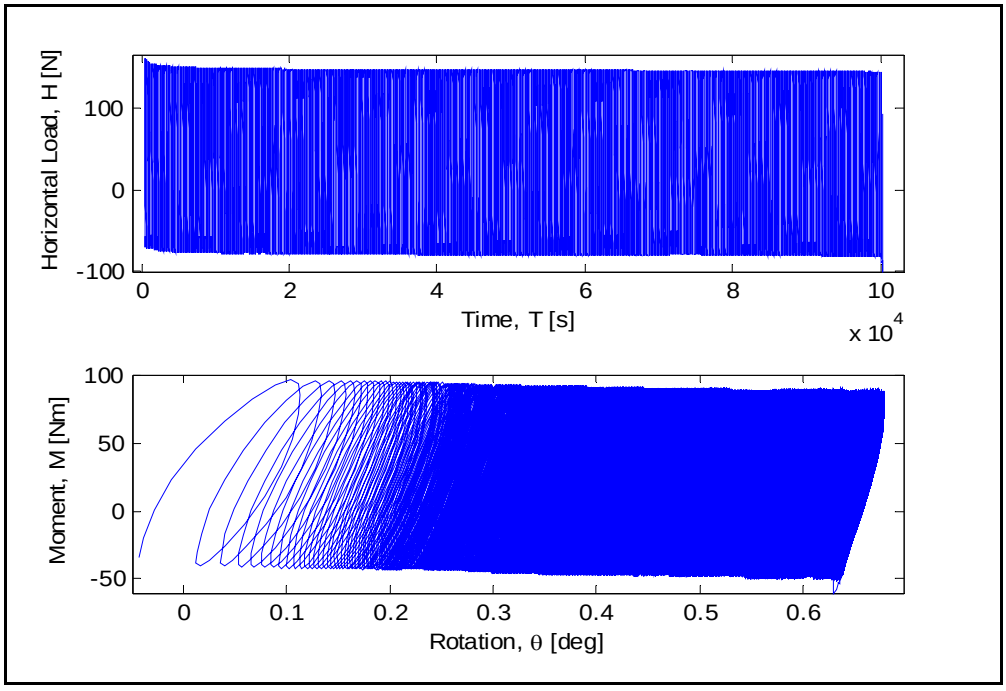

Maximum accumulated rotation [deg] | 0.678

Maximum and minimum moment [Nm]

Mmax	Mmin
88.8	-48.04

ζb	ζc
0.48	-0.54

Post-Cyclic Phase

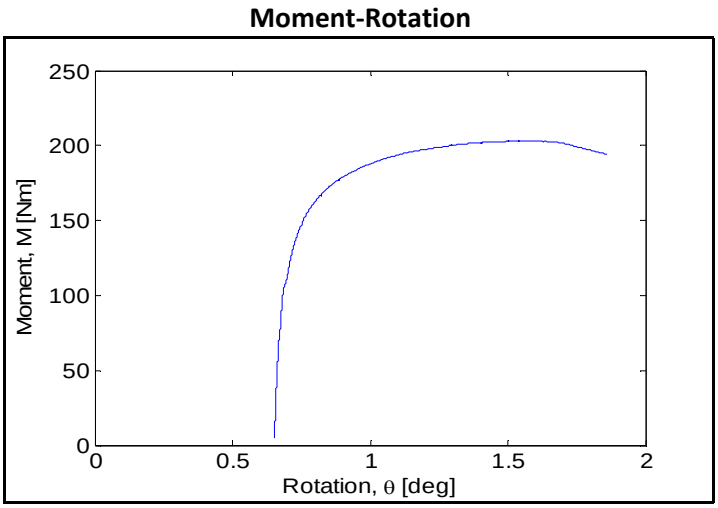

Maximum moment [Nm]	203.2
Rotation at maximum moment [deg]	1.6

Test equipment	Blue sandbox
User	Giulio & Aligi
Test name	C36
Date	04/10/2012

Bucket

Diameter [mm]	300
Embedment ratio	1

Test

Static or cyclic test	cyclic
Moment arm [mm]	596

General Comments

None

Soil Preparation and Installation Phase

Gradient applied

0.8

Cone Penetration Resistance

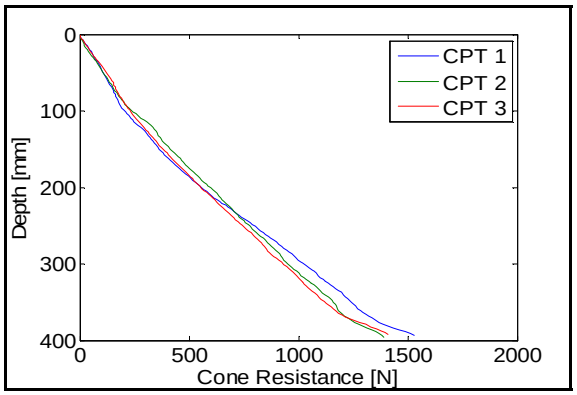

Installation Phase

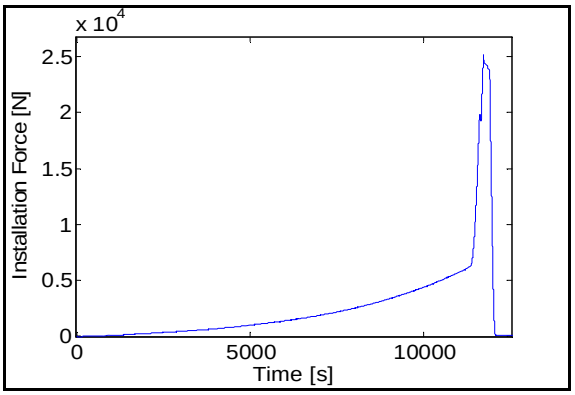

Relative density [%]

cpt 1	cpt 2	cpt 3	Average
98.68	99.99	97.71	98.79

Maximum installation force [N]	25149
Penetration depth [mm]	-

Cyclic Test Phase

Masses on the weight hangers [Kg]

M1	M2	M3
16.475	23.61	33

Number of cycles	10153
Loading period [s]	10

LVDTs-Time, Rotation-Time

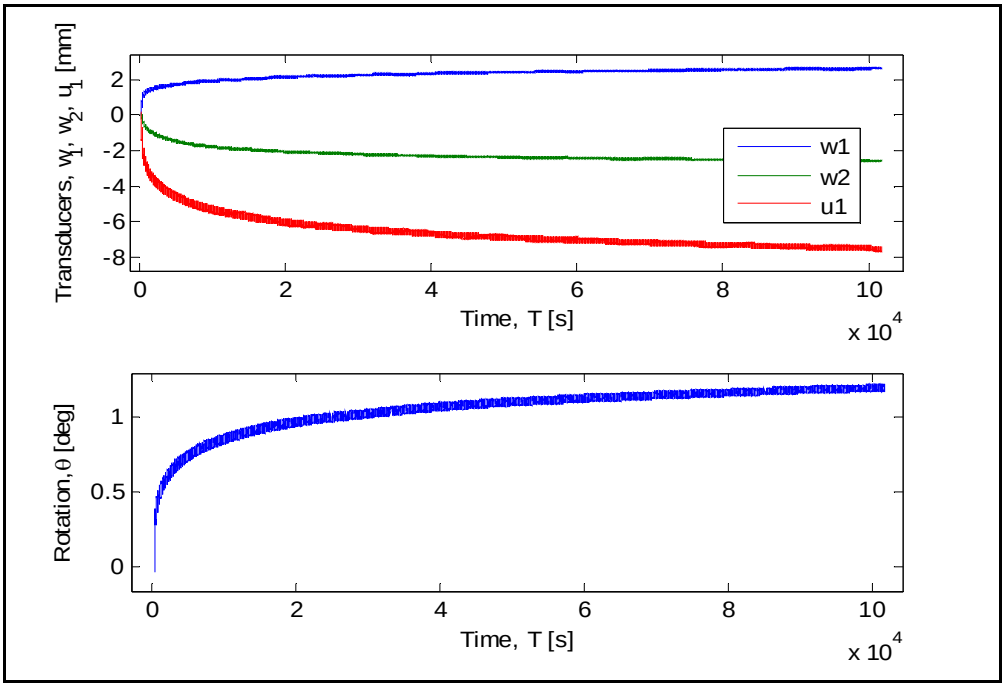

Horizontal Load-Time, Moment-Rotation

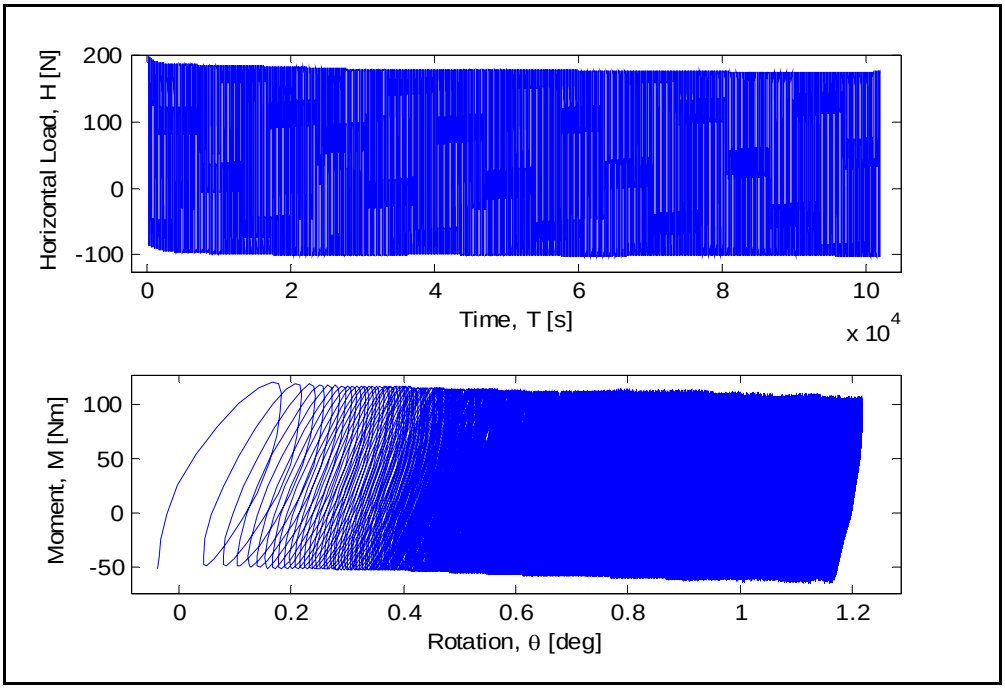

Maximum accumulated rotation [deg] | 1.216

Maximum and minimum moment [Nm]

Mmax	Mmin
106.84	-60.18

ζb	ζc
0.583	-0.563

Post-Cyclic Phase

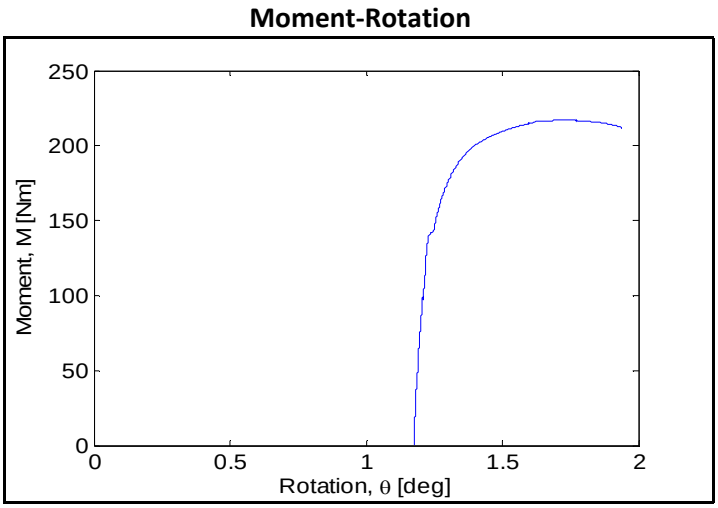

Maximum moment [Nm]	217.5
Rotation at maximum moment [deg]	1.71

Test equipment	Blue sandbox
User	Giulio & Aligi
Test name	C37
Date	08/10/2012

Bucket

Diameter [mm]	300
Embedment ratio	1

Test

Static or cyclic test	cyclic
Moment arm [mm]	596

General Comments

The installation force exceeded significantly 25 kN.

Soil Preparation and Installation Phase

Gradient applied

0.89

Cone Penetration Resistance

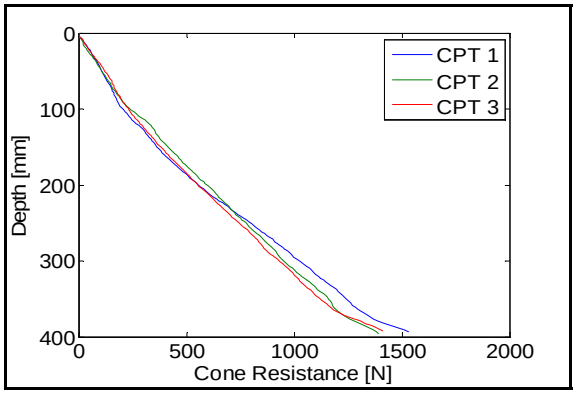

Installation Phase

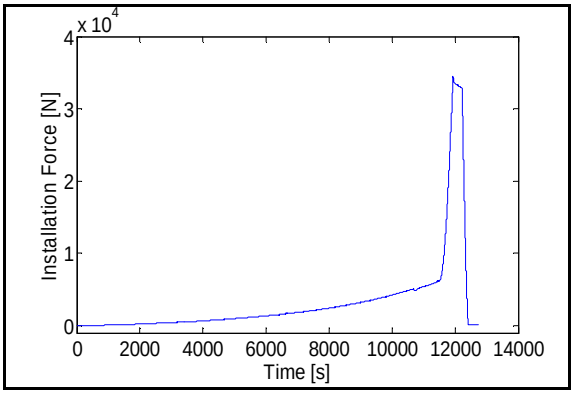

Relative density [%]

cpt 1	cpt 2	Icpt 3	Average
99.5	100.09	98.64	99.41

Maximum installation force [N]	34551
Penetration depth [mm]	-

Cyclic Test Phase

Masses on the weight hangers [Kg]

M1	M2	M3
19.575	27.93	33

Number of cycles	10083
Loading period [s]	10

LVDTs-Time, Rotation-Time

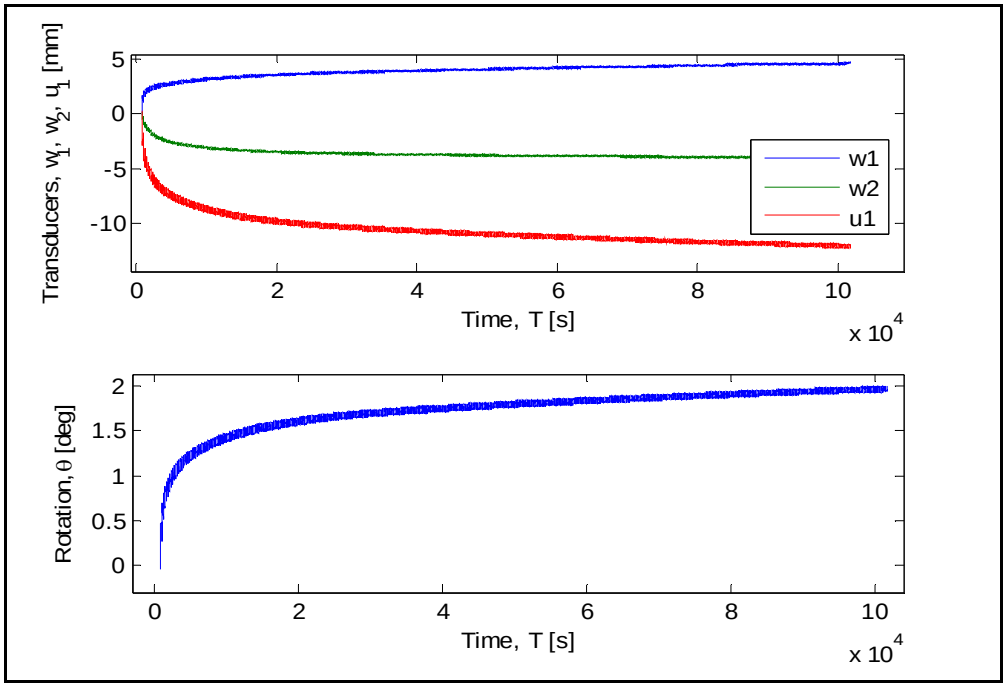

Horizontal Load-Time, Moment-Rotation

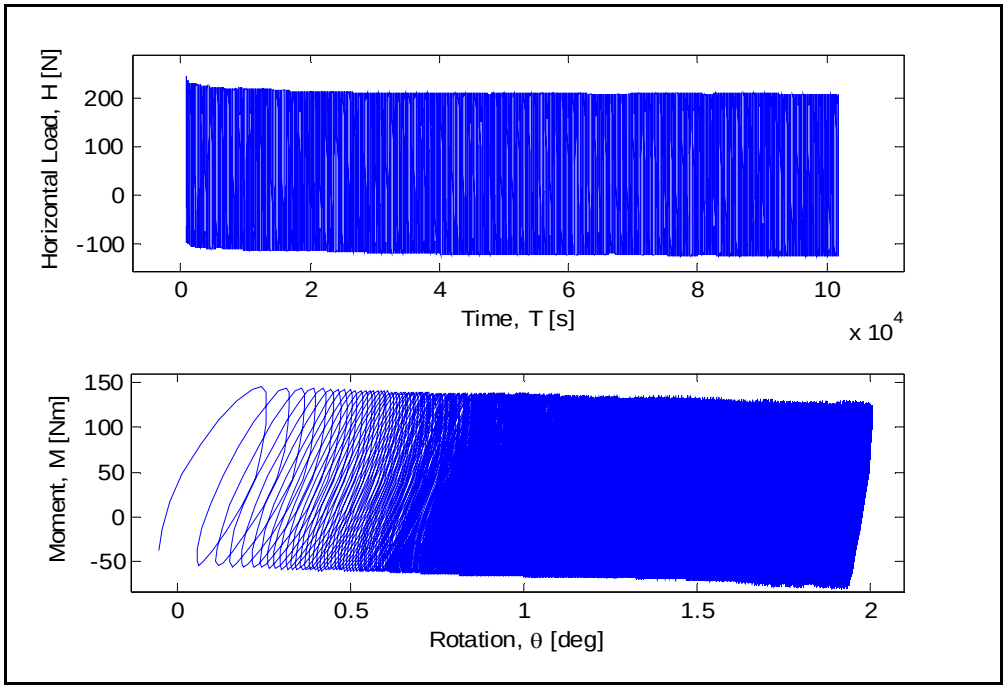

Maximum accumulated rotation [deg] | 2

Maximum and minimum moment [Nm]

Mmax	Mmin
126.03	-72.54

ζb	ζc
0.688	-0.576

Post-Cyclic Phase

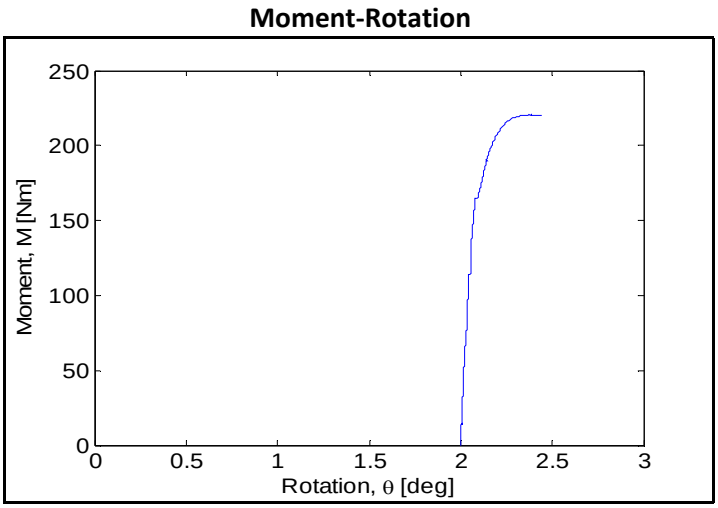

Maximum moment [Nm]	220.6
Rotation at maximum moment [deg]	2.376

Test equipment	Blue sandbox
User	Giulio & Aligi
Test name	C38
Date	11/10/2012

Bucket

Diameter [mm]	300
Embedment ratio	1

Test

Static or cyclic test	cyclic
Moment arm [mm]	596

General Comments

None

Soil Preparation and Installation Phase

Gradient applied

0.817

Cone Penetration Resistance

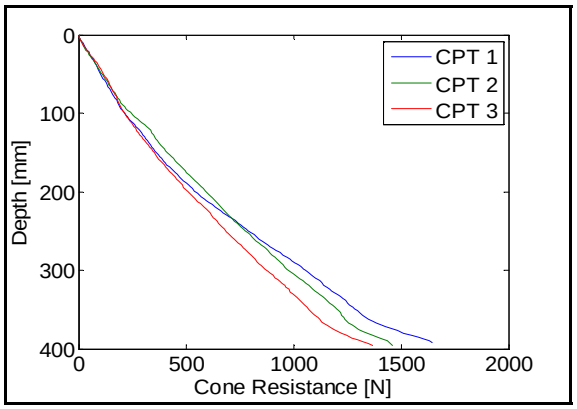

Installation Phase

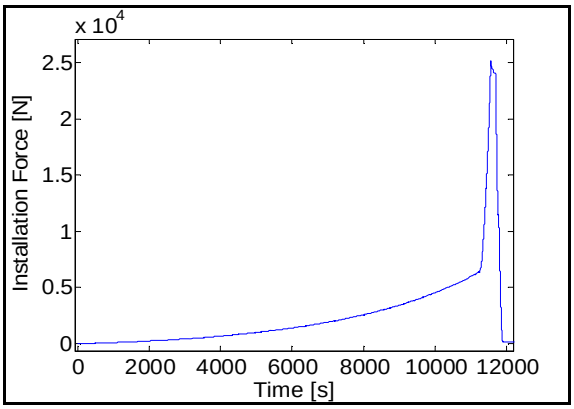

Relative density [%]

cpt 1	cpt 2	cpt 3	Average
99.92	100.5	96.69	99.03

Maximum installation force [N]	25152
Penetration depth [mm]	-

Cyclic Test Phase

Masses on the weight hangers [Kg]

M1	M2	M3
21.875	31.81	33

Number of cycles	10016
Loading period [s]	10

LVDTs-Time, Rotation-Time

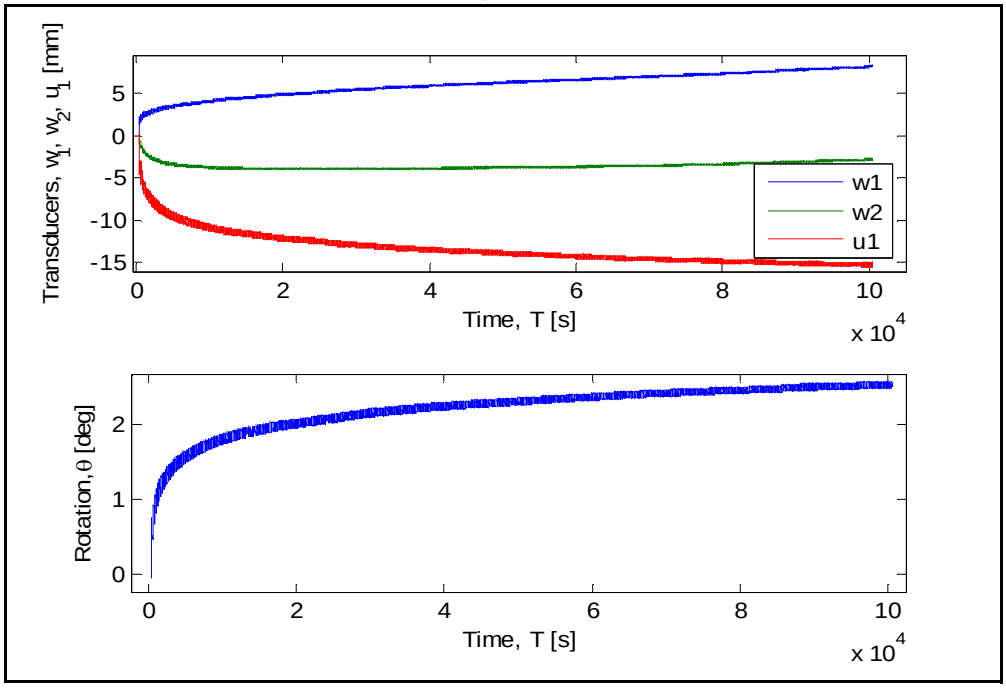

Horizontal Load-Time, Moment-Rotation

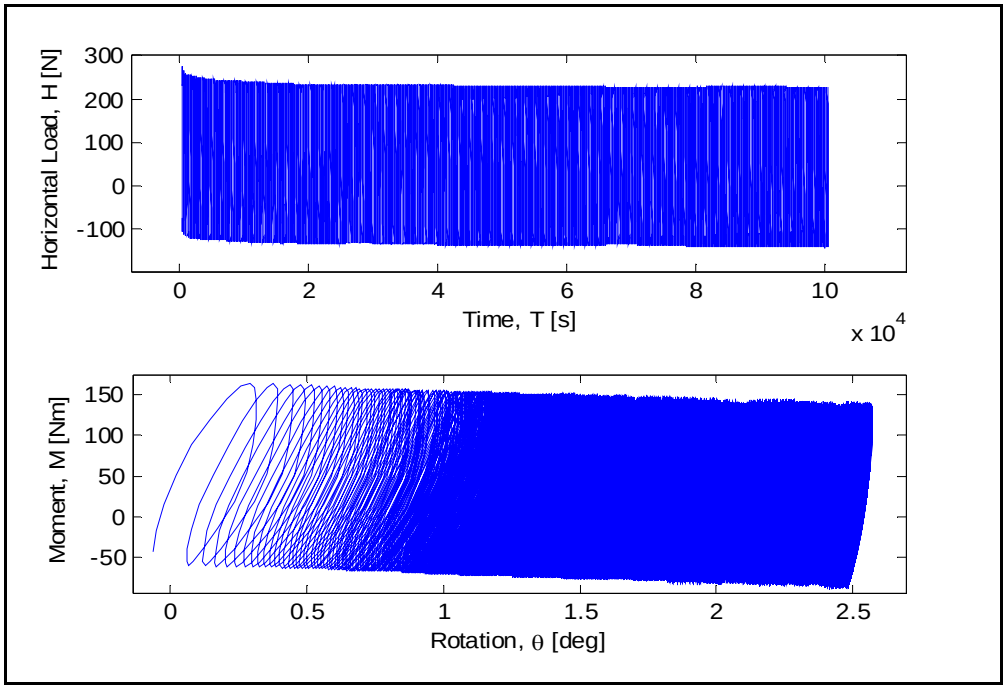

Maximum accumulated rotation [deg] | 2.574

Maximum and minimum moment [Nm]

Mmax	Mmin
139.03	-81

ζb	ζc
0.759	-0.583

Post-Cyclic Phase

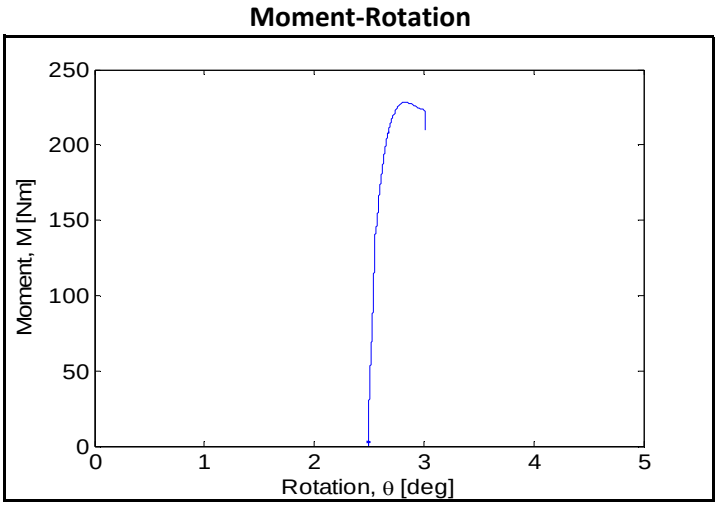

Maximum moment [Nm]	228.2
Rotation at maximum moment [deg]	2.839

Test equipment	Blue sandbox
User	Giulio & Aligi
Test name	C39
Date	15/10/2012

Bucket

Diameter [mm]	300
Embedment ratio	1

Test

Static or cyclic test	cyclic
Moment arm [mm]	596

General Comments

The post-cyclic test was not performed. The accumulated rotation of the bucket after cyclic loading was too large.

Soil Preparation and Installation Phase

Gradient applied

1.13

Cone Penetration Resistance

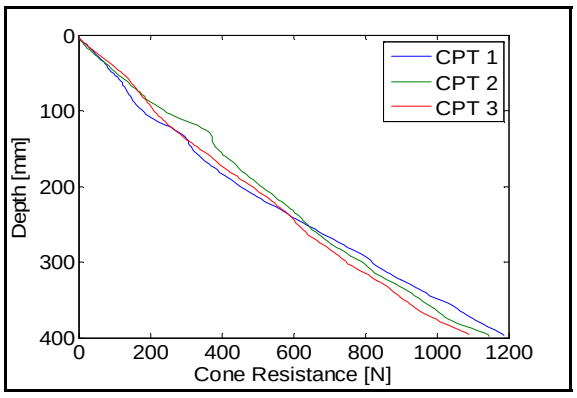

Installation Phase

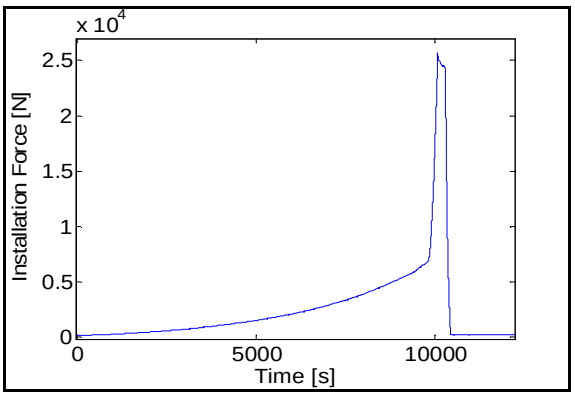

Relative density [%]

cpt 1	cpt 2	cpt 3	Average
94.1	96.12	93.83	94.68

Maximum installation force [N]	25668
Penetration depth [mm]	-

Cyclic Test Phase

Masses on the weight hangers [Kg]

M1	M2	M3
24.775	36.01	33

Number of cycles	9366
Loading period [s]	10

LVDTs-Time, Rotation-Time

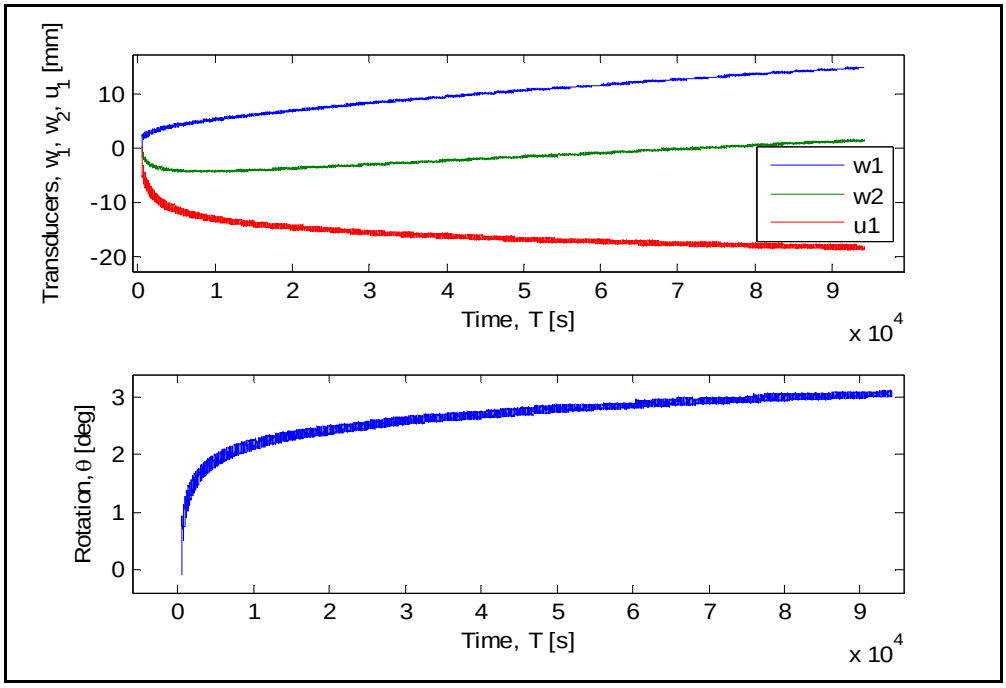

Horizontal Load-Time, Moment-Rotation

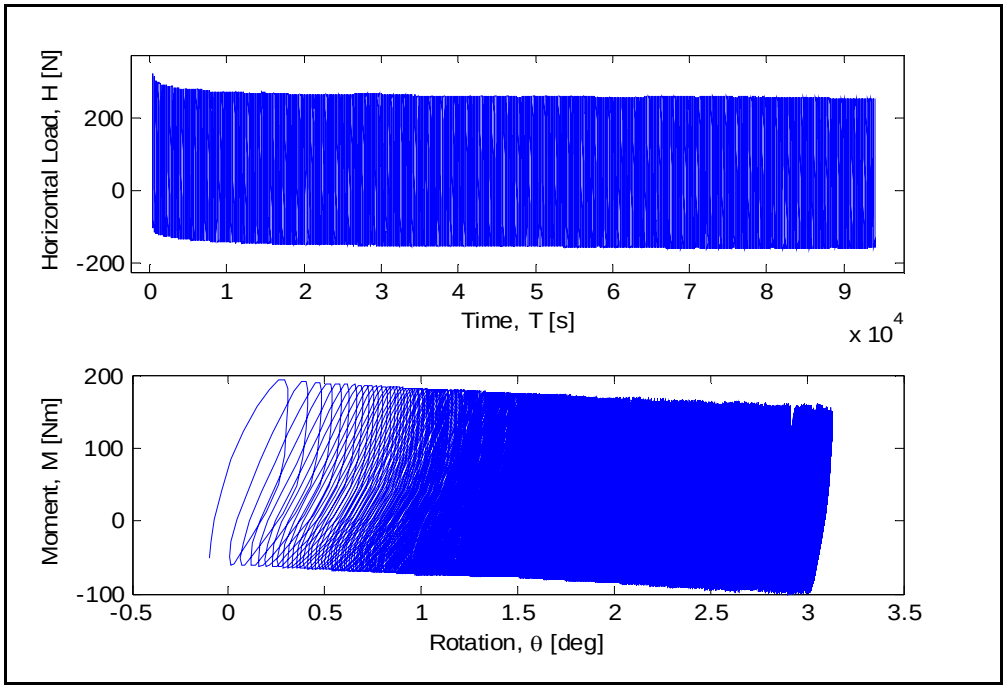

Maximum accumulated rotation [deg]	3.128

Maximum and minimum moment [Nm]

Mmax	Mmin
157.11	-92.18

ζb	ζc
0.857	-0.587

Post-Cyclic Phase

Moment-Rotation

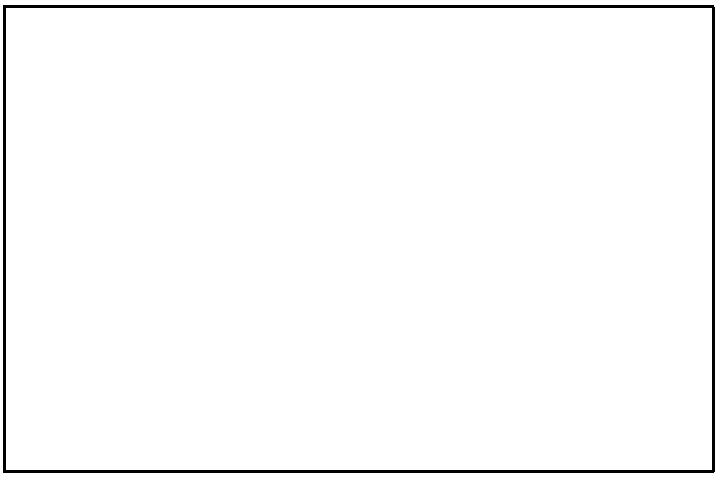

Maximum moment [Nm]	-
Rotation at maximum moment [deg]	-

Test equipment	Blue sandbox
User	Giulio & Aligi
Test name	C40
Date	23/10/2012

Bucket

Diameter [mm]	300
Embedment ratio	1

Test

Static or cyclic test	cyclic
Moment arm [mm]	596

General Comments

The penetration depth was measured by a magnet support.
The test was stopped after 144 cycles. The motor was not working correctly because overloaded

Soil Preparation and Installation Phase

Gradient applied

1.06

Cone Penetration Resistance

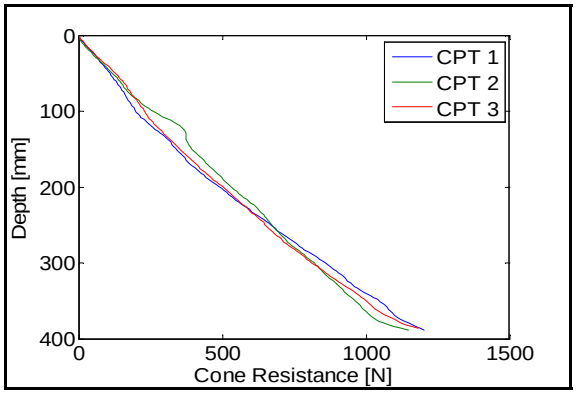

Installation Phase

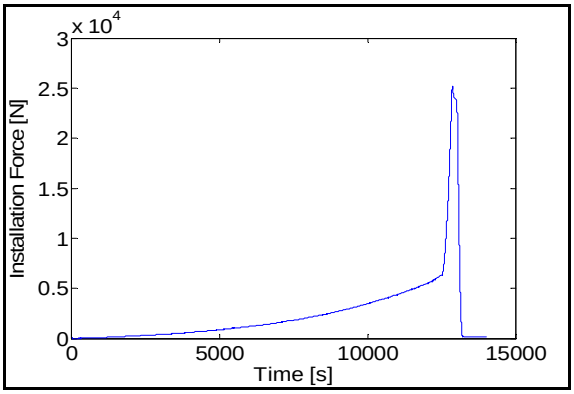

Relative density [%]

cpt 1	cpt 2	cpt 3	Average
95.56	97.25	95.68	96.17

Maximum installation force [N]	25125
Penetration depth [mm]	291.7

Cyclic Test Phase

Masses on the weight hangers [Kg]

M1	M2	M3
32.075	46.61	33

Number of cycles	108
Loading period [s]	10

LVDTs-Time, Rotation-Time

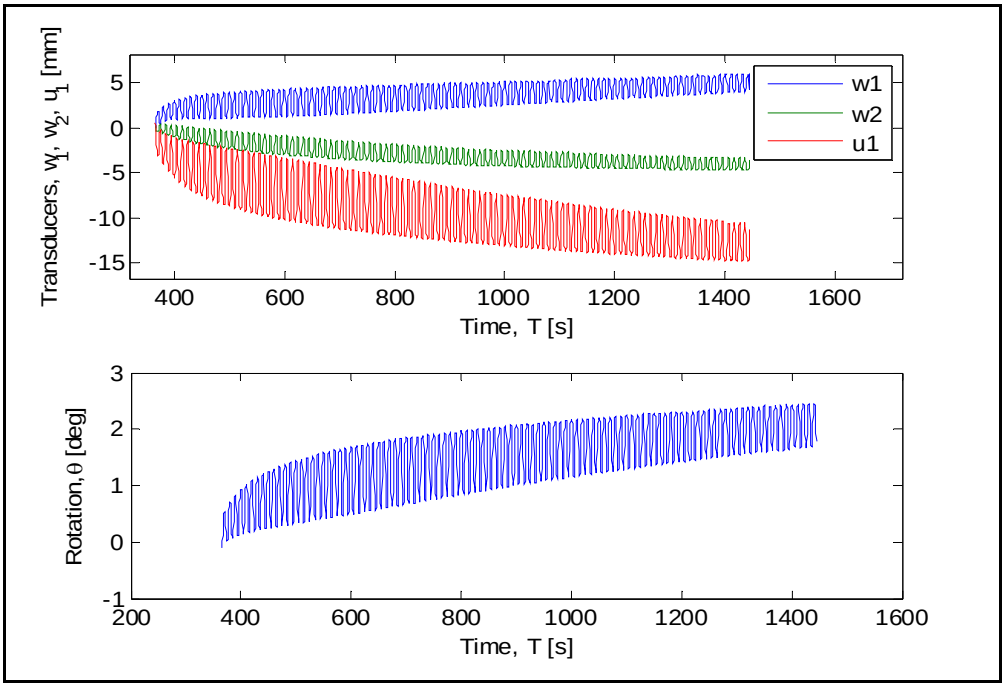

Horizontal Load-Time, Moment-Rotation

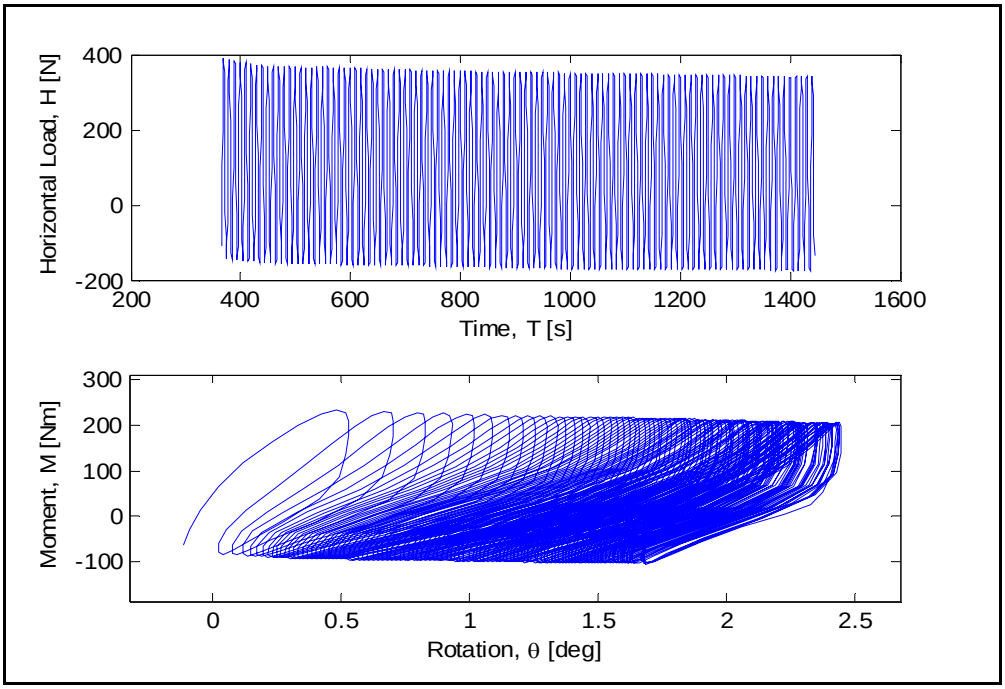

Maximum accumulated rotation [deg] | 2.451

Maximum and minimum moment [Nm]

Mmax	Mmin
211.84	-99.31

ζb	ζc
1.156	-0.469

Post-Cyclic Phase

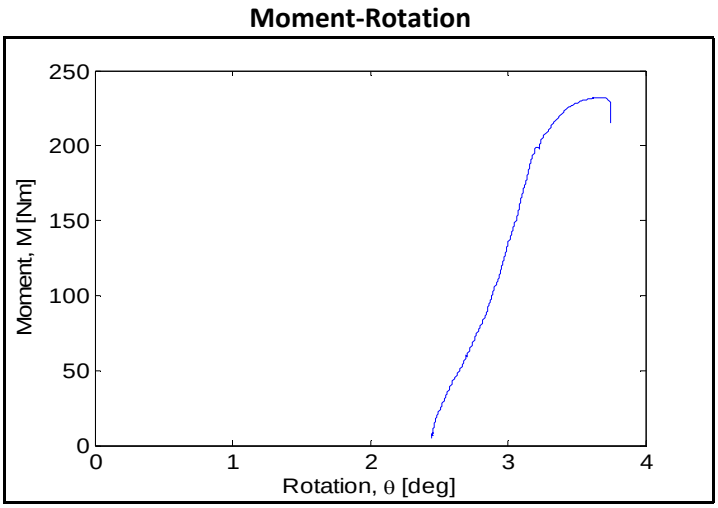

Maximum moment [Nm]	232.4
Rotation at maximum moment [deg]	3.659

Test equipment	Blue sandbox
User	Aligi & Giulio
Test name	C41
Date	15/11/2012

Bucket

Diameter [mm]	300
Embendment ratio	1

Test

Static or cyclic test	cyclic
Moment arm [mm]	596

General Comments

None

Soil Preparation and Installation Phase

Gradient applied

-

Cone Penetration Resistance

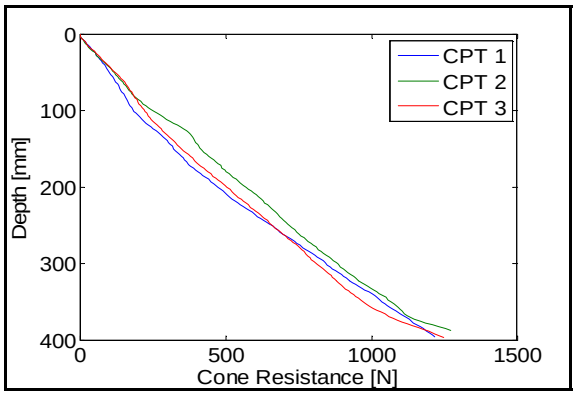

Installation Phase

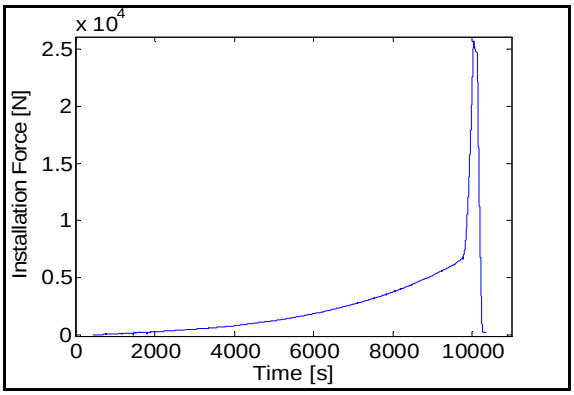

Relative density [%]

cpt 1	cpt 2	cpt 3	Average
94.79	98.85	95.53	96.39

Maximum installation force [N]	25731
Penetration depth [mm]	288.2

Cyclic Test Phase

Masses on the weight hangers [Kg]

M1	M2	M3
10.575	14.61	33

Number of cycles	10032
Loading period [sec]	10

Displacements-Time, Rotation-Time

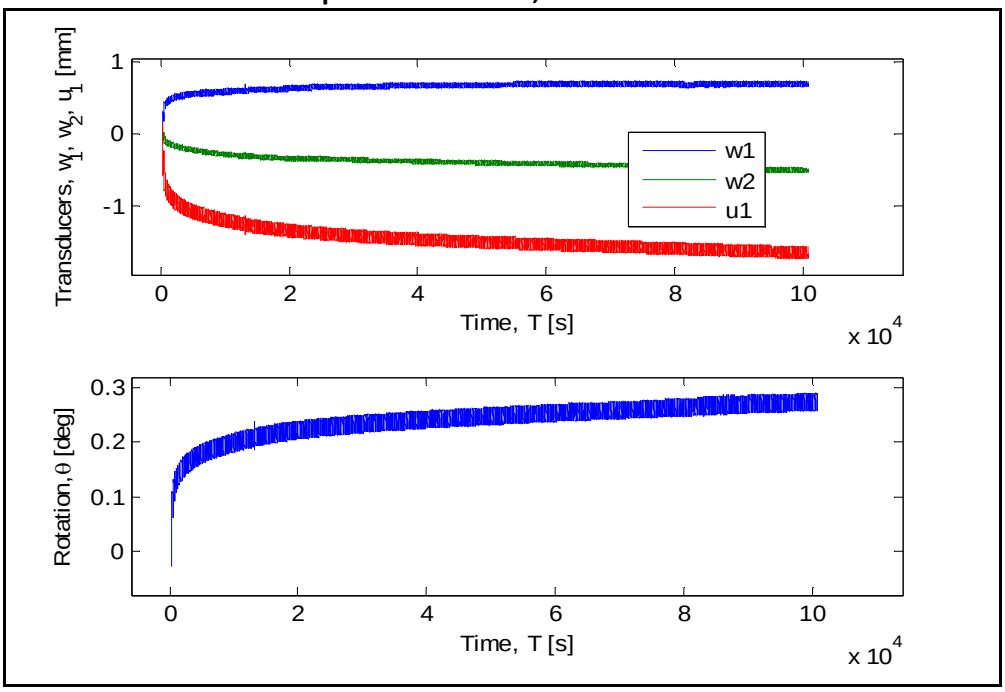

Horizontal Load-Time, Moment-Rotation

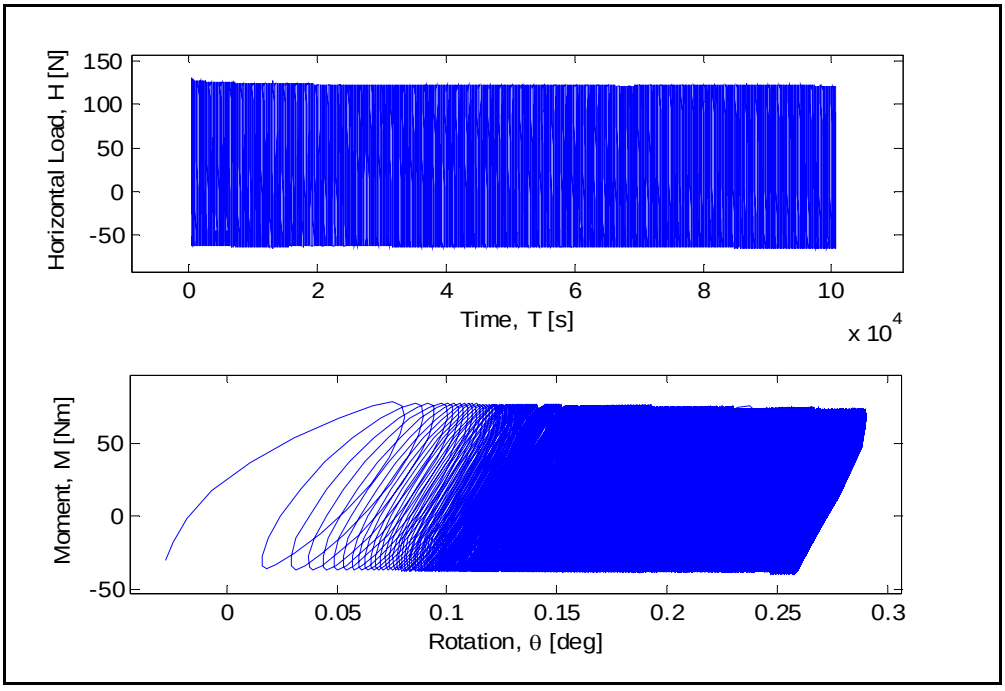

Maximum accumulated rotation [deg] | 0.29

Maximum and minimum moment [Nm]

Mmax	Mmin
73.62	-38.26

ζb	ζc
0.4	-0.52

Post-Cyclic Phase

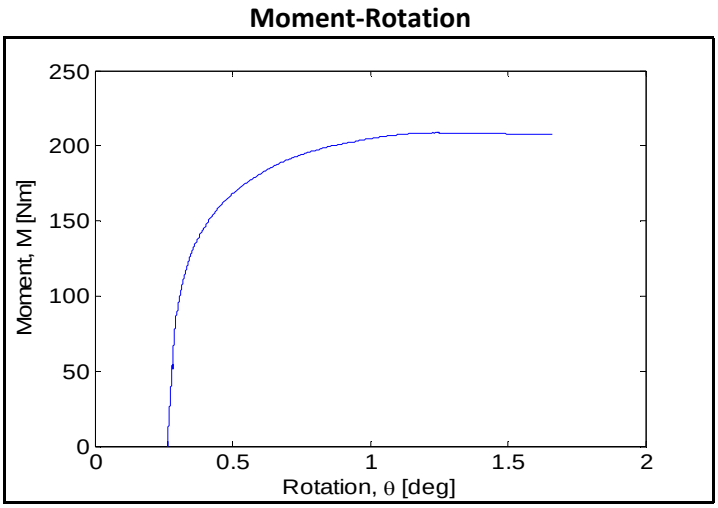

Maximum moment [Nm]	208.8
Rotation at maximum moment [deg]	1.23

Test equipment	Blue sandbox
User	Aligi & Giulio
Test name	C42
Date	22/11/2012

Bucket

Diameter [mm]	300
Embedment ratio	1

Test

Static or cyclic test	cyclic
Moment arm [mm]	596

General Comments

The installation depth was not measured

Soil Preparation and Installation Phase

Gradient applied

0.96

Cone Penetration Resistance

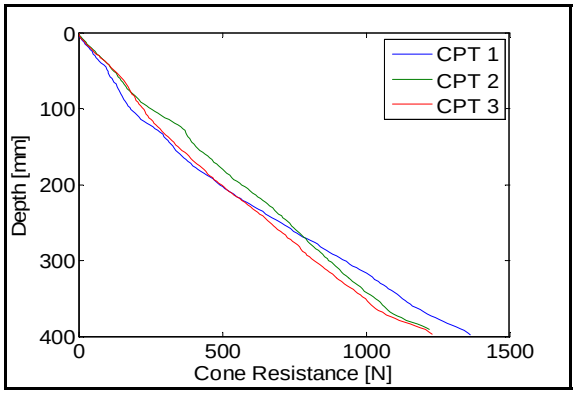

Installation Phase

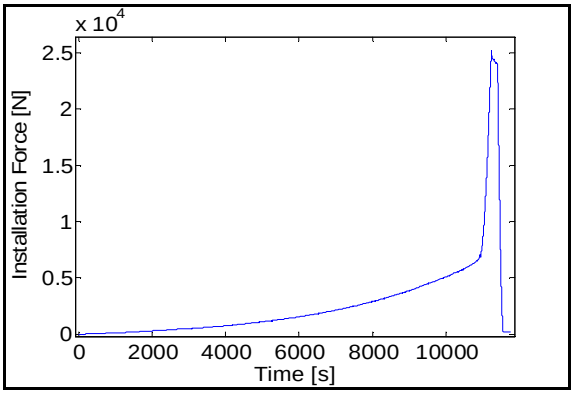

Relative density [%]

cpt 1	cpt 2	cpt 3	Average
96.31	98.6	95.58	96.83

Maximum installation force [N]	25212
Penetration depth [mm]	-

Cyclic Test Phase

Masses on the weight hangers [Kg]

M1	M2	M3
10.575	14.61	33

Number of cycles	10124
Loading period [s]	20

LVDTs-Time, Rotation-Time

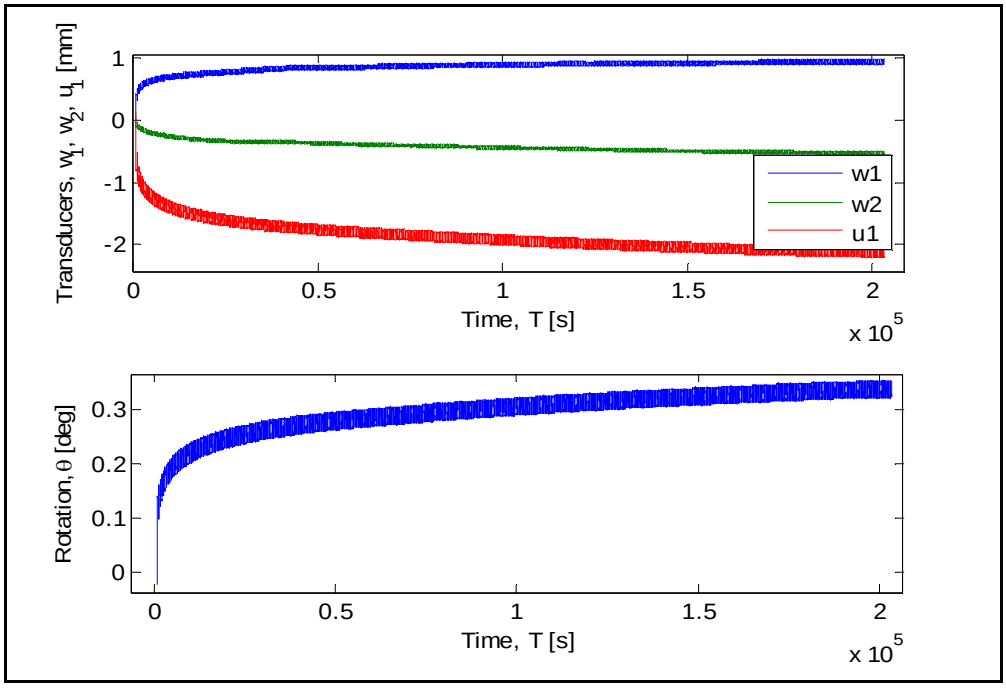

Horizontal Load-Time, Moment-Rotation

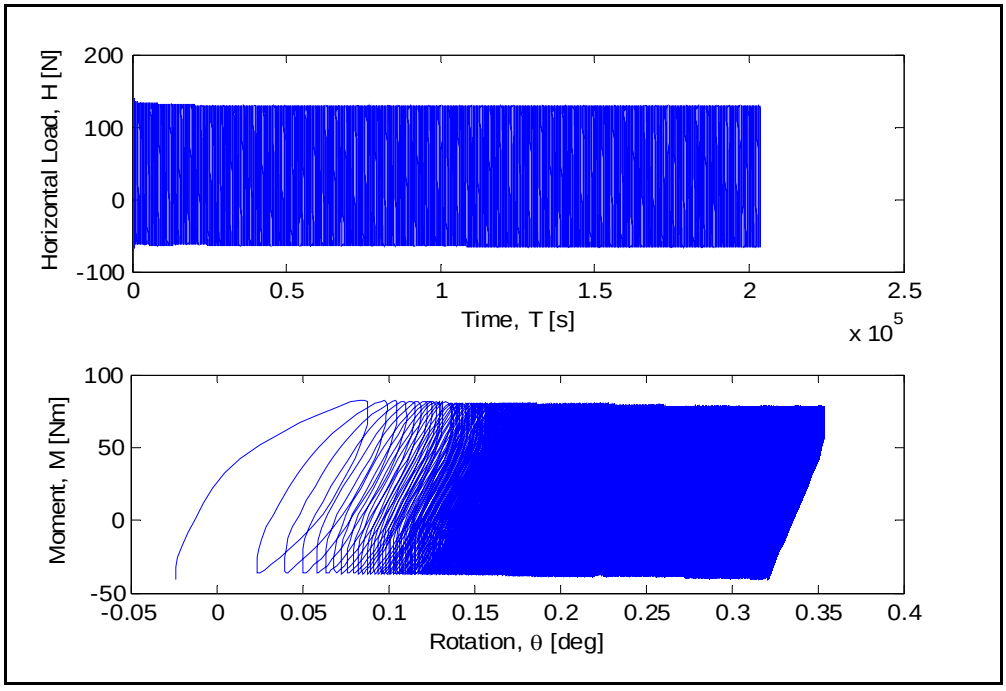

Maximum accumulated rotation [deg] 0.354

Maximum and minimum moment [Nm]

Mmax	Mmin
77.53	-38.78

ζb	ζc
0.423	-0.5

Post-Cyclic Phase

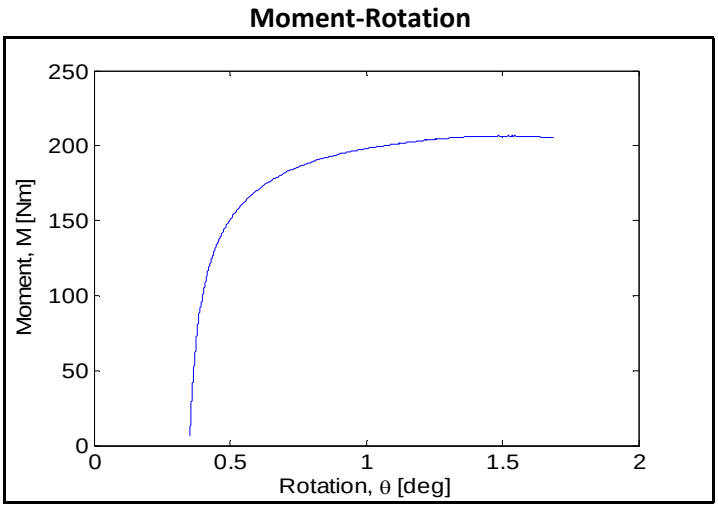

Maximum moment [Nm]	206.5
Rotation at maximum moment [deg]	1.488

Test equipment	Blue sandbox
User	Giulio
Test name	C44
Date	15.01.2013

Bucket

Diameter [mm]	300
Embedment ratio	1

Test

Static or cyclic test	cyclic
Moment arm [mm]	596

General Comments

None

Soil Preparation and Installation Phase

Gradient applied

0.956

Cone Penetration Resistance

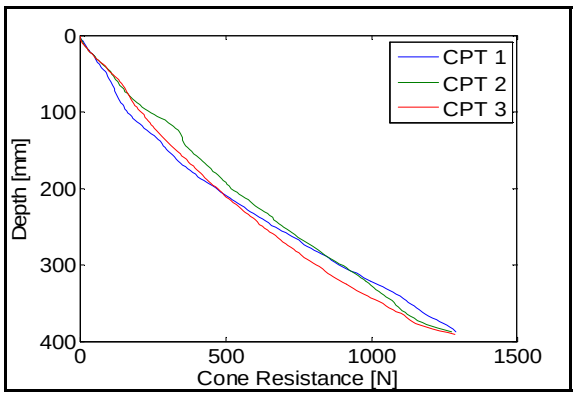

Installation Phase

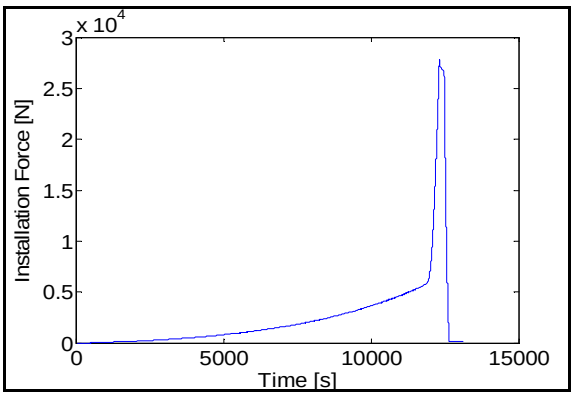

Relative density

cpt 1	cpt 2	cpt 3	Average
94.93	97.93	94.87	95.91

Maximum installation force [N]	27798
Penetration depth [mm]	288.25

Cyclic Test Phase

Masses on the weight hangers [Kg]

M1	M2	M3
10.575	14.61	33

Number of cycles	10148
Loading period [s]	30

LVDTs-Time, Rotation-Time

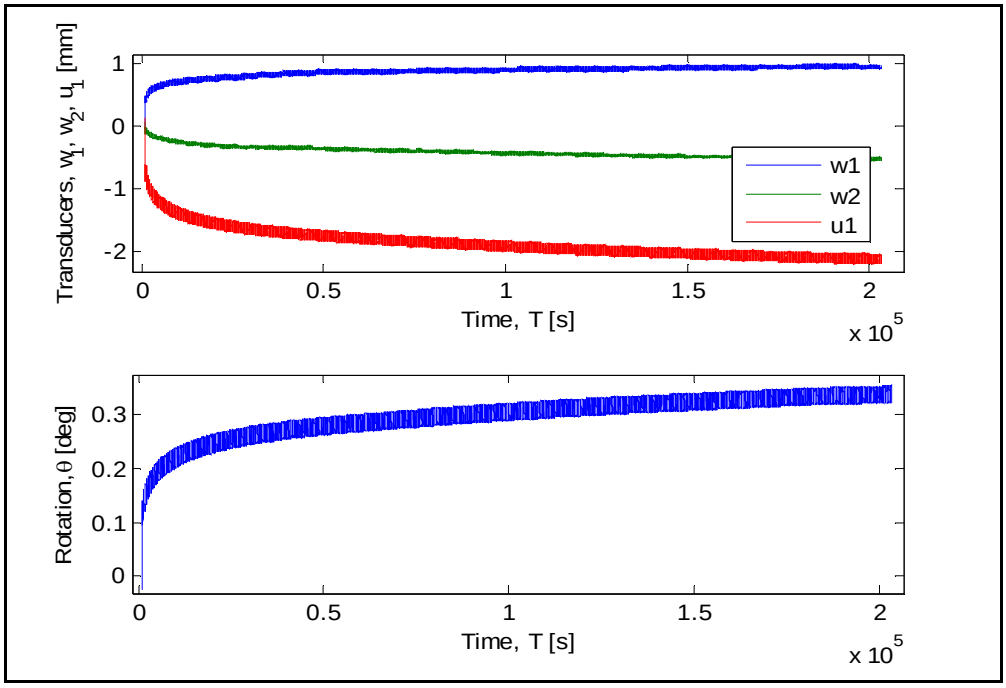

Horizontal Load-Time, Moment-Rotation

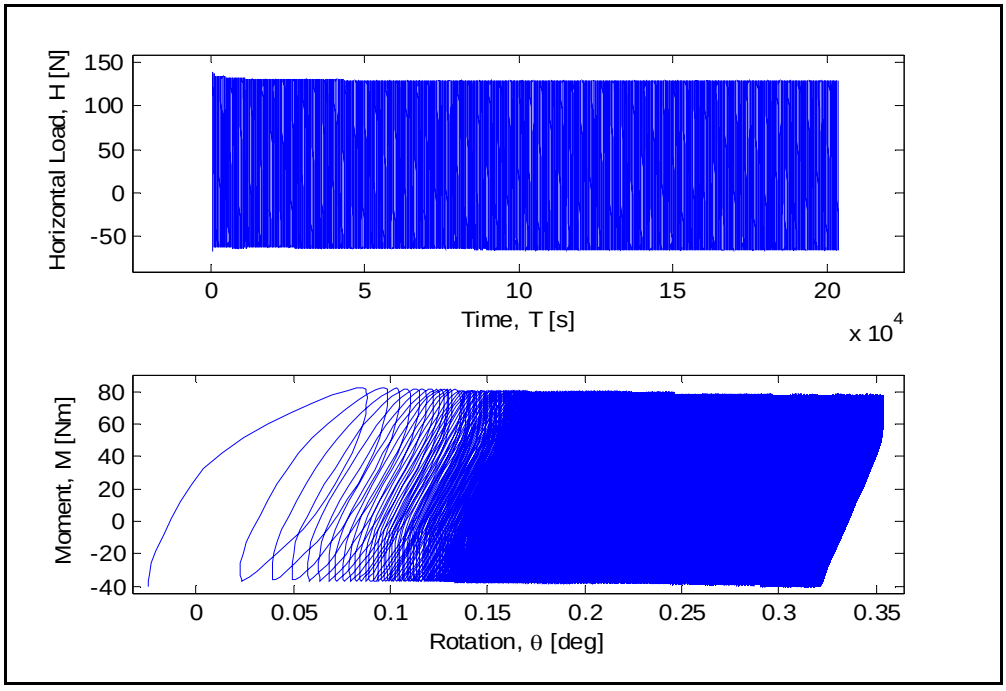

Maximum accumulated rotation [deg]	0.277

Maximum and minimum moment [Nm]

Mmax	Mmin
71.3	-42.66

ζb	ζc
0.269	-0.426

Post-Cyclic Phase

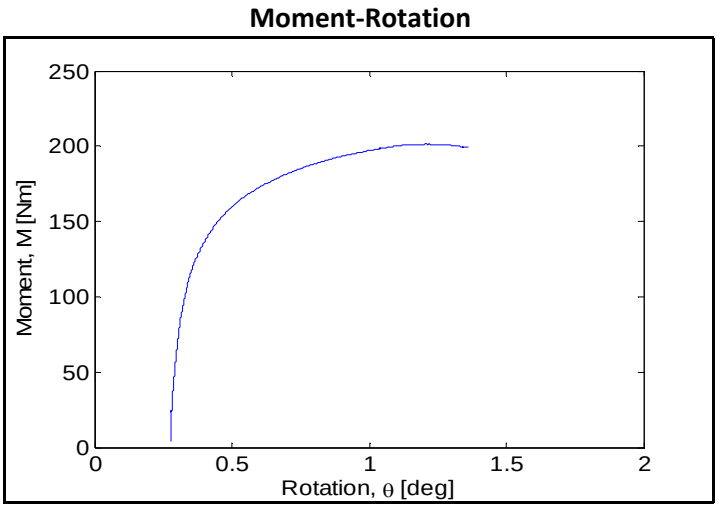

Maximum moment [Nm]	201.4
Rotation at maximum moment [deg]	1.191

Test equipment	Blue sandbox
User	Giulio
Test name	C45
Date	04/02/2013

Bucket

Diameter [mm]	300
Embedment ratio	1

Test

Static or cyclic test	cyclic
Moment arm [mm]	596

General Comments

Soil Preparation and Installation Phase

Gradient applied

-

Cone Penetration Resistance

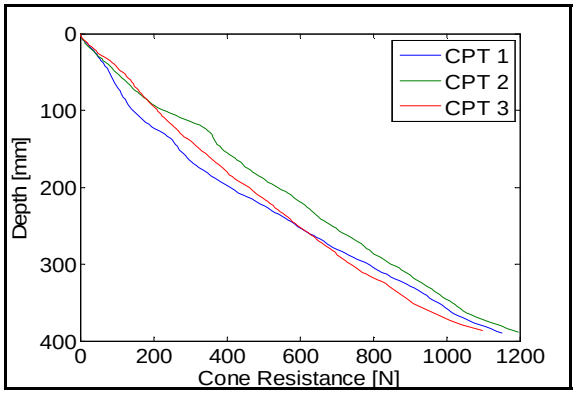

Installation Phase

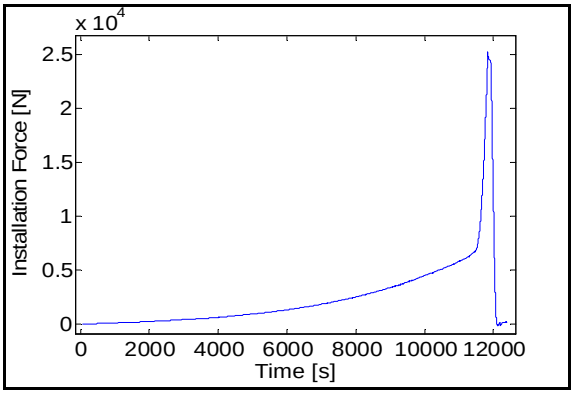

Relative density

cpt 1	cpt 2	cpt 3	Average
91.46	97.38	93.3	94.05

Maximum installation force [N]	25185
Penetration depth [mm]	287.66

Cyclic Test Phase

Masses on the weight hangers [Kg]

M1	M2	M3
10.575	14.61	33

Number of cycles	10070
Loading period [s]	5

LVDTs-Time, Rotation-Time

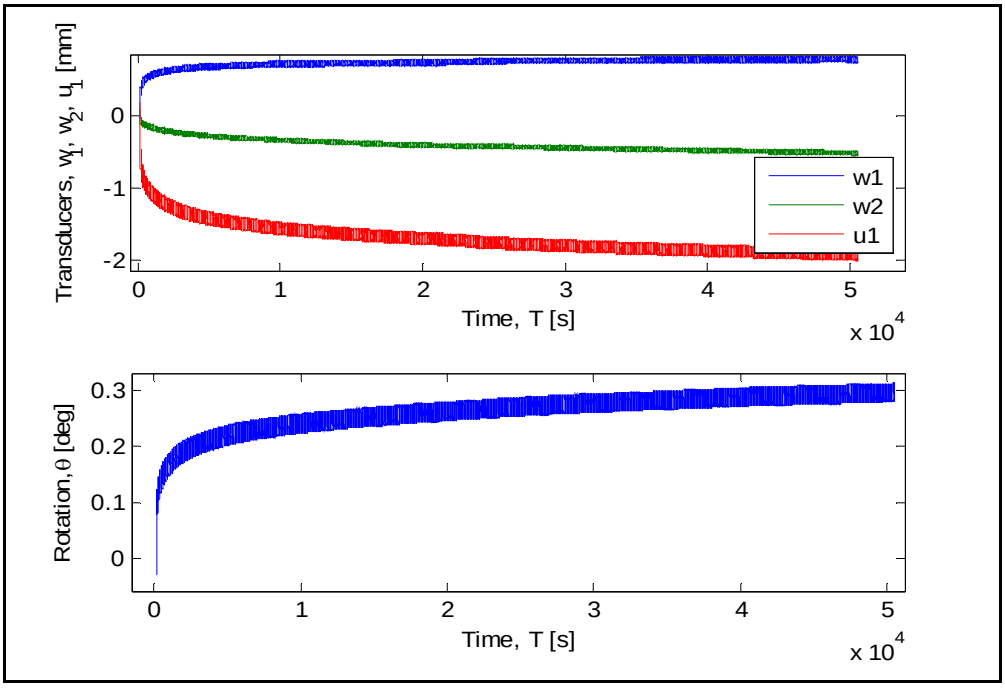

Horizontal Load-Time, Moment-Rotation

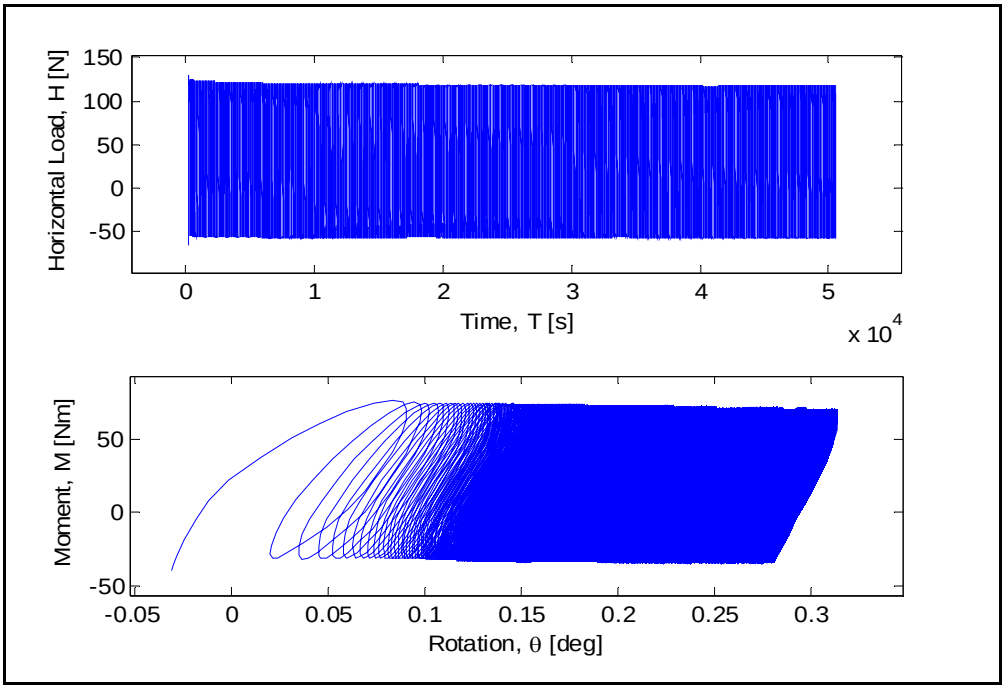

Maximum accumulated rotation [deg] | 0.3141

Maximum and minimum moment [Nm]

Mmax	Mmin
70.94	-34.02

ζb	ζc
0.387	-0.48

Post-Cyclic Phase

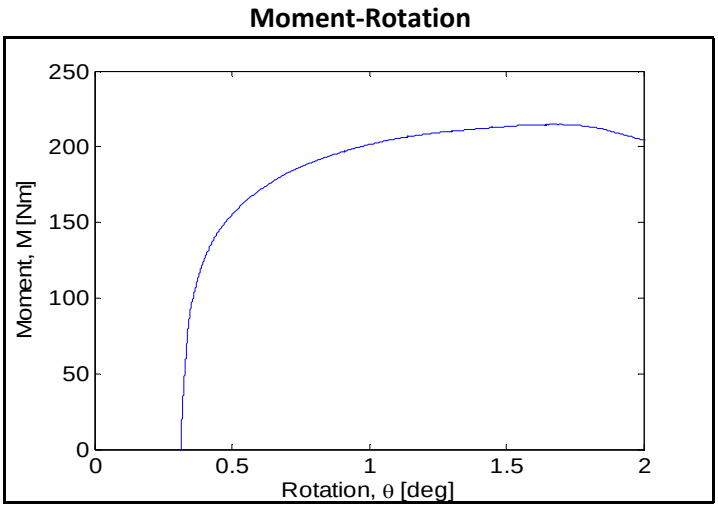

Maximum moment [Nm]	214.8
Rotation at maximum moment [deg]	1.66

Test equipment	Blue sandbox
User	Giulio
Test name	C46
Date	13/02/2013

Bucket

Diameter [mm]	300
Embedment ratio	1

Test

Static or cyclic test	cyclic
Moment arm [mm]	596

General Comments

None

Soil Preparation and Installation Phase

Gradient applied

1.06

Cone Penetration Resistance

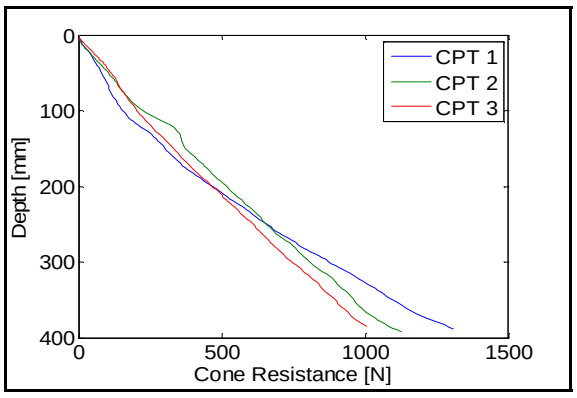

Installation Phase

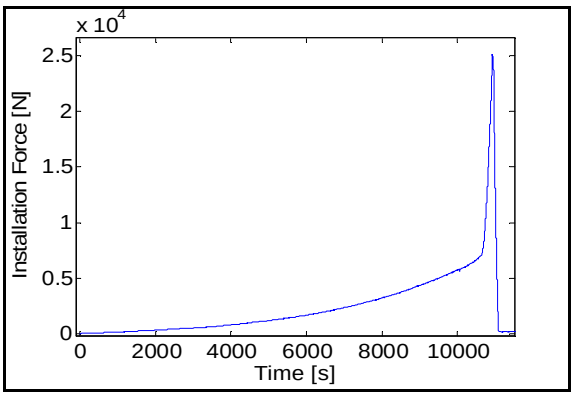

Relative density [%]

cpt 1	cpt 2	cpt 3	Average
94.51	96.18	93.32	94.67

Maximum installation force [N]	25206
Penetration depth [mm]	280.9

Cyclic Test Phase

Masses on the weight hangers [Kg]

M1	M2	M3
10.575	14.61	33

Number of cycles	10031
Loading period [Sec]	40

LVDTs-Time, Rotation-Time

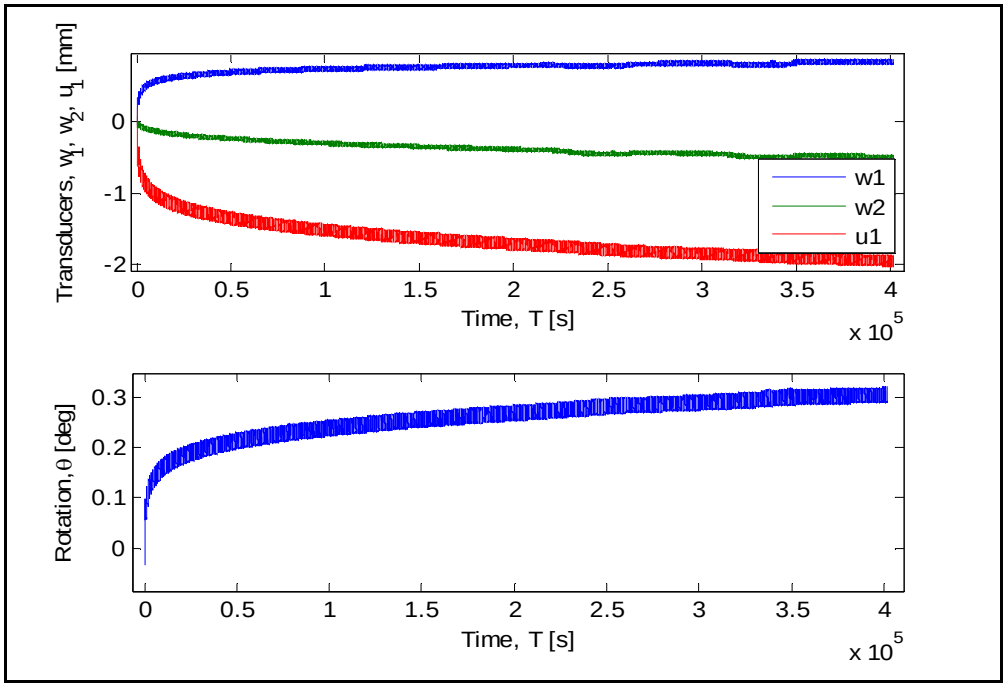

Horizonatl Load-Time, Moment-Rotation

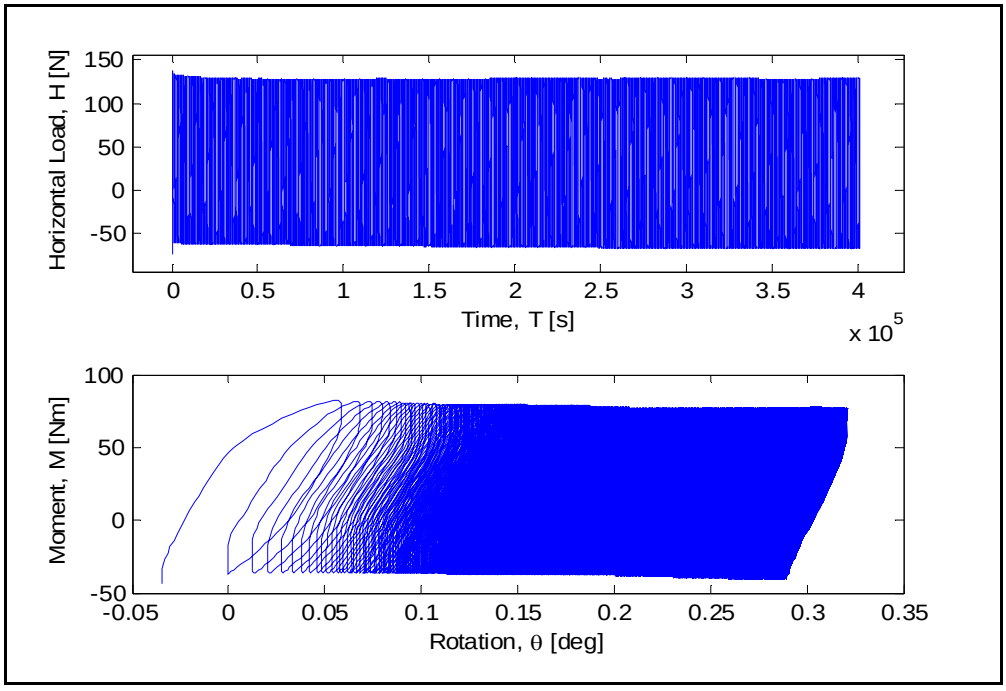

Maximum accumulated rotation [deg] | 0.321

Maximum and minimum moment [Nm]

Mmax	Mmin
76.91	-39.07

ζb	ζc
0.419	-0.508

Post-Cyclic Phase

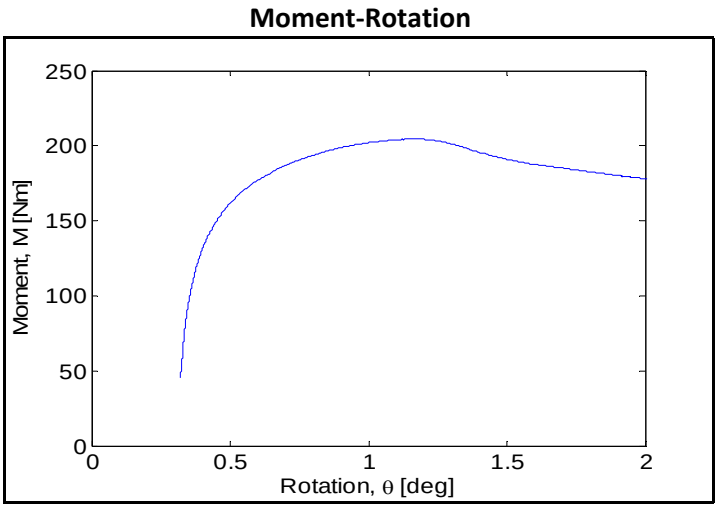

Maximum moment [Nm]	204.5
Rotation at maximum moment [deg]	1.1995

Test equipment	Blue sandbox
User	Aligi
Test name	C47
Date	13/03/2013

Bucket

Diameter [mm]	300
Embedment ratio	1

Test

Static or cyclic test	cyclic
Moment arm [mm]	596

General Comments

None

Soil Preparation and Installation Phase

Gradient applied

1.06

Cone Penetration Resistance

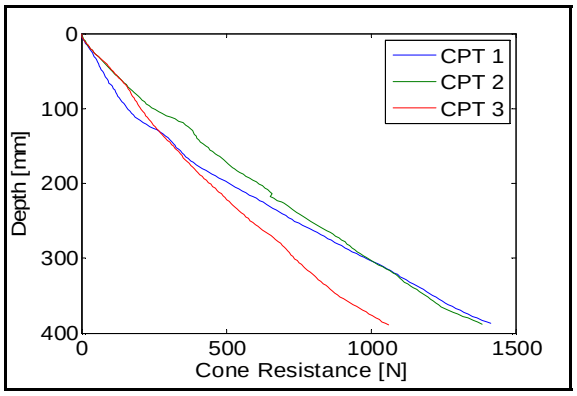

Installation Phase

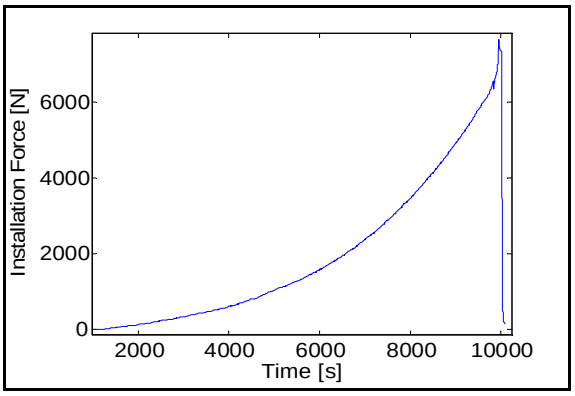

Relative density [%]

cpt 1	cpt 2	cpt 3	Average
96.98	101.02	92.67	96.89

Maximum installation force [N]	7659
Penetration depth [mm]	282.4

Cyclic Test Phase

Masses on the weight hangers [Kg]

M1	M2	M3
-	-	33

Number of cycles	50001
Loading period [s]	10

LVDTs-Time, Rotation-Time

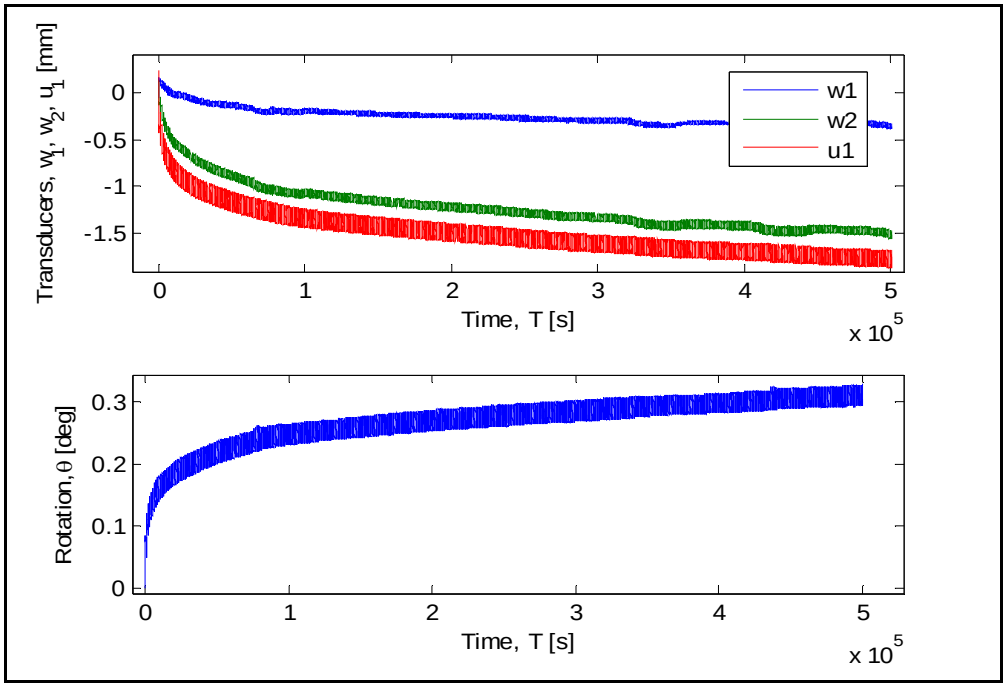

Horizontal Load-Time, Moment-Rotation

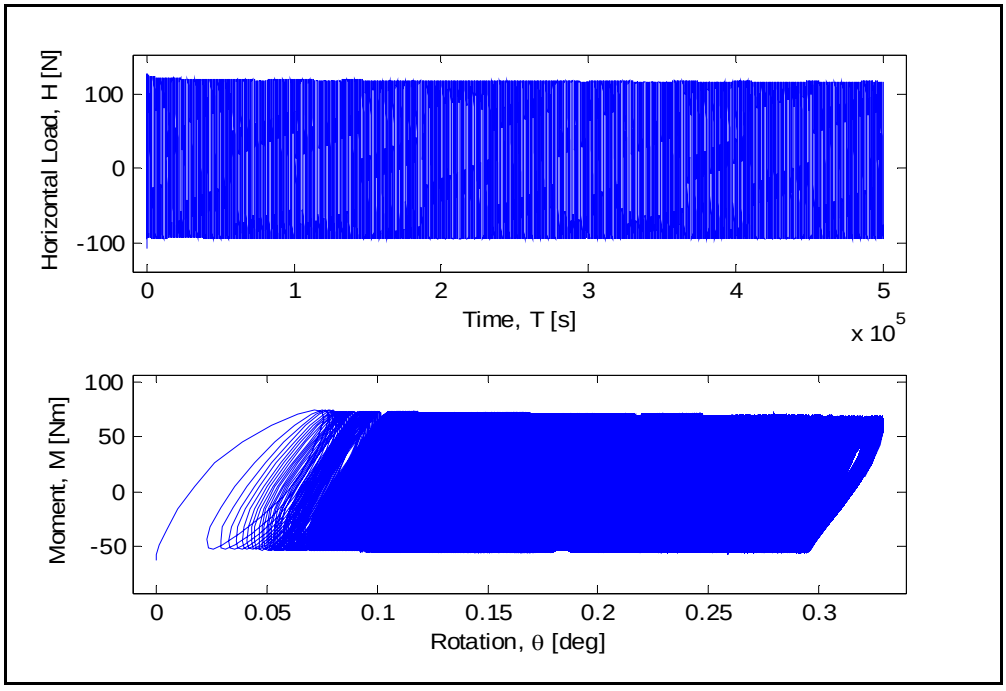

Maximum accumulated rotation [deg]	0.283

Maximum and minimum moment [Nm]

Mmax	Mmin
69.35	-55.23

ζb	ζc
0.378	-0.796

Post-Cyclic Phase

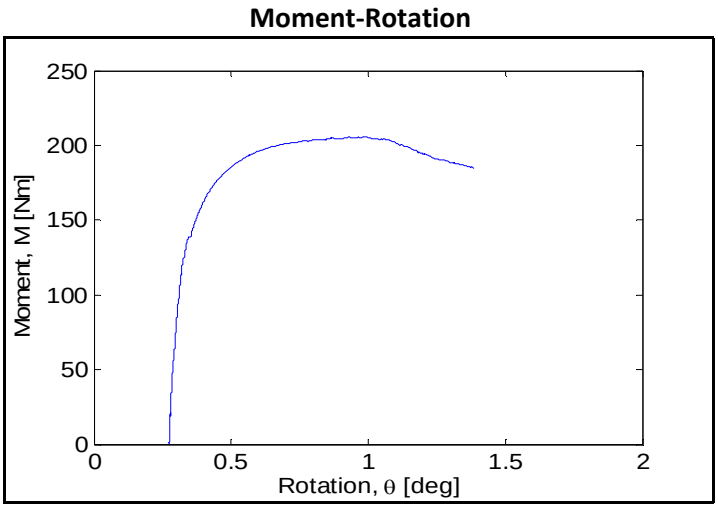

Maximum moment [Nm]	205.5
Rotation at maximum moment [deg]	0.98

Test equipment	Blue sandbox
User	Aligi
Test name	S48
Date	20/03/2013

Bucket

Diameter [mm]	300
Embedment ratio	0.5

Test

Static or cyclic test	static
Moment arm [mm]	0.596

General Comments

None

Soil Preparation & Installation Phase

Gradient applied

1.08

Cone Penetration Resistance

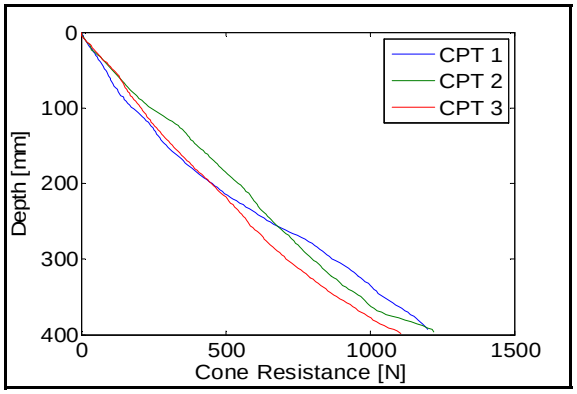

Installation Phase

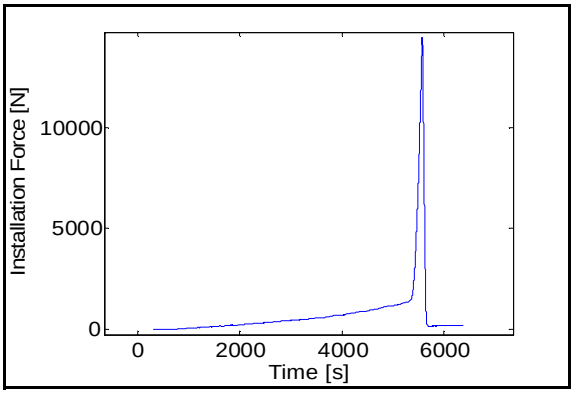

Relative density [%]

cpt 1	cpt 2	cpt 3	Average
94.4	96.9	92.52	94.61

Maximum installation force [N]	14500
Penetration depth [mm]	143.3

Horizontal and Vertical displacement-Rotation

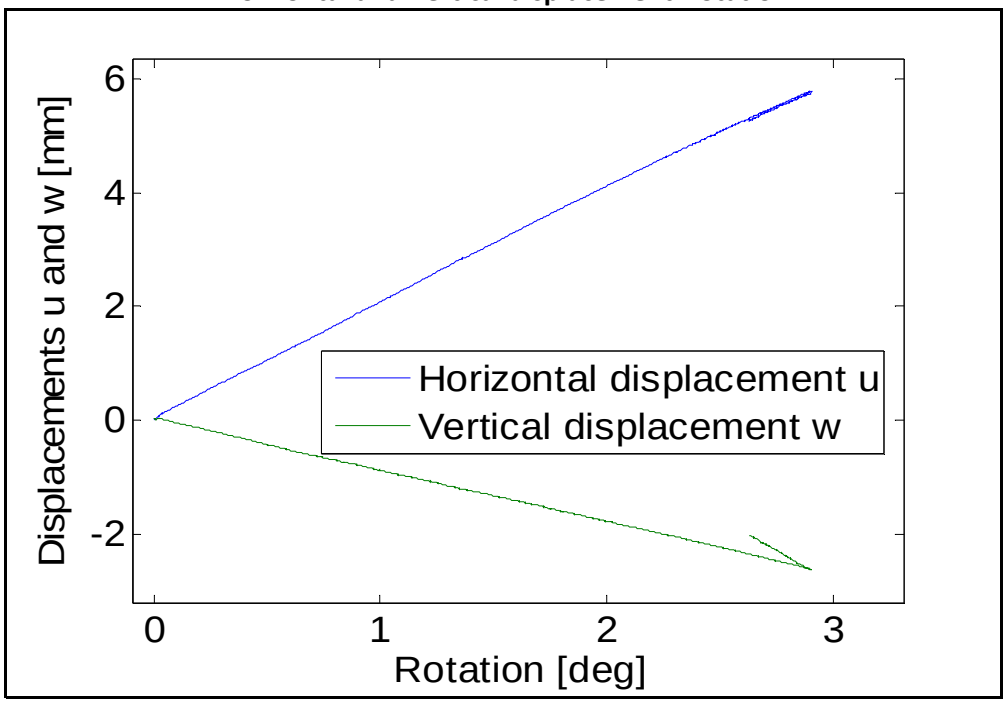

Moment-Rotation

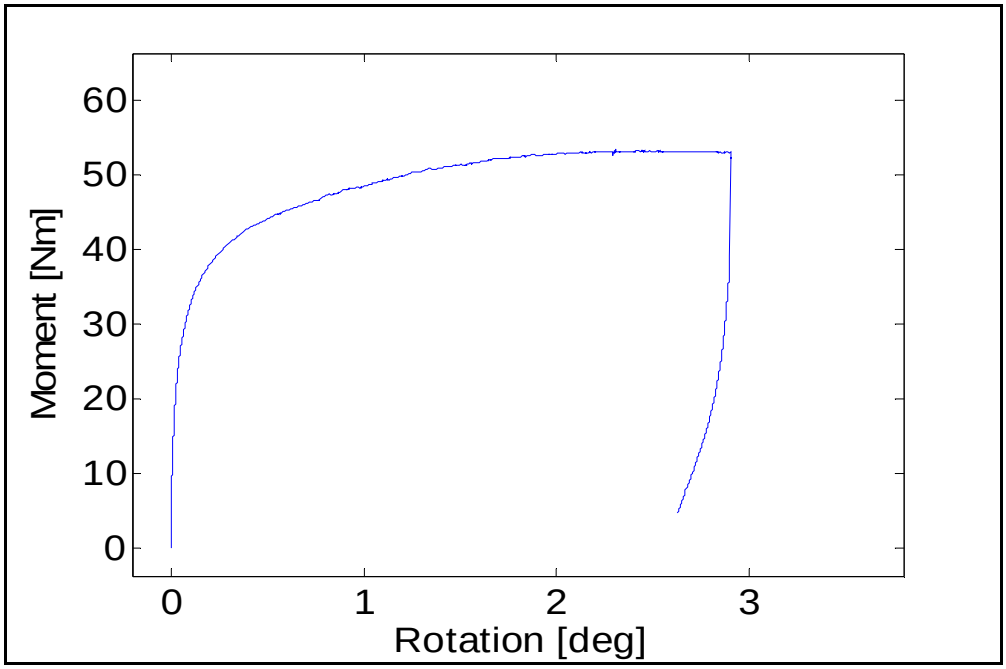

Maximum moment [Nm]	53.46
Rotation at maximum moment [deg]	2.308

Test equipment	Blue sandbox
User	Aligi
Test name	C49
Date	22/03/2013

Bucket

Diameter [mm]	300
Embedment ratio	0.5

Test

Static or cyclic test	cyclic
Moment arm [mm]	596

General Comments

Problem in the very first cycle, it did not measure the first displacement since the wrong set up assistant was loaded. The test was restarted after 5 cycles with load-after.
The weight hangers were changed as well since they were way too heavy.
The measurements were not tared, I tared them on General.m

Soil Preparation and Installation Phase

Gradient applied

1.08

Cone Penetration Resistance

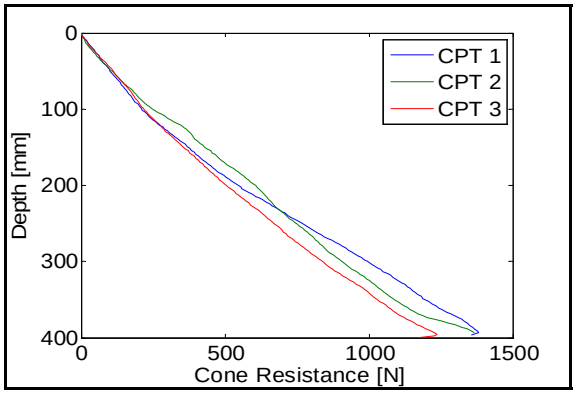

Installation Phase

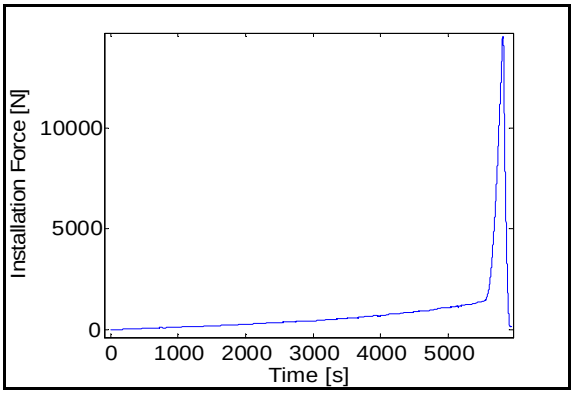

Relative density [%]

cpt 1	cpt 2	cpt 3	Average
98.99	99.8	96.12	98.30

Maximum installation force [N]	14540
Penetration depth [mm]	142.93

Cyclic Test Phase

Masses on the weight hangers [Kg]

M1	M2	M3
0.6	1.75	31.5

Number of cycles	74917
Loading period [sec]	10

Displacements-Time, Rotation-Time

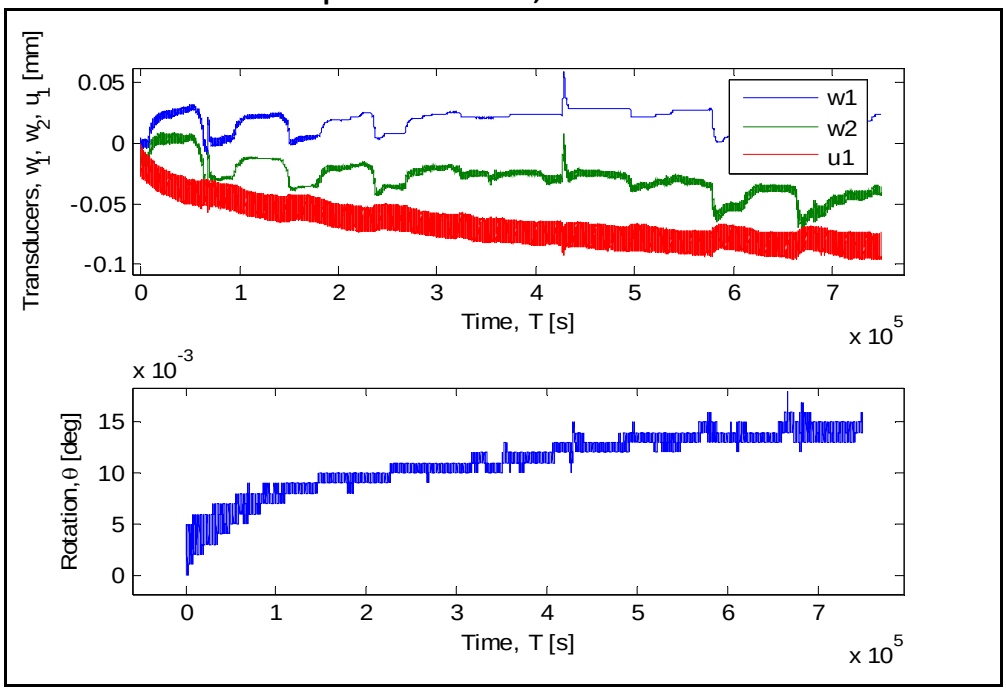

Horizontal Load-Time, Moment-Rotation

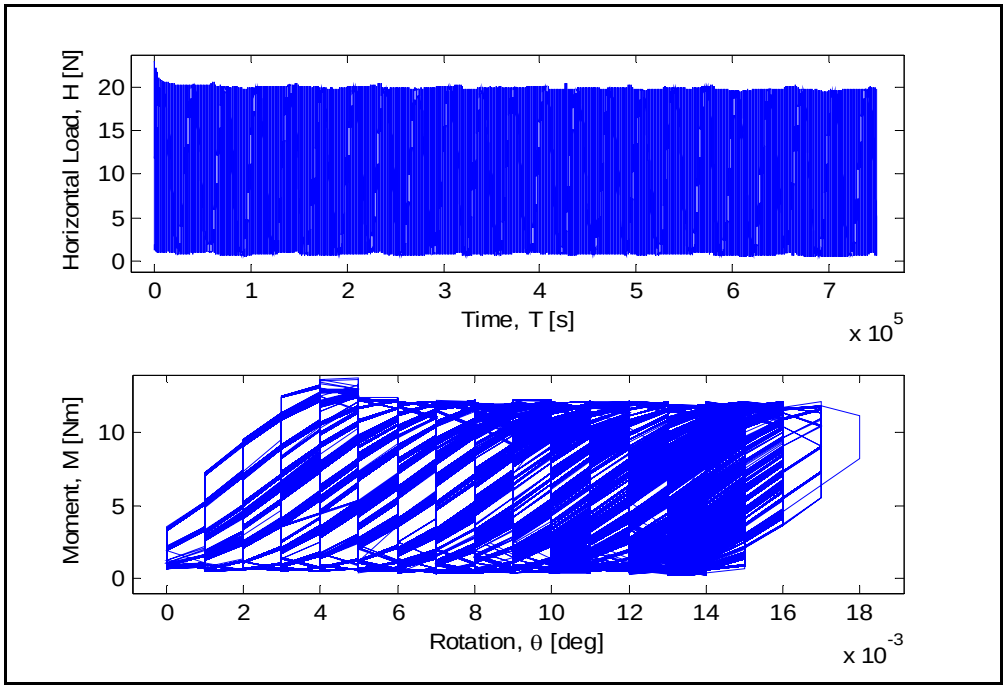

Maximum accumulated rotation [deg] | 0.017

Maximum and minimum moment [Nm]

Mmax	Mmin
11.95	0.44

ζb	ζc
0.22	0.037

Post-Cyclic Phase

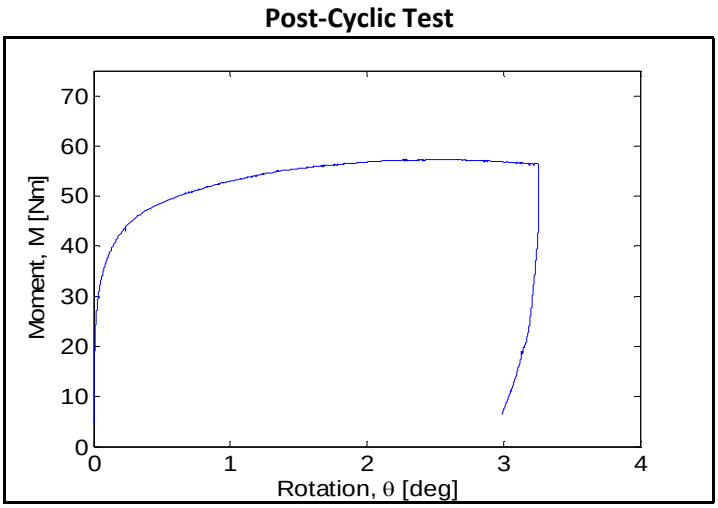

Maximum moment [Nm]	57.37
Rotation at maximum moment [Deg]	2.502

Test equipment	Blue sandbox
User	Aligi
Test name	C50
Date	06/04/2013

Bucket

Diameter [mm]	300
Embedment ratio	0.5

Test

Static or cyclic test	cyclic
Moment arm [mm]	596

General Comments

The load was adjusted four times within the first twenty cycles.

Soil Preparation and Installation Phase

Gradient applied

1.08

Cone Penetration Resistance

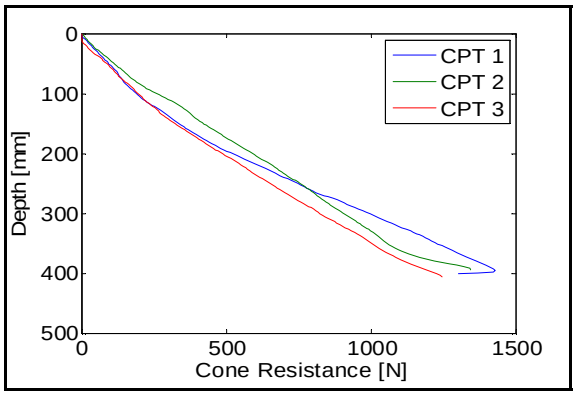

Installation Phase

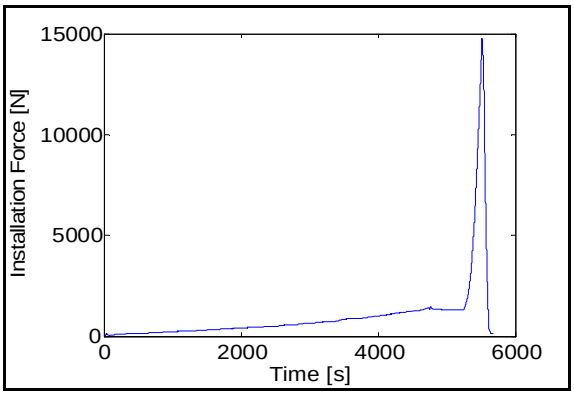

Relative density [%]

cpt 1	cpt 2	cpt 3	Average
98.01	99.51	94.72	97.41

Maximum installation force [N]	14800
Penetration depth [mm]	129

Cyclic Test Phase

Masses on the weight hangers [Kg]

M1	M2	M3
1.43	2.4	31.5

Number of cycles	9953
Loading period [s]	10

Displacements-Time, Rotation-Time

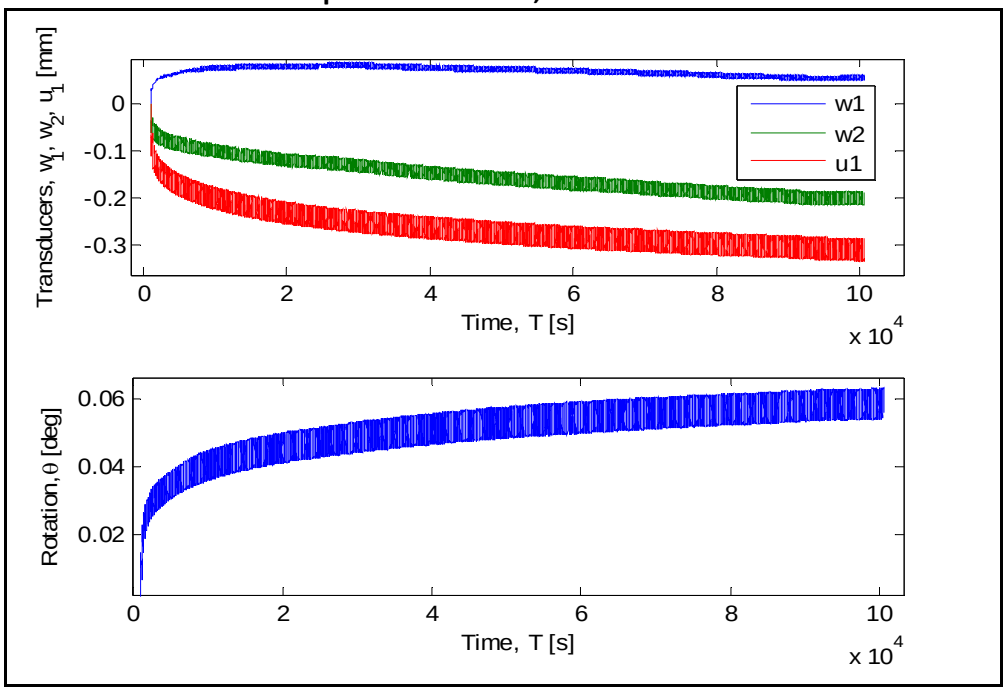

Horizontal Load-Time, Moment-Rotation

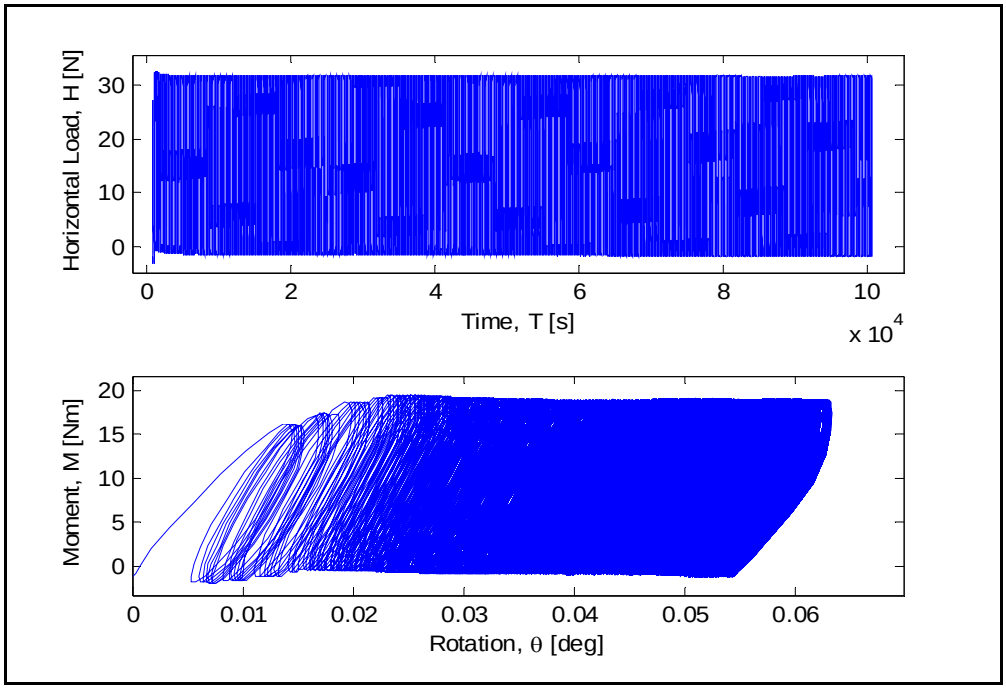

Maximum accumulated rotation [deg] | 0.0634

Maximum and minimum moment [Nm]

Mmax	Mmin
18.99	0.35

ζb	ζc
0.35	-0.054

Post-Cyclic Phase

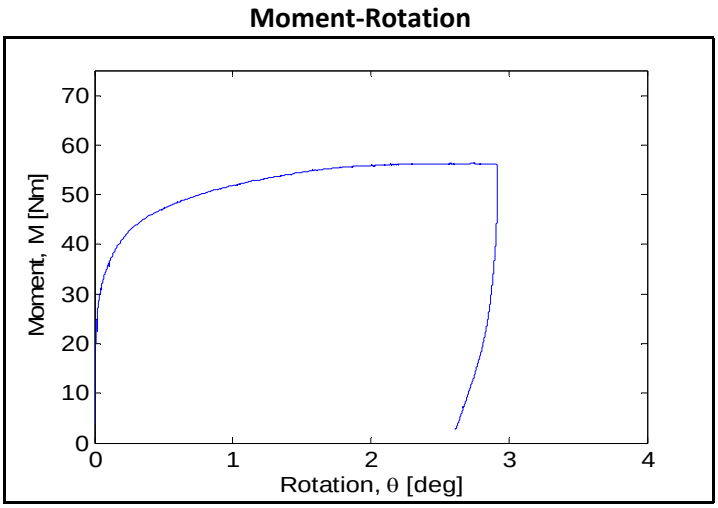

Maximum moment [Nm]	56.26
Rotation at maximum moment [Deg]	2.52

Test equipment	Blue sandbox
User	Aligi
Test name	C51
Date	10/04/2013

Bucket

Diameter [mm]	300
Embedment ratio	0.5

Test

Static or cyclic test	cyclic
Moment arm [mm]	596

General Comments

The second CPT was not corectly performed

Soil Preparation and Installation Phase

Gradient applied

1.08

Cone Penetration Resistance

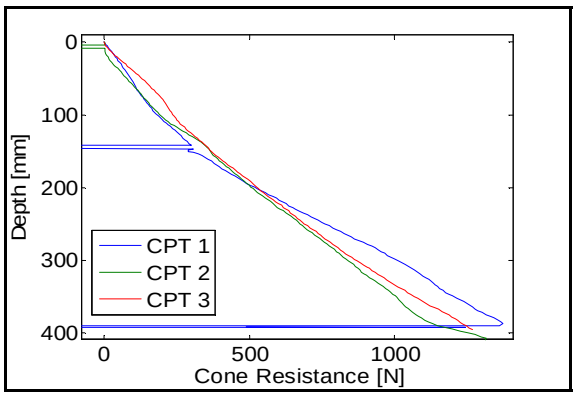

Installation Phase

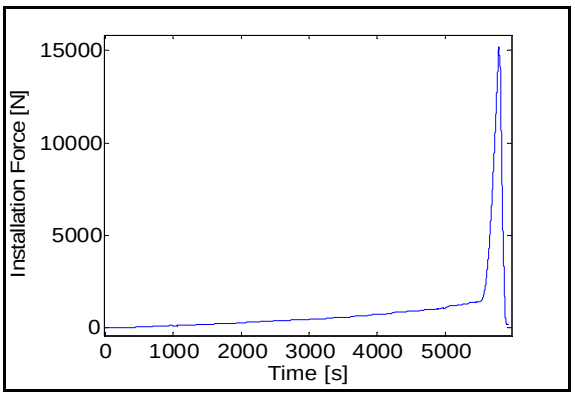

Relative density [%]

cpt 1	cpt 2	cpt 3	Average
98.59	-	97.33	97.96

Maximum installation force [N]	15200
Penetration depth [mm]	143

Cyclic Test Phase

Masses on the weight hangers [Kg]

M1	M2	M3
2.15	3.37	31.5

Number of cycles	10089
Loading period [s]	10

LVDTs-Time, Rotation-Time

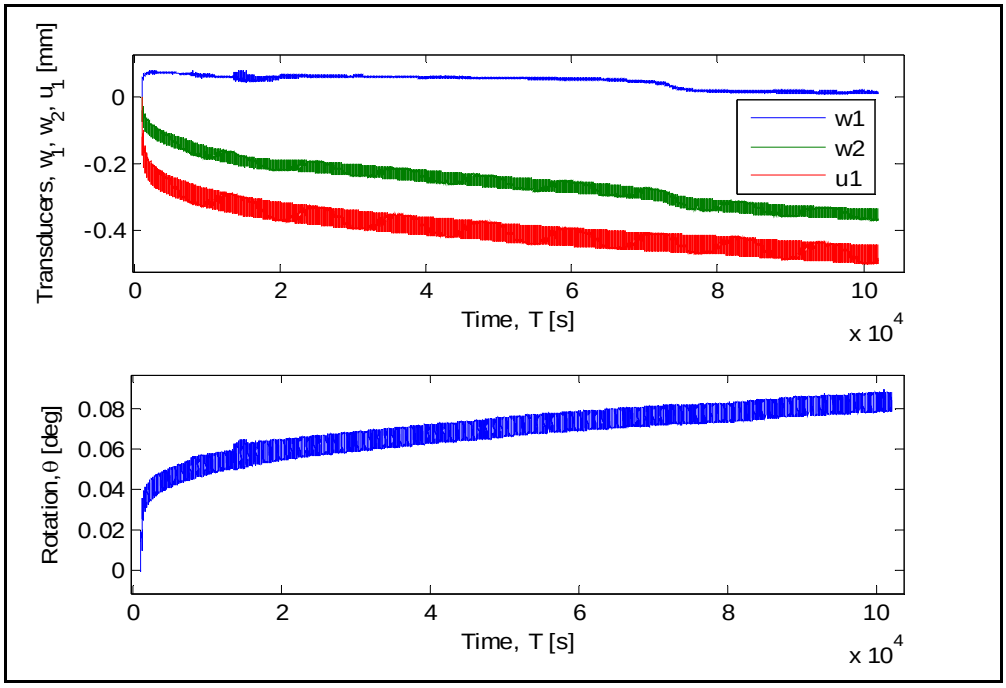

HorizontalLoad-Time, Moment-Rotation

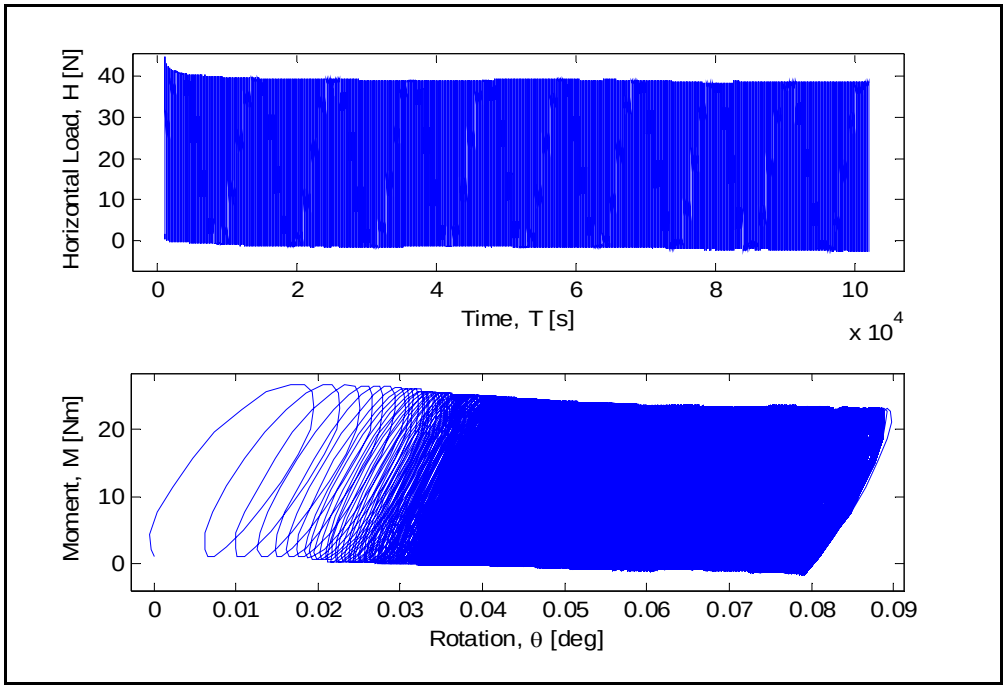

Maximum accumulated rotation [deg] | 0.0888

Maximum and minimum moment [Nm]

Mmax	Mmin
23.29	0

ζb	ζc
0.435	-0.041

Post-Cyclic Phase

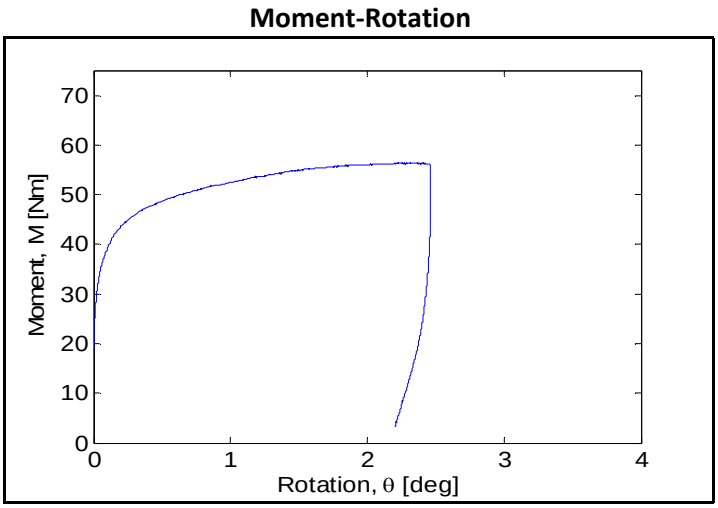

Maximum moment [Nm]	56.4
Rotation at maximum moment [deg]	2.319

Test equipment	Blue sandbox
User	Aligi
Test name	S52
Date	19/04/2013

Bucket

Diameter [mm]	300
Embedment ratio	0.5

Test

Static or cyclic test	static
Moment arm [mm]	0.596

General Comments

None

Soil Preparation & Installation Phase

Gradient applied

1.08

Cone Penetration Resistance

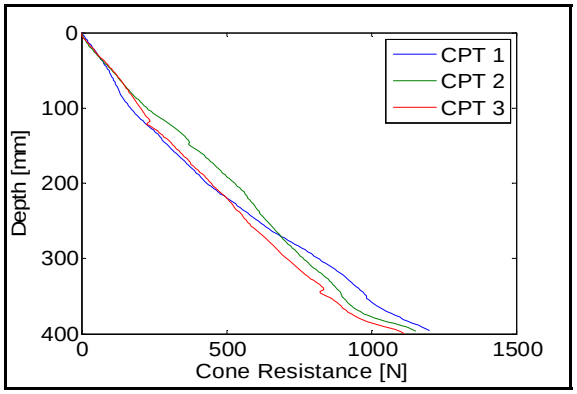

Installation Phase

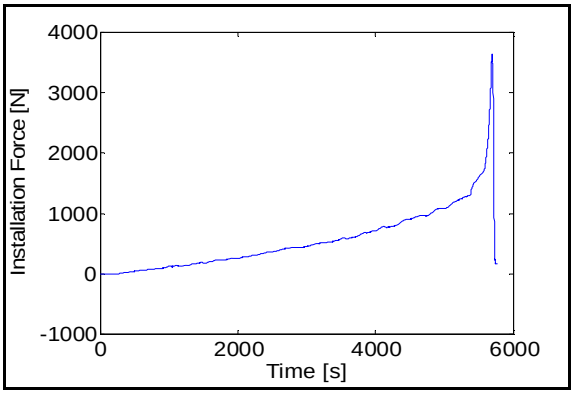

Relative density [%]

cpt 1	cpt 2	cpt 3	Average
93.09	95.45	92.1	93.55

Maximum installation force [N]	3639
Penetration depth [mm]	140

Horizontal and Vertical displacement-Rotation

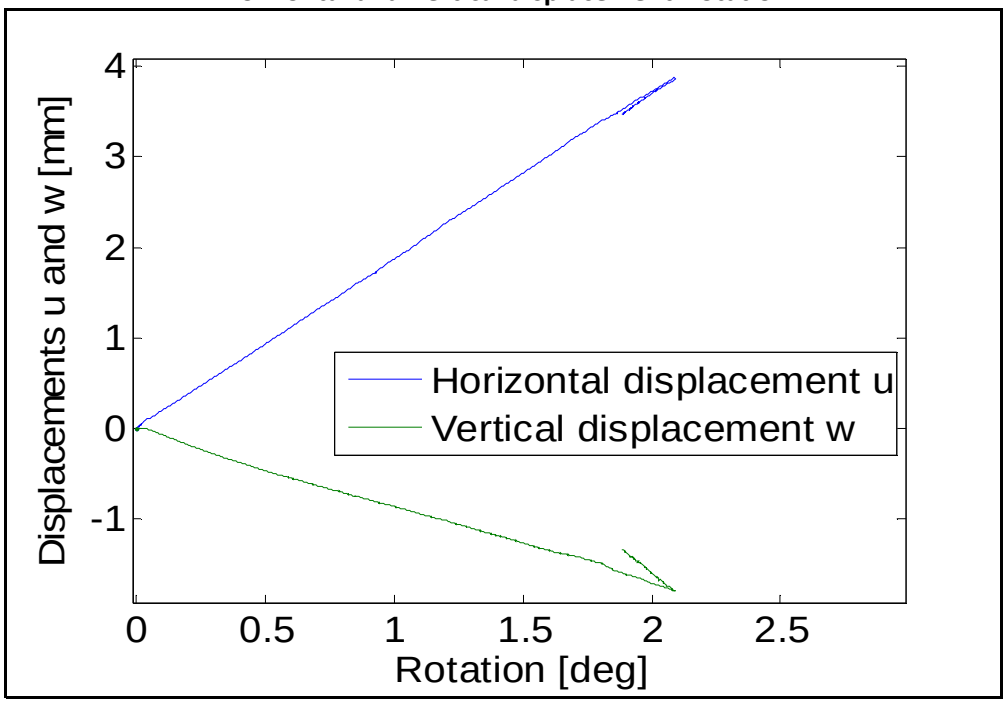

Moment-Rotation

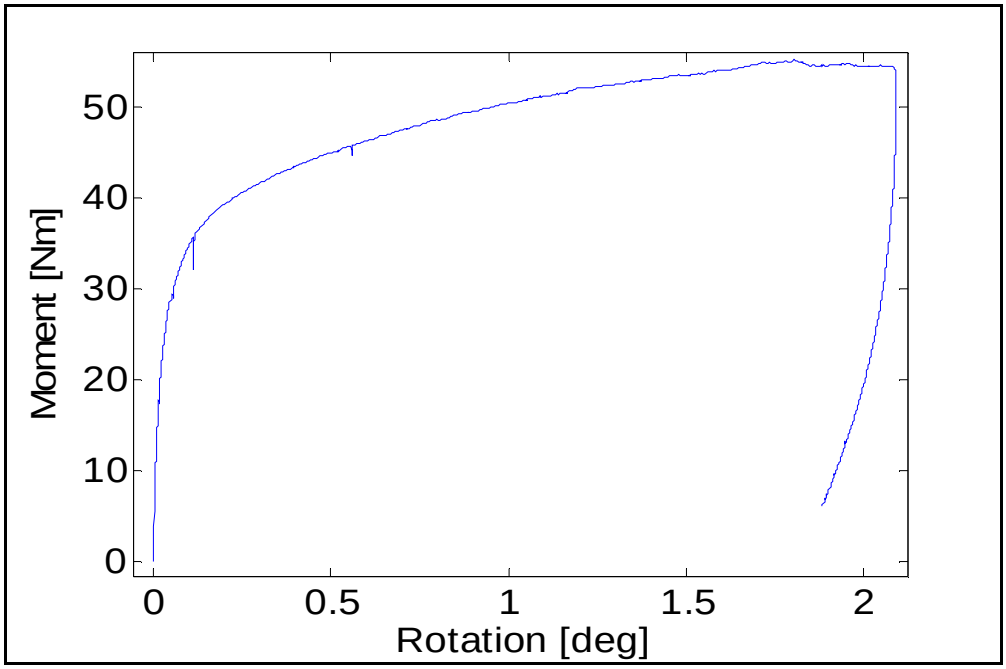

Maximum moment [Nm]	55.18
Rotation at maximum moment [deg]	1.8

Test equipment	Blue sandbox
User	Aligi
Test name	C53
Date	24/04/2013

Bucket

Diameter [mm]	300
Embedment ratio	0.5

Test

Static or cyclic test	cyclic
Moment arm [mm]	596

General Comments

The installation was split into two separate files.

Soil Preparation and Installation Phase

Gradient applied

1.08

Cone Penetration Resistance

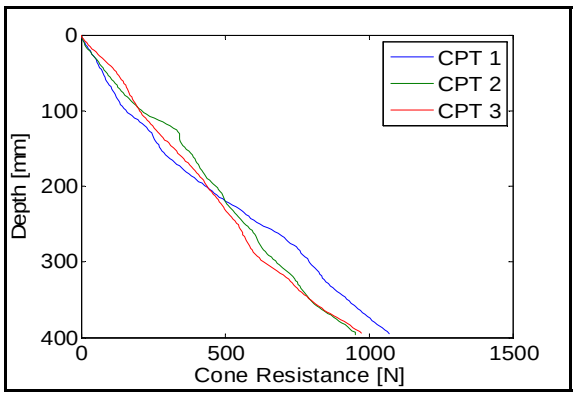

Installation Phase

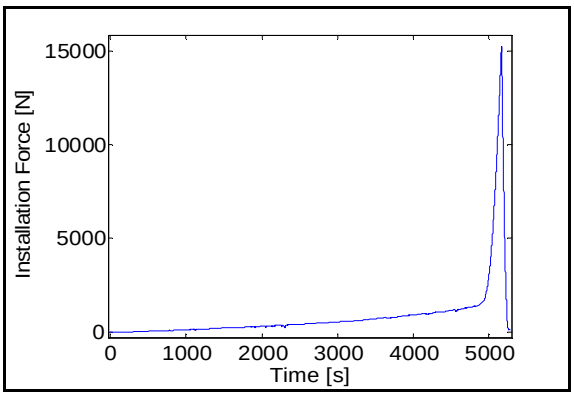

Relative density [%]

cpt 1	cpt 2	cpt 3	Average
92.23	92.79	91.12	92.05

Maximum installation force [N]	15234
Penetration depth [mm]	142.74

Cyclic Test Phase

Masses on the weight hangers [Kg]

M1	M2	M3
-	-	31.5

Number of cycles	16068
Loading period [s]	10

LVDTs-Time, Rotation-Time

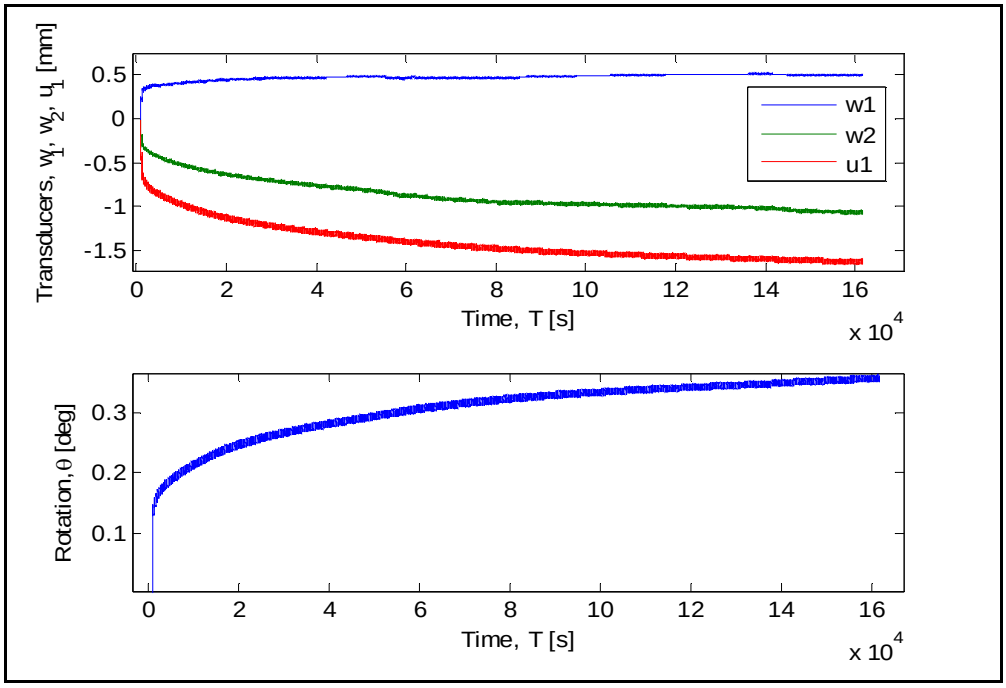

Horizontal Load-Time, Moment-Rotation

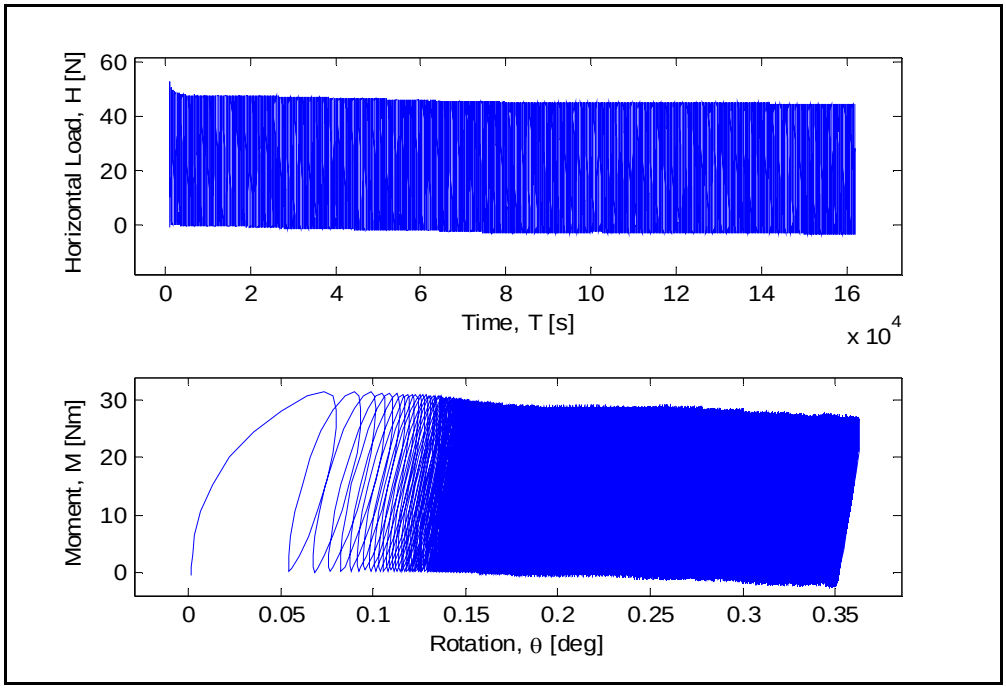

Maximum accumulated rotation [deg] | 0.362

Maximum and minimum moment [Nm]

Mmax	Mmin
27.47	-1.34

ζb	ζc
0.51	-0.049

Post-Cyclic Phase

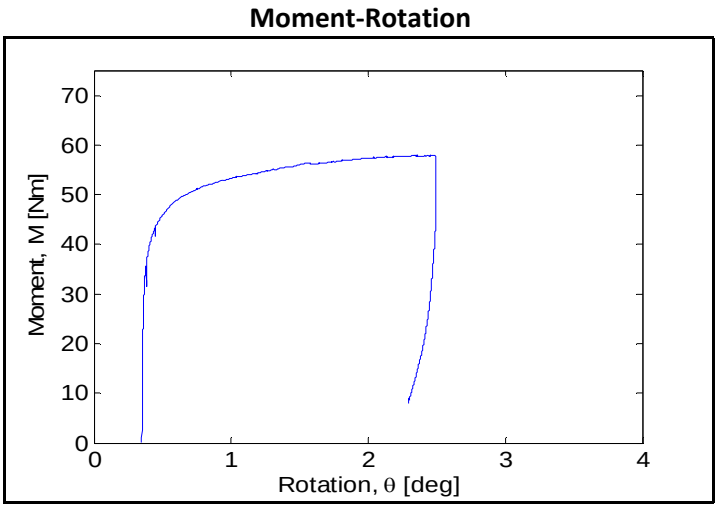

Maximum moment [Nm]	-
Rotation at maximum moment [deg]	-

Test equipment	Blue sandbox
User	Aligi
Test name	C54
Date	28/09/2013

Bucket

Diameter [mm]	300
Embedment ratio	0.5

Test

Static or cyclic test	cyclic
Moment arm [mm]	596

General Comments

The data present a clear discontinuity in terms of w1 and w2 at N = 15000.
The CPT calibration factor changed. From 2600 to 1363 to 1 mV/V

Soil Preparation and Installation Phase

Gradient applied

0.96

Cone Penetration Resistance

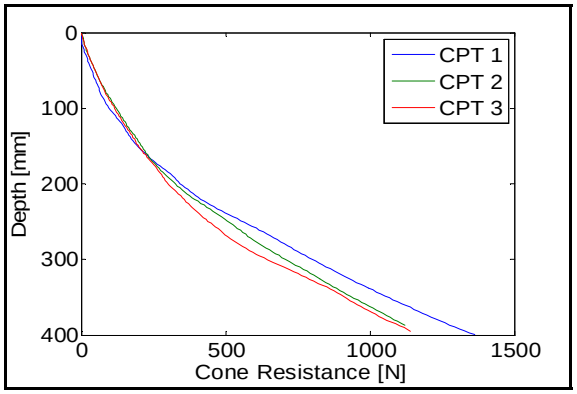

Installation Phase

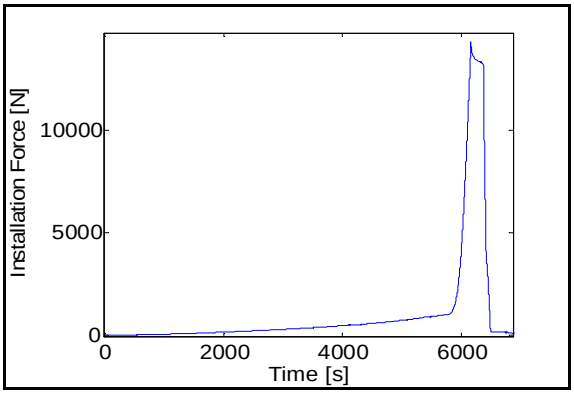

Relative density [%]

cpt 1	cpt 2	cpt 3	Average
89.13	87.52	85.99	87.54667

Maximum installation force [N]	14301
Penetration depth [mm]	145.7

Cyclic Test Phase

Masses on the weight hangers [Kg]

M1	M2	M3
1.225	2.3	31.5

Number of cycles	16327
Loading period [s]	10

LVDTs-Time, Rotation-Time

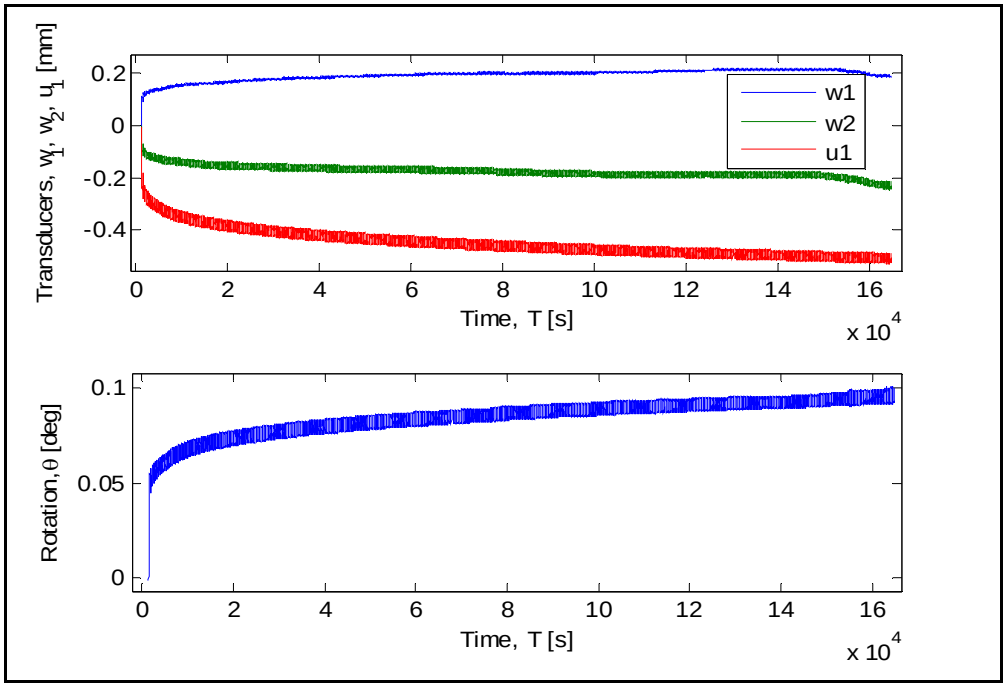

Horizontal Load-Time, Moment-Rotation

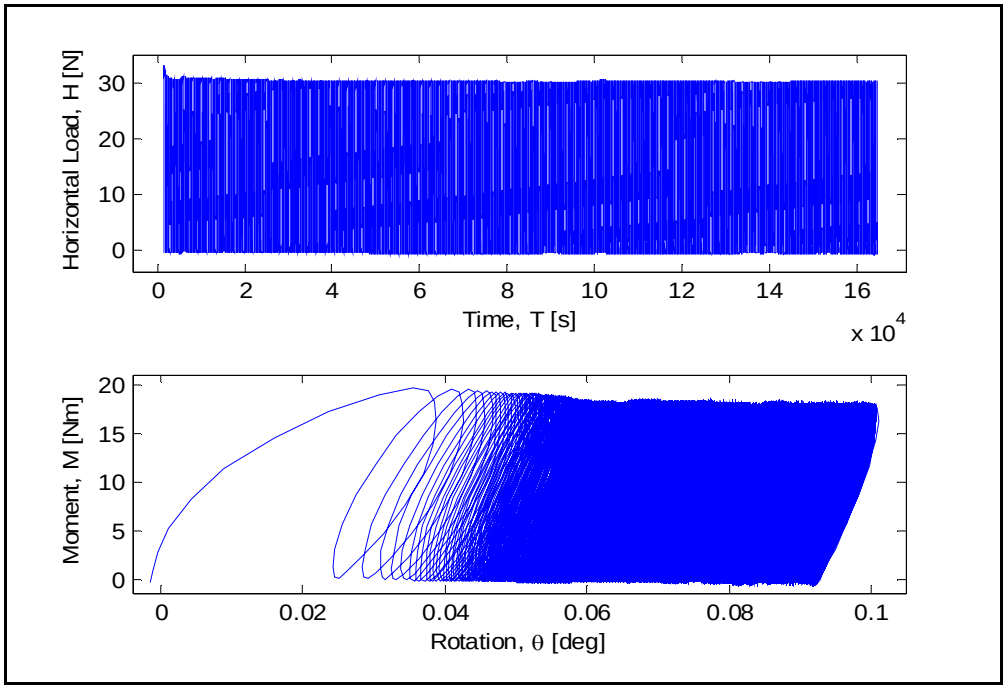

Maximum accumulated rotation [deg] | 0.099

Maximum and minimum moment [Nm]

Mmax	Mmin
18.13	-0.341

ζb	ζc
0.3329	-0.0188

Post-Cyclic Phase

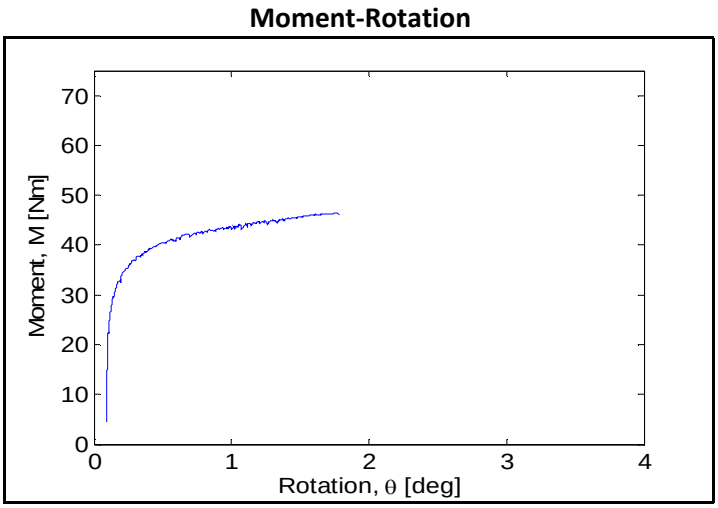

Maximum moment [Nm]	46.4
Rotation at maximum moment [deg]	1.778

Test equipment	Blue sandbox
User	Aligi
Test name	C55
Date	01/10/2013

Bucket

Diameter [mm]	300
Embedment ratio	0.5

Test

Static or cyclic test	cyclic
Moment arm [mm]	596

General Comments

I did not tare the system before starting running the test. I zeroed all the measurements just in the 'general.mat' script.
The LVDTs u1 and w2 were switched by accident. I switched them back in terms of column in general.mat

Soil Preparation and Installation Phase

Gradient applied

0.96

Cone Penetration Resistance

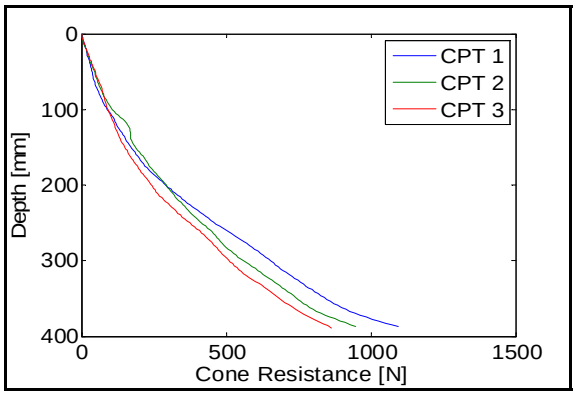

Installation Phase

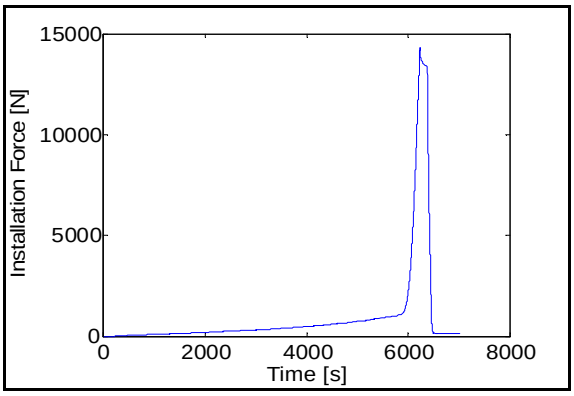

Relative density [%]

cpt 1	cpt 2	cpt 3	Average
84.26	83.47	79.91	82.55

Maximum installation force [N]	14325
Penetration depth [mm]	145.2

Cyclic Test Phase

Masses on the weight hangers [Kg]

M1	M2	M3
1.435	2.95	31.5

Number of cycles	15233
Loading period [s]	10

LVDTs-Time, Rotation-Time

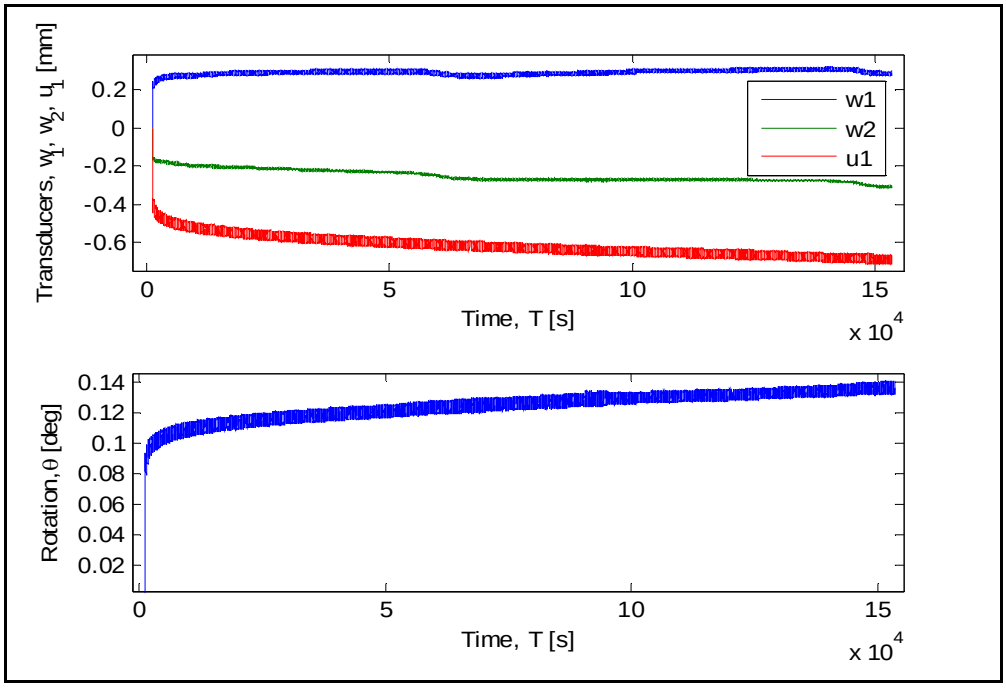

Horizontal Load-Time, Moment-Rotation

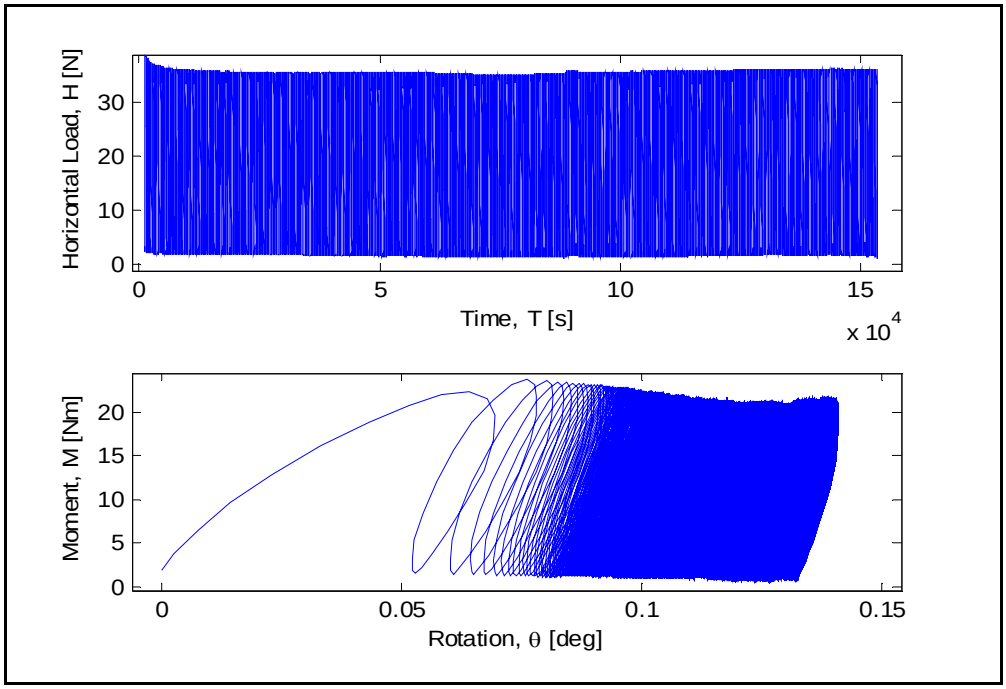

Maximum accumulated rotation [deg]	0.1407

Maximum and minimum moment [Nm]

Mmax	Mmin
21.28	0.857

ζB	ζC
0.39	0.04

Post-Cyclic Phase

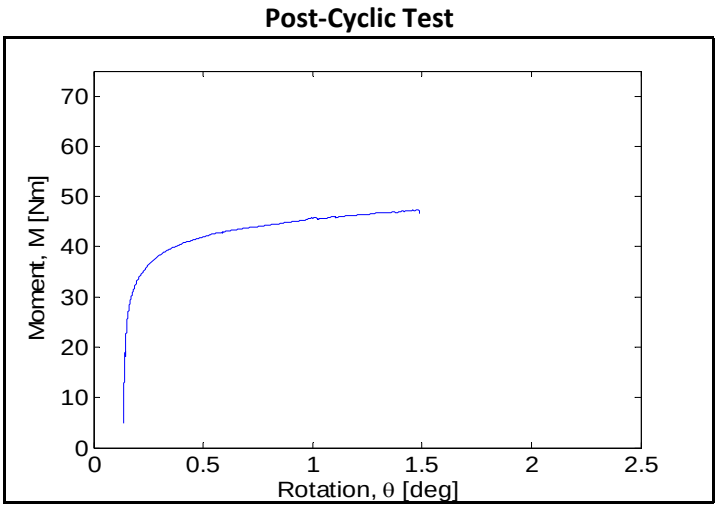

Maximum moment [Nm]	47.3
Rotation at maximum moment [deg]	2.646

Test equipment	Blue sandbox
User	Aligi
Test name	S56
Date	04/10/2013

Bucket

Diameter [mm]	300
Embedment ratio	0.75

Test

Static or cyclic test	static
Moment arm [mm]	0.596

General Comments

This test was the first quasi-statit reference for buckets d/D = 0.75.
We had quite an issue in mounting the loading tower. The support plate did not fit with the screw on the bucket lid. Finally we decided to run the test anyway by bolting the loading tower through the support in tension (that on the left).
The LVDT 'u1' was not fitted properly and it could not measure the first hundreds data.
The LVDT was then moved closer to the plates and therefore could restart taking measurements.

Soil Preparation & Installation Phase

Gradient applied

1.08

Cone Penetration Resistance

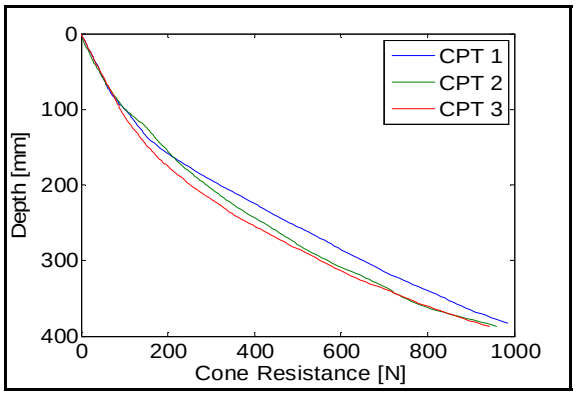

Installation Phase

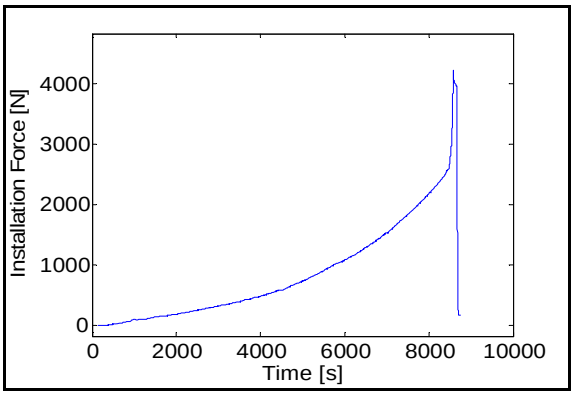

Relative density [%]

cpt 1	cpt 2	cpt 3	Average
85.03	83.35	81.08	83.15

Maximum installation force [N]	4218
Penetration depth [mm]	215.86

Horizontal and Vertical displacement-Rotation

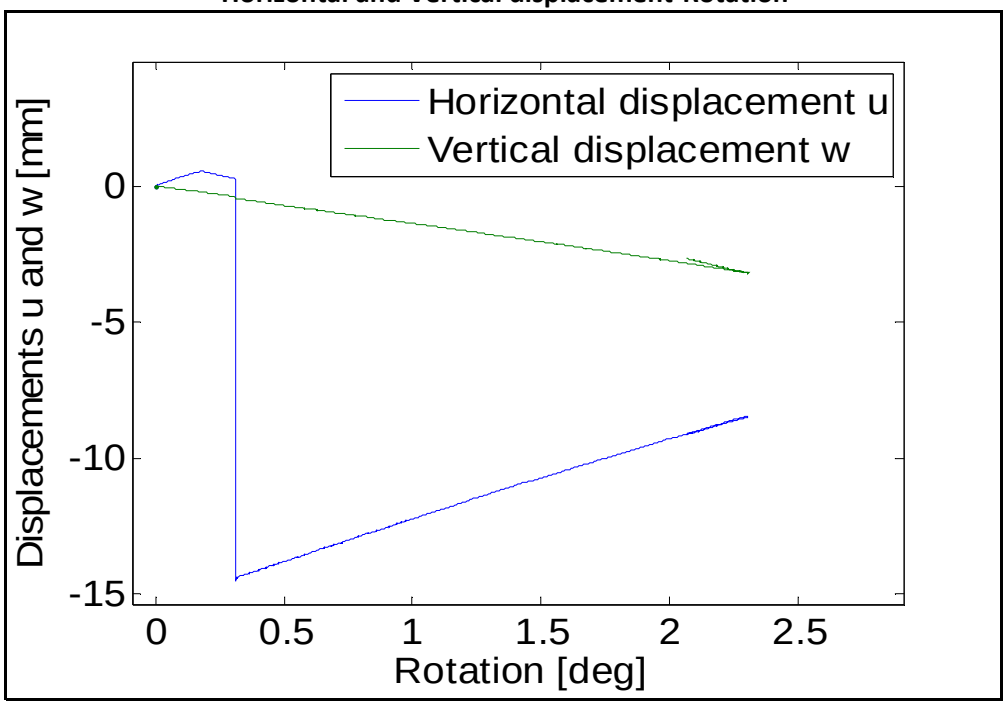

Moment-Rotation

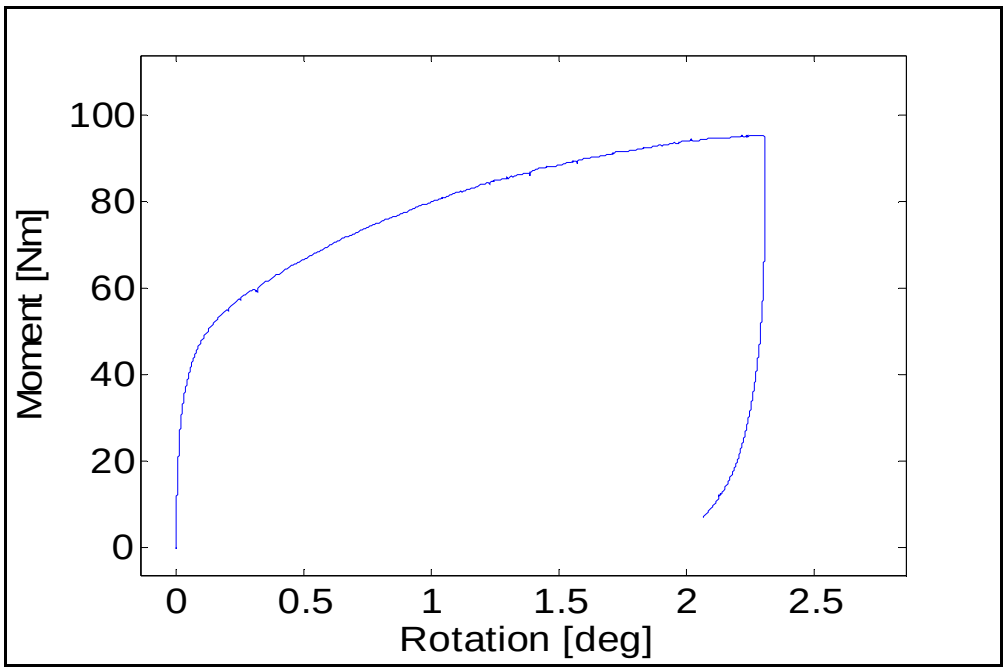

Maximum moment [Nm]	95.35
Rotation at maximum moment [deg]	2.29

Test equipment	Blue sandbox
User	Aligi
Test name	S57
Date	08/10/2013

Bucket

Diameter [mm]	300
Embedment ratio	0.75

Test

Static or cyclic test	static
Moment arm [mm]	0.596

General Comments

None

Soil Preparation & Installation Phase

Gradient applied

1.08

Cone Penetration Resistance

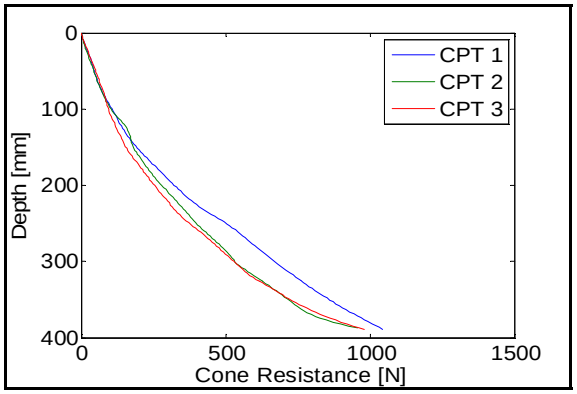

Installation Phase

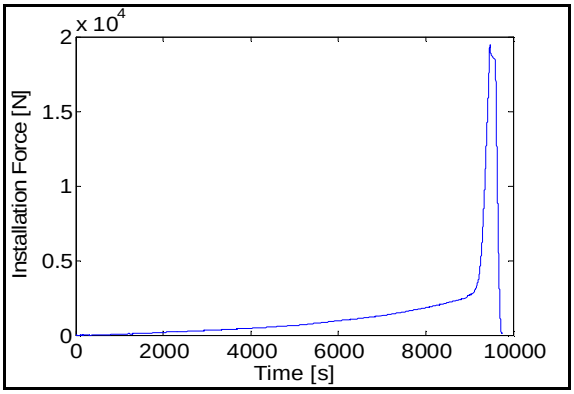

Relative density [%]

cpt 1	cpt 2	cpt 3	Average
85.93	82.49	80.87	83.10

Maximum installation force [N]	19464
Penetration depth [mm]	218.32

Horizontal and Vertical displacement-Rotation

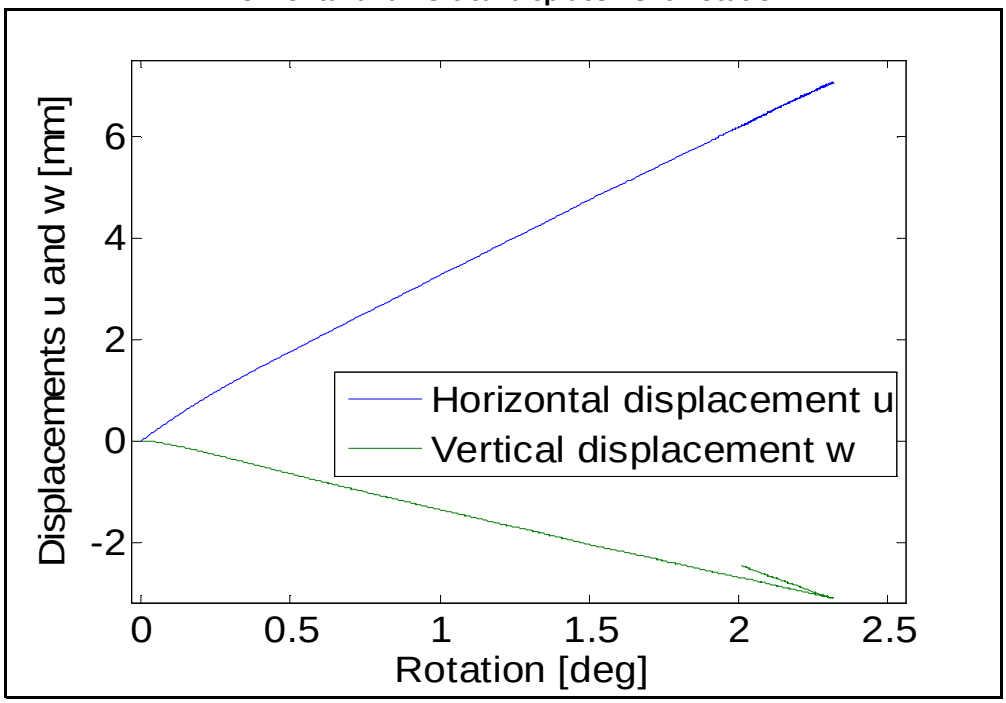

Moment-Rotation

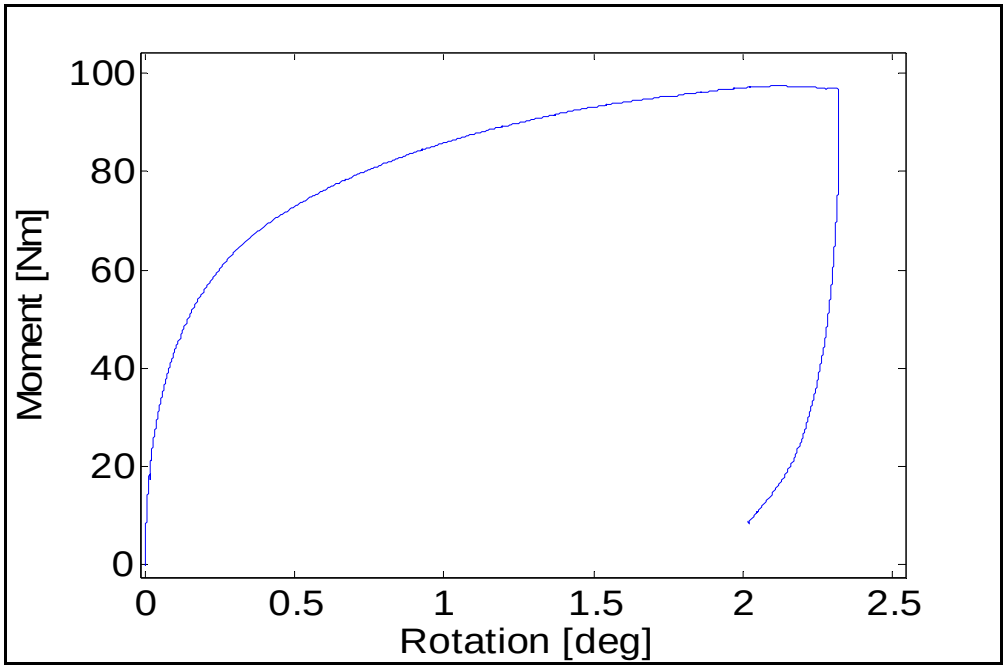

Maximum moment [Nm]	97.53
Rotation at maximum moment [deg]	2.12

Test equipment	Blue sandbox
User	Aligi
Test name	C58
Date	12/10/2013

Bucket

Diameter [mm]	300
Embedment ratio	0.75

Test

Static or cyclic test	cyclic
Moment arm [mm]	596

General Comments

None

Soil Preparation and Installation Phase

Gradient applied

0.96

Cone Penetration Resistance

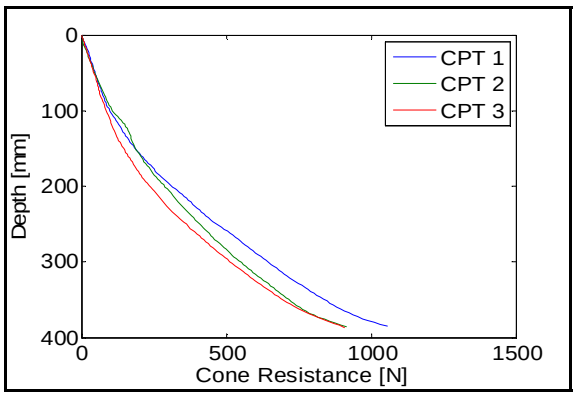

Installation Phase

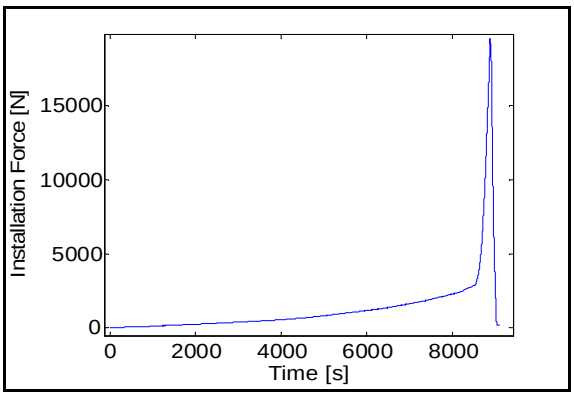

Relative density [%]

Id cpt 1	Id cpt 2	Id cpt 3	Average
84.97	82.93	79.51	82.47

Maximum installation force [N]	19530
Penetration depth [mm]	217.6

Cyclic Test Phase

Masses on the weight hangers [Kg]

M1	M2	M3
1.23	2.54	31.5

Number of cycles	34459
Loading period [s]	10

LVDTs-Time, Rotation-Time

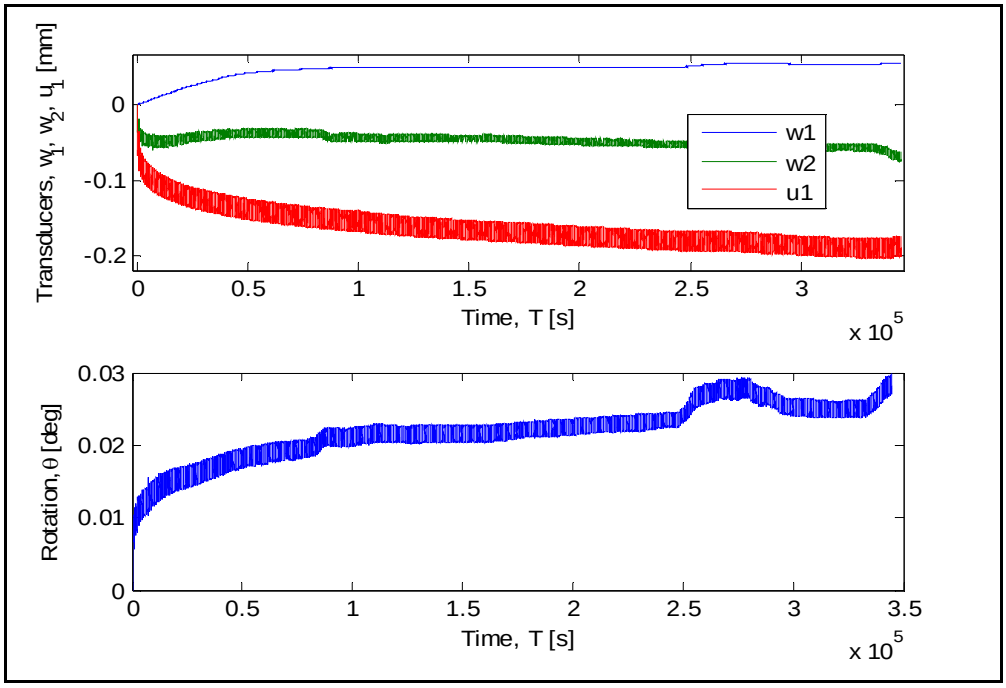

Horizontal Load-Time, Moment-Rotation

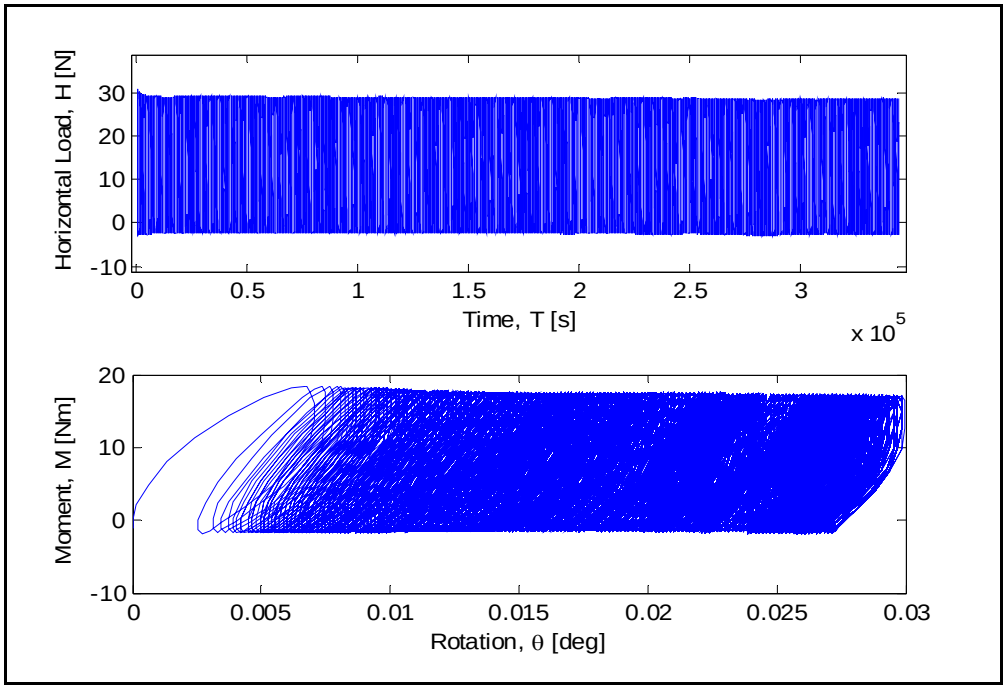

Maximum accumulated rotation [deg] | 0.03

Maximum and minimum moment [Nm]

Mmax	Mmin
17.25	-1.53

ζb	ζc
0.177	-0.09

Post-Cyclic Phase

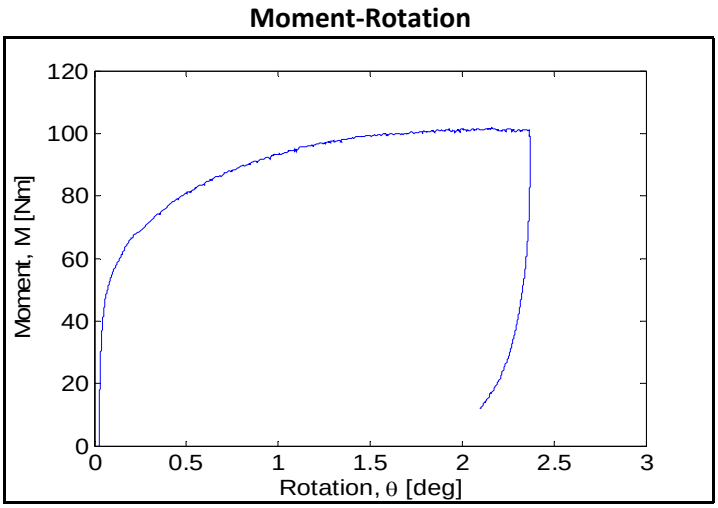

Maximum moment [Nm]	101.7
Rotation at maximum moment [deg]	2.16

Test equipment	Blue sandbox
User	Aligi
Test name	C59
Date	17/10/2013

Bucket

Diameter [mm]	300
Embedment ratio	0.75

Test

Static or cyclic test	cyclic
Moment arm [mm]	596

General Comments

None

Soil Preparation and Installation Phase

Gradient applied

0.96

Cone Penetration Resistance

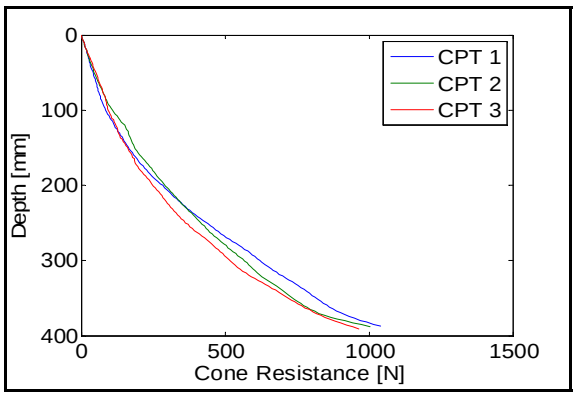

Installation Phase

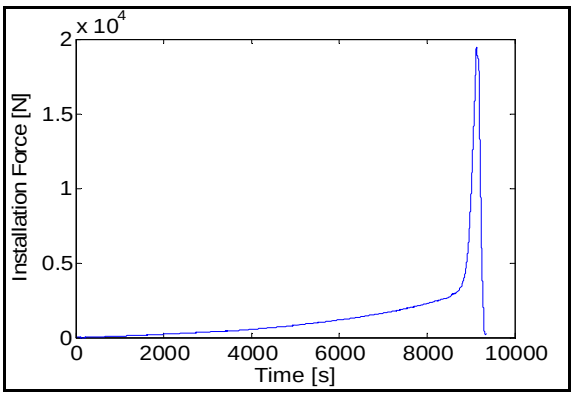

Relative density [%]

cpt 1	cpt 2	cpt 3	Average
83.18	83.49	80.75	82.47

Maximum installation force [N]	19425
Penetration depth [mm]	216.345

Cyclic Test Phase

Masses on the weight hangers [Kg]

M1	M2	M3
1.92	3.54	31.5

Number of cycles	9984
Loading period [s]	10

LVDTs-Time, Rotation-Time

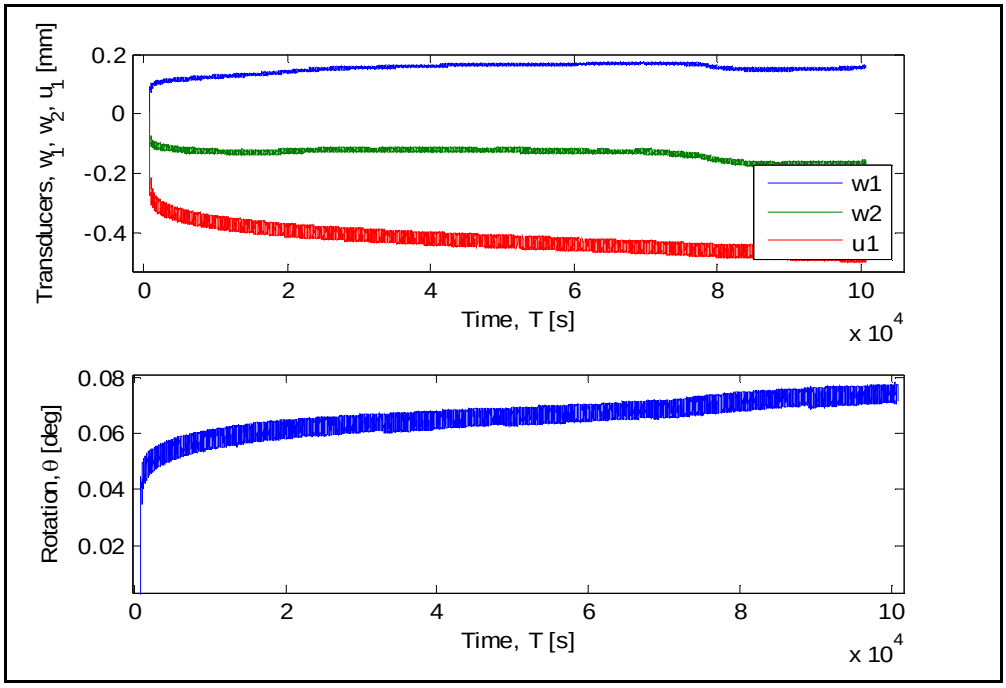

Horizontal Load-Time, Moment-Rotation

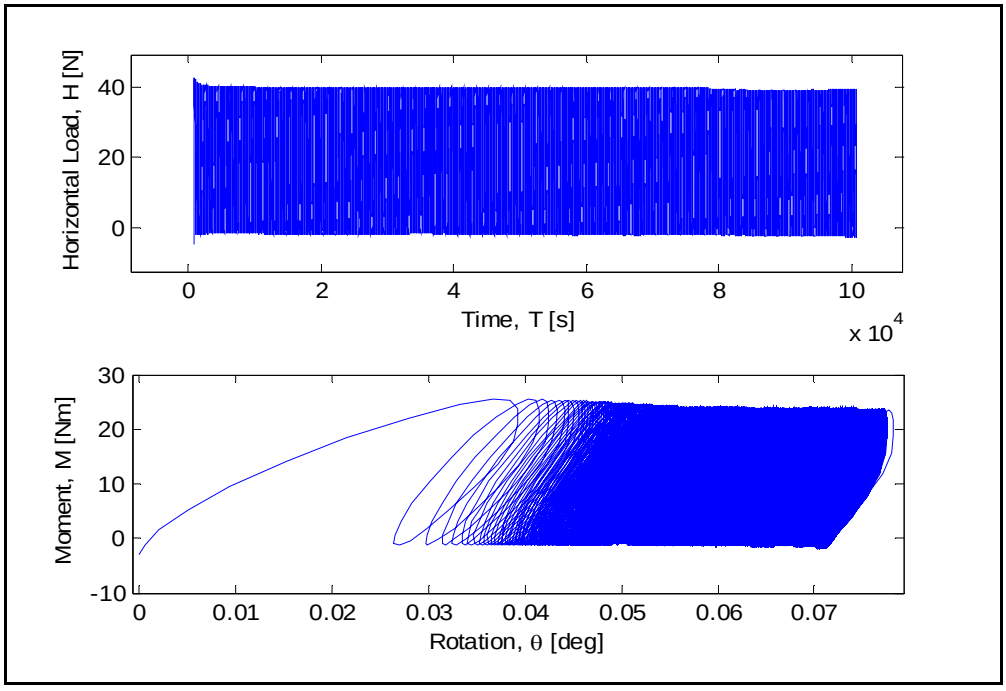

Maximum accumulated rotation [deg] | 0.0783

Maximum and minimum moment [Nm]

Mmax	Mmin
23.76	-1.315

ζb	ζc
0.244	-0.055

Post-Cyclic Phase

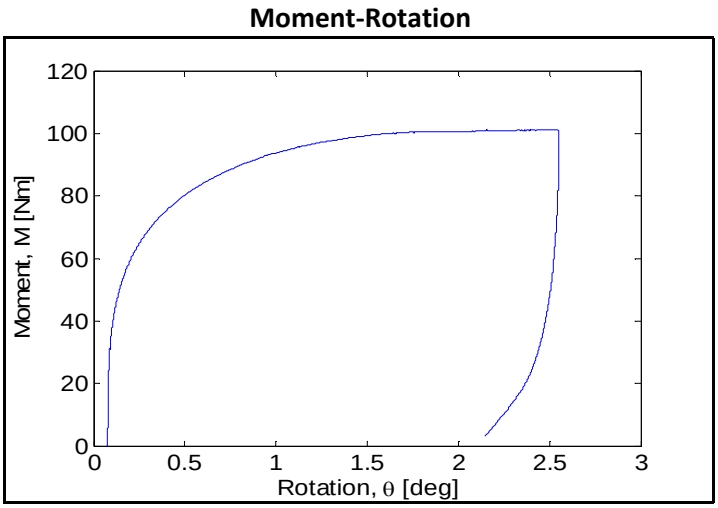

Failure moment [Nm]	101.2
Rotation at failure [deg]	2.4

Test equipment	Blue sandbox
User	Aligi
Test name	C60
Date	25/10/2013

Bucket

Diameter [mm]	300
Embedment ratio	0.75

Test

Static or cyclic test	cyclic
Moment arm [mm]	596

General Comments

During the CPT1 the hydraulic system leaked oil. It was not possible to terminate the test correctly.
The flat part in the installation phase is due to the self-stopping device.

Soil Preparation and Installation Phase

Gradient applied

0.96

Cone Penetration Resistance

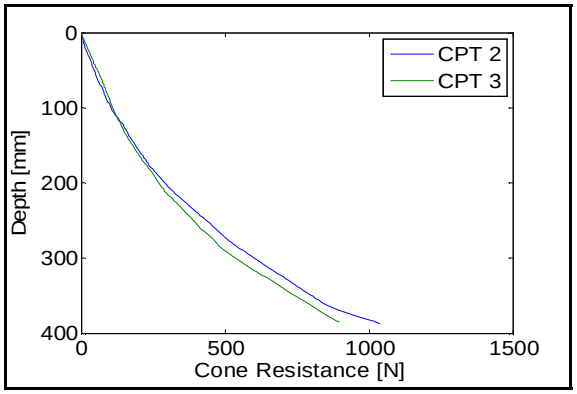

Installation Phase

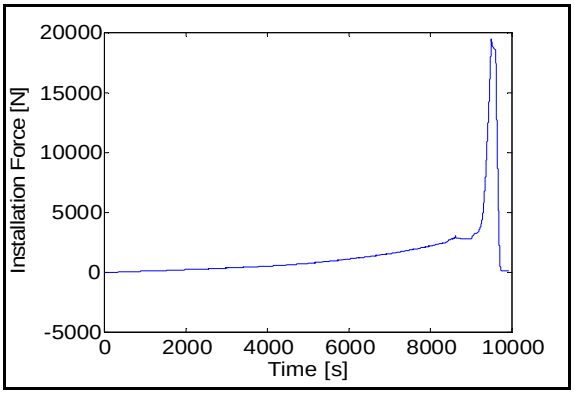

Relative density [%]

cpt 1	cpt 2	cpt 3	Average
-	84.11	82.27	83.19

Maximum installation force [N]	19008
Penetration depth [mm]	216.641

Cyclic Test Phase

Masses on the weight hangers [Kg]

M1	M2	M3
2.04	4.48	31.5

Number of cycles	10058
Loading period [s]	10

LVDTs-Time, Rotation-Time

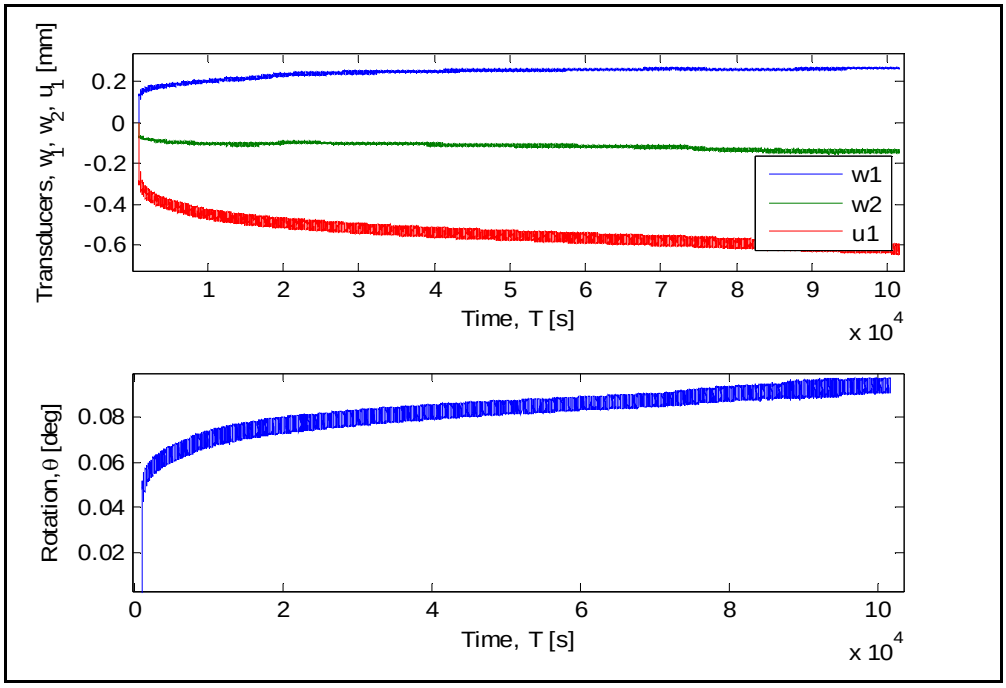

Horizontal Load-Time, Moment-Rotation

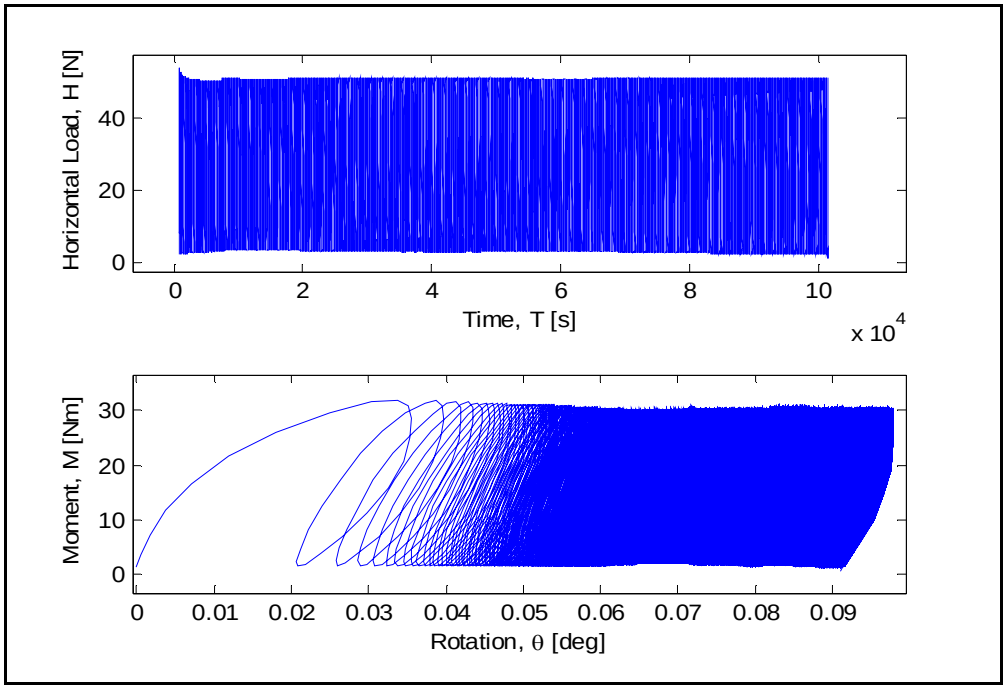

Maximum accumulated rotation [deg] | 0.0978

Maximum and minimum moment [Nm]

Mmax	Mmin
30.39	1.66

ζb	ζc
0.312	0.0547

Post-Cyclic Phase

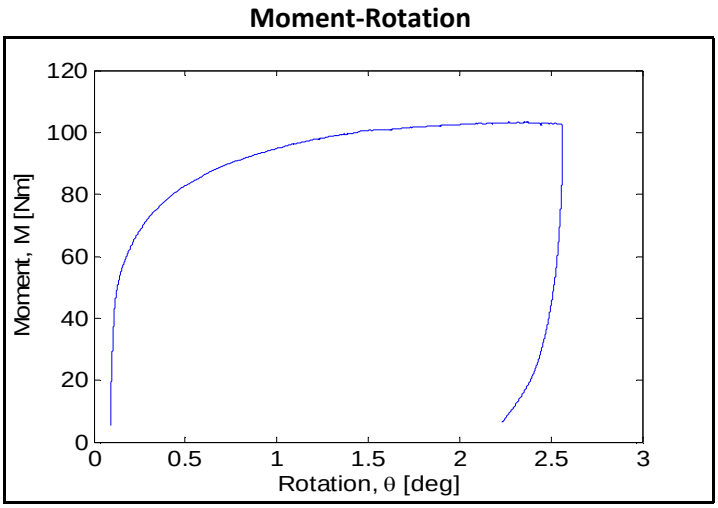

Maximum moment [Nm]	103.2
Rotation at maximum moment [deg]	2.27

Test equipment	Blue sandbox
User	Aligi
Test name	C61
Date	25/10/2013

Bucket

Diameter [mm]	300
Embedment ratio	0.75

Test

Static or cyclic test	cyclic
Moment arm [mm]	596

General Comments

The load cel during installation did not work.

Soil Preparation and Installation Phase

Gradient applied

0.96

Cone Penetration Resistance

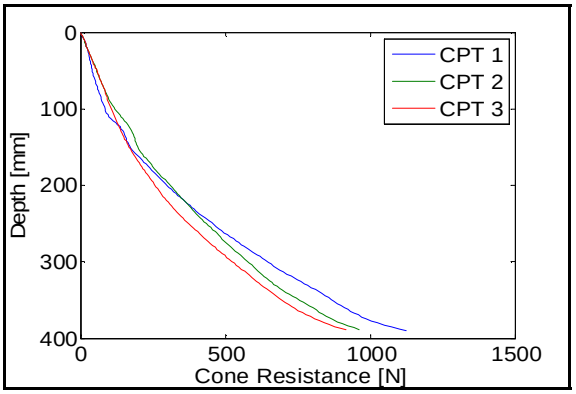

Installation Phase

Relative density [%]

cpt 1	cpt 2	cpt 3	Average
84.51	84.5	81.21	83.41

Maximum installation force [N]	-
Penetration depth [mm]	-

Cyclic Test Phase

Masses on the weight hangers [Kg]

M1	M2	M3
2.92	4.06	31.5

Number of cycles	18116
Loading period [s]	10

LVDTs-Time, Rotation-Time

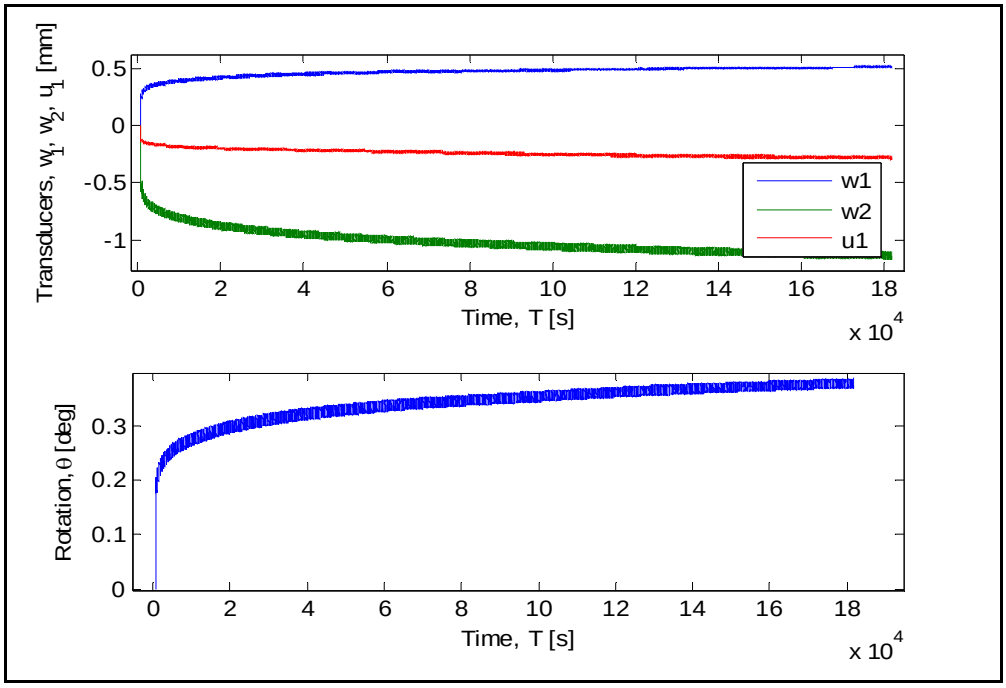

Horizontal Load-Time, Moment-Rotation

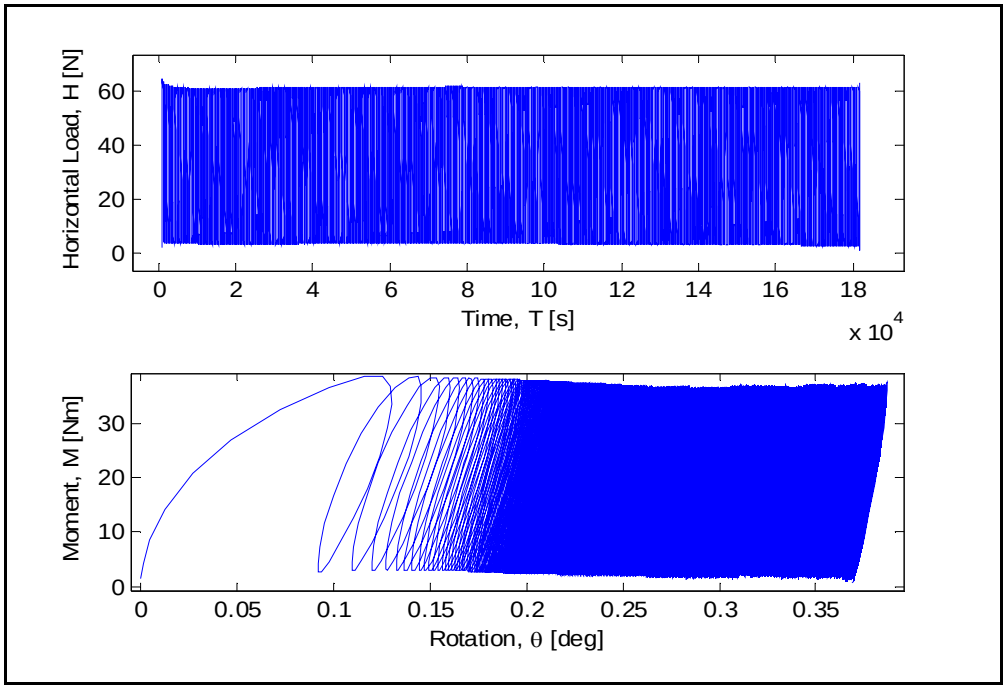

Maximum accumulated rotation [deg] | 0.3874

Maximum and minimum moment [Nm]

Mmax	Mmin
36,71	1.95

ζb	ζc
0.376	0.053

Post-Cyclic Phase

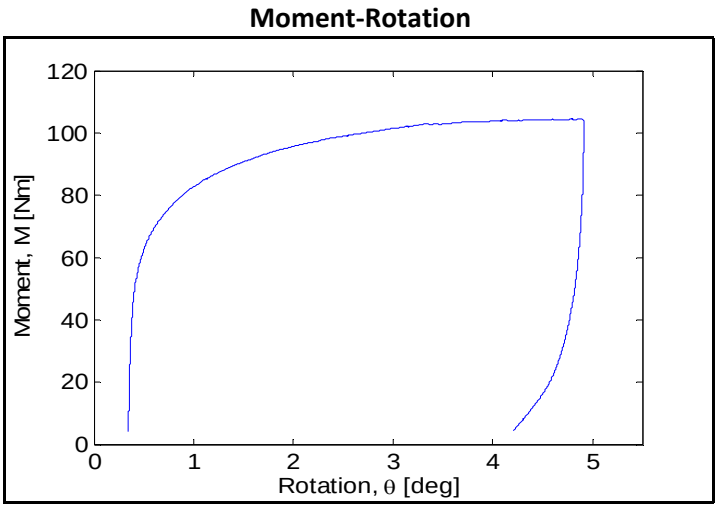

Maximum moment [Nm]	104.5
Rotation at maximum moment [deg]	4.88

Test equipment	Yellow sandbox
User	Aligi
Test name	S63
Date	02/12/2013

Bucket	
Diameter [mm]	300
Embendment ratio	0.75
Test	
Static or cyclic test	static

General Comments

Soil Preparation & Test Phase

Cone Penetration Resistance

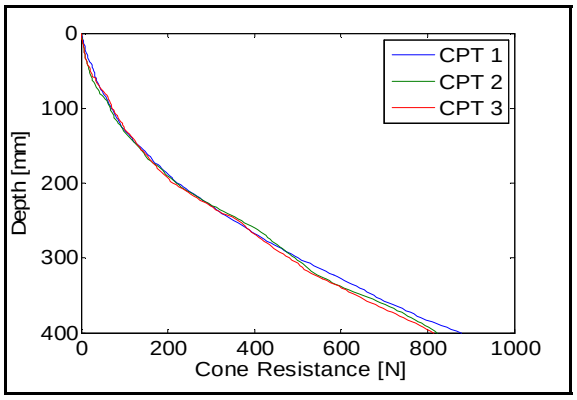

Test Phase

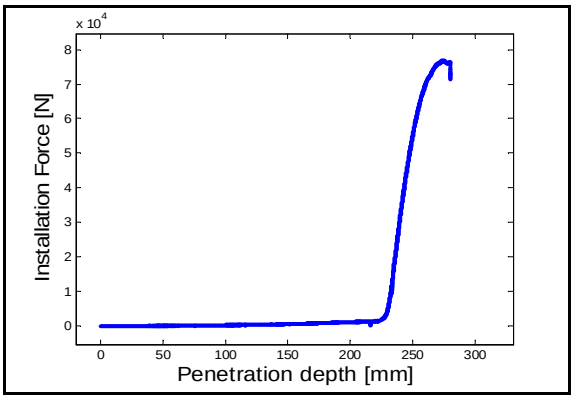

Relative density [%]

Id cpt 1	Id cpt 2	Id cpt 3	Average
78.32	77.85	77.73	77.97

Test equipment	Yellow sandbox
User	Aligi
Test name	S64
Date	03/12/2013

Bucket

Diameter [mm]	300
Embendment ratio	1

Test

Static or cyclic test	static

General Comments

Soil Preparation & Test Phase

Cone Penetration Resistance

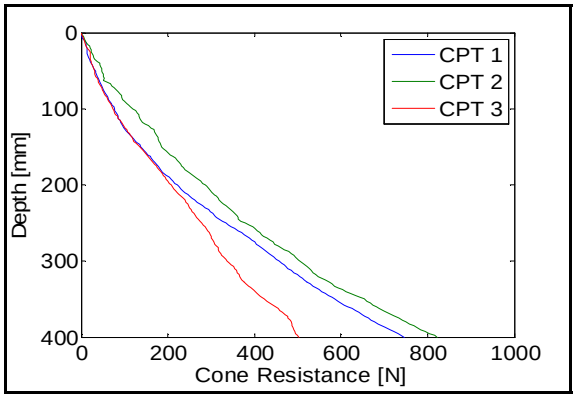

Test Phase

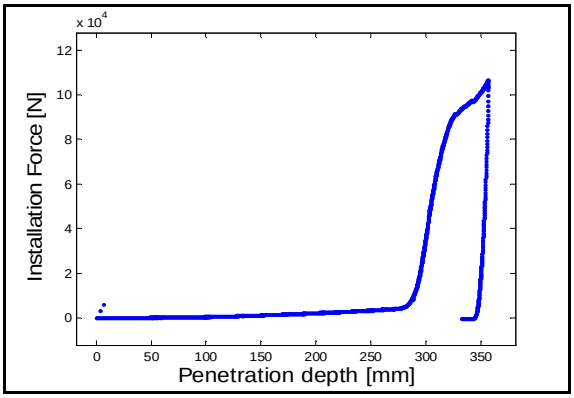

Relative density [%]

Id cpt 1	Id cpt 2	Id cpt 3	Average
77.1	81.92	73.15	77.39

ISSN 1901-7294
DCE Thesis No. 68